DISSERTATION

# A COMPREHENSIVE APPROACH TO MODELING MUSCULOSKELETAL AGING AND INJURY: AN EMPHASIS ON NRF2-RELATED PATHOGENESIS

Submitted by

Kendra M. Andrie

Department of Microbiology, Immunology, and Pathology

In partial fulfillment of the requirements

For the Degree of Doctor of Philosophy

Colorado State University

Fort Collins, Colorado

Spring 2021

Doctoral Committee:

Advisor: Kelly S. Santangelo

Karyn Hamilton
Laurie Goodrich
Brendan Podell
Juan Muñoz Gutiérrez
Benjamin Miller

ABSTRACT

A COMPREHENSIVE APPROACH TO MODELING MUSCULOSKELETAL AGING AND INJURY: AN EMPHASIS ON NRF2-RELATED PATHOGENESIS

Osteoarthritis (OA) is a degenerative joint disease that affects over 730 million people globally, over 30 million Americans, and is the leading cause of disability in adults. The underlying pathogenesis is multifactorial and largely undetermined, with a variety of cellular pathways and risk factors contributing to disease onset and progression. The crux of this work is that downregulation in nuclear factor erythroid-2 related factor-2 (Nrf2)-signaling in musculoskeletal tissue serves as a central driver for persistent low-grade inflammation, dysregulation of redox homeostasis, mitochondrial dysfunction, and protein dyshomeostasis, all of which contribute to OA progression. To explore the role of this pathway in OA, we utilized the Hartley OA-prone guinea pig model, which develops naturally occurring idiopathic disease with pathology that mimics human disease. My global hypothesis is supported by preliminary data that demonstrates that aging Hartley guinea pig knee joint tissues have decreased expression of Nrf2 mRNA and protein, which coincides with disease onset and remains decreased throughout OA progression. We investigated the utility of a novel nutraceutical and Nrf2-activator in delaying both the onset and progression of idiopathic OA in this model. The ultimate goal of this work is to (1) identify key molecular pathways involved in the etiopathogenesis of OA, with a particular focus on the contribution of the Nrf2 pathway; (2) investigate the utility of a novel nutraceutical and Nrf2-activator in delaying the onset and/or progression of OA in the Hartley guinea pig, and (3) examine the effects of Nrf2-activation on long bone strength. The inclusion of a musculoskeletal condition beyond OA was also pursued; as such, the clinical and histologic manifestations of a novel rectus femoris myotendinous junction injury model was characterized in rats. Ultimately, this work seeks to advance the understanding of musculoskeletal aging and injury through the analysis of key structural and functional outcome measures to further develop appropriate therapeutic targets for disease prevention and treatment.

ACKNOWLEDGMENTS

I would like to thank Dr. Kelly Santangelo for your support and mentorship throughout my residency and PhD training. You fostered a collaborative, transparent, respectful work environment that created a positive atmosphere for continued achievement and growth. My time spent in your lab has provided me with the necessary tools and confidence needed as I embark on my career as a young pathologist and independent scientist. I would like to express gratitude to all the pathologists and residents at the CSU VDL and my PhD committee members Drs. Karyn Hamilton, Juan Muñoz Gutiérrez, Benjamin Miller, Brendan Podell, and Laurie Goodrich.

This work would not have been accomplished without the collaborative efforts of current and former lab members including Rob Musci, Lauren Radakovich, Katie Sikes, Sydney Bork, Ariel Timkovich, Alexa Spittler, Margaret Campbell, Richard Martinez, Joseph Sanford, Sara Wist, Owen Wahl, Daniel Palmer, Maureen Walsh, Lindsey Burton, Mary Afzali, and Zack Valenti. Thank you for your efforts in animal handling and the overall success of these projects. Further, I appreciate the financial support and opportunities provided by the CSU VDL and NIH (5T32OD010437-18, R21 AG054713-02).

Lastly, I would like to thank my parents, Stan and Karen Andrie, and my husband, Kurt Fennema, for their continued emotional, moral, physical, mental, and financial support throughout my academic career. To my mother, I am forever grateful for you and the value you place on education. Your appreciation for science and medicine fostered my passion within the field which served as a central driver throughout my academic pursuits. The educational opportunities and support you have provided has deeply broadened my understanding and perspective of the world. To my father, your career has exemplified the true meaning of strong leadership and hard work. I am beyond thankful for the leadership qualities and relentless drive for success and achievement you have instilled in me. To my darling husband, I am forever grateful and thankful for your wisdom, sympathetic ear, love, and friendship. Your genuinely happy disposition brings so much joy to this world and I am forever grateful to share our time here together.

TABLE OF CONTENTS

LIST OF TABLES

LIST OF FIGURES

# CHAPTER 1: THE HARTLEY GUINEA PIG MODEL OF IDIOPATHIC OSTEOARTHRITIS

## 1.1: Overview

Idiopathic osteoarthritis (OA) is a degenerative joint disease that is a leading cause of disability in adults. The underlying pathogenesis is multifactorial and largely undetermined, with a variety of cellular pathways and risk factors contributing to disease onset and progression. Laboratory animal models, both genetically engineered and spontaneous mutants, are employed to better understand the pathophysiology of disease and to develop safe and effective therapeutics to halt disease progression. The Hartley Guinea pig is emerging as a unique laboratory animal model of spontaneous idiopathic musculoskeletal aging, or musculoskeletal "inflammaging". This OA-prone guinea pig model develops naturally occurring idiopathic OA with pathology that mimics human disease. Further, their inflammaging phenotype is characterized by patterns of local and systemic inflammation that are associated with knee joint degeneration. This overarching goal of this chapter is to: (1) characterize structural, molecular, and clinical manifestations of idiopathic OA in aging male and female Hartley guinea pigs and, (2) identify molecular pathways for therapeutic target. Further, this work highlights sex as a key biological variable in the etiopathogenesis of OA. In summary, this chapter provides preliminary data which shaped my global hypothesis and provides rationale for the investigation of the utility of a novel phytochemical and Nrf2-activator in mitigating OA onset (Chapter 2) and/or progression (Chapter 3) in the Hartley Guinea pig.

## 1.2: Introduction

Osteoarthritis (OA) is a degenerative joint disease that is the most common cause of disability in older adults, affecting up to 30 million people, and 30-50% of some demographics[1–3]. There are three major subsets of OA: (1) primary or idiopathic, (2) secondary or post-traumatic OA (PTOA), and (3) rheumatoid or inflammatory. Primary osteoarthritis is unique in that is it is relatively spontaneous with no underlying traumatic injury or hypersensitivity reaction driving local or systemic pathology. The pathogenesis of primary OA is complex, multifactorial, and largely undetermined with a variety of susceptibility genes and

molecular pathways involved in disease onset and progression. A major limitation in managing OA is the lack of therapeutics that can slow the onset and/or progression of clinical and/or structural manifestations of disease. Interventions are focused on pain modification and when unsuccessful often result in immobility and depression [4]. Economic impacts of OA are vast. Arthritis-attributable lost wages are reportedly $164 billion which is equivalent to $4,040 less pay for an adult with arthritis compared to an non-arthritic adult, highlighting the economic impact this disease can have on individual families[5]. Further, treatment for patients with end-stage disease often results in invasive surgeries and complete joint replacement, which further contributes to overall arthritis-attributable medical costs and the large economic burden of this condition on the United States economy [5,6]. The World Health Organization estimates by the year 2050 the number of adults over the age of 60 will double, with the possibility of this demographic increasing from 605 million to 2 billion [7]. Our aging population combined with a relative lack of available therapeutics highlights a critical need to study this disease and discover novel therapeutic targets to delay the onset and halt the progression of joint degeneration and associated functional decline.

### 1.2.1: Animals Models of Idiopathic Osteoarthritis

Given the idiopathic nature of disease, few small laboratory animal models of spontaneous primary OA are available. Spontaneous models of primary OA can be broadly classified into two categories: (1) genetically engineered and (2) naturally occurring models [8]. Genetically engineered mutant mouse models manipulate structural or non-structural cartilage constituents by means of transgenic or knockout mutation and are commonly employed to study the effects of a specific gene of interest on cartilage integrity. Similar to other genetically engineered mutant mice these models have inherent limitations; more specifically, they are constrained by their translatability, as naturally occurring OA is largely accepted as a heterogenous polygenic degenerative disease with a variety of susceptibility genes contributing to disease onset and progression [9]. Regardless of these limitations, genetically engineered models significantly contribute to our understanding of OA pathogenesis and are instrumental in drug development through phenotypic rescue experimentation.

Naturally occurring models of spontaneous osteoarthritis are valuable as their susceptibility genes are uncertain and likely polygenic, more closely mimicking the human condition. Fewer models of naturally occurring disease in small laboratory animals are available and are limited to aging C57BL/6 mice, BALB/c mice, STR/ort mice, and Hartley guinea pigs.

Spontaneous osteoarthritis is described in aging C57BL/6 and Balb/c mice [10–13]. In both strains, age related cartilage degeneration first develops around 1 year. In C57BL/6 mice OA lesion distribution is somewhat conflicting as some groups describe pathology most severely manifesting in the medial compartment [10,11], while others have demonstrated more severe changes in the lateral compartment [12,14]. In BALB/c mice the most severe region of joint degeneration is along the patellar femoral groove with minor lesions documented in both the medial and lateral compartments [12,14]. STR/Ort mice were derived from an extensive breeding program which utilized tandem selection in CBA mice to investigate carcinogen resistance [15]. Spontaneous mutations resulted in a piebald mutation disrupting monoamine oxidase and catecholamine activity and metabolism and animals develop early onset obesity and spontaneous OA [16]. In this strain OA onset is initiated around 20-weeks and cartilage degeneration in males is more severe than females [17]. These mice are a unique model in that they may better characterize asymptomatic spontaneous knee OA; clinical manifestations of disease are thought to be derived from structural changes within the joint rather than a manifestation of pain [18]. This was demonstrated by an absence of gait modification when animals with end-stage disease were administered non-steroidal anti-inflammatory drugs (NSAIDs) or opioid antagonists and thus, investigators concluded this model has utility in more directly measuring manifestations of structural joint degeneration without the complicating factor of pain [18]. However, the SR/ort mouse has its limitations as they develop spontaneous hepatomas, obstructive urinary tract disorders, and have polymorphisms in the sacral segments which creates variations in the pelvic girdle which my lead to kinematic alterations in the hindlimb extremities and confound interpretations of mobility assessments [19]. Collectively, all mouse models are somewhat limited by their small tissue samples, challenging assessments of skeletal maturity, and limited tool repertoire available to longitudinally assess disease progression.

#### 1.2.1.1: Hartley Guinea Pig as an Underutilized Strain and Model of Symptomatic Knee OA

The outbred Dunkin Hartley Guinea pig serves as a unique but underutilized preclinical laboratory animal model of spontaneous idiopathic musculoskeletal aging. There are both potential mechanistic and translational strengths of this strain in musculoskeletal research as it holds potential as a useful preclinical model that may encompass systemic idiopathic musculoskeletal decline in cartilage, bone, and muscle similar to humans. Of interest, skeletal maturity occurs around 3-4 months of age [20], and degenerative pathologies are described in both skeletal muscle myofibers [21] and articular cartilage [22] by 15-months. More specifically, this strain develops disease onset between 3-5 months of age in at least one joint, and by 8-12 months the disease is bilateral and end-stage [22,23]. Both humans and the Hartley guinea pig develop more severe disease on the medial weight bearing aspect of the joint. By one year of age Hartley's tend to have marked degeneration and loss of medial tibial articular cartilage with subsequent subchondral bone sclerosis [22,23]. Standardized scoring systems have been developed to assess quantitative changes within the knee joint both histologically [22] and using microcomputed tomography (uCT) [24,25]. Recently, a uCT scoring system was developed that characterizes clinically relevant structural changes in aging Hartley guinea pigs with knee joint OA which serves as a useful noninvasive tool to monitor the longitudinal effects of disease progression [24].

Compared to large animals, guinea pigs are relatively affordable to obtain and house, rapidly grow and mature, are easy to handle, and provide large tissue samples for multidisciplinary analyses. Similar to humans, guinea pigs have a nutritional requirement for Vitamin C in collagen synthesis. In contrast to the SRT/ort mouse, the Hartley guinea pigs may more accurately model clinically relevant symptomatic knee OA as gait analysis, specifically stride length, is modifiable by administration of NSAIDs [26]. This may measure the effects of both pain and functional mobility and serve as a noninvasive clinically relevant alternative tool (to structural modification as endpoints) to monitor disease progression longitudinally and validate biomarkers against [27].

As with all animal models of disease, there are inherent limitations. It is recognized that these animals differ from the general human population in that (1) they are quadrupeds, (2) they may have open growth

plates during initial OA onset, (3) occasionally have ossifying menisci and infrapatellar fat pads, and (4) are albino. Considering Hartley guinea pigs as quadrupeds, one may hypothesize they would not develop severe knee OA as, compared to bipeds, their weight is distributed more evenly across 4 rather than 2 joints. Further, one may suspect that they would develop more severe OA in their shoulder or elbow as quadrupeds distribute 63% of their body weight on their forelimbs [28]. Despite these intuitions, Hartley guinea pigs develop severe knee joint OA in the absence of forelimb disease which suggests that effects of local inflammation and tissue damage supersedes the influence of weight gain or bearing on disease progression. Another potential concern of the Hartley guinea pig is that OA onset can precede growth plate closure, a feature that is not typically characteristic of adult human disease but has been seen with obese adolescents. To address this limitation, our group records femur and tibia lengths bi-weekly and can estimate a time frame when growth plate closure occurs. This unique feature is of interest, however, as early-onset OA is becoming more prevalent in obese young adults. It has been argued that, in a subset of Hartley guinea pigs, as well as in mice, the menisci and infrapatellar fat pads of aging animals ossify and may contribute to joint instability [29]. The degree and location of intraarticular mineralization can be evaluated longitudinally using uCT and at the study endpoint via uCT and histopathology. Lastly, albinism in people is an inherited disorder of defective melanin production that is primary characterized by an oculocutaneous syndrome. To date, no studies have linked albinism in people to primary osteoarthritis. Future directions in this vein include investigating signaling pathways that modulate melanin gene products to determine how dysregulation may disrupt redox homeostasis and further contribute to primary OA in this model. Finally, as with all lab animal models, drug efficacy and safety in the laboratory does not directly translate to larger animals or humans. Smaller models may be favored in early proof of concept investigations and early drug screening studies while larger animals may be used to verify these findings before human clinical trials are implemented [30]. Currently the Hartley guinea pig serves as the most affordable, best described, arguably the best translational animal model for studying idiopathic osteoarthritis in a preclinical laboratory setting.

### 1.2.1.2: Anatomy and Histopathology of the Guinea Pig Knee Joint

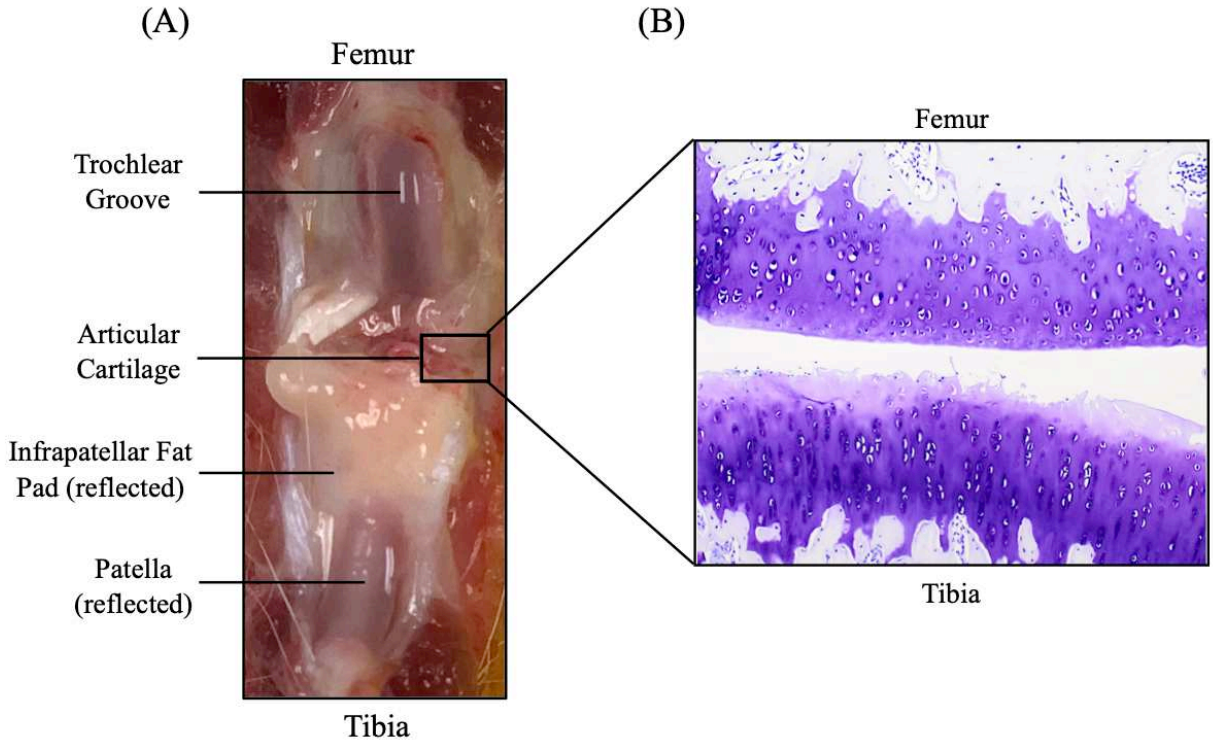


**Figure 1.1. Articular Cartilage.** (**A**) Gross image of a guinea pig knee joint displaying the tibiofemoral articulation and its intimate association with the infrapatellar fat pad. (**B**) Histologically articular cartilage is an avascular, alymphatic, and aneural paucicellular tissue composed of chondrocytes organized into three zones (superficial, middle, and deep) all supported by a collagen and proteoglycan rich extracellular matrix. A variably distinct tidemark delineates the deep cartilage zone from the calcified cartilage. Underneath the calcified cartilage is subchondral bone. Toluidine blue, 40x.

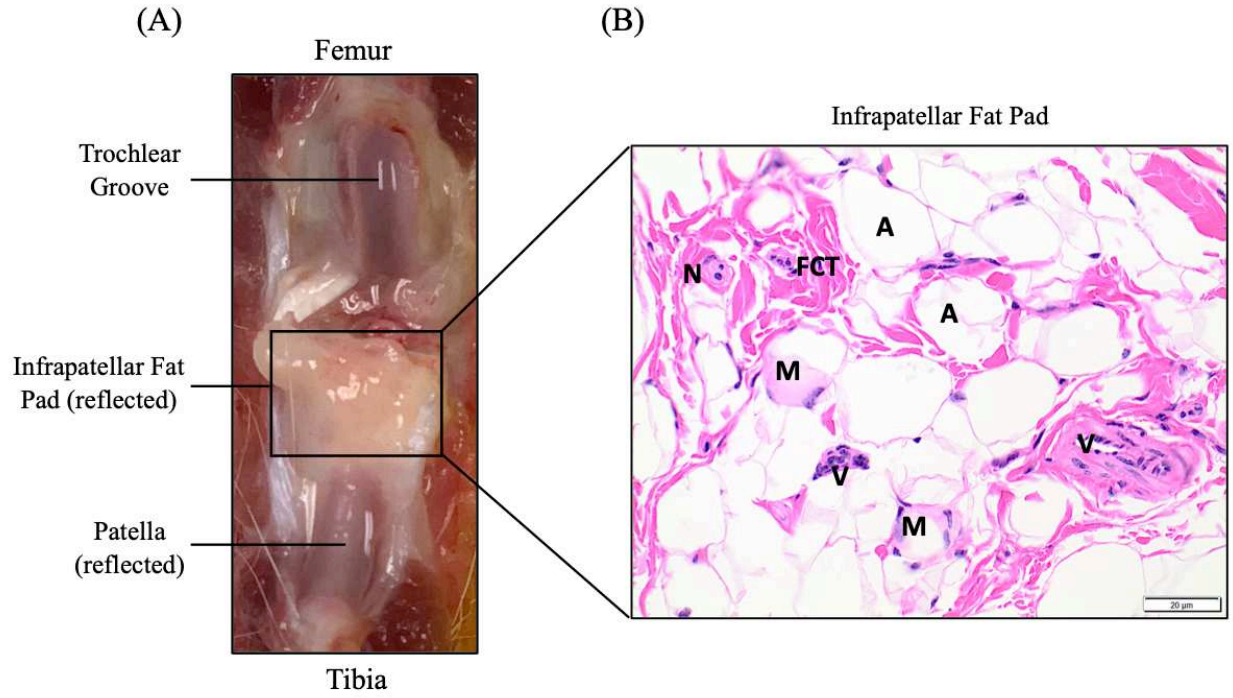


**Figure 1.2. The Infrapatellar Fat Pad.** (**A**) Gross image of a guinea pig knee joint displaying the infrapatellar fat pad (reflected), a relatively large intracapsular extrasynovial white fat depot intimately associated with the knee joint cavity just distal to the patella. (**B**) The infrapatellar fat pad contains well differentiated adipocytes (A), macrophages (M), vessels (V), nerves (N), and fibrous connective tissue (FCT). H&E, 40x, bar 20um.

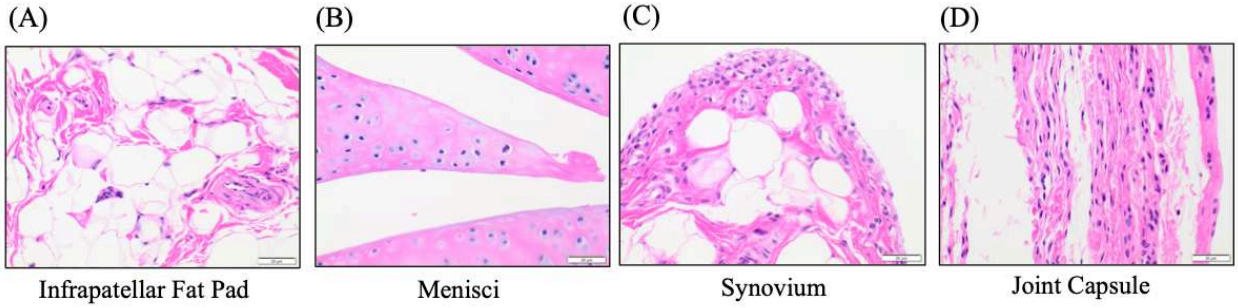


**Figure 1.3. Intracapsular Knee Joint Tissues**. Intracapsular knee joint tissues contributing to the local environmental milieu include the: (**A**) infrapatellar fat pad, (**B**) menisci, (**C**) synovial membranes, (**D**) fibrous joint capsule, and articular cartilage. H&E, 40x, bar 20um.

Osteoarthritis is considered “a disease of the joint as an organ” – the anatomy and interplay between articular cartilage and nearby tissues are integral in disease progression [31]. Typical pathologic features of OA include: (1) narrowing of the joint space, (2) degeneration of menisci and ligaments, (3) synovial hypertrophy and hyperplasia, (4) joint effusion, (5) expansion of the joint capsule, (6) eburnation and thickening of subchondral bone, and (7) osteophyte formation. Nearby structures, such as the infrapatellar fat pad, menisci, synovial membranes, and joint capsule all contribute to maintenance of synovial fluid and the local microenvironmental milieu. Disruption or induction of these structures can stimulate cascades that perpetuate inflammatory and protease activity locally within the joint and serve as independent and collaborative drivers in OA pathology.

### 1.2.2: Pathogenesis of Idiopathic Knee Osteoarthritis

The pathogenesis of primary idiopathic knee OA is complex multifactorial and largely undetermined with a variety of local tissues and mediators driving disease progression. In a healthy joint there is a somewhat balance of anabolic and catabolic enzymes which keeps the joint in a relatively homeostatic state. In an arthritic degenerative joint, there is increased expression of catabolic enzymes which cleave extracellular matrix components, particularly collagens and proteoglycans, causing joint degeneration.

Type II collagen (COL2A1) serves as the main scaffold for major ECM proteoglycans and other non-glycosylated ECM proteins. Indeed, degeneration of the COL2A1 backbone is recognized as a defining feature of OA in animals and humans [12,32,33]. Aggrecan, a proteoglycan and another essential structural component of the ECM, protects articular cartilage from compression forces [34]. In Hartley guinea pigs, matrix metalloproteinases (MMPs) with collagenase activity are activated as early as 2 months of age prior to the onset of OA and phenotypic changes consisted with collagen fiber and aggrecan denaturation manifest in the early stages of disease. Potential sources of metalloproteinases and similar mediators driving joint degeneration include chondrocytes as well as nearby structures within the joint, including the infrapatellar fat pad (IFP), menisci, synovium, and joint capsule. Traditionally, principle upstream mediators driving transcriptional upregulation of MMPs include IL1β [35–37], TNFα [38], and IL-6 [39].

Obesity and aging, as well as inflammation and stress associated with both of these conditions, perpetuate and independently drive local and systemic mediators of OA and exacerbate degenerative joint disease and joint instability. Histologically articular cartilage degeneration manifests most severely along the medial tibial plateau, the most significant weight bearing aspect of the knee joint. As hyaline cartilage is naturally of low cellularity with limited renewal capacity, healing often occurs through fibrocartilage replacement which is primarily composed of type I collagen, and thus lacks the unique functional tensile and compressive characteristics of type II collagens and aggrecan characteristic of hyaline cartilage [40].

Osteoarthritis along with many other age-associated pathologies is recognized as a sexually dimorphic disease [41–45]. However, historically research designs in laboratory animals employed non-breeder males only despite that women represent a disproportionate number of patients with severe OA [46]. It was not until 2015 that the NIH released a notice (NOT-OD-15-102) that accounted for sex a biological variable and that it be factored into research designs, analyses, and reporting. Thus, it is only somewhat recently that the field has committed efforts towards increasing our understand and improving health outcomes specifically for women.

In this study we sought to characterize age- and sex-associated changes in articular cartilage and knee joint tissues at the histologic, mRNA, protein, and clinical level to better characterize innate mechanisms driving joint degeneration and immobility in aging male and female Hartley guinea pigs. Long term, the goal of this work is to further develop biomarkers through all stages of disease and drug development including how we define and characterize OA disease burden, investigation, prognosis, intervention efficacy, and diagnosis (BIPED) [27].

## 1.3: Materials and Methods

### 1.3.1: Animals and Study Design

All Hartley guinea pigs (n=56) were procured from Charles River Laboratories (Wilmington, MA). Male (n=14) and female (n=14) Hartley guinea pigs (total n=28) aged 1.5 months were aged for 3.5 months at

Colorado State University and sacrificed at 5-months-old. Male (n=14) and female (n=14) Hartley guinea pigs (total n=28) aged 4.5 months were aged for 10.5 months at Colorado State University and sacrificed at 15-months-old. Procedures were approved by the university's Institutional Animal Care and Use Committee (19-9129A) and were performed in accordance with the NIH Guide for the Care and Use of Laboratory Animals. Animals were maintained at Colorado State University's Laboratory Animal Resources housing facilities and were monitored daily by a veterinarian. Guinea pigs were singly housed in solid bottom cages and provided *ad libitum* access to water and regular chow diet. Hay cubes were withheld.

### 1.3.2: ANY-maze™ Open Field Enclosure Monitoring

Animals were acclimated over a 2-week period, before the onset of the study, to an open circular field behavior monitoring system (ANY-maze™, Wood Dale, IL) to assess voluntary physical activity. Animals' activities were recorded, and data were collected for 10 consecutive minutes on a monthly basis throughout the study. Videos were analyzed for the following parameters: total distance traveled (m), average speed (m/s), time mobile (s), % time mobile, time in hut (s), % time in hut, and average moving speed (m/s).

### 1.3.3: Harvests and Tissue Collection

Body weights were recorded immediately before harvest. Animals were anesthetized with a mixture of isoflurane and oxygen and transferred to a carbon dioxide chamber for euthanasia. Complete necropsy was performed by a veterinary pathologist to rule out co-morbidities. The right hind limb was disarticulated at the coxofemoral joint. Upon arthrotomy, the articular surfaces of the knee were: (1) flushed with 500 µl PBS, (2) patellar, patella-femoral groove, femoral condylar, and tibial plateau surfaces, along with the menisci, were scraped and pooled cartilage flakes stored in RNALater, and (3) the infrapatellar fat pad removed and stored in Allprotect Tissue Reagent. All tissues were stored at -80°C until further processing. The left hind limb was removed, left intact, stored *in situ* in 10% neutral buffered formalin for 48 hours and transferred to PBS.

### 1.3.4: Histology and OARSI Histopathology Grading

The left hindlimbs were decalcified over 6-weeks in $Ca^{2+}$EDTA. Limbs were trimmed in the medial sagittal plane, embedded in cassettes, processed, and 5uM paraffin sections were mounted onto charged slides. Slides were stained with hematoxylin and eosin (H&E) and toluidine blue for histopathologic examination and OARSI grading, respectively. Medial tibial plateaus were examined and graded based on established grading schemes provided by *Kraus et al.*[22]. Knee joints were scored by a veterinary pathologist in duplicate as well as in random order, blinded to sex- and age-group.

### 1.3.5: Articular Cartilage and Infrapatellar Fat Pad Gene Expression

A custom NanoString nCounter 100-code gene panel for targeted mRNA analysis was utilized. Total mRNA, from pooled articular cartilage or the infrapatellar fat pad of the right knee joint, was extracted using TRIzol reagent and Qiagen RNeasy and RNeasy Lipid Mini Kits according to the manufacturer's instructions. Samples were analyzed in collaboration with Nanostring Technologies at the University of Arizona Genetics Core. Eukaryotic elongation factor 1 alpha (EFF1a) was used as a housekeeper gene for normalization.

### 1.3.6: Immunohistochemistry (IHC)

To semi-quantitatively assess selected gene expression outcomes at the functional protein level, IHC was implemented using antibodies against Nrf2 (ThermoFisher Scientific, PA-38312, rabbit polyclonal, dilution of 1:100) and NAD(P)H dehydrogenase (quinone-1) detoxification enzyme (NQ01, Abcam ab34173, rabbit polyclonal, dilution of 1:400). Heat-induced epitope retrieval was performed on a Leica Bond-RX automated stainer using BOND Epitope Retrieval Solution 1 (citrate buffer) for 420 minutes at 55°C. Blocking was performed using 3% peroxide followed by 2.5% donkey serum. Labeling was performed on an automated staining platform. DAB was used as the chromogen and immunoreactions were visualized using commercial detection systems. Slides were counterstained with hematoxylin. Sequential steps of the immunostaining procedure were performed on negative controls following incubation. Photomicrographs

from the medial tibial plateau were semi-quantitatively analyzed by measuring the mean immuno-positive surface area using VisioPharm® software (Westminster, CO).

### 1.3.7: Statistics

Two-way ANOVA was utilized to evaluate the effects of age (5 vs 15 months) and sex (male vs female) on various outcome measures. Bonferroni's method was performed *post-hoc* for multiple comparison testing between groups. On all graphs, two-way ANOVA results and associated p-values are listed below the X-axis; significance was defined as a p-value $<0.05$ and a trend was defined $0.05<p<0.15$. Bonferroni's multiple comparison results are depicted on the graphs; significant differences are depicted using brackets and asterisk above the data points *(*$0.01<p<0.05$; ** $0.001<p<0.01$ ; *** $0.0001<p<0.001$; **** $p<0.0001$)*; trends (*$0.05<p<0.15$)* are depicted below data points with brackets and p-values. All analyses were performed using GraphPad Prism Version 9.0 (San Diego, CA, USA).

## 1.4: Results

### 1.4.1: Histopathology - Toluidine Blue Staining and OARSI Grading

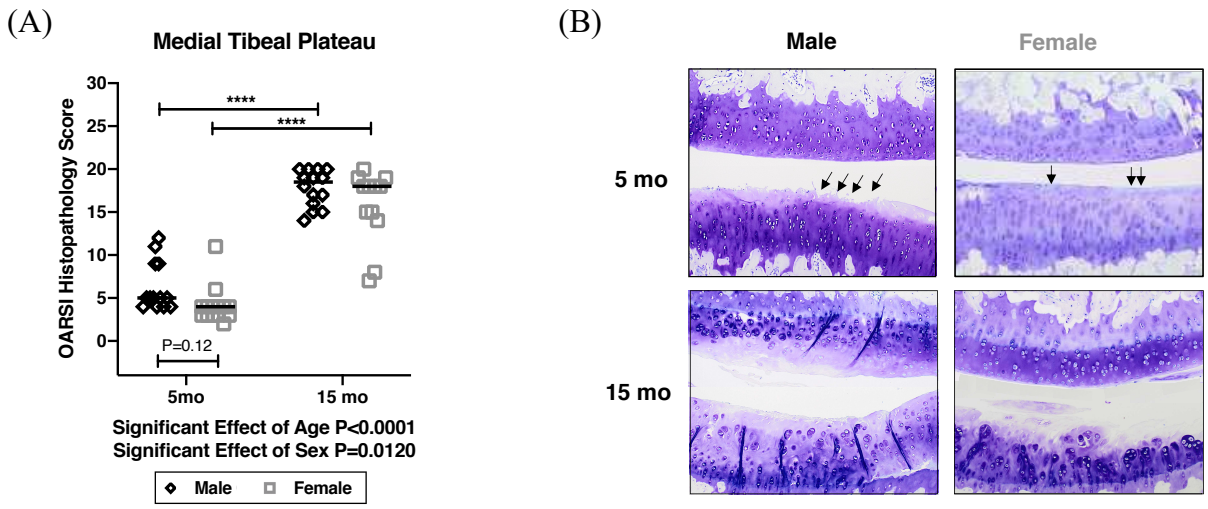


**Figure 1.4. Osteoarthritis of the medial tibial plateau in aging Hartley guinea pigs.**
(**A**) Medial tibial plateau (MTP) median OARSI histopathology scores for OA in 5-month and 15-month-old male (black diamonds) and female (grey squares) Hartley guinea pigs. (**B**) Representative medial tibial plateau toluidine blue photomicrographs from 5-month (top row) and 15-month (bottom row) male (left column) and female (right column) Hartley guinea pigs. Femoral condyles and tibial plateaus are on the top and bottom of each image, respectively. **** *p<0.0001,* mo=months

As anticipated, medial tibial plateau histologic OA scores were significantly (**Figure 1.4A, p<0.0001**) higher in 15-month compared to 5-month-old animals. Females had significantly (**Figure 1.4A, p=0.0120**) lower OA scores compared to males. Representative photomicrographs demonstrate mild degenerative OA changes representing the onset of disease in 5-month-old animals; characteristic lesions include loss of proteoglycan and chondrocytes as well as fibrillation and fissuring (black arrows) in the superficial zone. Severe degenerative changes representing end-stage disease are depicted in 15-month-old animals; characteristic lesions include: loss of proteoglycan and chondrocytes in all three zones of cartilage, presence of hypertrophied chondrocytes and large multicellular chondrones, and fibrillations and clefts extending along the tidemark in between the deep zone and calcified cartilage layer.

### 1.4.2: Nanostring Targeted mRNA Analysis – Cartilage

#### 1.4.2.1: Articular Cartilage Structure

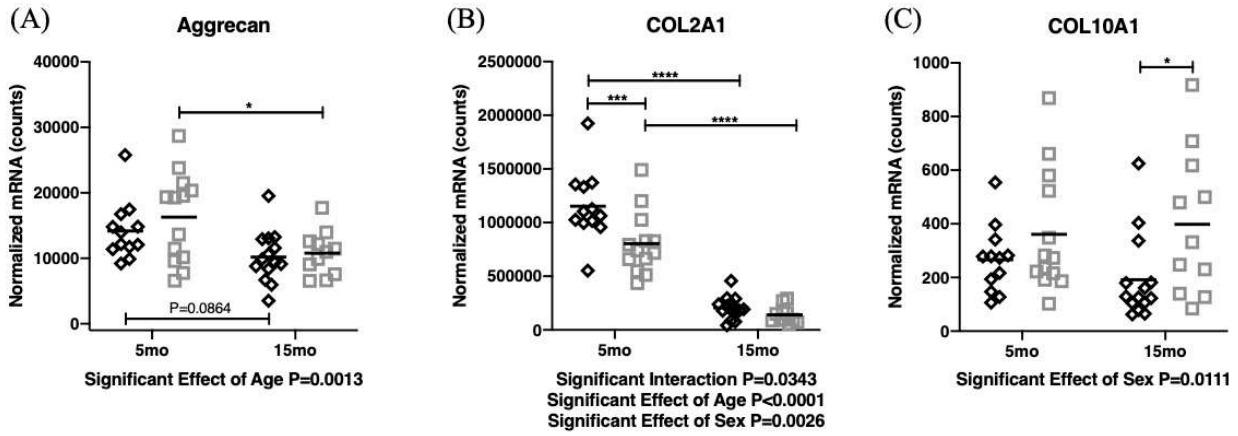


**Figure 1.5. Normalized mRNA counts for select structural extracellular matrix constituents expressed in aging Hartley guinea pig knee joint articular cartilage**. Articular cartilage mean mRNA expression levels of (**A**) aggrecan, (**B**) collagen type II alpha I chain (COL2A1), and (**C**) collagen type X alpha I chain (COL10A1) in 5-month and 15-month-old male and female guinea pigs.
**0.01<p<0.05; ** 0.001<p<0.01 ; *** 0.0001<p<0.001; **** p<0.0001,* mo=months

As expected, with age there is a significant decline in the expression of the major articular cartilage constituents aggrecan (**Figure 1.5A, p=0.0013**) and COL2A1 (**Figure 1.5B, p<0.0001**). Females have significantly lower mRNA levels of COL2A1 (**Figure 1.5B, p<0.0026**) compared to males. COL10A1, a minor collagen and less abundant component of the ECM, is expressed significantly higher in females (**Figure 1.5C, p=0.0111**) compared to males.

### 1.4.2.2: Articular Cartilage Oxidant Sensing (Nrf2-ARE)

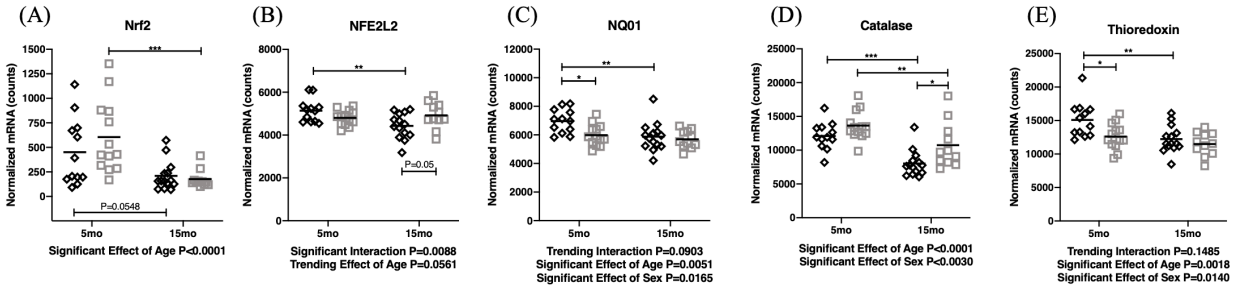


**Figure 1.6. Normalized mRNA counts for select stress sensing transcription factors and antioxidants expressed in aging Hartley guinea pig knee joint articular cartilage**. Articular cartilage mean mRNA expression levels of (**A**) nuclear factor erythroid 2 related factor 2 (Nrf2) oxidant sensing transcription factor, (**B**) nuclear factor erythroid 2 like 2 (NFE2L2) oxidant sensing transcription factor variant, (**C**) NAD(P)H dehydrogenase (quinone-1) (NQ01) detoxification enzyme, (**D**) catalase antioxidant, and (**E**) thioredoxin antioxidant in 5-month and 15-month-old male and female guinea pigs. **0.01<p<0.05; ** 0.001<p<0.01 ; *** 0.0001<p<0.001; **** p<0.0001,* mo=months

Of interest, with age there is a decline in the expression of the oxidant/stress-sensing transcription factor Nrf2 and NFE2L2 (**Figure 1.6A-B, p=0<0.0001 and p=0.0581**) and a significant decline in nuclear factor erythroid-2 related factor-2 antioxidant-response-element (Nrf2-ARE) regulated antioxidants NQ01 (**Figure 1.6C, p=0.0051**), catalase (**Figure 1.6D, p<0.0001**), and thioredoxin (**Figure 1.6E, p=0.0018**). Compared to males, females have significantly decreased expression levels of NQ01 (**Figure 1.6C, p=0.0165**) and thioredoxin (**Figure 1.6E, p=0.0140**) and significantly higher expression levels of catalase (**Figure 1.6D, p=0.0030**).

### 1.4.2.3: Articular Cartilage Iron-Regulator and Trafficking Proteins

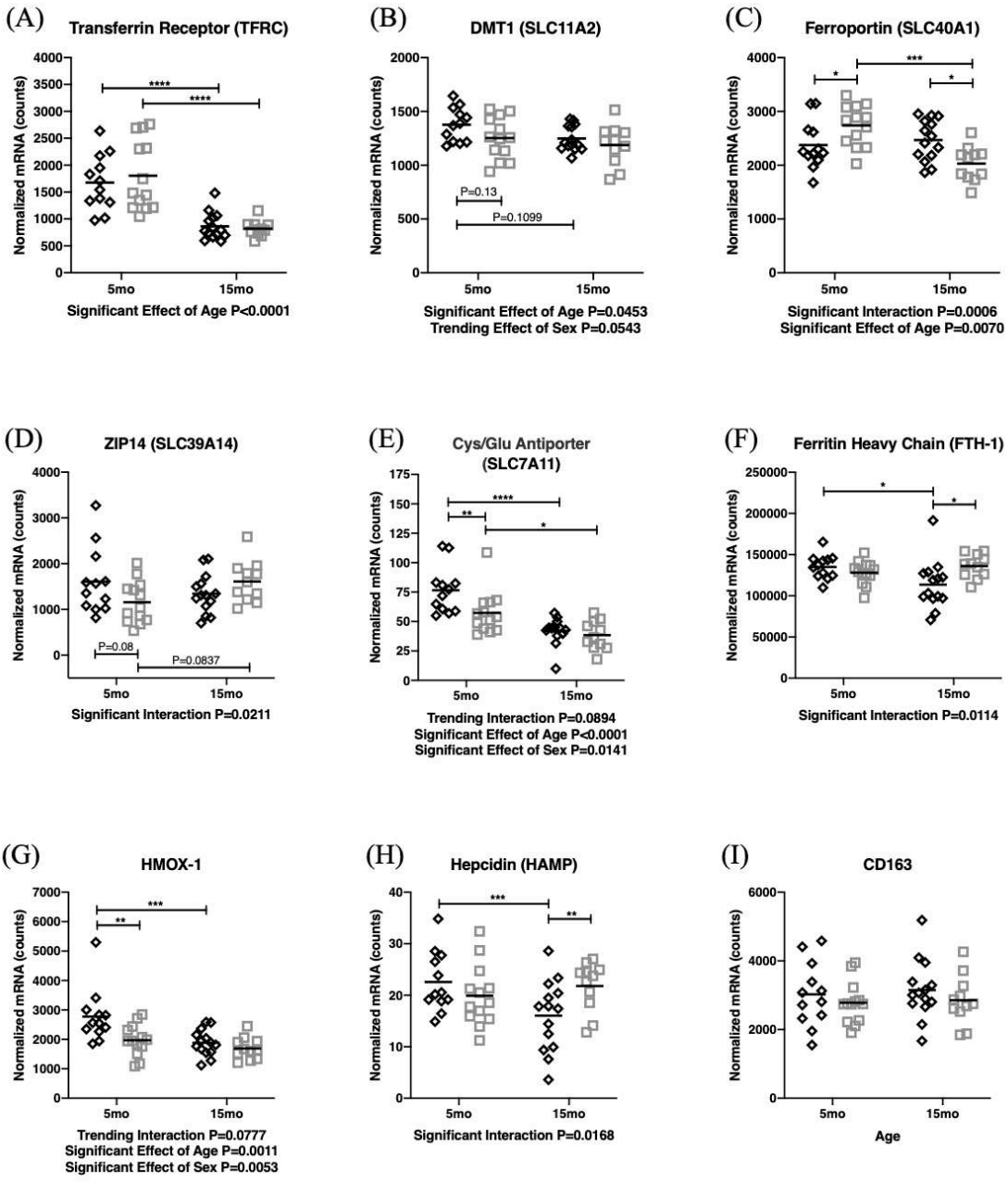


**Figure 1.7. Normalized mRNA counts for select iron-regulator and trafficking proteins expressed in aging Hartley guinea pig knee joint articular cartilage**. Articular cartilage mean mRNA expression levels of the (**A**) transferrin receptor (TFRC), (**B**) DMT1 iron transporter (SLC11A2), (**C**) ferroportin iron exporter (SLC40A1), (**D**) ZIP14 iron transporter (SLC39A14), (**E**) cystine/glutamate antiporter (SLC7A11, preserver of redox balance via glutathione regulation), (**F**) ferritin heavy chain (FTH-1), (**G**) heme oxygenase-1 antioxidant (HMOX-1), (**H**) hepcidin (HAMP), and (**I**) the macrophage hemoglobin/haptoglobin scavenger receptor (CD163), in 5-month and 15-month-old male and female guinea pigs. **0.01<p<0.05; ** 0.001<p<0.01 ; *** 0.0001<p<0.001; **** p<0.0001,* mo=months

Of note, 15-month-old Hartley guinea pigs have decreased expression of the transferrin receptor (**Figure 1.7A, p<0.0001**), DMT1 iron transporter (**Figure 1.7B, p=0.0453**), ferroportin (**Figure 1.7C, p=0.0070**), cystine/glutamate antiporter (**Figure 1.7E, p<0.0001**), and heme oxygenase-1 antioxidant (**Figure 1.7G, p=0.0011**). Compared to males, females have decreased expression levels of the cystine/glutamate antiporter (**Figure 1.7E, p=0.0141**), and heme oxygenase-1 antioxidant (**Figure 1.7G, p=0.0053**). There is a significant sex-age interaction on the expression of ferroportin (**Figure 1.7C, p=0.0006**), ZIP14 iron transporter (**Figure 1.7D, p=0.0211**), ferritin heavy chain (**Figure 1.7F, p=0.0114**), and hepcidin (**Figure 1.7H, p=0.0168**).

### 1.4.3: Nanostring Targeted mRNA analysis - Infrapatellar Fat Pad

#### 1.4.3.1: Infrapatellar Fat Pad Adipokine Expression

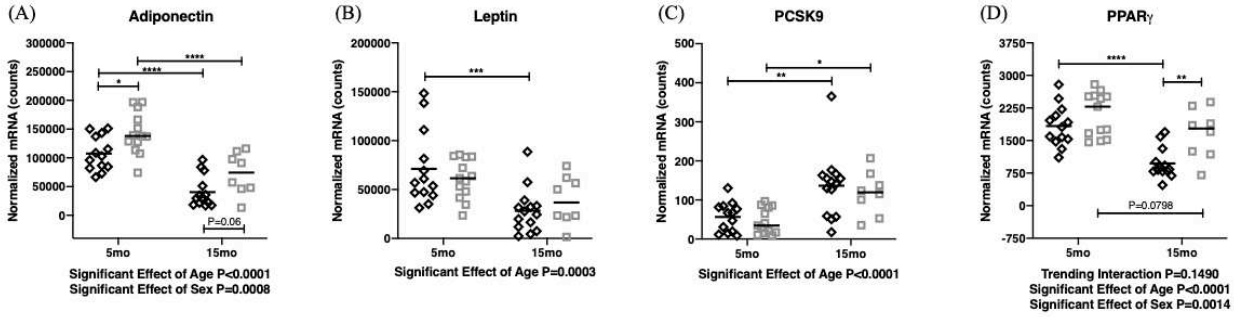


**Figure 1.8. Normalized mRNA counts for select adipokines expressed in aging Hartley guinea pig infrapatellar fat pads.** Infrapatellar fat pad mean mRNA expression levels of (**A**) adiponectin, (**B**) leptin, (**C**) proprotein convertase subtilisin/kexin Type 9 (PCSK9), and (**D**) peroxisome proliferator activated receptor gamma (PPARγ) in 5-month and 15-month-old male and female guinea pigs. **0.01<p<0.05; ** 0.001<p<0.01 ; *** 0.0001<p<0.001; **** p<0.0001,* mo=months

As expected, relatively high expression levels of adiponectin and leptin confirms the adipose nature of the IFP. Fifteen-month-old Hartley guinea pigs have significantly decreased levels of adiponectin (**Figure 1.8A, p<0.0001**), leptin (**Figure 1.8B, p=0.0003**), and PPARγ (**Figure 1.8D, p<0.0001**), and increased levels of PCSK9 (**Figure 1.8C, p<0.0001**). Compared to males, females have significantly higher expression of adiponectin (**Figure 1.8A, p=0.0008**) and PPARγ (**Figure 1.8D, p=0.0014**).

### 1.4.3.2: Infrapatellar Fat Pad Metalloproteinases, Protease Inhibitors, and Mediators of OA

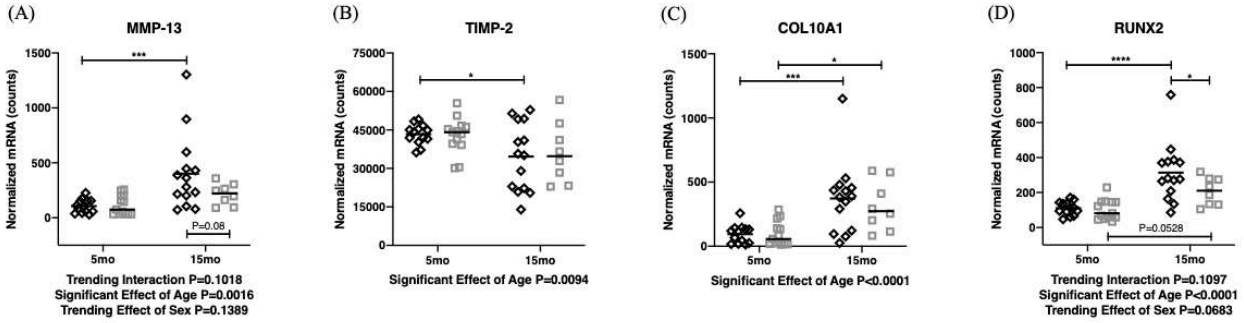


**Figure 1.9. Normalized mRNA counts for select matrix metalloproteinases, protease inhibitors, and mediators of OA expressed in aging Hartley guinea pig infrapatellar fat pads.** Infrapatellar fat pad mean mRNA expression levels of (**A**) matrix metalloproteinase-13/collagenase-3 (MMP-13), (**B**) tissue inhibitor of matrix metalloproteinase-2 (TIMP-2), (**C**) collagen type X alpha I chain (COL10A1), and (**D**) runt-related transcription factor 2 (RUNX2) in 5-month and 15-month-old male and female guinea pigs. **0.01<p<0.05; ** 0.001<p<0.01 ; *** 0.0001<p<0.001; **** p<0.0001,* mo=months

As anticipated, 15-month-old guinea pigs have significantly higher mRNA expression levels of MMP-13 (**Figure 1.9A, p=0.0016**), COL10A1 (**Figure 1.9C, p<0.0001**), and RUNX2 (**Figure 1.9D, p<0.0001**) and significantly decreased expression levels of TIMP2 (**Figure 1.9B, p=0.0094**), compared to 5-month-old animals.

### 1.4.3.3: Infrapatellar Fat Pad Pro-Inflammatory Mediators and Alarmins

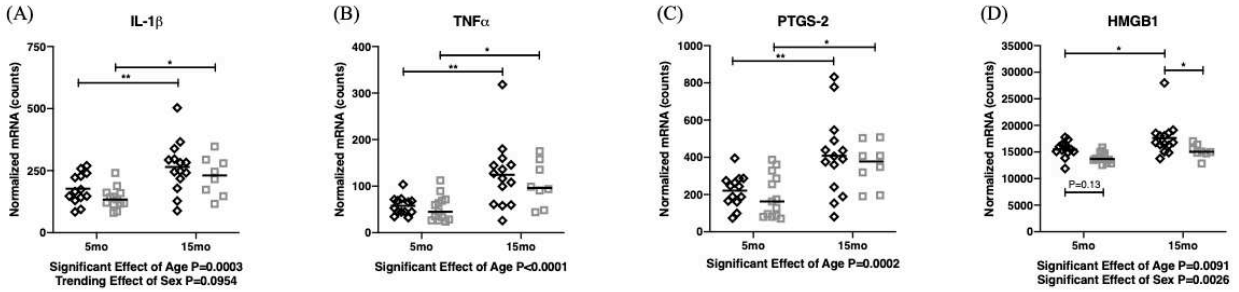


**Figure 1.10. Normalized mRNA counts for select pro-inflammatory cytokines and alarmins expressed in aging Hartley guinea pig infrapatellar fat pads.** Infrapatellar fat pad mean mRNA expression levels of (**A**) interleukin-1beta (IL-1β), (**B**) tumor necrosis factor-alpha (TNFα), (**C**) prostaglandin G/H synthase-2 (PTGS-2, inducible COX2), and (**D**) high mobility group box-1 (HMGB-1) in 5-month and 15-month-old male and female guinea pigs.
**0.01<p<0.05; ** 0.001<p<0.01 ; *** 0.0001<p<0.001; **** p<0.0001,* mo=months

As anticipated, 15-month-old guinea pigs have significantly higher mRNA expression levels of IL-1β (**Figure 1.10A, p=0.0003**), TNFα (**Figure 1.10B, p<0.0001**), PTGS-2 (**Figure 1.10C, p=0.0002**) and HMGB-1 (**Figure 1.10D, p=0.0091)**, compared to 5-month-old animals. Compared to males, females have significantly lower levels of HMGB-1 (**Figure 1.10D, p=0.0026**).

### 1.4.4: Immunohistochemistry and Advanced Imaging

#### 1.4.4.1: Nuclear factor erythroid-2-related factor-2 Immunohistochemistry

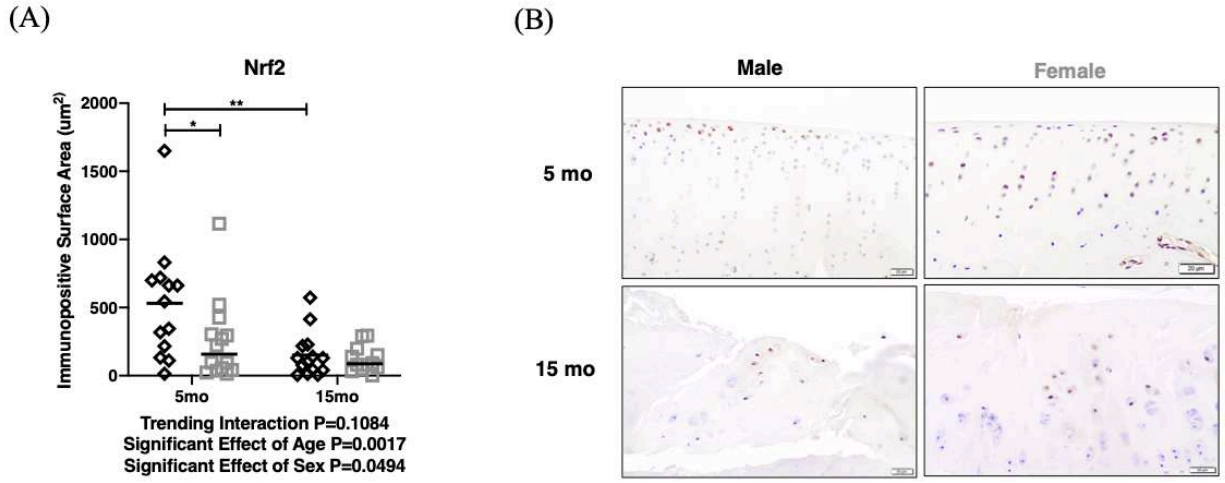


**Figure 1.11. Medial tibial plateau Nrf2 immunoexpression in aging Hartley guinea pigs.** (**A**) Nrf2 mean immunopositive surface area of the medial tibial plateau in 5-month and 15-month-old Hartley guinea pigs. (**B**) Representative Nrf2 immunohistochemistry photomicrographs of the medial tibial plateau from 5-month (top row) and 15-month (bottom row) male (left column) and female (right column) Hartley guinea pigs.
40x; bar=20um; **0.01<p<0.05; **0.001<p<0.01 ; *** 0.0001<p<0.001; **** p<0.0001,* mo=months

Of interest, 15-month-old animals have significantly decreased medial tibial plateau functional protein expression levels of the oxidant/stress-sensing transcription factor Nrf2 (**Figure 1.11A, p=0.0017**). Further, females have significantly decreased expression levels of Nrf2 (**Figure 1.11A, p=0.0494**) compared to males. Representative immunohistochemistry photomicrographs from 5-month-old animals (with mild degenerative OA changes) demonstrate mild to moderate chondrocyte nuclear immunolabeling in the superficial (5-month-old males) and middle (5-month-old females) zones. Photomicrographs from 15-month-old animals exhibit marked degenerative OA changes with loss of chondrocytes and degenerative matrix combined with diminished Nrf2-immunolabeling. There is mild to moderate nuclear labeling in intact chondrocytes.

### 1.4.4.2: NAD(P)H dehydrogenase (quinone 1) Immunohistochemistry

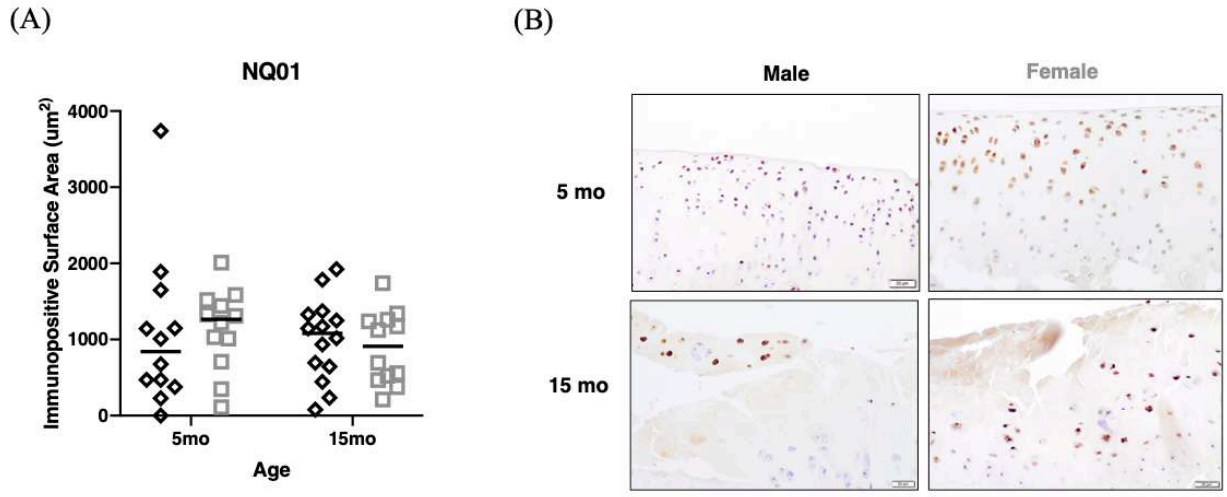


**Figure 1.12. Medial tibial plateau NQ01 immunoexpression in aging Hartley guinea pigs.** (**A**) NQ01 mean immunopositive surface area of the medial tibial plateau in 5-month and 15-month-old Hartley guinea pigs. (**B**) Representative NQ01 immunohistochemistry photomicrographs of the medial tibial plateau from 5-month (top row) and 15-month (bottom row) male (left column) and female (right column) Hartley guinea pigs.
40x; bar=20um; **0.01<p<0.05; **0.001<p<0.01 ; *** 0.0001<p<0.001; **** p<0.0001,* mo=months

There were no significant effects of age, sex, or age-sex interactions on medial tibial plateau NQ01 protein immunoexpression levels. Of note, 5-month-old animals exhibit moderate diffuse cytoplasmic immunolabeling throughout all three layers of cartilage (**Figure 1.12B)**. Fifteen-month-old animals with more advanced OA demonstrate enhanced immunolabeling in fewer chondrocytes, with increased expression surrounding regions of chondrocyte loss and matrix degradation (**Figure 1.12B)**.

### 1.4.5: Voluntary Mobility Determined by ANY-maze™ Open Field Enclosure Monitoring

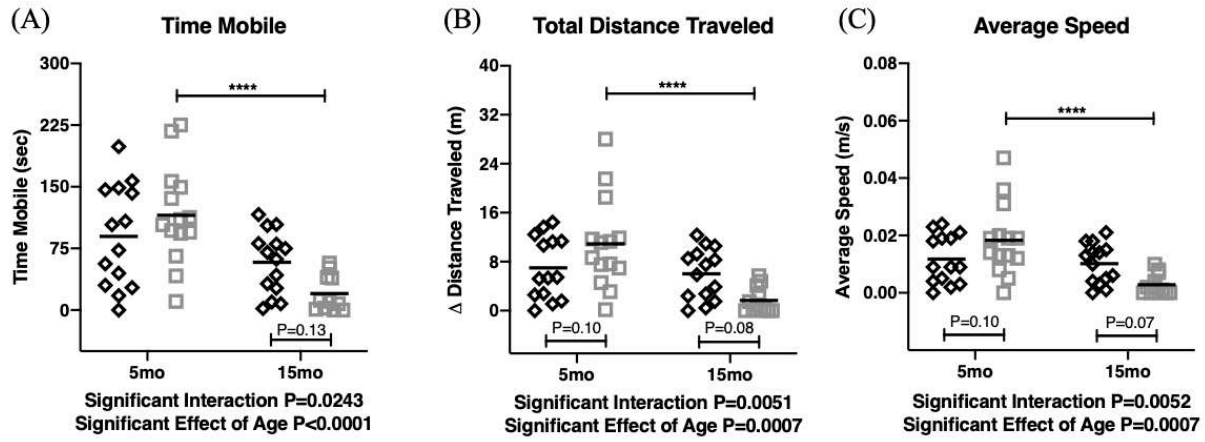


**Figure 1.13. ANY-maze™ open field monitoring in aging Hartley guinea pigs.** (**A**) Mean time mobile, (**B**) total distance traveled, and (**C**) average speed in 5-month- and 15-month-old Hartley guinea pigs exposed to an open field for 10-minutes.
**0.01<p<0.05; **0.001<p<0.01; *** 0.0001<p<0.001; **** p<0.0001,* mo=months

There were significant interactions and effects of age on time mobile (**Figure 1.13A**), total distance traveled (**Figure 1.13B**), and average speed (**Figure 1.13C**) when animals were exposed to an open field for ten minutes. Specifically, 15-month-old Hartley guinea pigs spent significantly less time mobile, traveled significantly shorted distances, at a lower average speed compared to 5-month-old animals (**Figure 1.13A. p<0.0001; Figure 1.13B. p=0.0007; Figure 1.13C. p=0.0007,** respectively).

## 1.5: Discussion

### 1.5.1: Articular Cartilage

This study characterized the *in-vivo* phenotypic, molecular, and clinical manifestations of guinea pig knee joint degeneration in an idiopathic model of spontaneous osteoarthritis. Both sexes were employed to investigate sex-specific markers of OA disease burden with age. As expected, 15-month-old animals exhibited severe degenerative joint disease and knee joint pathology that closely mimicked that described in humans, and as previously described in the Hartley guinea pig model of spontaneous OA [24,47]. Further,

noteworthy differences in whole knee joint OA scores and concurrent variations in articular cartilage and IFP gene expression profiles suggests sex-specificity in OA onset and progression in the model.

While aging is known as a significant risk factor in idiopathic OA, there are many other risk factors that contribute to both disease onset and progression, including genetics, obesity, and importantly, sex [48]. In this study we demonstrated significant sex differences in OA severity and concurrent differences in gene expression profiles in articular cartilage and the IFP between males and females, consistent with reports that describe OA as a sexual dimorphic disease [41–43,46,49]. These key sex differences in the molecular mechanism driving the initial onset of OA play a role in disease progression and may dictate how males and females respond differently to treatment strategies. Opposite to what is described in people, our study identified males as more at risk for advanced OA compared to females. However, the OARSI histopathology recommendations for histological assessments of osteoarthritis in the guinea pig are primarily based off studies in non-breeder males; modificaitons to this grading scheme may be necessary to more accurately characterize OA pathology in aging Hartley females. Of note, compared to age-matched males female Hartley guinea pig have thinner articular cartilage, more widespread surface replacement with fibrocartilage, and more severe subchondral bone sclerosis in end-state disease, all OA features that are not incorporated into the OARSI grading scheme and features which likely contributing to OA progression and clinical aspects of disease. Future work includes characterizing longitudinal phenotypic OA changes in females using both uCT and histopathology.

Aggrecan and type II collagen serve as the two main cartilage constituents that are responsible for structural, compressive, and tensile strength of hyaline cartilage. As anticipated, microscopically there was an age-related decline in articular cartilage structural integrity, toluidine blue staining, and aggrecan and COL2A1 mRNA expression in both male and female guinea pigs. This parallels characteristic OA pathology and correlations described in mice, guinea pigs, and humans [12,33,50,51]. Collagen X, a minor collagen in hyaline cartilage, is a more specific marker of the hypertrophic zone of the growth plate and calcified articular cartilage; it plays a functional role in endochondral ossification and calcification [52]. In contrast to other matrix collagens, upregulation of COL10A1 serves as a marker of chondrocyte

hypertrophy and an increased expression may lead to calcification, ossification, and osteophyte formation in the joint. Compared to males, females had higher COL10A1 mRNA counts consistent with stiffer cartilage matrix that more readily ossify, sclerose, and form osteophytes.

Nrf2 is an oxidant- and stress-sensing transcription factor that regulates the expression of cellular defense mechanisms. Nrf2 activity diminishes with age, and thus the elderly are more susceptible to a variety of oxidative stress driven diseases [53]. In aging guinea pig articular cartilage there is a decrease in Nrf2 expression at both the mRNA and protein level and a subsequent decline in the Nrf2-mediated transcriptional regulation of antioxidants including NQ01, catalase, and thioredoxin. Another protective role of Nrf2 is its transcriptional regulation of iron, heme, and globin scavenging proteins. Unbound iron is highly reactive and generates free radicals that can drive oxidative damage. Nrf2 is able to counter iron-induced oxidative damage by transcriptional upregulation of ferritin (a major iron intracellular storage protein), ferroportin (an iron cellular export protein), and heme-oxygenase-1 (HMOX-1, a heat shock protein that counteracts heme toxicity) [54]. Indeed, in aging Hartley Guinea pig articular cartilage there is a significant decrease in ferroportin, ferritin (in males), and HMOX-1, as well as other iron-regulator proteins including the transferrin receptor, DMT1 iron transporter, and the SLC7A11 cystine/glutamate antiporter. Of note, there is an age-sex interaction on the expression of ferroportin and ferritin. More specifically, aged females have decreased ferroportin and increased ferritin and thus may efficiently respond to iron insults in early OA but lose their iron- and oxidant-sensing capabilities in late-stage disease. Further, males demonstrate the inverse effect with increased ferroportin and decreased ferritin levels with age. Collectively, these results suggest that age-related functional decline in Nrf2-signaling in musculoskeletal tissues serves as a local driver of oxidative damage and persistent low-grade inflammation which contributes to OA pathogenesis, and thus leads to my central hypothesis:

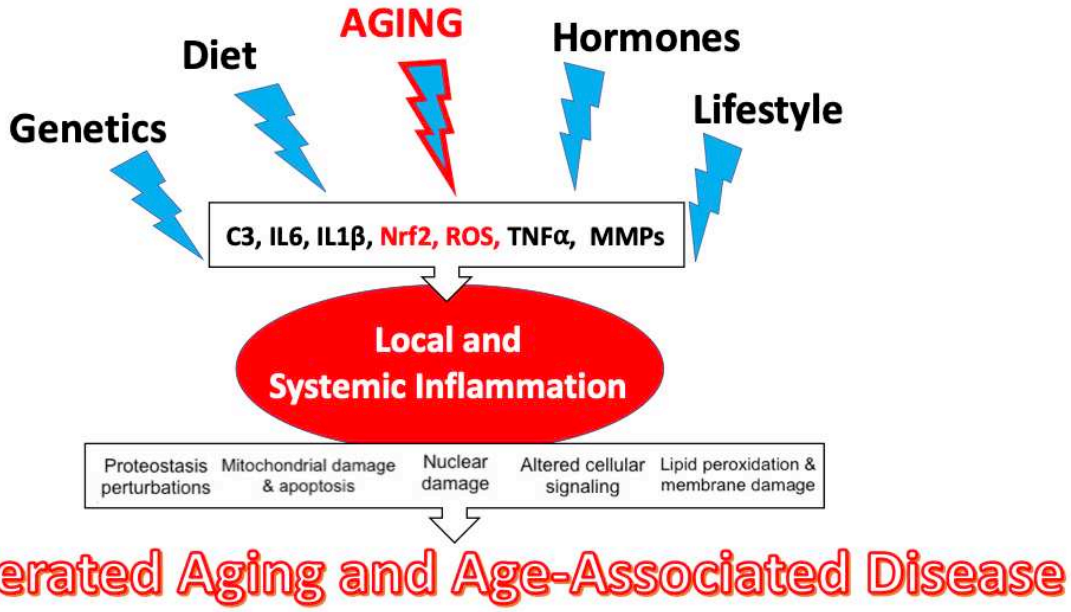


**Figure 1.14. Global Hypothesis**. Inflammation and oxidative stress have been recognized as closely integrated entities in OA pathology. Many contributing risk factors, including genetics, diet, stress associated with aging, hormonal imbalances, and a variety of lifestyle factors collectively contribute to decreased Nrf2-transcription systemically and locally within the joint. Subsequent depletion of oxygen-processing enzymes and free radical scavenging drives inflammation, cellular damage, and accelerates aging and age-associated disease, such as osteoarthritis. We hypothesize that phytochemical activation and stabilization (chapters 2 and 3) of the Nrf2-cytoprotective pathway will up regulate cytoprotective enzymes, mitigate intracellular ROS, and delay the onset and progression of OA in the Hartley guinea pig.

### 1.5.2: Infrapatellar Fat Pad

The IFP is composed of white adipose tissue which functions as a metabolically dynamic organ and plays a multifaceted role in joint homeostasis. Functional advantages of the IFP include its ability distribute synovial fluid, lubricate the joint, provide stability by occupying potential dead space, and shock absorption [55,56]. As a relatively large fat depot, it can signal in a paracrine, autocrine, endocrine, and juxtacrine manner communicating locally to the joint and remotely to the nervous (central, peripheral, adrenal) and immune systems [57]. The presence of intracapsular adipocytes, macrophages, and leukocytes poses a liability as these mediators have the potential to source pro-inflammatory and chondrodegenerative cytokines such as interleukins and proteases and thus contribute as a local driver in the pathogenesis of knee OA.

Work by Gierman et al. demonstrated that patients with end-stage OA have distinct metabolic profiles in their IFP that are regulated by OA rather than systemic basal metabolic changes [58]. In contrast, the inflammatory nature of the IFP may signal differentially in lean, healthy, and obese individuals, as diet composition and obesity were shown to have differential effects on the local IFP microenvironment. Specifically, obese animals fed ad libitum on a regular chow diet and animals consuming a high fat calorie restricted diet both had pro-inflammatory profiles and more severe OA compared to animals consuming a calorie restricted regular chow diet, suggesting that changes in diet and thus systemic basal metabolism may contribute to IFP inflammatory activity and drive OA [59].

Adiponectin and leptin are two adipokines that play an integral role in glucose and fatty acid metabolism, as well as hunger regulation and energy metabolism, respectively. The association of these adipokines and the development of OA is somewhat controversial [55]. In this study local IFP adiponectin mRNA levels inversely correlated with OA severity in both males and females. Further, males demonstrated decreased adiponectin expression compared to females, and had comparatively significantly advanced OA. Similar patterns of adiponectin expression in both plasma and synovial fluid are documented in human OA patients, and *in vitro* studies have demonstrated a chondroprotective role of this adipokine in OA progression [60,61]. However, conflicting reports demonstrate increased adiponectin expression in chondrocytes from OA patients, and other authors demonstrated this adipokine plays a catabolic role in matrix degeneration [62,63]. This reported catabolic effect of adiponectin in cartilage is inconsistent with our study as mRNA levels from both articular cartilage and the IFP of aging Hartley guinea pigs demonstrated a significant decrease in adiponectin expression with OA severity (Supplemental Tables 2.1 and 3.1). Leptin, another adipokine implemented in OA pathogenesis, is reportedly increased both locally within synovial fluid and systemically within plasma, and positively correlated with OA severity in people [64]. Of note, obese patients have high circulating levels of leptin, but overall a functional deficiency through decreased leptin sensitivity at the cellular receptor. In this study, knee fat stores from both sexes had decreased leptin expression with age. This expression pattern may exhibit a similar clinical sequelae as decreased production

may mimic the clinical manifestation of functional deficiency associated with leptin resistance in obese individuals.

Aged Hartley guinea pig IFPs have increased expression of the pro-inflammatory cytokines IL1β, TNFα, PTGS-2, and HMGB1 and articular cartilage has histologic features of end-stage joint degeneration. Further, IFPs from 15-month-old animals demonstrate increased COL10A1 and RUNX2 expression which is well reported to correlate with advanced OA [14,51], and may even serves as a drvier for the formation of extraskeletal ossifying chondromas which are recognized as drivers of knee pain and OA in people [65]. Of interest, there is a significant increase in MMP and a concurrent decrease in TIMP transcriptional activity in IFPs from aging animals. Specifically, TIMP-2, a broad inhibitor of MMPs with a high specificity for MMP2, activity is decreased in the IFP of 15-month-old male and female animals. In accord, articular cartilage MMP2 activity is increased with advanced OA. Collectively, these data suggest tight regulation and crosstalk between the IFP and articular cartilage of the knee joint, and thus the IFP may serve as a plausible regional target for disease modification. Further, these data are in consensus with other reports which suggest the IFP plays a significant role in sourcing pro-inflammatory mediators and proteases driving local destruction of articular cartilage [55,58,66,67]. However, the association between adiposity, local and systemic functional adipokine activity, metabolism, inflammation, and OA warrants further investigation.

### 1.5.3: Clinical Assessment of Voluntary Mobility

The most common clinical presenting complaint of OA patients is pain which is often associated with decreased functional mobility. Further, behavior traits, such as anxiety- and depressive-like activity, may represent a manifestation of chronic low-grade pain which may impair a patient's ability to cope with acute painful stimuli associated with movement [68]. Despite this, few studies aim to assess clinically relevant spontaneous biomechanical and behavioral influences of OA the functional level. In this study, clinical assessments of voluntary mobility were determined by ANY-maze™ behavioral monitoring tracking software. Both male and female 15-month-old Hartley guinea pigs with severe OA spent significantly less

time mobile, traveled significantly shorted distances, at a lower average speed compared to 5-month-old animals. Some animals in the late stages of disease demonstrated task noncompliance, defined as refusal to move when exposed to an open field. These changes in mobility associated with age and end-stage OA may serve as a noninvasive clinical measurement of disability due to direct structural joint damage and/or pain associated with OA. Further, this data serves as a baseline tool in measuring OA disease burden over time and aids in determining the clinical efficacy of an intervention strategy in managing OA.

### 1.5.4: Future Directions

Currently there is a lack of a large-scale gene expression profiling study characterizing both articular cartilage and infrapatellar fat pad mRNA levels in both male and female Hartley guinea pigs. This study characterized age- and sex- specific effects on mRNA expression in these tissues, however advanced analysis, including pathway analysis and principal component analysis combined with a dimension reduction technique may better correlate meaningful biomarkers between the sexes and OA progression. Further, this study documents a significant decline in COL2A1 expression in the knee joint of male and female Hartley guinea pigs, which is a described feature of temporal mandibular joint degeneration (TMJ) in COL2A1 mutant mice [50]. Future directions include longitudinally characterizing the degree of TMJ degeneration, using both uCT and histopathology, of non-weight bearing fibrocartilaginous joints in aging male and female Hartley guinea pigs.

## 1.6: Conclusions

This study demonstrates key sex differences in OA severity and gene and protein expression profiles consistent with OA representing a sexual dimorphic disease. Of particular interest, both male and female aging Hartley guinea pig knee joint tissues have decreased Nrf2 levels at both the mRNA and protein level which coincides with advanced-stage disease. These age-linked findings have led to the global hypothesis that downregulation in Nrf2/ARE-signaling in musculoskeletal tissue serves as a central driver for persistent low-grade inflammation, dysregulation of redox homeostasis, all of which contribute to OA progression.

With this in mind, the objective of the current thesis dissertation is to investigate if treatment with a Nrf2 activator mitigates the onset (Chapter 2) and/or progression (Chapter 3) of osteoarthritis in the Hartley guinea pig. Our long-term goal is to identify therapeutic targets in the Nrf2 pathway so appropriate intervention strategies can be implemented for disease prevention and management.

# CHAPTER 2: PHYTOCHEMICAL NRF2-ACTIVATION MODIFIES MOLECULAR AND CLINICAL BUT NOT PHENOTYPIC MANIFESTATIONS OF EARLY OSTEOARTHRITIS IN THE HARTLEY GUINEA PIG

## 2.1: Overview

This chapter seeks to investigate the utility of a novel Nrf2-activator (Nrf2a) in delaying the onset of idiopathic osteoarthritis (OA) in the Hartley guinea pig. The foundation of this work is based on the premise that: (1) it has been shown that dysregulation of Nrf2/ARE-signaling plays a role in many age-related non-OA pathologies; (2) the underlying pathogenesis of many inflammatory and age-related diseases has been associated with the toxic effects of ROS in tissues; and (3) downregulation of the Nrf2-pathway in aging knee joint tissue is associated with OA in both male and female Hartley guinea pigs (Chapter 1). The chapter will use a combination of structural, molecular, and *in vivo* functional outcomes to assess the effects of 3-month Nrf2a treatment on characteristic OA outcomes in the Hartley guinea pigs.

## 2.2: Introduction

A major limitation in managing OA is the lack of therapeutics that can slow the onset of disease. Patients are often treated for symptom modification with analgesics, such as nonsteroidal anti-inflammatory drugs; however, these medications only mask underlying pathology and are accompanied by unremittent side effects [69,70]. Compared to other tissues, articular cartilage is unique in that it is avascular, alymphatic, aneural, and paucicellular. Thus, chondrocytes have limited capacity to respond to damage and oxidative stress that accumulates with age.

There is a growing body of evidence that links the age-related imbalance of increased reactive oxygen species (ROS), chondrocyte cell death, and articular cartilage degeneration [71]. Nuclear factor erythroid-2 related factor-2 (Nrf2) is an oxidative stress induced cytoprotective transcription factor that, through binding to its promoter and antioxidant response element (ARE), serves as a master regulator of hundreds

of anti-inflammatory agents, phase I xenobiotic and phase II antioxidant enzymes, as well as enzymes with autophagic and proteasomal removal properties [72]. Indeed, Nrf2 activation generates hundreds of cellular proteins involved in free radical scavenging and cytoprotection. Functional alterations in Nrf2-signaling are implicated in a vast array of pathologies and age-related diseases, including carcinogenesis and chemoresistance [73–75], cardiovascular [76,77], and neurodegenerative disorders [78–80]. Further, Nrf2 has been recognized as an important mediator in cartilage homeostasis and osteoarthritis [71,81–83]. Of interest, in vivo mouse studies have demonstrated that Nrf2 is protective to cartilage and other joint tissues during the progression of various models of post-traumatic OA [84–86]. Additionally, Nrf2-knock out mice demonstrate more severe cartilage degeneration and accelerated overall disease progression in secondary OA models [83]. Despite this growing body of work in post-traumatic OA models, there is limited knowledge of the role of Nrf2 in the *in vivo* development of the progressive chondro-degenerative phenotype seen in primary idiopathic OA, and specifically in the translatable Hartley guinea pig model of spontaneous OA.

The Nrf2-pathway is down regulated in aging osteoarthritic knee joint tissue in both humans and Hartley guinea pigs, which intensifies oxidative stress under pathologic conditions [87,88]. Decreased Nrf2 activity and subsequent transcriptional downregulation of vital antioxidants (such as NQ01, thioredoxin, and superoxide dismutase) allows superoxide anions and hydrogen peroxides to cause unremitted protein damage altering cellular function. For example, increased ROS activity *in vitro* leads to both intracellular and extracellular damage causing chondrocyte apoptosis [88,89], collagen denaturation [90], and positive feedback loops further exacerbate cartilage degeneration [91]. In the Hartley guinea pig model of idiopathic OA, we have documented an age-associated decline in transcriptional and functional activity of Nrf2 in knee joint tissue. Thus, it is suspected the local knee joint microenvironment is uniquely susceptible to oxidative damage and thus a driver of cartilage damage throughout aging.

Nutraceuticals are relatively safe food- or plant-derived pharmaceutical alternatives that may pose a physiologic benefit in managing chronic diseases [69]. Currently, both glucosamine sulfate and chondroitin sulfate are classified as symptomatic slow-acting drugs for OA (SYSADOAs) and are often employed as

first line nutraceuticals in clinical management of disease [92–94]. Further, protandim and 6-gingerol were shown to both activate Nrf2 and diminished pro-inflammatory signaling *in vitro,* and expanded lifespan in mice *in vivo* [95]. PB125 (PB125, Pathway Bioscience, Denver, CO), a novel nutraceutical and Nrf2a, contains three bioactive ingredients extracted from rosemary (6.7% carnosol, R), ashwagandha (1% withaferin A), and sophora japonica (98% luteolin, L) that synergistically both activate and stabilize the Nrf2 pathway [96]. As we documented an age-related decline in Nrf2 activity in aging Hartley knee joint tissue (Chapter 1) we were interested in investigating the utility of this Nrf2-activating nutraceutical in delaying OA in the Hartley guinea pig.

Naturally hyaline cartilage is of low cellularity with limited renewal capacity and to date there are no readily available therapeutics that can restore chondrocytes or the extracellular matrix to its quiescent state. Thus, we took the approach of preemptive Nrf2a supplementation before the onset of disease in attempt to delay molecular, phenotypic, and clinical manifestations of early-stage disease [40]. We hypothesized that animals treated with PB125 before the onset of knee OA would have differential gene expression profiles within articular cartilage and the infrapatellar fat pad (IFP), decreased whole knee joint OA scores, and modified clinical parameters, including differential voluntary activity levels and gait patterns, during open field enclosure monitoring and obligatory gait analysis, respectively. The overarching goals of this chapter is to assess the utility of a novel phytochemical and Nrf2a in delaying or preventing clinical and/or structural manifestations of *early* OA in the Hartley guinea pig.

## 2.3: Materials and Methods

### 2.3.1: Animals and Study Design

All Hartley guinea pigs (n=56, aged 1.5 months) were procured from Charles River Laboratories (Wilmington, MA). Procedures were approved by the university's Institutional Animal Care and Use Committee (19-9129A) and were performed in accordance with the NIH Guide for the Care and Use of Laboratory Animals. Animals were maintained at Colorado State University's Laboratory Animal

Resources housing facilities and were monitored daily by a veterinarian. Guinea pigs were singly housed in solid bottom cages and provided *ad libitum* access to water and regular chow diet. Hay cubes were withheld to ensure that the main source of phytochemicals was limited to the oral Nrf2 supplement.

After a 2-week acclimation period, male (n=28) and female (n=28) Hartley guinea pigs (total n=56) were randomly assigned to receive treatment with the Nrf2 activator PB125 or the delivery vehicle control (Ora-sweet Sugar Free Syrup Vehicle®, Paddock Laboratories, Minneapolis, MN). Nrf2a pigs received 8 mg/kg PB125 suspended in 1mg/kg Ora-sweet SF® vehicle while control pigs received a volume-based vehicle equivalent, only. Animals began treatment at 2-months-old, were dosed daily in the morning for 3 consecutive months, and sacrificed at 5-months-old, when mild OA changes representing early-stage disease were expected in control animals.

### 2.3.2: Harvests and Tissue Collection

Body weights were recorded immediately before harvest. Animals were anesthetized with a mixture of isoflurane and oxygen and transferred to a carbon dioxide chamber for euthanasia. Complete necropsy was performed by a veterinary pathologist to rule out comorbidities. The right hind limb was disarticulated at the coxofemoral joint. Upon arthrotomy, the articular surfaces of the knee were: (1) flushed with 500 µl PBS, (2) patellar, patella-femoral groove, femoral condylar, and tibial plateau surfaces, along with the menisci, were scraped and pooled cartilage flakes stored in RNALater, and (3) the IFP removed and stored in Allprotect Tissue Reagent. All tissues were stored at -80°C until further processing. The left hind limb was removed, left intact, stored *in situ* in 10% neutral buffered formalin for 48 hours and transferred to PBS.

### 2.3.3: Histology and OARSI Histopathology Grading

The left hindlimbs were decalcified over 6-weeks in $Ca^{2+}$EDTA. Limbs were trimmed in the medial sagittal plane, embedded in cassettes, processed, and 5uM paraffin sections were mounted onto charged slides. Slides were stained with hematoxylin and eosin (H&E) and toluidine blue for histopathologic examination and OARSI grading, respectively. Toluidine blue histologic grading was scored based on a modification (due to orientation in the sagittal plane) of established grading schemes provided by *Kraus et al.*[22] Knee joints were scored by a veterinary pathologist in duplicate as well as in random order, blinded to treatment group.

### 2.3.4: Nanostring Targeted mRNA Analysis

A custom NanoString nCounter 100-code gene panel for targeted mRNA analysis was utilized and consisted of Nrf2 and Nrf2 induced genes, as well as key mediators of inflammation and those implicated in OA pathogenesis. Total mRNA, from pooled articular cartilage or the IFP of the right knee joint, was extracted using TRIzol reagent and Qiagen RNeasy and RNeasy Lipid Mini Kits according to the manufacturer's instructions. Samples were analyzed in collaboration with Nanostring Technologies at the University of Arizona Genetics Core. Eukaryotic elongation factor 1 alpha (EFF1a) was used as a housekeeper gene for normalization. A complete gene list and normalized absolute mRNA counts from the articular cartilage and IFP are provided in Supplemental Tables 2.1 and 2.2, respectively.

### 2.3.5: Immunohistochemistry and Advanced Imaging

To semi-quantitatively assess selected gene expression outcomes at the functional protein level, IHC was implemented using antibodies against Nrf2 (ThermoFisher Scientific, PA-38312, rabbit polyclonal, dilution of 1:100) and NQ01 (Abcam ab34173, rabbit polyclonal, dilution of 1:400). Heat-induced epitope retrieval was performed on a Leica Bond-RX automated stainer using BOND Epitope Retrieval Solution 1 (citrate buffer) for 420 minutes at 55°C. Blocking was performed using 3% peroxide followed by 2.5% donkey serum. Labeling was performed on an automated staining platform. DAB was used as the chromogen and

immunoreactions were visualized using commercial detection systems. Slides were counterstained with hematoxylin. Sequential steps of the immunostaining procedure were performed on negative controls following incubation. Photomicrographs from the medial tibial plateau were quantitatively analyzed by measuring the mean immuno-positive surface area using VisioPharm® software (Westminster, CO).

### 2.3.6: ANY-maze™ Open Field Enclosure Monitoring

Animals were acclimated over a 2-week period, before the onset of the study, to an open circular field behavior monitoring system (ANY-maze™, Wood Dale, IL) to assess voluntary physical mobility. Animals' activities were recorded, and data were collected for 10 consecutive minutes on a monthly basis throughout the study. Videos were analyzed for the following parameters: total distance traveled (m), average speed (m/s), time mobile (s), % time mobile, time in hut (s), % time in hut, and average moving speed (m/s). See Supplemental Table 2.3 for full list of output variables and descriptive statistics.

### 2.3.7: DigiGait™ Treadmill-Based Gait Analysis

Animals were acclimated over a 2-week period before the onset of the study to a treadmill-based gait analysis system (DigiGait™, Mouse Specifics, Framingham, MA). Before the start of the study and on a monthly basis throughout guinea pigs were run on a flat treadmill at 55cm/sec and videos were analyzed for 22 gait parameters. See Supplemental Table 2.4 for full list of output variables and descriptive statistics.

### 2.3.8: Statistics

Gait analysis outcomes on stride length were selected as the primary outcome to determine the appropriate sample size as previous work demonstrated changes in stride length with anti-inflammatory treatment (Flunixin Meglumine) had an average effect size of 2.6 cm [26]. For our current study, we set an effect size of 1 cm for the power calculation, a power of 0.80 and significance (chance of Type I error) set at p=0.05

(Russ Lenth power calculator). Based on these values, we calculated an n=13 animals per treatment group and selected an n=14 per treatment group to account for the unexpected loss of animals.

Normality testing was performed on all outcome measures. Continuous variables - including gene and protein expression, as well as gait and behavior outcomes selectively at the 5-month time point (representing a snapshot effect after 3-months of treatment with a Nrf2a) - were expressed as *mean* raw counts, reactivity, or selected outcome measure, respectively. These outcomes were analyzed using two-way ANOVA (factors signifying sex and treatment) followed by multiple comparison *post hoc* correction via Bonferroni procedure. The longitudinal effects on gait and behavior were assessed using repeated measures t-test, or two-way ANOVA (depending on the inclusion or separation of sex, factors signifying time and treatment) followed by Tukey's multiple comparison *post hoc* tests.

Discrete variables – including total indices for OA pathology were expressed as *median* modified OARSI histopathology scores. These outcomes were analyzed using two-way ANOVA (factors signifying sex and treatment) followed by multiple comparison *post hoc* correction via Bonferroni procedure. For all tests, significance was set to $p<0.05$ and trends were identified as $0.05<p<0.15$. Analyses were performed using GraphPad Prism Version 9.0 (San Diego, CA, USA).

## 2.4: Results

### 2.4.1: OARSI Grading and Histopathology

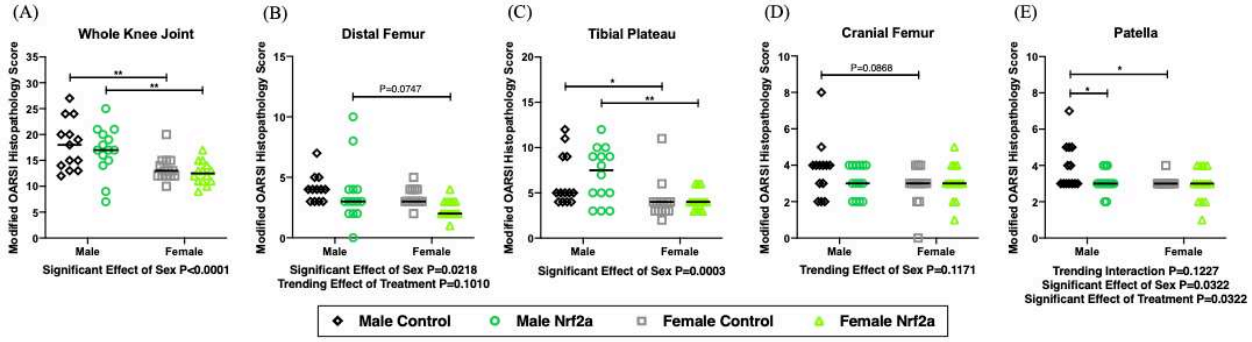


**Figure 2.1. Median OARSI histopathology scores for OA from control and Nrf2-activator treated guinea pigs. (A)** Whole knee joint median OARSI histopathology scores for OA in 5-month-old Hartley guinea pigs. Individual surface median OARSI histopathology scores of the (B) distal femur, (C) tibial plateau, (D) cranial femur, and (E) patella.
**0.01<p<0.05;* **** *0.001<p<0.01*

There were no significant effects of Nrf2a treatment on whole knee joint OA scores. However, there was a trending effect of PB125 treatment on decreasing distal femur OA scores (**p=0.10, Figure 2.1B**) and a significant effect of treatment in decreasing patellar OA scores (**p=0.03, 2 Figure 2.1E**); multiple comparisons revealed significance was driven by Nrf2a treatment in males (**p=0.01, Figure 2.1E**).

Sex had a significant effect on whole knee joint OA scores (**p<0.0001, Figure 2.1A**); control females had significantly lower whole knee joint OA scores compared to control males. When evaluating individual surface indices that comprise the whole knee joint score, control females had decreased scores along all surfaces evaluated (**Figure 2.1B-E**).

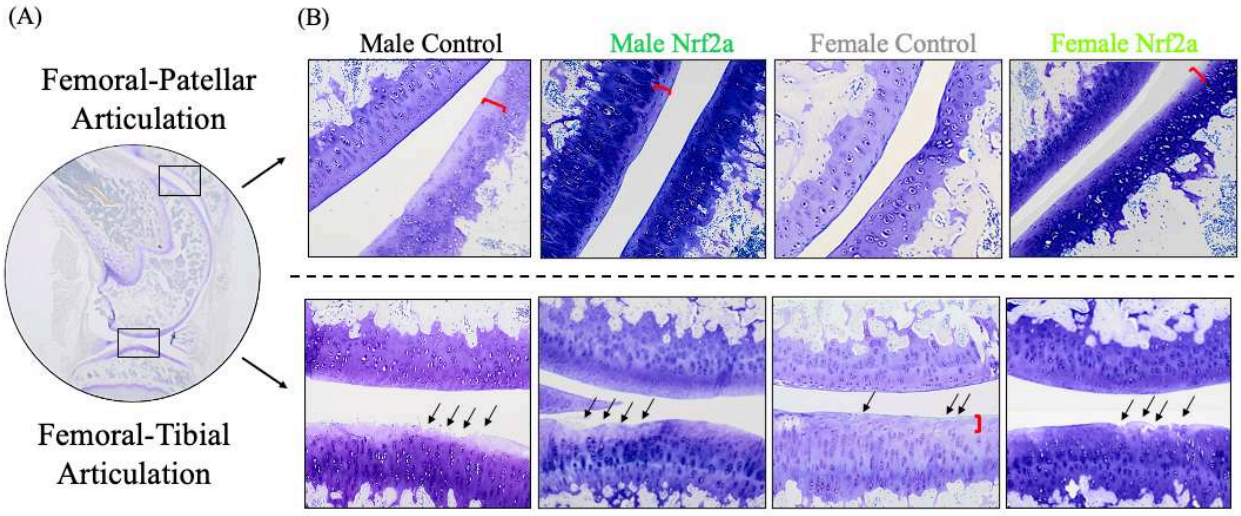


**Figure 2.2. Representative whole knee joint toluidine blue photomicrographs from 5-month-old control and Nrf2-activator treated Hartley guinea pigs. (A)** Subgross photomicrograph of the guinea pig whole knee joint trimmed in the sagittal plane. Boxes depict graded regions of interest which include the femoral patellar and femoral-tibial articular surfaces. (**B**) Representative photomicrographs of the femoral-patellar articulation (top row) and the femoral-tibial articulation (bottom row). Red brackets depict proteoglycan loss; black arrows highlight fissures and cartilage loss in the superficial to middle zones. *Toluidine blue, 40x.*

Representative photomicrographs demonstrate mild degenerative OA changes representing the onset of disease in 5-month-old animals; characteristic lesions include loss of proteoglycan and chondrocytes (**Figure 2.2B, red brackets**) as well as mild fibrillation and fissuring (**Figure 2.2B, black arrows**) in the superficial zone. Of interest, although no significant effects of treatment on whole knee joint OA scores were appreciated in either sex, animals treated with a Nrf2a have richer knee joint proteoglycan content characterized by diffusely darker and brighter blue/purple toluidine blue staining on all surfaces

### 2.4.2: Nanostring Targeted mRNA Analysis

#### 2.4.2.1: Articular Cartilage

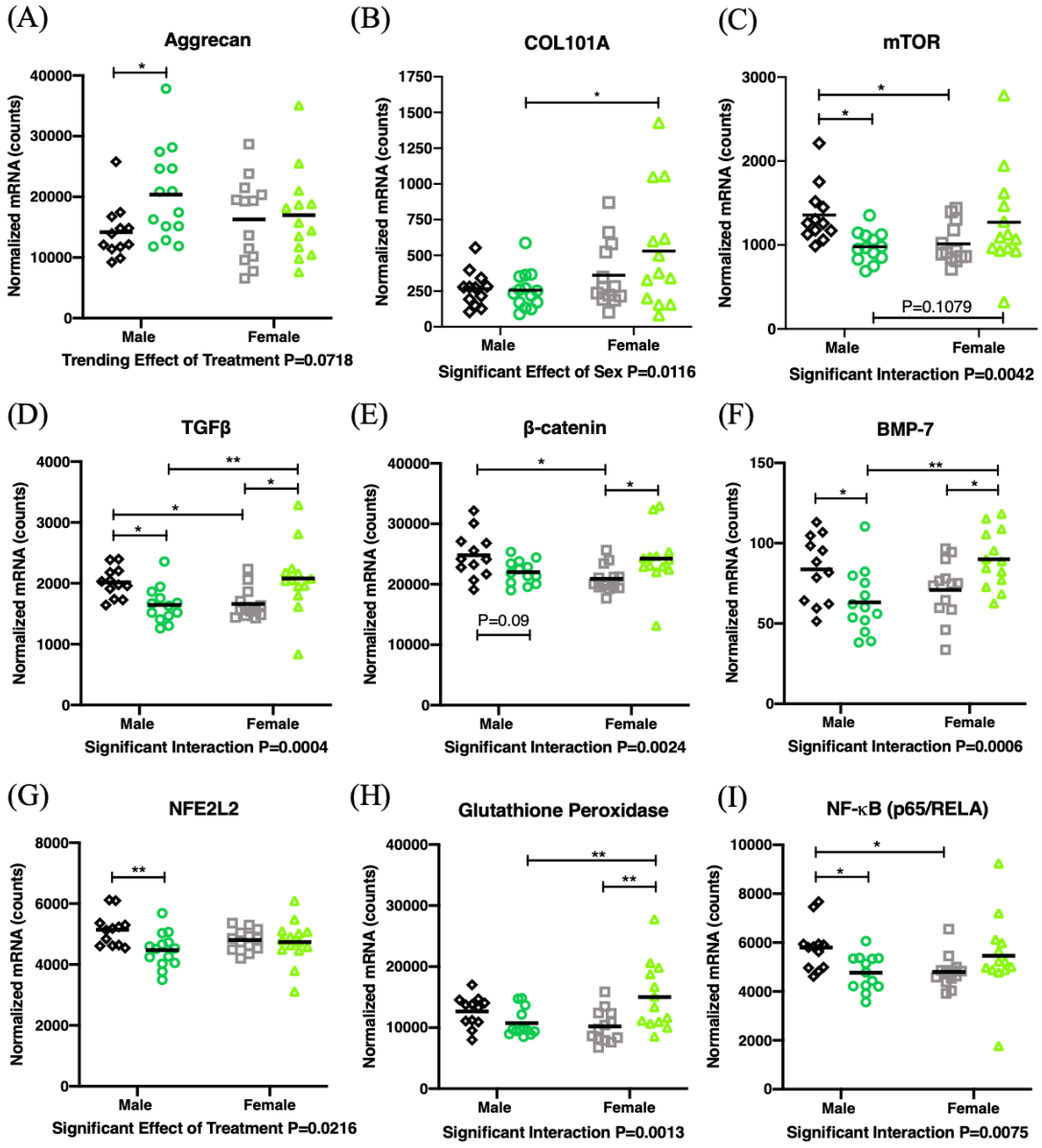


**Figure 2.3. Normalized mRNA counts for select constituents of the extracellular matrix, anabolic markers of OA, and the Nrf2-signaling pathway in articular cartilage from 5-month-old control and Nrf2-activator treated Hartley guinea pigs.** Articular cartilage mean mRNA expression levels of (**A**) aggrecan, (**B**) collagen type X alpha I chain (COL10A1), (**C**) mechanistic target of rapamycin (mTOR), (**D**) transforming growth factor-β (TGF-β), (**E**) β-catenin, (**F**) bone morphogenic protein-7 (BMP-7), (**G**) nuclear factor erythroid-2 related factor-2 (NFE2L2) oxidant sensing transcription factor, (**H**) glutathione peroxidase, and (**I**) nuclear factor κ-light-chain enhancer of activated B-cells (NF-κB, p65, RELA). **0.01<p<0.05; ** 0.001<p<0.01 ; *** 0.0001<p<0.001; **** p<0.0001*

Nrf2a treated males had a significant increase in aggrecan (**p=0.04, Figure 2.3A**) and a concurrent decrease in TGFβ (**p=0.01, Figure 2.3D**), β-catenin (**p=0.09, Figure 2.3E**), BMP7 **(p=0.02, Figure 2.3F**), NFE2L2 (**p=0.008, Figure 2.3G**), and NF-κB (**p=0.04, Figure 2.3I**) expression. Nrf2a treated females demonstrated no significant changes in aggrecan expression but an increase in TGFβ (**p=0.02, Figure 2.3D**), β-catenin (**p=0.03, Figure 2.3F**), and glutathione peroxidase (**p=0.002, Figure 2.3H**) expression.

Many genes were variably expressed between the sexes, translatable to similar sex-based gene expression patterns reported in people [49]. Specifically, there was a decrease in: mTOR (**p=0.05, Figure 2.3C**), TGFβ (**p=0.03, Figure 2.3D**), β-catenin (**p=0.01, Figure 2.3E**), and NF-κB (**p=0.05**, **Figure 2.3I**) in control females compared to control males. As mentioned above, these females also have significantly decreased OA scores (**Figure 2.3A**).

Lastly, there were significant sex-treatment interactions on the expression of mTOR (**p=0.004, Figure 2.3C**), TGFβ (**p=0.0004, Figure 2.3D**), β-catenin (**p=0.002, Figure 2.3E**), BMP-7 (**p=0.0006**, **Figure 2.3F**), glutathione peroxidase (**p=0.001, Figure 2.3H**), and NF-κB (**p=0.0007, Figure 2.3I**).

### 2.4.2.2: Infrapatellar Fat Pad

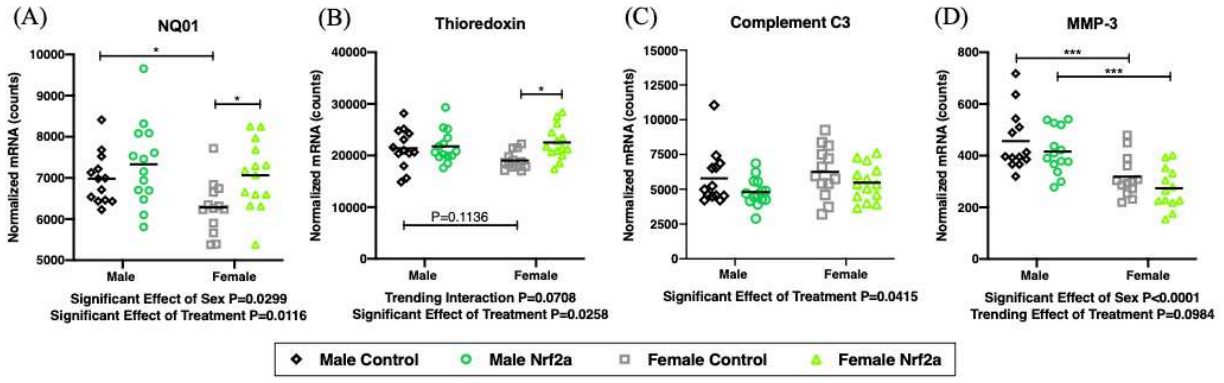


**Figure 2.4. Normalized mRNA counts for select antioxidants, pro-inflammatory, and catalytic mediators in infrapatellar fat pads from 5-month-old control and Nrf2-activator treated Hartley guinea pigs.** IFP mean mRNA expression levels of (**A**) NAD(P)H dehydrogenase quinone-1 (NQ01) detoxification enzyme, (**B**) thioredoxin antioxidant, (**C**) complement C3, and (**D**) matrix metalloproteinase-3 (MMP-3). **0.01<p<0.05; ** 0.001<p<0.01 ; *** 0.0001<p<0.001; **** p<0.0001*

Nrf2a treated animals expressed significantly increased levels of the cytoprotective enzymes NQ01 (**p=0.01, Figure 2.4A**) and thioredoxin **(p=0.02, Figure 2.4B**), and decreased levels of the pro-inflammatory mediator complement C3 (**p=0.04, Figure 2.4C**) and protease MMP-3 (**p=0.09, Figure 2.4D**). There was a significant effect of sex on the expression of NQ01 (**p=0.02, Figure 2.4A**) and MMP-3 (**p<0.0001, Figure 2.4D**); specifically, males had significantly higher expression compare to females.

### 2.4.3: Immunohistochemistry and Advanced Imaging

#### 2.4.3.1: Nuclear factor erythroid-2-related factor-2

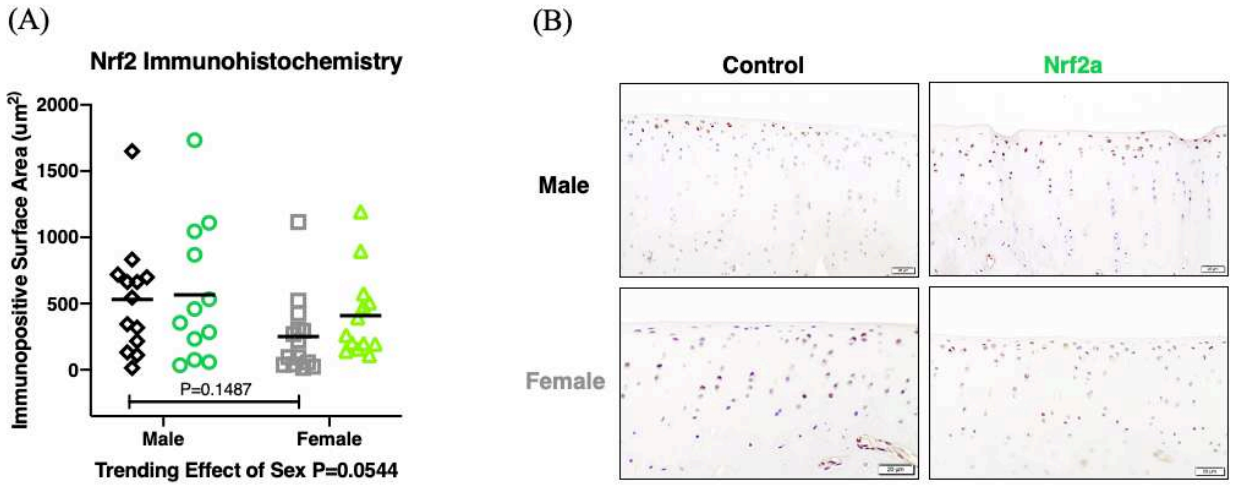


**Figure 2.5. Medial tibial plateau Nrf2 immunoexpression in control and Nrf2-activator treated Hartley guinea pigs.** (**A**) Nrf2 mean immunopositive surface area of the medial tibial plateau in 5-month-old control and Nrf2a treated Hartley guinea pigs. (**B**) Representative Nrf2 immunohistochemistry photomicrographs of the medial tibial plateau from male (top row), female (bottom row), control (left column), and Nrf2a treated (right column) Hartley guinea pigs. 40x; bar=20um; **0.01<p<0.05; **0.001<p<0.01; *** 0.0001<p<0.001; **** p<0.0001*

There were no appreciable effects of Nrf2a supplementation on medial tibial plateau Nrf2 immunoexpression levels. There was a trending deccreasea in Nrf2 expression in females compared to males (**p=0.0544, Figure 2.5A**). Representative immunohistochemistry photomicrographs demonstrate mild to moderate chondrocyte nuclear immunolabeling in the superficial zone of males and similar expression patterns in both the superficial and middle zone of females.

### 2.4.3.2: NAD(P)H dehydrogenase quinone 1

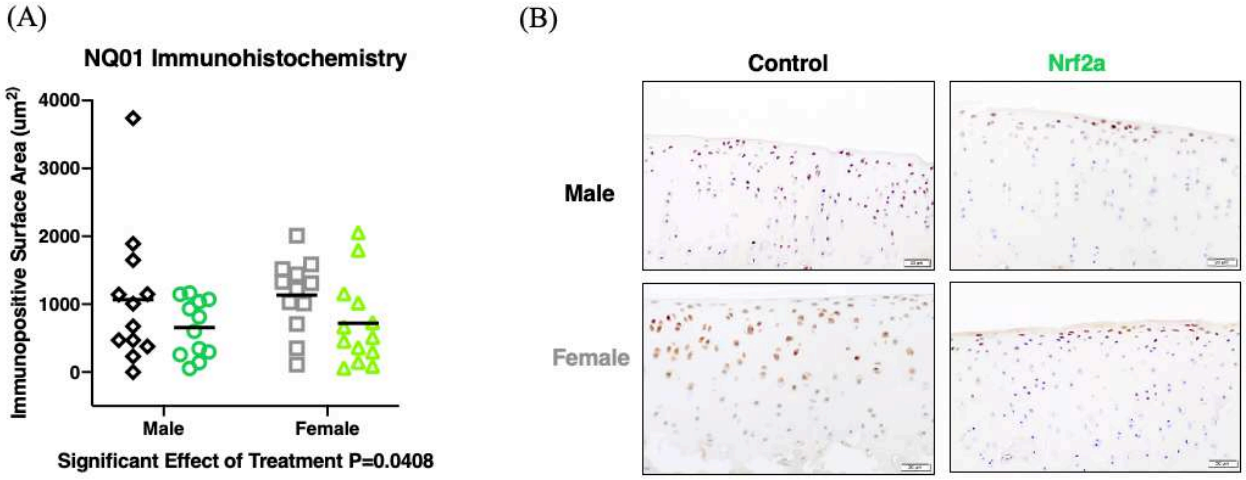


**Figure 2.6. Medial tibial plateau NQ01 immunoexpression in control and Nrf2-activator treated Hartley guinea pigs.** (**A**) NQ01 mean immunopositive surface area of the medial tibial plateau in 5-month-old control and Nrf2a treated Hartley guinea pigs. (**B**) Representative NQ01 immunohistochemistry photomicrographs of the medial tibial plateau from male (top row), female (bottom row), control (left column), and Nrf2a treated (right column) Hartley guinea pigs. 40x; bar=20um; **0.01<p<0.05; **0.001<p<0.01; *** 0.0001<p<0.001; **** p<0.0001*

There was a significant effect of Nrf2a treatment on medial tibial plateau NQ01 immunoexpression (**p=0.04, Figure 2.6A**). Specifically, NQ01 activity was decreased in both males and females treated with PB125; *post hoc* tests did not indicate significance was driven by one sex. Representative immunohistochemistry photomicrographs demonstrate moderate chondrocyte nuclear immunolabeling in the superficial zone of control and PB125 treated males, moderate to strong diffuse nuclear and cytoplasmic immunolabeling in control females, and mild to moderate nuclear and cytoplasmic immunolabeling in the superficial zone of PB125 treated females (**Figure 2.6B**).

### 2.4.4: ANY-maze™ Open Field Enclosure Monitoring

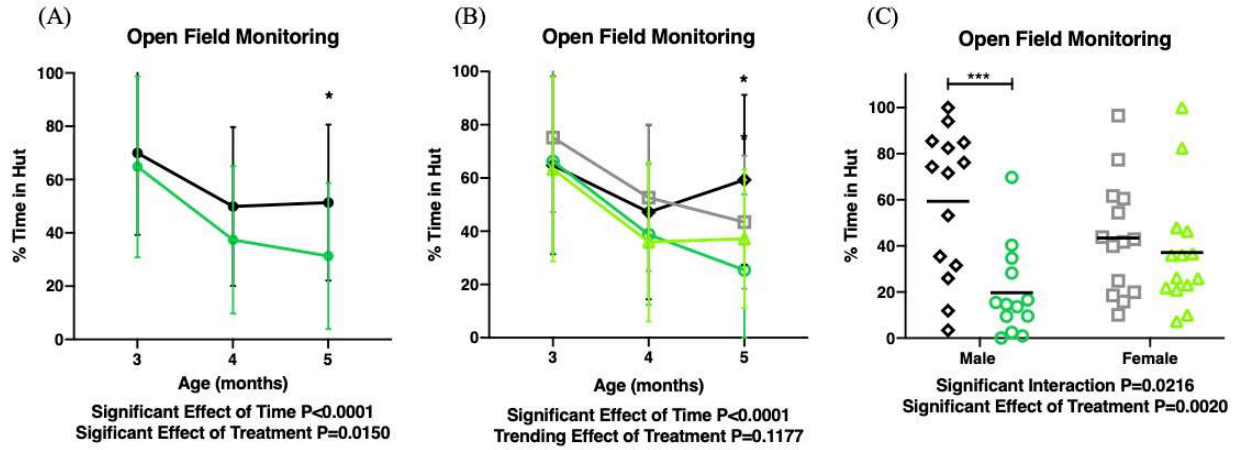


**Figure 2.7. ANY-maze™ open field monitoring displaying percentage of time spent in hut when exposed to an open field for 10-minutes.** (**A**) Longitudinal tracking of mean percentage of time spent in hut throughout the study duration in control (black dots and line) and Nrf2a (green dots and line) treated guinea pigs. (**B**) Longitudinal tracking of individual group mean percentage of time spent in hut in male controls (black diamond and line), female controls (gray squares and line), Nrf2a treated males (green circles and line), and Nrf2a treated females (neon green triangles and line). (**C**) Mean percentage of time spent in hut at the study end point after 3 consecutive months of Nrf2a treatment or vehicle control.
**0.01<p<0.05; **0.001<p<0.01 ; *** 0.0001<p<0.001; **** p<0.0001*

There were significant effects of time and treatment on the percentage of time animals spent in hut when exposed to an open field for ten minutes (**p<0.001 and p=0.01, Figure 2.7A, respectively).** Specifically, Nrf2a treated animals spent significantly less time in hut after 3 months of treatment (**p=0.03, Figure 2.7A**). When investigating the effects of sex, significance was driven by treatment in males (**p=0.03, Figure 2.7B**). A snapshot of the percentage of time each group spent in hut after 3 months of treatment (representing the study endpoint) demonstrated a significant sex-treatment interaction (**p=0.02, Figure 2.7C**) and significant effects of treatment (**p=0.002, Figure 2.7C**). Tukey's multiple comparisons revealed significance was driven by Nrf2a treated males (**p=0.03, Figure 2.7C**).

### 2.4.5: DigiGait™ Treadmill-Based Gait Analysis

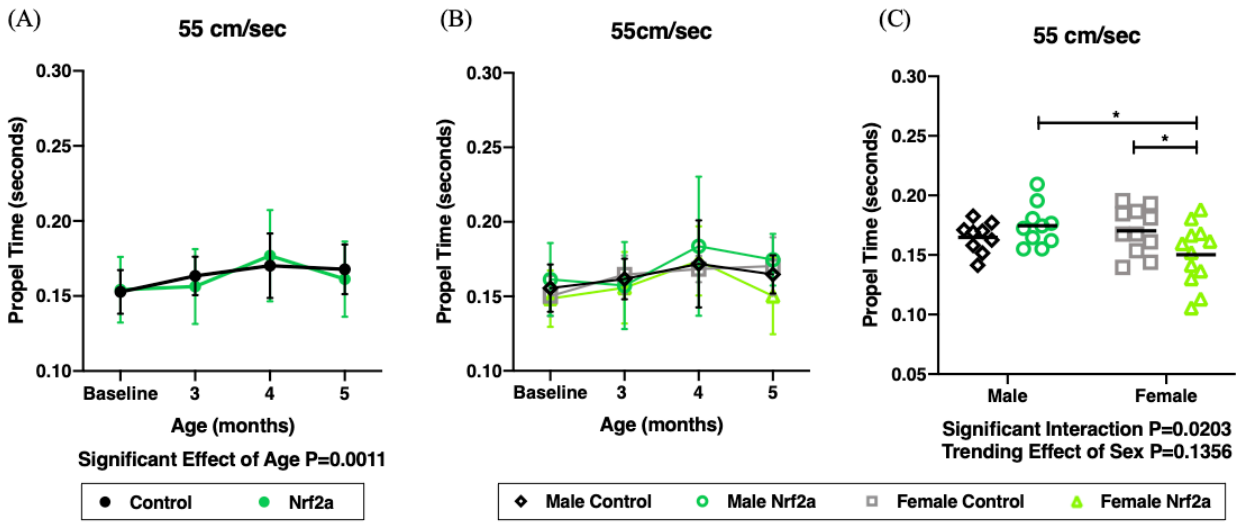


**Figure 2.8. Mean propel time during obligatory running at 55cm/sec.** (**A**) Longitudinal tracking of mean propel time throughout the study duration in control (black dots and line) and Nrf2a (green dots and line) treated guinea pigs. (**B**) Longitudinal tracking of individual group mean propel times in male controls (black diamond and line), female controls (gray squares and line), Nrf2a treated males (green circles and line), and Nrf2a treated females (neon green triangles and line). (**C**) Mean propel time at the study end point after 3 consecutive months of treatment with a Nrf2a or vehicle control.
**0.01<p<0.05; **0.001<p<0.01 ; *** 0.0001<p<0.001; **** p<0.0001*

There was a significant effect of age (or duration into the study) on mean propel time (**p=0.001, Figure 2.8A**). Individual group mean propel times over the duration of the study are depicted in Figure 2.8B. A snapshot of propel time after 3 months of treatment (representing the study endpoint) demonstrated a significant sex-treatment interaction (**p=0.02, Figure 2.8C**) and trending effect of sex (**p=0.13, Figure 2.8C**) on mean propel time. Tukey's multiple comparison *post hoc* testing revealed a significant decline in mean propel time in females treated with a Nrf2a (**p=0.04, Figure 2.8C**).

## 2.5: Discussion

This study investigated the utility of a novel nutraceutical and Nrf2a in delaying the onset of early OA using the spontaneous, non-induced, and highly translatable Hartley guinea pig model of idiopathic OA. As previously alluded, articular cartilage is naturally of low cellularity with limited renewal capacity and once

damaged there are limited to no therapeutics available that restore chondrocytes and the extracellular matrix to their native quiescent state. Therefore, in this study we took the approach of preemptive Nrf2a supplementation before the onset of OA in attempt to delay phenotypic and clinical manifestations of early disease. Three months of Nrf2a supplementation modified gene and protein expression patterns in both cartilage and the IFP, significantly decreased patellar OA scores, and altered clinical (behavioral and gait) patterns characteristic of early-stage disease; however, whole knee joint pathology scores did not significant differ with treatment.

Molecularly, articular cartilage homeostasis is achieved by a relative balance between catalytic degradation (mediated by inflammatory cytokines and proteases), and anabolic synthesis (mediated by growth factors and protease inhibitors) rates. Indeed, when chondrocytes are stimulated through various modes of injury, they often respond through the acquisition of a hypertrophied phenotype (characterized by COL10A1 expression) and lose their function in extracellular matrix maintenance and stabilization. As previously mentioned, 3-month Nrf2a treatment did not modify whole knee joint phenotypic manifestations of early OA. However, Nrf2a treated animals had increased aggrecan mRNA expression within articular cartilage, diffusely richer proteoglycan stores on all articular surfaces, and decreased femur and patellar individual surface OA scores. Although the consensus on aggrecan production and turnover in OA is somewhat controversial [97–99], reports have demonstrated that during the early stages of joint degeneration increased aggrecan production may serve a protective role in stabilizing the ECM and inhibiting more advanced joint destruction [34,40]. Of note, PB125 treated males demonstrate increased aggrecan expression and a simultaneous decrease in anabolic mediators (TGFβ, BMP-7, β-catenin) as well as decreased mTOR activity. Collectively, these pathways may enhance chondrocyte protein recycling through means of autophagy which may serve as a benefit in balancing knee joint homeostasis in early OA and pose a desirable secondary mechanistic property of PB125 beyond Nrf2 activation. Further, inflammatory cytokines (such as IL1β, TNFα, and C3) have been shown to not only increase the production of matrix metalloproteinases but also inhibit chondrocyte functional activity by decreasing the production

of vital ECM proteins, such as aggrecan, thus driving ECM dyshomeostasis and joint degeneration [34,100]. In this study both PB125 treated males and females demonstrated decreased IFP expression levels of MMP3 and complement C3 consistent with treatment serving a beneficial protective role in maintain cartilage homeostasis by delaying ECM degeneration and increasing aggrecan production, respectively. Lastly, articular cartilage from females treated with PB125 demonstrated increased expression of the anabolic growth factors TGFβ, β-catenin, and BMP-7 which, in the absence of concurrent histologic OA lesions, may suggest Nrf2a treated females are primed for ECM maintenance and may respond more rapidly or efficiently when cartilage damage is recognized and repair is needed [101–104].

Previously, Nrf2 has been recognized as an important mediator in cartilage homeostasis *in vitro* [71,81–83]. In this study PB125 treatment *in vivo* did not significantly alter medial tibial plateau Nrf2 expression at the functional level; however, compared to control males, control females had decreased Nrf2 expression and PB125 supplementation tended to increase Nrf2 activity selectively in females. In further support of this, we demonstrated altered transcriptional activity of a number of Nrf2-induced antioxidants in female articular cartilage and IFPs. More specifically, articular cartilage exhibited increased glutathione peroxidase activity, which may serve as a benefit as cartilage from human OA patients have significant down-regulation of the glutathione peroxidase gene [105]. Further, in the IFPs of females treated with PB125 there was increased thioredoxin and NQ01 expression. Thioredoxin, an NADPH-oxidase dependent antioxidant, serves as one of the main control mechanisms for recycling peroxiredoxins which ultimately mitigates hydrogen peroxide induced cellular stress. Overexpression of thioredoxins minimized joint destruction in a mouse model of inflammatory osteoarthritis [71,106]. NQ01, a Nrf2-induced quinone reductase, is uniquely relevant as it can reduce endogenous catechol estrogens generated in estrogen metabolism [107]. Under conditions of oxidative stress catechol estrogens undergo oxidation and become reactive quinones that drive the Fenton reaction, ultimately releasing toxic iron from ferritin and further perpetuating free radical damage [15,54,108,109]. Although the NQ01 immunoexpression along the medial tibial plateau was decreased with PB125 treatment, PB125 treated females demonstrated increased

transcriptional activity of NQ01 in the IFP which may play a protective role in local mitigation of estrogen-induced oxidative stress within the knee joint.

As the major presenting complaint in a clinical setting associated with OA is painful and/or decreased mobility [26,110], our group sought to characterize a number of functional and clinically relevant outcome measures. Traditional methods utilized to detect pain in rodents include behavioral based observational scoring systems; however, assessment of these behaviors in guinea pigs can be subtle, non-reproducible, and subjective [111]. In this study, overhead enclosure monitoring and computer-aided gait analysis were used to assess voluntary and obligatory functional mobility, respectively.

When exposed to an open field monitoring system, there were not significant effects of Nrf2a treatment on total distance traveled, average speed, or time spent mobile (Supplemental Table 2.3). This was not completely unexpected as at this early study endpoint animals do not always experience symptomatic disease. Of note, during enclosure monitoring Nrf2a treated animals spent significantly less time in hut, with significance driven by Nrf2a treated males. The clinical significance of this finding remains undetermined; however, it is plausible that time spent in hut may symbolize: (1) avoidance of new or threatening places; (2) anxiety-like behavior [68,112]; (3) its own type of movement noncompliance; and/or (4) may represent differences in nesting behaviors between the sexes.

As expected, propel time (time after the paw reaches maximum contact area during the stance phase of the stride [113]) steadily increased during obligatory running (at 55cm/sec) throughout the initial duration of the study. This fixed increase in propel time stabilized around 4-months of age, a time which represents cessation in long bone growth and skeletal maturity in the Hartley guinea pig [20]. As animals' femur lengths and thus stride length was increasing, the relative treadmill belt speed from the guinea pig perspective was somewhat decreased and likely accounts for this steady increase in propel time. Of interest, at 5-months of age, after skeletal maturity has been established, propel time is maintained in control animals but decreased in Nrf2a treated females. This decrease in propel time suggests a higher degree of strength and control in the propulsion phase of the gait cycle [113]. However, of note, as previously stated by *Poulet*

*at al.,* Digigait measurements of brake and propel time have not been validated by force plate analysis and this is an inherent limitation of this outcome variable [18].

This work has revealed that PB125 has the potential to both activate the Nrf2-pathway and also work through a vast number of other anti-inflammatory and anabolic pathways implemented in OA pathogenesis. However, as with all nutraceuticals, the efficacy and safety of this class of compounds is controversial as they are limited by their quality, structure, purification, and labeling which is variably regulated or completely unregulated in many countries [92,114]. Collectively, this work may serve as promise in future investigations looking at the utility of PB125 as novel nutraceutical in *delaying the progression* of OA during more advanced end-stage disease. Future studies are warranted to assess the efficacy of PB125 to potentially act as a SYSADOA when managing OA patients with long-term disease.

# CHAPTER 3: UTILIZATION OF A PHYTOCHEMICAL NRF2-ACTIVATOR DELAYS THE PROGRESSION OF OSTEOARTHRITIS IN THE HARTLEY GUINEA PIG

## 3.1: Overview

The aim of this chapter is to investigate the utility of prolonged PB125 Nrf2-activator treatment in delaying the progression of OA in the Hartley guinea pig. The foundation of this effort is based on the established premise that: (1) we have documented an age-associated decline in transcriptional and functional activity of Nrf2 in knee joint tissue (Chapter 1), and (2) during the early-stages of OA, PB125 treatment modified gait patterns and activity levels, transcriptional activity in articular cartilage and the IFP, and mitigated patellofemoral knee joint OA (Chapter 2). Thus, for this study we took the approach of long term Nrf2-activator supplementation starting at OA-onset (5-months) and continuing treatment throughout the middle (7-9 months) and end-stages (10-15 months) of disease to determine the long-term effects of prolonged Nrf2-activation on knee joint health.

## 3.2: Introduction

As introduced in section 2.2, current clinical treatment strategies for managing OA are lacking, which highlights a critical need to develop novel therapeutics to enhance functional mobility and improve quality of life in patients with OA. Continuous long-term treatment with Nrf2-activators is an intriguing management approach as Nrf2-activators have previously shown promise in lifespan extension in preclinical mouse models. More specifically, work from the National Institute of Health Interventions Testing Program (NIH-ITP) has demonstrated that the Nrf2-activator, Protandim, significantly increased median lifespan in male mice [115]. Nrf2-activators, particularly PB125, may hold potential in acting as a SYSADOA when managing OA patients with long-term disease. In support of this, we have demonstrated that 3-months of PB125 treatment in the early stages of OA modified functional mobility outcomes and transcriptional activity with guinea pig knee joint tissues. Further, in the early stages of OA Nrf2-activator treatment diminished OA pathology in the patellofemoral compartment. Thus, the aim of this chapter is to

investigate the utility of prolonged PB125 treatment in delaying the progression of OA during more advanced end-stage disease.

We hypothesized that animals treated for 10 consecutive months with PB125, initially during the onset of knee OA and continuously throughout OA development, would have differential gene and protein expression profiles within articular cartilage and the infrapatellar fat pad (IFP), decreased whole knee joint OA scores, and increased mobility during open field enclosure monitoring. The overarching goals of this chapter is to assess the utility of a novel phytochemical and Nrf2a in delaying the progression of clinical and/or structural manifestations of late-stage OA in the Hartley guinea pig.

## 3.3: Materials and Methods

### 3.3.1: Animals and Study Design

All Hartley guinea pigs (n=56, aged 4.5 months) were procured from Charles River Laboratories (Wilmington, MA). Procedures were approved by the university's Institutional Animal Care and Use Committee (19-9129A) and were performed in accordance with the NIH Guide for the Care and Use of Laboratory Animals. Animals were maintained at Colorado State University's Laboratory Animal Resources housing facilities and were monitored daily by a veterinarian. Guinea pigs were singly housed in solid bottom cages and provided *ad libitum* access to water and regular chow diet. Hay cubes were withheld to ensure that the main source of phytochemicals was limited to the oral Nrf2 supplement.

After a 2-week acclimation period, male (n=28) and female (n=28) Hartley guinea pigs (total n=56) were randomly assigned to receive treatment with the Nrf2 activator PB125 or the delivery vehicle control (Ora-sweet Sugar Free Syrup Vehicle®, Paddock Laboratories, Minneapolis, MN). Nrf2a pigs received 8 mg/kg PB125 suspended in 1mg/kg Ora-sweet SF® vehicle while control pigs received a volume-based vehicle equivalent, only. Animals began treatment at 5-months-old, were dosed daily in the morning for 10

consecutive months, and sacrificed at 15-months-old, when severe OA changes representing end-stage disease were expected in control animals.

### 3.3.2: ANY-maze™ Open Field Enclosure Monitoring

Animals were acclimated over a 2-week period, before the onset of the study, to an open circular field behavior monitoring system (ANY-maze™, Wood Dale, IL) to assess voluntary physical activity. Animals' activities were recorded, and data were collected for 10 consecutive minutes on a monthly basis throughout the study. Videos were analyzed for the following parameters: total distance traveled (m), average speed (m/s), time mobile (s), % time mobile, time in hut (s), % time in hut, and average moving speed (m/s). Additionally, guinea pig ANY-maze task noncompliance was documented as the refusal to move when exposed to the open circular field.

### 3.3.3: Harvests and Tissue Collection

Body weights were recorded immediately before harvest. Animals were anesthetized with a mixture of isoflurane and oxygen and transferred to a carbon dioxide chamber for euthanasia. Complete necropsy was performed by a veterinary pathologist to rule out comorbidities. The right hind limb was disarticulated at the coxofemoral joint. Upon arthrotomy, the articular surfaces of the knee were: (1) flushed with 500 µl PBS, (2) patellar, patella-femoral groove, femoral condylar, and tibial plateau surfaces, along with the menisci, were scraped and pooled cartilage flakes stored in RNALater, and (3) the IFP removed and stored in Allprotect Tissue Reagent. All tissues were stored at -80°C until further processing. The left hind limb was removed, left intact, stored *in situ* in 10% neutral buffered formalin for 48 hours and transferred to PBS.

### 3.3.4: Histology and OARSI Histopathology Grading

The left hindlimbs were decalcified over 6-weeks in $Ca^{2+}$EDTA. Limbs were trimmed in the coronal plane, embedded in cassettes, processed, and 5uM paraffin sections were mounted onto charged slides and

stained with toluidine blue. Slides were graded by a veterinary pathologist (in duplicate and random order, blinded to treatment group) based on established grading schemes provided by *Kraus et al.*[22].

### 3.3.5: Targeted mRNA Analysis Utilizing Nanostring

A custom NanoString nCounter 100-code gene panel for targeted mRNA analysis was utilized and consisted of Nrf2 and Nrf2 induced genes, as well as key mediators of inflammation and those implicated in OA pathogenesis. Total mRNA, from pooled articular cartilage or the IFP of the right knee joint, was extracted using TRIzol reagent and Qiagen RNeasy and RNeasy Lipid Mini Kits according to the manufacturer's instructions. Samples were analyzed in collaboration with Nanostring Technologies at the University of Arizona Genetics Core. Eukaryotic elongation factor 1 alpha (EFF1a) was used as a housekeeper gene for normalization. A complete gene list and normalized absolute mRNA counts from the articular cartilage and IFP are provided in Supplemental Tables 3.1 and 3.2, respectively.

### 3.3.6: Immunohistochemistry and Advanced Imaging

To semi-quantitatively assess selected gene expression outcomes at the functional protein level, IHC was implemented using antibodies against Nrf2 (ThermoFisher Scientific, PA-38312, rabbit polyclonal, dilution of 1:100) and NQ01 (Abcam ab34173, rabbit polyclonal, dilution of 1:400). Heat-induced epitope retrieval was performed on a Leica Bond-RX automated stainer using BOND Epitope Retrieval Solution 1 (citrate buffer) for 420 minutes at 55°C. Blocking was performed using 3% peroxide followed by 2.5% donkey serum. Labeling was performed on an automated staining platform. DAB was used as the chromogen and immunoreactions were visualized using commercial detection systems. Slides were counterstained with hematoxylin. Sequential steps of the immunostaining procedure were performed on negative controls following incubation. Photomicrographs from the medial tibial plateau were quantitatively analyzed by measuring the mean immuno-positive surface area using VisioPharm® software (Westminster, CO).

### 3.3.7: Statistics

Two-way ANOVA was utilized to evaluate the effects of sex and treatment on various outcome measures. Bonferroni's method was performed *post-hoc* for multiple comparison testing between groups. On all graphs, two-way ANOVA results and associated p-values are listed below the X-axis; significance was defined as a p-value $<0.05$ and a trend was defined $0.05<p<0.15$. Bonferroni's multiple comparison results are depicted on the graphs; significant differences are depicted using brackets and asterisk above the data points *(*$0.01<p<0.05$; ** $0.001<p<0.01$; *** $0.0001<p<0.001$; **** $p<0.0001$)*; trends (*$0.05<p<0.15$)* are depicted below data points with brackets and p-values.

Kaplan Meier curves combined with long rank and Gehan-Breslow-Wilcoxon tests were utilized to assess the probability of sustained voluntary mobility throughout the 40-week study period. The "event" was task noncompliance and defined as number of weeks into the study until an animal did not move (i.e., zero distanced traveled when exposed to the open circular field). Remaining individuals that maintained mobility throughout the entire 40-week study duration were censored at the 40-week study endpoint. All analyses were performed using GraphPad Prism Version 9.0 (San Diego, CA, USA).

### 3.4: Results

#### 3.4.1: Histology and OARSI Histopathology Grading

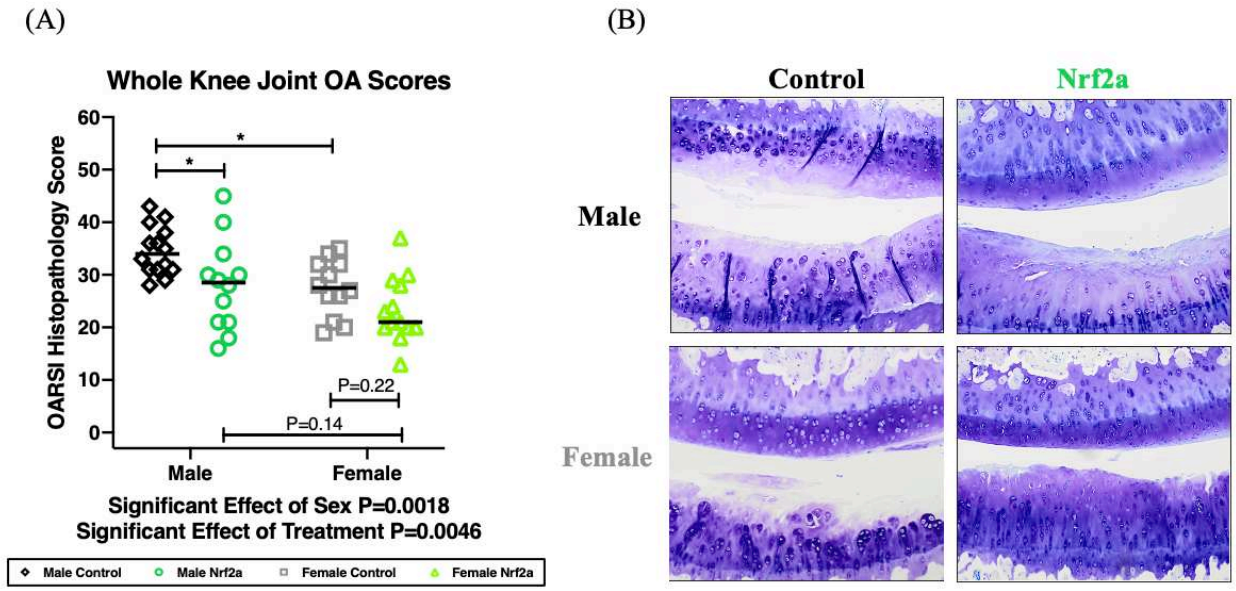


**Figure 3.1. Median OARSI histopathology scores for OA from control and Nrf2-activator treat guinea pigs.** (**A)** Whole knee joint median OARSI histopathology scores for OA in 15-month-old control and Nrf2a treated Hartley guinea pigs. (**B**) Representative medial tibial plateau toluidine blue photomicrographs from male (top row) and female (bottom row) control (left column) and Nrf2a treated (right column) Hartley guinea pigs. Femoral condyles and tibial plateaus are on the top and bottom of each image, respectively. *Toluidine blue, 40x *0.01<p<0.05; ** 0.001<p<0.01 ; *** 0.0001<p<0.001; **** p<0.0001*

There was a significant effect of sex and treatment on whole knee joint OA scores (**p=0.0018 and p=0.0045, respectively 3.1A**). Males had significantly higher OA scores compared to females. Nrf2a treatment significantly decreased whole knee joint OA scores; multiple comparison *post hoc* testing revealed significance was driven by Nrf2a-treated males. Representative toluidine blue photomicrographs of the femoral-tibial articulation are depicted in 3.1B. Severe degenerative changes representing end-stage disease are depicted in 15-month-old control animals; characteristic lesions include: loss of proteoglycan and chondrocytes in all three zones of cartilage, presence of hypertrophied chondrocytes and large multicellular chondrones, and fibrillations and clefts extending along the tidemark in between the deep zone

and calcified cartilage layer. Nrf2-activator treated males and females have proteoglycan and chondrocyte loss in all three zones, however articular cartilage structure is better maintained.

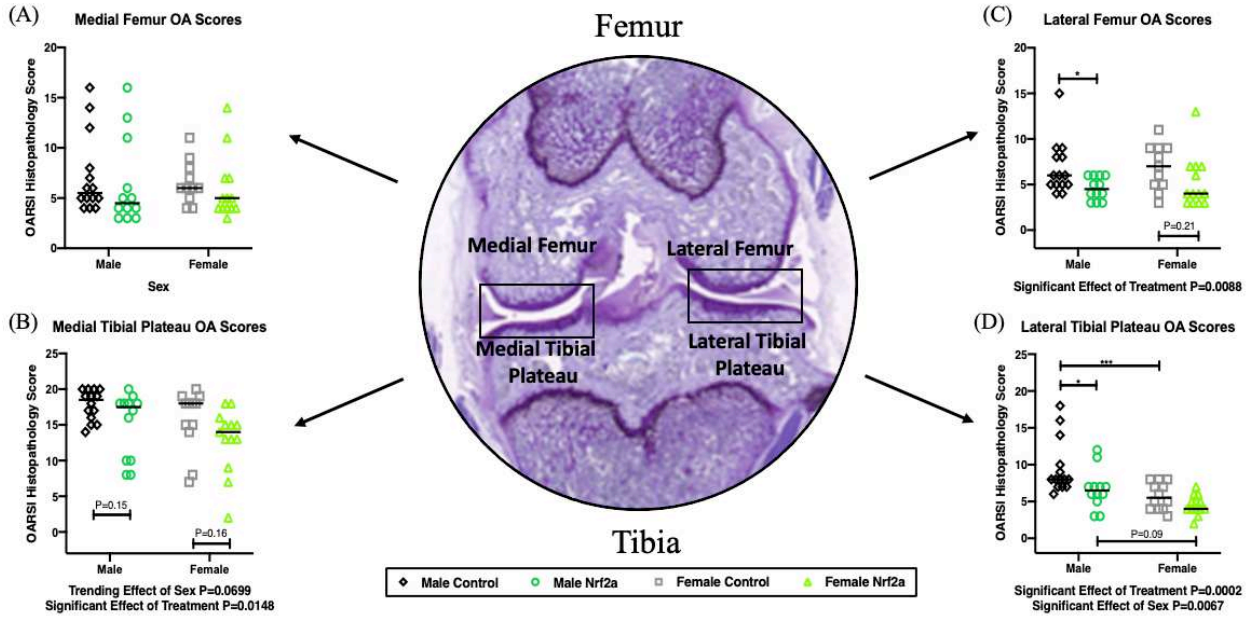


**Figure 3.2. Median individual surface OARSI histopathology scores for OA from control and Nrf2-activator treated guinea pigs.** Subgross toluidine blue photomicrograph of a guinea pig knee joint trimmed in the coronal plane and individual surface median OARSI histopathology scores for OA of the (**A**) medial femur, (**B**) medial tibial plateau, (**C**) lateral femur, and (**D**) lateral tibial plateau. **0.01<p<0.05; ** 0.001<p<0.01; *** 0.0001<p<0.001*

There is a significant effect of treatment on decreasing median medial tibial plateau (**p=0.01, Figure 3.2B**), lateral femur (**p=0.008, Figure 3.2C**), and lateral tibial plateau (**p=0.006, Figure 3.2D**) OA scores. Females have significantly decreased lateral tibial plateau median OA scores compared to males (**p=0.006, Figure 3.2D**).

### 3.4.2: Nanostring Targeted mRNA Analysis

#### 3.4.2.1: Articular Cartilage

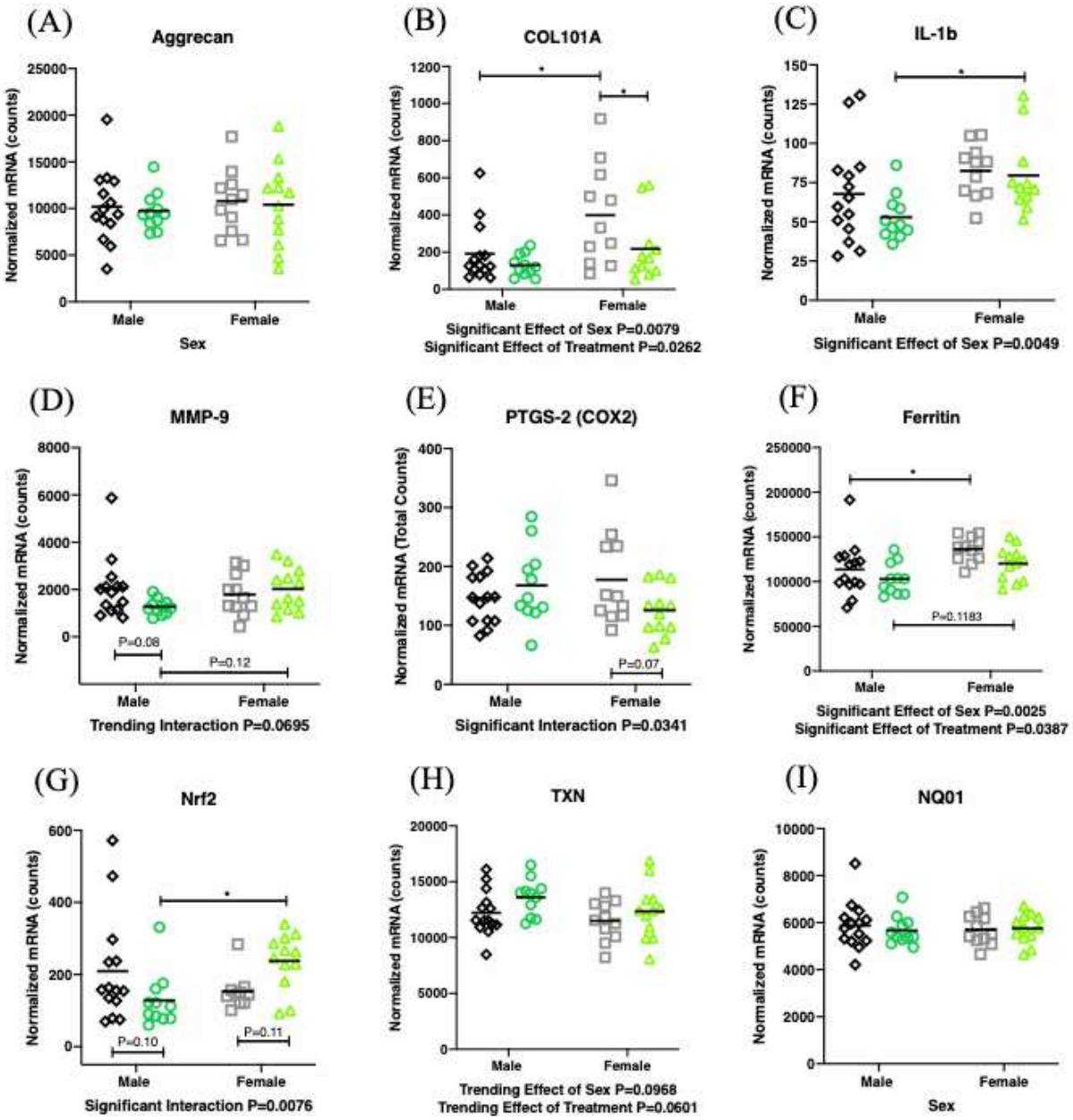


**Figure 3.3. Normalized mRNA counts for select extracellular matrix constituents, pro-inflammatory, catalytic, and Nrf2-signaling mediators expressed in control and Nrf2-activator treated Hartley guinea pig knee joint articular cartilage.** Articular cartilage mean mRNA expression levels of (**A**) aggrecan, (**B**) collagen type X alpha I chain (COL10A1), (**C**) interleukin-1 beta (IL1β), (**D**) matrix metalloproteinase-9 (MMP-9), (**E**) prostaglandin G/H synthase (PTGS-2, COX-2), (**F**) ferritin heavy chain, (**G**) nuclear factor erythroid-2-related factor-2 (Nrf2), (**H**) thioredoxin (TXN), and (**I**) NAD(P)H dehydrogenase quinone 1 (NQ01). *$*0.01<p<0.05$*

Ten-month treatment with a Nrf2a did not have significant effects on aggrecan expression (**Figure 3.3A**). There was a significant effect of sex (**p=0.008, Figure 3.3B**) and treatment (**p=0.03, Figure 3.3B**) on COL101A expression; control females had significantly higher COL101A expression levels compared to control males and Nrf2a supplementation significantly decreased COL101A expression in females (**Figure 3.3B**). Additionally, there was a significant effect of sex on IL-1β expression (**p=0.0049, Figure 3.3C**); females had higher expression levels compared to males. Nrf2a treatment tended to decrease mean IL-1β counts in both sexes. Nrf2a treated males had a trending (**p=0.08, Figure 3.3D**) decreased in MMP-9 expression. There was a significant (**p=0.03, Figure 3.3E**) interaction on the expression of PTGS-2; Nrf2a treated females had a trending (**p=0.07, Figure 3.3E**) decreased in PTGS2 expression. There was a significant effect of sex (**p=0.003, Figure 3.3F**) and treatment (**p=0.04, Figure 3.3F**) on ferritin expression; control females had significantly higher ferritin expression levels compared to control males and Nrf2a supplementation decreased ferritin levels in both sexes. There was a significant sex-treatment interaction on Nrf2 expression (**p=0.007; Figure 3.3G**). There was a trending effect of treatment on increasing thioredoxin levels (**p=0.06; Figure 3.3H**). Ten-month treatment with a Nrf2a did not have significant effects on NQ01 mRNA expression (**Figure 3.3I**).

### 3.4.2.2: Infrapatellar Fat Pad

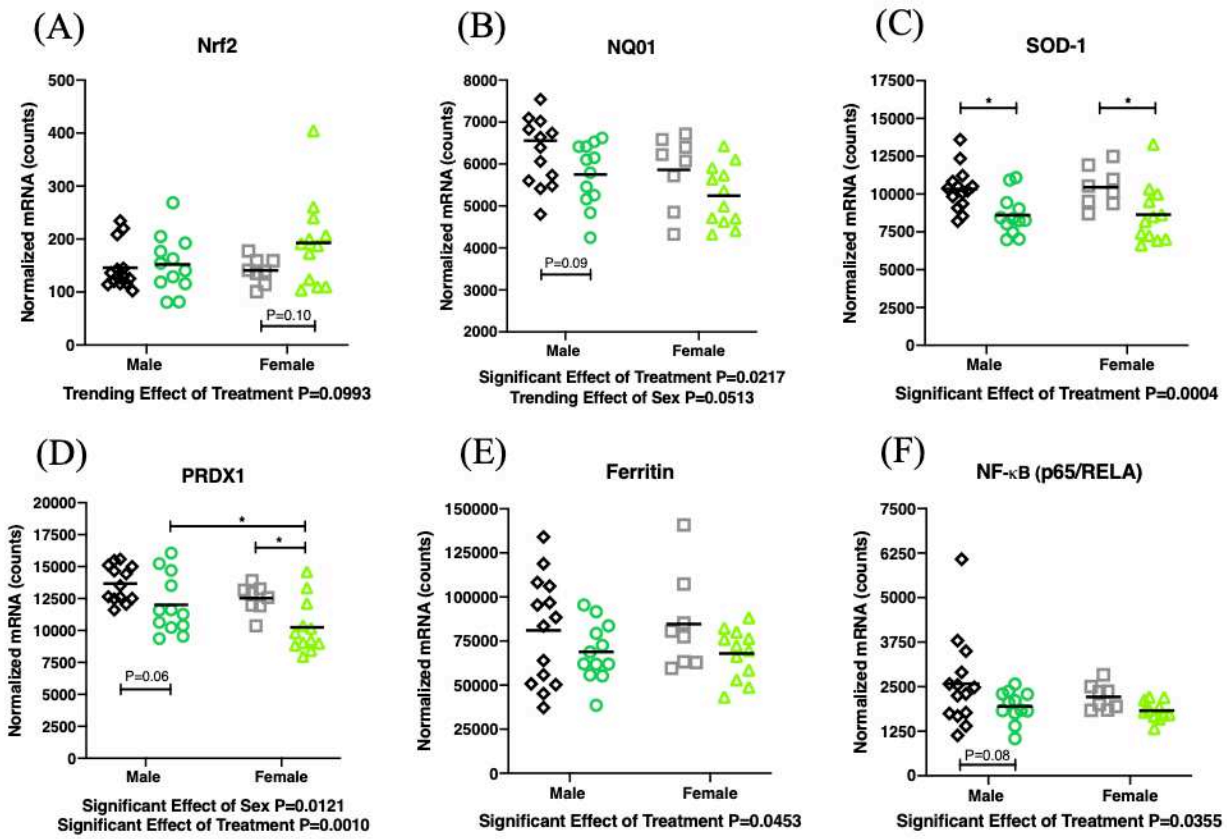


**Figure 3.4. Normalized mRNA counts for select Nrf2-ARE regulated genes, iron storage proteins, and inflammatory mediators expressed in control and Nrf2-activator treated Hartley guinea pig infrapatellar fat pads.** IFP mean mRNA expression levels of (**A**) nuclear factor erythroid-2-related factor-2 (Nrf2), (**B**) NAD(P)H dehydrogenase quinone 1 (NQ01), (**C**) superoxide dismutase-1 (SOD-1), (**D**) peroxiredoxin-1 (PRDX1), (**E**) ferritin heavy chain, and (**F**) nuclear factor κ-light-chain enhancer of activated B-cells (NF-κB, p65, RELA). **0.01<p<0.05*

There was a trending (**p=0.09, Figure 3.4A**) effect of Nrf2a treatment on increasing Nrf2 mRNA expression in IFPs. Nrf2a treatment significantly decreased IFP NQ01 (**p=0.02, Figure 3.4B**), SOD-1 (**p=0.0004, Figure 3.4C**), PRDX1 (**p=0.001, Figure 3.4D**), ferritin (**p=0.04, Figure 3.4E**), and NF-κB (**p=0.03, Figure 3.4F**) mRNA expression.

### 3.4.3: Immunohistochemistry and Advanced Imaging

#### 3.4.3.1: Nuclear factor erythroid-2-related factor-2

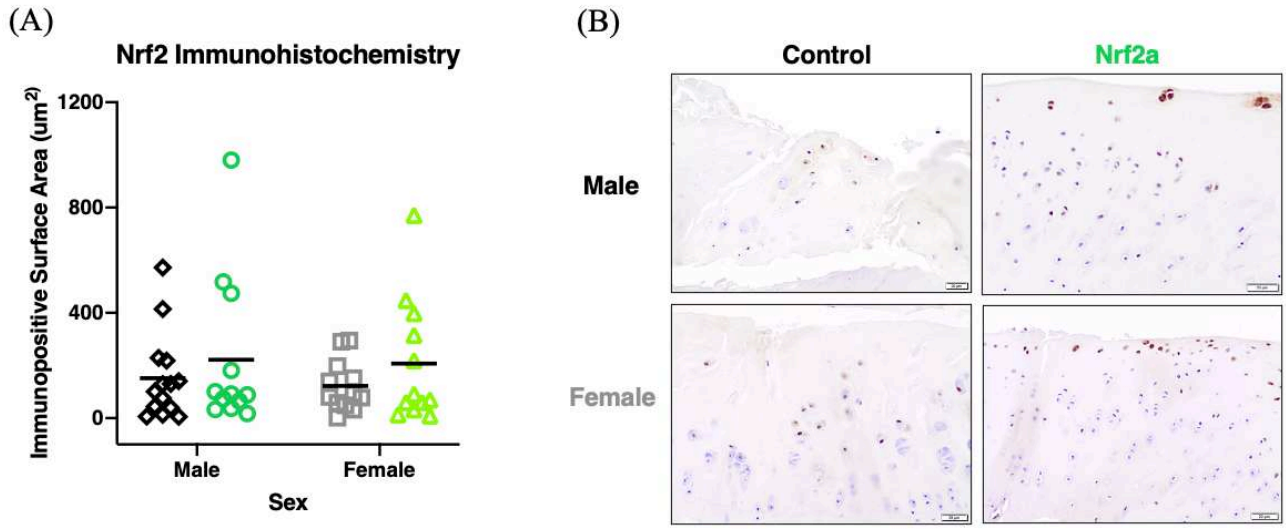


**Figure 3.5. Medial tibial plateau Nrf2 immunoexpression in control and Nrf2-activator treated Hartley guinea pigs.** (**A**) Nrf2 mean immunopositive surface area of the medial tibial plateau in 15-month-old control and Nrf2a treated Hartley guinea pigs. (**B**) Representative Nrf2 immunohistochemistry photomicrographs of the medial tibial plateau from male (top row), female (bottom row), control (left column), and Nrf2a treated (right column) Hartley guinea pigs. 40x; bar=20um; **0.01<p<0.05; **0.001<p<0.01; *** 0.0001<p<0.001; **** p<0.0001*

There were no significant effects of age, sex, or age-sex interactions on medial tibial plateau mean Nrf2 immunoexpression at the functional level. Of note, 15-month-old control animals exhibited more localized nuclear immunolabeling and Nrf2a treated animals exhibited more diffuse nuclear and cytoplasmic immunolabeling, with increased labeling intesity in regions of chondrocyte loss and matrix degradation.

### 3.4.3.2: NAD(P)H dehydrogenase quinone 1

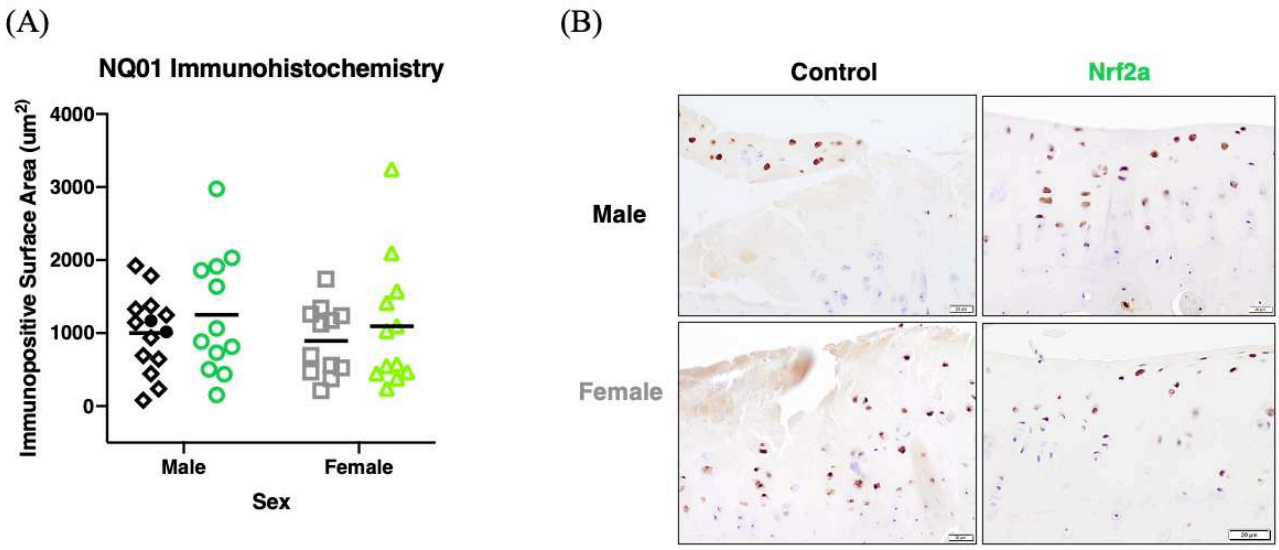


**Figure 3.6. Medial tibial plateau NQ01 immunoexpression in control and Nrf2-activator treated Hartley guinea pigs.** (**A**) NQ01 mean immunopositive surface area of the medial tibial plateau in 15-month-old control and Nrf2a treated Hartley guinea pigs. (**B**) Representative NQ01 immunohistochemistry photomicrographs of the medial tibial plateau from male (top row), female (bottom row), control (left column), and Nrf2a treated (right column) Hartley guinea pigs. 40x; bar=20um; **0.01<p<0.05; **0.001<p<0.01; *** 0.0001<p<0.001; **** p<0.0001*

There were no significant effects of age, sex, or age-sex interactions on medial tibial plateau mean NQ01 immunoexpression at the functional level. NQ01 labeling is primarily cytoplasmic in both control and Nrf2a treated animals.

### 3.4.4: Voluntary Mobility Determined by ANY-maze™ Open Field Enclosure Monitoring

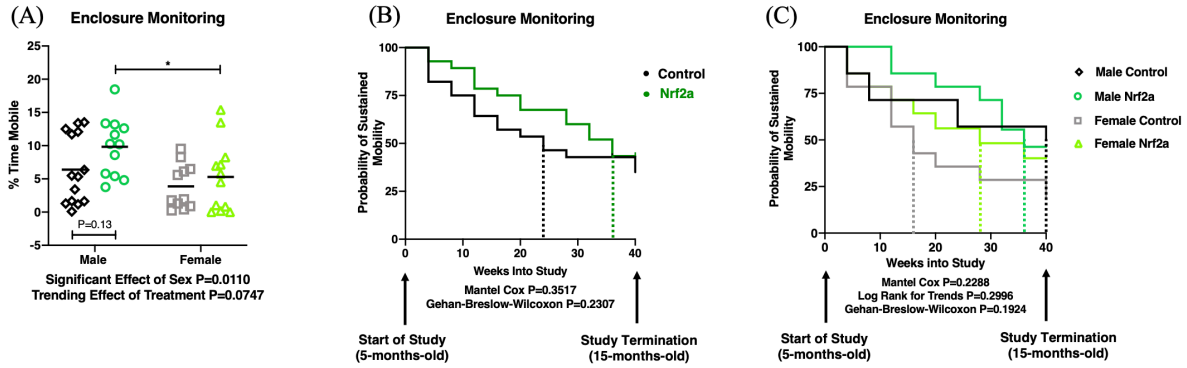


**Figure 3.7. Voluntary mobility determined by ANY-maze™ open field enclosure monitoring in control and Nrf2-activator treated Hartley guinea pigs.** (**A**) Mean percent time mobile at the 40-week study endpoint and (**B**) Kaplan-Meier curves depicting the probability of sustained mobility throughout the 40-week study period in control and Nrf2-activator treated guinea pigs. (**C**) Kaplan-Meier curves depicting individual group probability of sustained mobility throughout the 40-week study period. Dotted lines represent the age at which each group loses 50% mobility.

A snapshot of the percentage of time each group spent mobile after 10 consecutive months of treatment (representing the study endpoint) demonstrated significant effects of sex and trending effects of treatment on the percentage of time animals spent mobile (**p=0.01 and p=0.07, Figure 3.7A, respectively).** Males spent significantly more time mobile compared to females. Nrf2a treated animals tended to spend more time mobile compared to controls.

Kaplan-Meier curves depicting the probability of sustained voluntary mobility throughout the 40-week study period demonstrate Nrf2a treated animals are more likely to maintain mobility. Although not statistically significant, control guinea pigs tended to lose mobility more rapidly than those treated with a Nrf2a (**Figure 3.7B**, hazard ratio=1.402, CI=0.6884 to 2.856; median ratio=0.666, CI=0.3360 to 1.323). Further, PB125 treated males tend to have a relative increase in mobility compared to controls until about 32 weeks into the study. However, 50% of treated males loss mobility at 36 weeks, while 50% of control males maintained mobility the entire 40-week study duration (remaining animals were censored at this time). For the majority of the study, females treated with a Nrf2a maintained their mobility compared to female controls. Approximately 50% of control females loss mobility around 16 weeks, while Nrf2a treated females sustained voluntary mobility until about 28 weeks (**Figure 3.7C**, see vertical dotted lines).

### 3.5: Discussion

This study investigated the utility of a novel nutraceutical and Nrf2a in delaying the progression of end-stage OA in the Hartley guinea pig. Nrf2a supplementation was initiated at 5-months, administered orally daily, and the study was terminated at 15-months when severe OA representing end-stage disease was anticipated in control animals. Pharmacokinetic analyses demonstrated plasma levels of withaferin A, and luteolin peaked between 20-60 minutes post oral dosing (as determined by HPLC/MS/MS, see Supplemental Figure 3.1), thus, confirming adequate systemic delivery of these two components of PB125. We demonstrated that long term treatment with PB125: (1) mitigated knee joint OA, (2) modified articular cartilage and IFP gene expression profiles, and (3) modified voluntary mobility patterns characteristic of end-stage disease.

Histopathology and toluidine blue special stains revealed significant effects of Nrf2a treatment on mitigating whole knee joint OA scores. More specifically, PB125-treated animals had decreased OA scores along the medial and lateral tibial plateaus and within the lateral compartment of the femur. In accordance, Nrf2-activator treated females demonstrated a significant decline in articular cartilage Col10A1 expression. The role of Col10A1 expression in the development of OA is somewhat controversial as it is recognized as a minor collagen in the extracellular matrix; however, it also represents the only documented molecular marker of chondrocyte hypertrophy [116]. As chondrocyte differentiation and hypertrophy are essential for endochondral bone formation, increased Col10A1 activity in OA poses a detriment as it serves as a molecular driver of osteophyte formation and subchondral bone sclerosis, features which are both characteristic of end-stage disease. Despite this fact, in C57BL/6 and Balb/c mice there was a lack of Col10A1 expression in joint compartments prone to the development of OA [14]. However, in other mouse models, chondrocyte hypertrophy was stimulated in chondrogenic cell lines exposed to ROS and these cells subsequently underwent apoptosis and increased the production of markers of angiogenesis, and calcification, both *in vitro* and *in vivo* [117]. Further, this group demonstrated that treatment with an antioxidant, N-acetyl cysteine, decreased ROS and inhibited chondrocyte hypertrophy and apoptosis [117].

In accordance with these findings, 10-month treatment with PB125 diminished chondrocyte Col10A1 expression in both sexes; *post hoc* testing revealed significance was primarily driven in females. Thus, in our study, we suspect diminished Col10A1 expression may have played a protective role in delaying osteophyte formation and subchondral bone sclerosis, two pathologic hallmarks of end-stage disease.

Phytochemical Nrf2-activation with PB125 increased Nrf2 mRNA expression in female articular cartilage. Further, both PB125 treated males and female demonstrated increased articular cartilage expression levels of thioredoxin in 5-month-old (Chapter 2) and 15-month-old animals treated for 3-months and 10-months with PB125, respectively. As previously noted, thioredoxin, an NADPH-oxidase dependent antioxidant, serves as one of the main control mechanisms for recycling peroxiredoxins which ultimately mitigates hydrogen peroxide induced cellular stress. While some studies have demonstrated overexpression of thioredoxin minimizes joint destruction in models of inflammatory osteoarthritis [71,106], others have documented thioredoxin serves as a biomarker of oxidative stress in patients with rheumatoid arthritis [118]. In our study, patients with increased thioredoxin mRNA levels had diminished OA scores, suggesting this may play a beneficial role in idiopathic OA, potentially by combating ROS induced oxidative stress and inflammation by means of Nrf2-activation. We previously demonstrated 3-month Nrf2-activator treatment increased NQ01, thioredoxin, and glutathione peroxidase activity (Chapter 2); conversely, 10-month Nrf2-activator treatment decreased IFP ARE-dependent antioxidants NQ01, SOD-1, and peroxiredoxin. Of interest, the IFP also demonstrated decrease expression of NF-κB mediated inflammation. While the biological significance of this is unknown, it may plausible that transcription of these ARE-cytoprotective antioxidants is downregulated due to decreased need (i.e., increased stability at the functional level, and/or decreased local endogenous ROS stimulation) or long-term treatment with PB125 may result in local tolerance of Nrf2-activity in musculoskeletal tissues.

Nrf2 is emerging as a key regulator in iron, heme, and hemoglobin metabolism [54]. Of interest, knee joint tissue (articular cartilage and IFPs) from OA-resistant Strain 13 (S13) guinea pigs can detect and respond to systemic changes in iron status [119]. Further, systemic iron overload in S13 guinea pigs exacerbated OA and increased IL1-β and ferritin expression in knee joint tissue. This is in contrast to, but

consistent with our findings, as animals treated long term with a Nrf2-activator had diminished OA scores and decreased IL1-β and ferritin expression in both articular cartilage and the IFP knee joint compartments. Of note, Nrf2-activator treated guinea pigs had similar ferritin mRNA expression levels of those characterized in young S13 OA-resistant control guinea pigs [119]. In accord, transcriptional repression of ferritin reflects systemically low iron levels [120], which may serve as a benefit as increased ferritin levels are associated with symptomatic knee OA in man [121]. Future work is needed to rigorously assess the effects of Nrf2-activation on systemic and local iron stores at the function levels to determine the potential interplay between ROS, Nrf2, and iron metabolism in OA pathogenesis.

When assessing voluntary locomotor activity there was an increased trend in the percentage of time PB125-treated guinea pigs spent mobile while exposed to an open field. Mobility curves were not significantly different between groups; however, the likelihood (or probability) of immobility is lower in guinea pigs receiving Nrf2a-treatment. More specifically, the median time in which 50% of control guinea pigs lost mobility was 24-weeks into the study while 50% of Nrf2a treated guinea pigs sustained mobility until 36-weeks. When investigating the effects of sex, it is of note that Nrf2a treated females tended to sustain voluntary mobility compared to female controls. More specifically, the median time in which 50% of Nrf2a treated females sustained mobility was about 28-weeeks, while 50% of control females were immobile by week 16. Furthermore, Nrf2a treated males exhibited steady maintenance in mobility as characterized by a more gradual decline in steepness of their mobility curve up until about 32 weeks when compared to all other groups.

While this data provides a compelling link between PB125 treatment and mitigation of phenotypic and clinical characteristics of OA, there are inherit limitations. It is recognized that PB125 treatment was dosed once daily, and thus Nrf2 was only exogenously stimulated once per day. A potentially more beneficial approach may be lower Nrf2a doses more frequently administered throughout the day, perhaps in the food supply. However, supplementation in food poses a challenge, as commercial guinea pig food sources undergo heat treatments that could inactivate crucial phytochemical ingredients in PB125, and thus this is why we selected a once daily dosing strategy. Further, pharmacokinetic analyses demonstrated plasma

levels of withaferin A and luteolin peaked between 20-60 minutes post oral dosing, however; carnosol was not readily detected (Supplemental Figure 3.1). Of note, PB125 delivery was optimized in monogastric foregut fermenters and it is plausible that hindgut cecal fermenters, such as the guinea pig, may have significant effects on drug metabolism, transformation, and bioavailability. It is also possible that bioactive levels of carnosol peaked in between data points and thus was not detected by our collection methods. An additional limitation of this study was the lack of *in vivo* serial blood monitoring and *ex vivo* systemic organ histology and, thus, we cannot comment on the overall safety and systemic effects of long term PB125 and Ora-sweet Sugar Free Syrup Vehicle® control supplementation. However, no changes in food intake, weight, or gastrointestinal habits were observed during the study period. Further, as demonstrated in both our short term (Chapter 2) and long term (Chapter 3) studies, it is recognized that gene expression outcome measures do not always directly correlate to protein abundance and function. A plausible explanation for this is that samples collected for mRNA analyses were pooled from the tibial plateaus, femoral condyles and the menisci, however; immunohistochemistry was quantified exclusively along the medial tibial plateau. To better complement mRNA data, future work is necessary to investigate additional proteins and their functional abundance throughout the entire knee joint.

In conclusion, current clinical treatment and strategies for managing OA are limited which highlights a critical need to investigate novel therapeutics for disease management. Nrf2-activators, specifically PB125, may hold promise in acting as a SYSADOA when managing OA patients with long-term disease. Future studies are necessary to further evaluate the efficacy and safety of this nutraceutical in mitigating the age-related decline in structural and functional mobility associated with osteoarthritis in the elderly.

# CHAPTER 4: PHYTOCHEMICAL ACTIVATION OF NRF2 INCREASES FEMORAL LONG BONE STRENGTH IN SKELETALLY MATURE FEMALE HARTLEY GUINEA PIGS

## 4.1: Overview

An imbalance of reactive oxygen species and subsequent oxidative damage are emerging as key contributors to the pathogenesis of degenerative bone disorders, such as osteoporosis. Nuclear factor-erythroid 2-related factor-2 (Nrf2) is a transcription factor that serves as a master regulator of anti-inflammatory agents, phase I xenobiotic, and phase II antioxidant enzymes, all of which serve a cytoprotective role in combating disease progression. We hypothesized that oral administration of a novel phytochemical Nrf2-activator would increase long bone strength in aging Hartley guinea pigs prone to musculoskeletal decline. In this study we also characterized bone strength and structure in aging male and female Hartley Guinea pigs to assess the potential utility of this species as an animal model of age-related bone decline. Male (n=56) and female (n=56) guinea pigs were randomly assigned to receive daily oral treatment with either the Nrf2 activator PB125 or vehicle control for a consecutive 3-months (starting at 2-months) or 10-months (starting at 5-months). Outcome measures included: (1) ANY-maze™ enclosure monitoring, (2) biomechanical testing, and (3) quantitative microcomputed tomography. Treatment with a Nrf2-activator resulted in increased long bone strength as determined by ultimate bending stress, long bone stiffness, and femoral head trabecular number in aging female Hartley guinea pigs. Further, Nrf2-activator treatment decreased mid-diaphyseal cortical canal spacing. Collectively, this work suggests Nrf2-activation may serve as a promising target and preventive measure in managing the age-related decline in bone mass and quality and thus potentially fracture risk documented in patients with osteoporosis.

## 4.2: Introduction

The World Health Organization estimates that by the year 2050 the number of adults over the age of 60 will double, with the possibility of this demographic increasing from 605 million to 2 billion people [7].

Primary osteoporosis, the age-associated decline in both bone mass and quality, is a significant risk factor for fracture in aging populations. Anatomically, the most common location of osteoporotic fractures are the femur and vertebrae [122], both of which pose detrimental effects on overall quality of life. Like other age-related conditions, there is a growing body of evidence for a compelling link between age-associated increases in reactive oxygen species (ROS) and cellular oxidative stress with diminished bone quality and quantity, thus proposing that increased ROS serve as a central driver in the pathogenesis of osteoporosis.

Indeed, current literature suggests ROS are key contributors to osteoporosis via both steroid-dependent and steroid-independent mechanisms. The age-associated loss of sex steroids, most notably characterized in post-menopausal women, reportedly accelerates oxidant-induced effects of aging on bone via diminished estrogen receptor signaling [123]. Further, a mouse model of oxidative stress induced bone loss via antioxidant depletion (by means of experimental glutathione deficiency by buthionine sulfoximine administration) mechanistically mimicked ovariectomy-induced estrogen deficiency bone loss [124]. On a structural level, both male and female aging C57BL/6 mice demonstrate age-related decreases in bone strength, bone mineral density, remodeling, and formation rates. These changes were temporally associated with signaling pathways that increase ROS (via diminished glutathione reductase activity) and activate mediators of apoptosis (p53) and negatively modify markers of cellular longevity ($p66^{shc}$) [123]. On a cellular level, several groups have demonstrated increased ROS trigger osteoblast and osteocyte apoptosis, as well as osteoclastogenesis, all of which alter bone homeostasis, drive remodeling, and diminish bone quality and strength over time [123–125]. Collectively, there are a variety of ROS-sensing cells within musculoskeletal tissues that are responsible for bone modeling and remodeling, which can alter strength at the macroscopic tissue level [126].

Nuclear factor erythroid 2 related factor 2 (Nrf2) is a transcription factor that responds to oxidative stress by increasing the transcription of cytoprotective genes involved in a variety of cellular defense mechanisms. Functional alterations in Nrf2-signaling are implicated in a vast array of pathologies, including carcinogenesis and chemoprevention [75,127], cardiovascular [77,128], neurodegenerative [80], and inflammatory diseases [129].

Numerous studies are in support of Nrf2-activation playing a central role in bone matrix homeostasis and maintenance. More specifically, Nrf2 is known to play a pivotal role in fracture healing [130], bone resorption [131], and bone formation rates [132]. For the current study, our group utilized a novel Nrf2-activator (PB125, Pathways Bioscience, Denver CO) comprised of three synergistically acting phytochemicals (rosemary extract, ashwagandha extract, and luteolin) that collectively activate and stabilize the Nrf2-pathway [96]. Of interest, luteolin, one of the three active ingredients in PB125, supplementation alone decreased serum lipid peroxidase levels, increased glutathione peroxidase levels, and decreased the expression of the osteoclast marker NFATc1 in ovariectomized rats [133]. Further, curcumin was protective against hydrogen peroxide-induced stress and promoted osteoblast survival via GSK3β-Nrf2 signaling [132]. Unexpectedly, in a mouse model of inflammatory arthritis, Nrf2-knockout animals experienced unanticipated spontaneous bone fractures [134]. Based on these data, we have strong rationale for objectively testing the utility of PB125 to increase long bone strength in an animal model of musculoskeletal aging.

For this work we employed the Hartley guinea pig – a unique but underutilized preclinical model of musculoskeletal decline. Our group is interested in both the potential mechanistic and translational strengths of this strain in bone research as it holds potential as a useful preclinical model that may encompass systemic idiopathic musculoskeletal decline similar to humans. Of interest, skeletal maturity occurs around 3-4 months of age [20], and degenerative pathologies are well described in both skeletal muscle myofibers [21] and articular cartilage [22] by 15-months. As skeletal muscle dysfunction, articular cartilage degeneration, and bone remodeling and deterioration often occur jointly with aging [21,135,136], we sought to: (1) characterize the effects of age and sex on structural, geometric and mechanical long properties of on skeletally mature (5-month-old) and middle-aged (15-month-old) control Hartley guinea pig long bones and (2) determine the effects of short- and long-term administration of a novel phytochemical Nrf2-activator on long bone strength. We hypothesized that sex and age would have significant effects on long bone strength over time and that phytochemical Nrf2-activation would increase bone strength in male and female Hartley guinea pigs.

## 4.3: Material and Methods

### 4.3.1: Study Design

All Hartley guinea pigs (n=112) were procured from Charles River Laboratories (Wilmington, MA). Procedures were approved by the university's Institutional Animal Care and Use Committee (19-9129A) and were performed in accordance with the NIH Guide for the Care and Use of Laboratory Animals. Animals were maintained at Colorado State University's Laboratory Animal Resources housing facilities and were monitored daily by a veterinarian. Guinea pigs were singly housed in solid bottom cages and provided *ad libitum* access to water and regular chow diet. Hay cubes were withheld to ensure that the main source of phytochemicals was limited to the oral Nrf2 supplement. Animals were divided into two study groups, with both sexes equally represented.

Short term (3-month treatment group): Male (n=28) and female (n=28) Hartley guinea pigs (total n=56) aged 1.5 months were randomly assigned into the following groups: treatment with the Nrf2 activator (PB125) and control, with both sexes equally represented (n=14 per sex). Long term (10-month treatment group): Male (n=28) and female (n=28) Hartley guinea pigs (total n=56) aged 4.5 months were randomly assigned into the following groups: treatment with the Nrf2a and control with both sexes equally represented (n=14 per sex).

After a 2-week acclimation period, guinea pigs began a daily oral dosing regimen. Nrf2a pigs received 8mg/kg PB125 suspended in 1mg/kg Ora-sweet SF® vehicle while control pigs received a volume-based vehicle equivalent, only. Short term animals began treatment at 2-months-old, were dosed daily for 3 consecutive months, and sacrificed at 5-months-old. Long term animals began treatment at 5-months-old, were dosed daily for 10 consecutive months, and sacrificed at 15-months-old.

### 4.3.2: ANY-maze™ open field enclosure monitoring

Animals were acclimated over a 2-week period, before the onset of the study, to an open circular field behavior monitoring system (ANY-maze™, Wood Dale, IL) to assess voluntary physical activity. Animals'

activities were recorded, and data were collected for 10 consecutive minutes on a monthly basis throughout the study. Videos were analyzed for the following parameters: total distance traveled (m), average speed (m/s), time mobile (s), % time mobile, time in hut (s), % time in hut, and average moving speed (m/s) (Supplemental Table 4.1).

### 4.3.3: Harvests and Tissue Collection

Body weights were recorded immediately before harvest. Animals were anesthetized with a mixture of isoflurane and oxygen and transferred to a carbon dioxide chamber for euthanasia. Complete necropsy was performed by a veterinary pathologist to rule out co-morbidities. The right hind limb was disarticulated at the coxofemoral joint and the femur was isolated, wrapped in PBS-soaked gauze, and frozen at -18°C until further processing.

### 4.3.4: Quantitative Microcomputed Tomography (μCT) Bone Measurements

Prior to biomechanical testing, femurs were thawed to room temperature and suspended in PBS for μCT scanning. Right femurs were scanned using the Scanco μCT scanner (Model UCT80, Scanco Medical AG, Bruttisellen, Switzerland) at an intensity of 70kVp and 113mA, and an isotropic resolution of 37μm was obtained. Thresholds and regions of interest were selected and analyzed using Scanco Medical Evaluator software. Three regions of interest (ROI) were included: (1) mid-diaphyseal cortex (region receiving the constant moment load in the subsequent four-point bending experiments) and representative subchondral trabecular bone compartments of the (2) femoral head and (3) femoral condyle. ROIs were selected to determine the effects of sex, age, and Nrf2a treatment on skeletal tissue structure with known relatively low turnover (diaphyseal cortical bone) and high turnover (femoral head and femoral condyle cancellous bone) rates.

### 4.3.5: Biomechanical Testing

After μCT, destructive four-point bending was utilized to determine ultimate bending stress at failure. A custom-built, adjustable aluminum fixture was used in conjunction with a servohydraulic materials testing system (MTS 858 Mini-Bionix II, MTS Systems Corp., Eden Prairie, MN, USA) outfitted with a 5kN capacity load cell. The femoral head to femoral condyle distance was measured using digital calipers, and the inner jaws of the apparatus were pla ced 1/3 of the distance proximal to the condyles and distal to the femoral head (**Figure 4.1**).

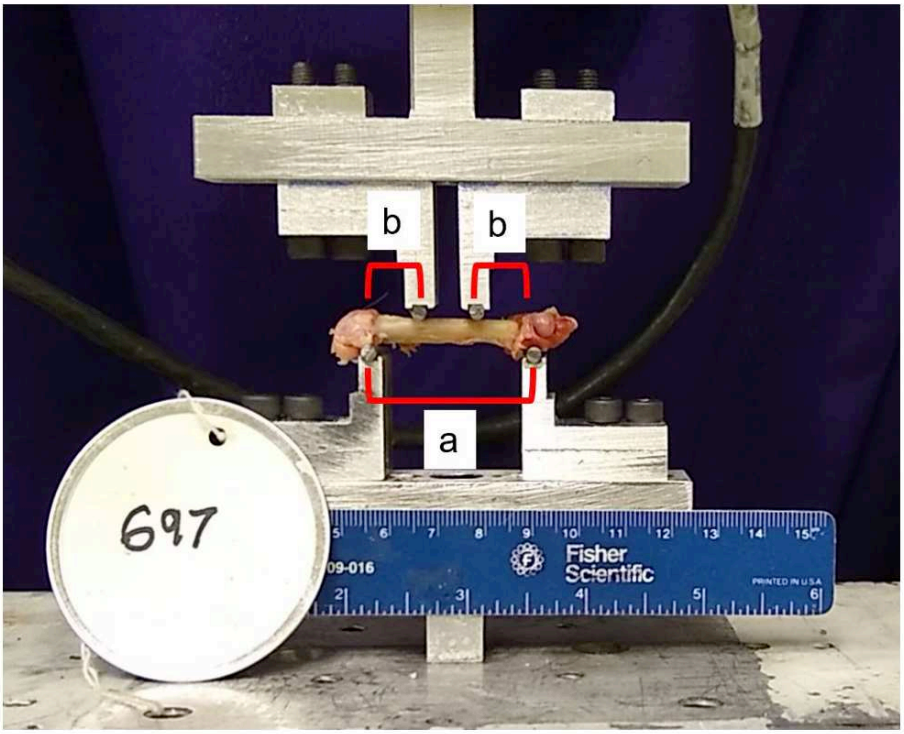


**Figure 4.1. Femoral four-point bending apparatus.** Femoral four-point bending apparatus displaying **(a)** lower bars set at the femoral head to femoral condyle length, and **(b)** upper bars inset at one-third of **(a)**. Force is applied to the anterior and mid-diaphyseal aspect of the right femur until failure.

A 1N load was used to reduce/eliminate system compliance and define the reference configuration. Subsequently, continuous crosshead displacement (0.1mm/s) was applied on the anterior mid-diaphyseal aspect of the right femur until bending failure was observed. Force-displacement data were transformed into moment-displacement data using the geometric configuration of the four-point bending apparatus. Force and geometry data were used to calculate bending stress ($\sigma$):

$$\sigma = M\,y/I$$

where M is applied bending moment (in N*mm), y is distance between the centroidal axis and the periosteal surface of the femur (in mm), and I is the area moment of inertia (in $mm^4$). Bending stress at failure was used as an assessment of long bone strength.

**4.3.6: Statistics**

Two-way ANOVA was utilized to evaluate the effects of age (5 vs 15 months) and sex on femoral long bone properties of vehicle control animals. Bonferroni's method was performed *post-hoc* for multiple comparison testing between groups.

To determine the effect of Nrf2-activator supplementation on femoral long bone mechanical property outcome measures, two-way (treatment, age) ANOVA's with Bonferroni's multiple comparison *post-hoc* testing was utilized. After grouped analyses (inclusion of sex), male and female guinea pigs were analyzed separately to determine the effect of Nrf2a on both sexes, independently. Further, unpaired Student's *t*-tests were utilized to evaluate each endpoint (5-months versus 15-months) and sex independently (Supplemental Tables 4.2 and 4.3).

On all graphs, two-way ANOVA results and associated p-values are listed below the X-axis; significance was defined as a p-value $<0.05$ and a trend was defined $0.05<p<0.15$. Bonferroni's multiple comparison results are depicted on the graphs; significant differences are depicted using brackets and asterisk above the data points *(* $0.01<p<0.05$; ** $0.001<p<0.01$; *** $0.0001<p<0.001$; **** $p<0.0001$)*; trends (*$0.05<p<0.15$)* are depicted below data points with brackets and p-values.

Correlation analyses were determined using Pearson tests; r-values, confidence intervals, and p-values are depicted in supplemental table 4.4. Data were analyzed in whole as a large group (n=112), and then analyzed with each sex and treatment separate (n=14). All analyses were performed using GraphPad Prism Version 9.0 (San Diego, CA, USA).

## 4.4: Results

### 4.4.1: Femur Strength, Structural Long Bone Properties, and Activity Levels of Aging Hartley Guinea Pigs

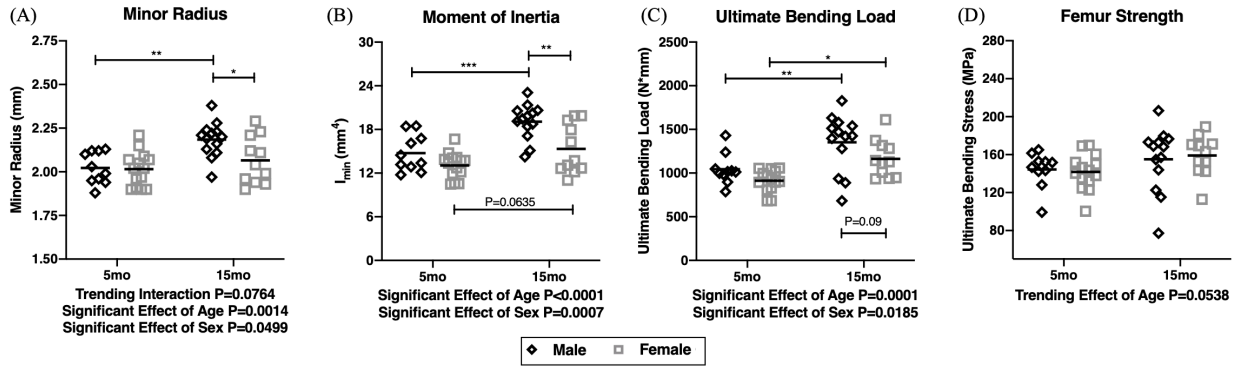


**Figure 4.2. Femoral long bone geometric and structural properties of young (5-months) and middle-aged (15-months) female and male Hartley Guinea pigs.** There is an age-associated significant increase in (**A**) minor radius, (**B**) moment of inertia, (**C**) ultimate bending load, and a trending increase in (**D**) femur strength. Females have significantly smaller radii (**A**) and decreased moment of inertia (**B**) and ultimate bending load (**C**). There is no difference in femur strength between the sexes. Means depicted with bars. * *0.01<P<0.05; ** 0.001<P<0.01 ; *** 0.0001<P<0.001; **** P<0.0001*

Femur strength was determined by destructive femoral four-point bending at 5-months and 15-months in male and female control guinea pigs. With age, and thus advanced skeletal maturity, there was a significant increase in body mass in both sexes; males weighed significantly more than females at both time points (Supplemental Table 4.2 & 4.3). Compared to 5-month-old animals, 15-month-old animals had a significant increase in femoral long bone geometric properties, experienced higher bending loads, and a trend for greater bone strength, as determined by minor radius and moment of inertia, ultimate bending load, and femur strength, respectively (**Figure 4.2**). Compared to age-matched males, females had significantly smaller radii, decreased moments of inertia, and decreased ultimate bending loads, yet there were no significant differences in overall strength (**Figure 4.2**).

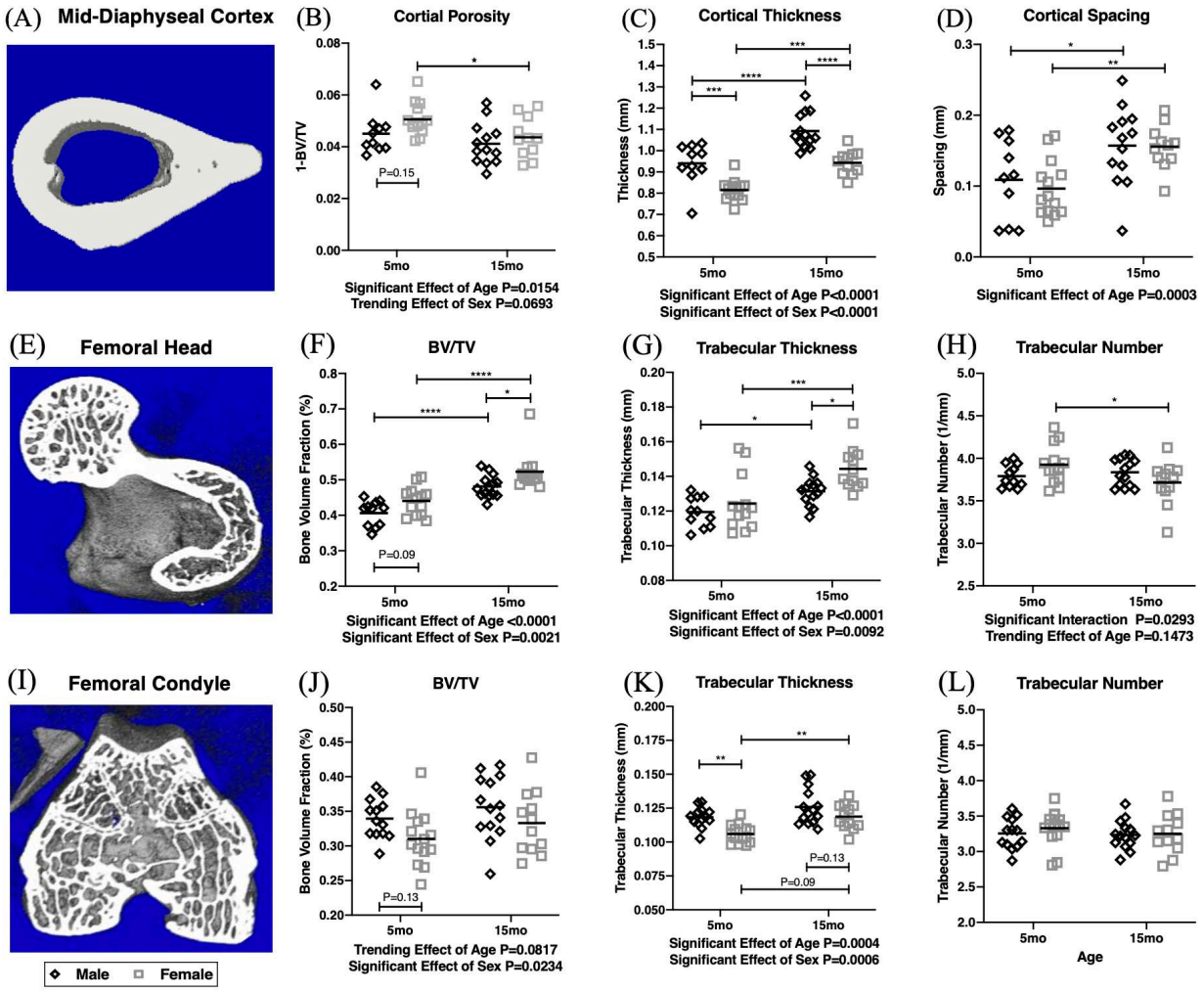


**Figure 4.3. Representative image renderings and selected microcomputed tomography structural properties of young (5 month) and middle-aged (15 month) male and female Hartley Guinea pigs.** Structural properties from the mid-diaphyseal cortex (**A-D**), femoral head (**E-H**), and femoral condyle (**I-L**). Means depicted with bars. * *0.01<P<0.05; ** 0.001<P<0.01 ; *** 0.0001<P<0.001; **** P<0.0001).*

Guinea pig age and sex had significant effects on femoral cortical (mid-diaphyseal) and trabecular (head and condyle) structural properties, as determined by μCT (**Figure 4.3**). These regions represent areas of relatively low and high bone turnover rates, respectively. Within the mid-diaphysis, there was an age-related increase in cortical thickness and canal spacing, with a decrease in cortical porosity (**Figure 4.3B-D**). Further, females had significantly thinner mid-diaphyseal cortices at both 5- and 15-months, compared to age-matched males (**Figure 4.3C**). Within the femoral head, there was an age-associated significant increase in bone volume fraction and trabecular thickness in both sexes (**Figure 4.3F-G**). However, when compared to sex-matched males, 15-month-old females had significantly increased femoral head bone

volume to trabecular volume (BV/TV) and trabecular thickness, yet an age-associated decline in femoral head trabecular number (**Figure 4.3F-H**). There was a significant effect of sex on femoral condylar trabecular bone microarchitecture. In contrast to femoral head cancellous bone properties, females had significantly decreased femoral condyle BV/TV and trabecular thickness compared to age-matched males (**Figure 4.3J-K**).

### 4.4.2: Open Field Enclosure Monitoring Activity Levels

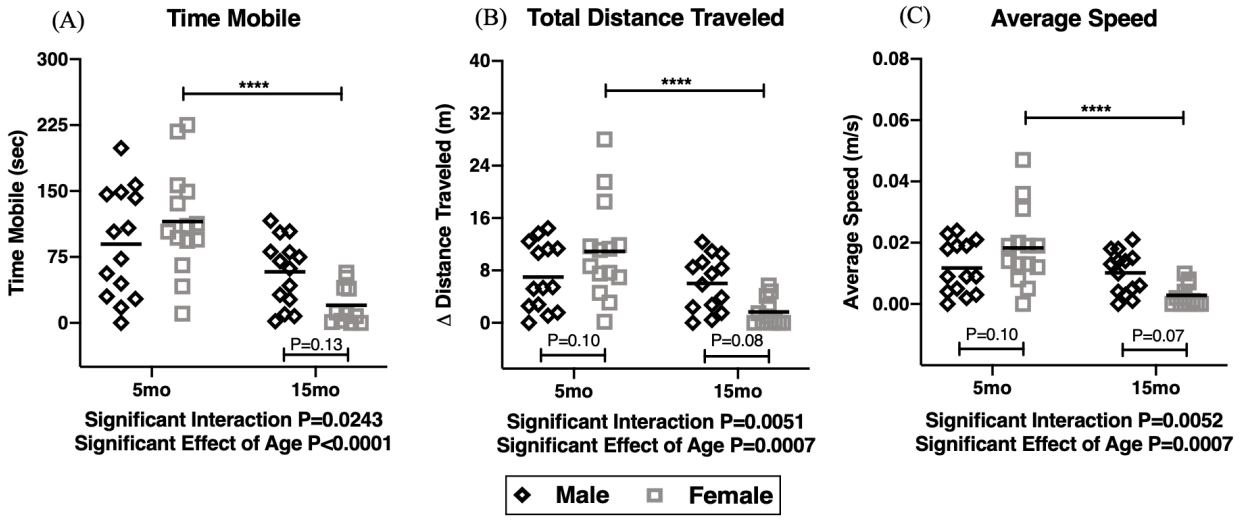


**Figure 4.4. ANY-maze open field monitoring.** There were significant interactions and effects of age on time mobile (**A**), total distance traveled (**B**), and average speed (**C**) when exposed to an open field for ten minutes. Means depicted with bars. * *0.01<P<0.05; ** 0.001<P<0.01 ; *** 0.0001<P<0.001; **** P<0.0001).*

ANYmaze™ enclosure monitoring revealed significant interactions and effects of age on Hartley Guinea pig activity levels (**Figure 4.4A-C**) when exposed to an open field for 10 minutes. At 5-months of age, compared to males, females tended to have increased activity, as characterized by increased time spent mobile (**Figure 4.4A**), increased mean distance traveled (**Figure 4.4B**), and increased average speeds (**Figure 4.4C**). In both sexes, aging significantly decreased the amount of time animals were mobile, the total distance traveled, and average speed (**Figure 4.4A-C**). Compared to their sex-matched counterparts, 15-month-old females spent significantly less time mobile, traveling significantly shorter distances and at a lower average speed (**Figure 4.4A-C**).

ANYmaze™ enclosure monitoring did not reveal any significant effects of Nrf2a treatment on male or female Hartley Guinea pig activity levels when exposed to an open field for 10 minutes (**Supplemental Table 1**). However, there was an inverse correlation between total distance travelled and ultimate bending stress (r=-0.2887, p=0.0050, Supplemental Table 4.4).

### 4.4.3: Effects of Nrf2-Activation on Long Bone Strength

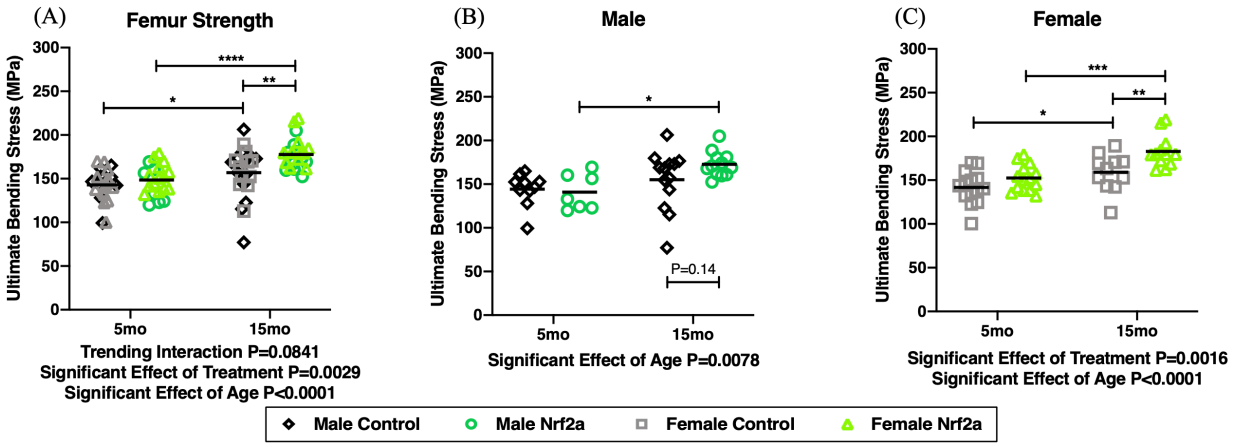


**Figure 4.5. Femur strength determined by femoral 4-point bending. (A)** Material properties of bone in 5-month and 15-month-old control and Nrf2-activator treated Hartley guinea pigs. (**B**) Material properties of bone in male and (**C**) females. Means depicted with bars * *0.01<P<0.05;* ** *0.001<P<0.01;* *** *0.0001<P<0.001;* **** *P<0.0001).*

There were no significant effects of long term Nrf2a supplementation on overall body mass (Supplemental Tables 4.2 and 4.3). Nrf2a treatment and treatment duration (3-month versus 10-month) significantly increased femoral ultimate bending stress at failure (**Figure 4.5A**). When investigating the effects of sex (**Figure 4.5B-C**), treatment-specific effects were predominately driven by 10-month Nrf2a treatment in females (**Figure 4.5C**).

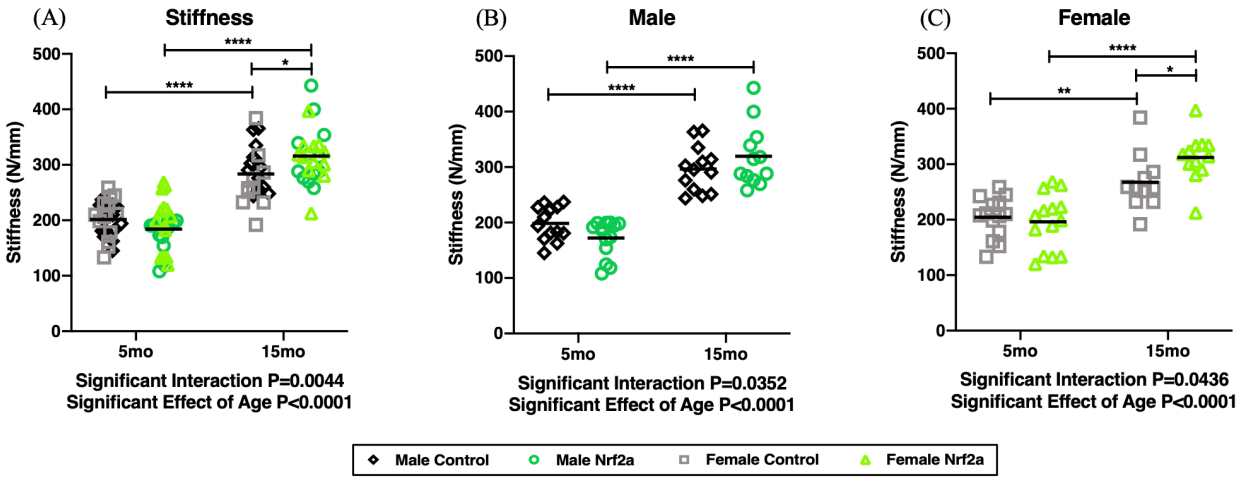


**Figure 4.6. Femur stiffness determined by femoral 4-point bending. (A)** Femur stiffness in 5-month and 15-month-old control and Nrf2-activator treated Hartley guinea pigs. (**B**) Femur stiffness in male and (**C**) females. Means depicted with bars ** 0.01<P<0.05; ** 0.001<P<0.01 ; *** 0.0001<P<0.001; **** P<0.0001).*

Fifteen-month-old animals treated for ten consecutive months with a Nrf2a demonstrated a significant interaction and effect of treatment duration on femur stiffness (**Figure 4.6A**); again, treatment-specific effects were also driven by long-term treatment in females (**Figure 4.6C**).


**Figure 4.7. Diaphyseal cortical spacing determined by microcomputed tomography. (A)** Cortical spacing in 5-month and 15-month-old control and Nrf2-activator treated Hartley guinea pigs. (**B**) Cortical spacing in male and (**C**) females. Means depicted with bars.

Lastly, there were significant effects of treatment on decreasing diaphyseal cortical canal spacing (**Figure 4.7C**) and increasing femoral head trabecular number (Supplemental Table 4.2) in long term treatment in females.

## 4.5: Discussion

The goals of our study were to: (1) characterize the effects of age and sex on skeletally mature (5-month-old) and middle-aged (15-month-old) Hartley guinea pig long bone properties to ultimately investigate the potential utility of this species as an animal model of age-related decline in bone qualities characteristic of early osteoporosis; and (2) determine the efficacy of long term Nrf2-activator treatment on increasing bone strength in this species. We demonstrated that both male and female control guinea pigs exhibit an increase in long bone strength from 5 to 15 months of age, and that 10-month supplementation with a Nrf2-activator significantly increased femoral strength in skeletally mature middle-aged females. ANYmaze™ enclosure monitoring characterized activity levels, and thus potential frequency of mechanical loading, on bone adaptations and overall strength in aging animals. There were significant interactions (age, sex) and effects of age on activity levels, but Nrf2a treatment had no significant effects on overall movement.

### 4.5.1: Characteristics of Aging on Male and Female Hartley Guinea Pigs Bone Properties

For this work we sought to better characterized bone strength and qualities in male and female Hartley guinea pigs as they represent a unique translational model of musculoskeletal aging that may encompass systemic idiopathic musculoskeletal decline similar to aging humans. Specifically, we were interested in investigating if the Hartley guinea pig may experience premature bone loss in the same timeframe as they experience joint degeneration [47] and muscle phenotypic shifts [21] characteristic of human aging.

On a microscopic level, commonly used rodent laboratory animals (mice and rats) in osteoporosis research are characterized by the predominance of primary bone over the lifespan with minimal to no osteonal remodeling with age [137]. In the guinea pig, primary bone predominates over their lifespan; however, with some regional variability, secondary osteons develop with age, which may better mimic remodeling properties of human bone. Thus, we investigated the biomechanical and microarchitecture properties of Hartley guinea pig long bones to better estimate their proximate bone age and translational utility compared to humans.

In our study, a number of biomechanical and microarchitecture outcome measures insinuate 15-month guinea pigs embody, from a bone perspective, skeletally mature middle-aged humans, rather than more advanced phases of bone loss characterized in aging populations. Compared to 5-month-old control animals, 15-month-old control animals had increased bone bending strength, and microcomputed tomography revealed a significant increase in: (1) diaphyseal cortical thickness, (2) femoral head BV/TV, and (3) femoral head trabecular thickness, while a decrease in cortical porosity. Collectively, these age-related changes in bone microarchitecture may represent normal growth patterns associated with skeletal maturity – including bone growth, modeling, and perhaps peak bone mass in this species – all of which contribute to the overall increase in the bending strength data observed at 15-months.

When investigating sex differences, specifically changes in bone microarchitecture and remodeling, as well as activity levels, female Hartley guinea pigs exhibit some early bone changes that necessitate further characterization of the effects of advanced aging on bone qualities in this strain. For example, at 5-months of age, a time point at which skeletal maturity should be reached, there is no significant difference between male and female minor bone radius; however, compared to males, females have significantly thinner diaphyseal-cortices. With age, there is no change in female radii; however, there is an increase in overall cortical thickness that may suggest limited endocortical resorption but increased periosteal apposition or proliferation, consistent with appositional growth after drift cessation [138]. In contrast, males demonstrate an age-associated increase in minor radius as well as an increase in cortical thickness, which may imply a balance between endocortical resorption and periosteal apposition, consistent with continued diametric modeling and cortical drift. These findings may propose key sex differences in the timeframe at which bone modeling is complete and remodeling is initiated. Specifically, compared to age-matched males, females may reach earlier transition times from modeling to remodeling, a finding which may suggest females demonstrate earlier onset skeletal maturity, and thus slightly advanced tissue aging, compared to age-matched males.

It is well recognized that physical inactivity diminishes the frequency of muscular contractile forces, and thus frequency of mechanical loading on bone, which serves as a clinical risk factor for bone resorption and

fragility fractures [139]. Open field monitoring revealed that with age Hartley guinea pigs are essentially inactive, and *post hoc* statistical analyses demonstrated 15-month-old females spent significantly less time mobile, traveling significantly shorter distances and at a lower average speed compared to their sex-matched 5-month counterparts. This natural age-related decline in mobility may serves as a clinically relevant and translational risk factor and warrants further investigation of more senior aged animals as a tractable model of inactivity- and age-related bone degeneration.

In this study, we selected the 5- and 15-month endpoints because these two ages represent a time in which there are consistently early and advanced indications of idiopathic joint degeneration and muscle remodeling, respectively. We acknowledge, and the current study has emphasized (as demonstrated by the increasing femur strength, trabecular and cortical measurements), that this age is not optimal to assess the effects of aging on bone turnover in this strain or species. BALB/C mice show age-related decrease in material properties of long bones around 20 months and numerous reports have documented the acceleration of bone loss when combined with early gonadectomy [123,140]. When considering the prolonged maximum lifespan of the companion guinea pig (12 years) compared to the Hartley guinea pigs (4-7 years), mice (2 years), and rats (4 years) [141], future work is needed to investigate bone quantity and quality at later ages, with and without gonadectomy.

### 4.5.2: Effects of Nrf2-Activation on Femur Strength in Hartley Guinea Pigs

We demonstrated, via destructive femoral 4-point bending, that 10-months of daily oral supplementation with a Nrf2-activator significantly increased femoral ultimate bending stress at failure and femur stiffness in middle-aged skeletally mature female Hartley guinea pigs. Strength, stiffness, and toughness are important mechanical parameters that are indicative of resistance to fracture [142]. It is well documented that mechanical loading enhances the anabolic activity of bone (Wolff's law) and thus may increase its strength [143]. In this study, there were no significant effects of Nrf2a treatment on overall body mass nor activity levels; yet there was an inverse correlation between ultimate bending stress and both body mass and activity levels in females treated for 10-months with a Nrf2a (Supplemental table 4). This finding may

suggest an alternative underlying mechanism, other than increased body mass or muscle adaptations, may be responsible for increased bone strength. It is well documented that bone mineral density (BMD) accounts for 70-75% of the variance in strength [144,145]. Although we did not explicitly measure BMD in this study (an inherent limitation of this study), we did not see significant effect of Nrf2a administration on other mineralized bone measurements such as trabecular BV/TV or cortical porosity. We hypothesize that alterations in bone microarchitecture and/or material tissue composition may be responsible for the increased bone strength and stiffness with Nrf2-activator supplementation.

Nrf2-activator treatment in 15-month-old female Hartley guinea pig significantly improved a number of architectural properties such as mid-diaphyseal cortical canal spacing and, femoral head trabecular number. An increase in femoral head trabecular number is of particular interest as this may be a beneficial adaptation in fracture resistance as femoral neck fractures are one of the most commonly reported morbidities in the osteoporotic condition [122].

In addition to bone mass and microarchitecture, the material tissue composition of bone is known to significantly effect bone turnover and contribute to overall bone strength [146]. Insights into rare musculoskeletal diseases, such as osteogenesis imperfecta and osteopetrosis, highlight the fundamental role of matrix constituents as these patients may have normal to increased bone mass and architecture but disrupted collagen cross-linking and mineralization [20]. We hypothesize that the effects of Nrf2a activation in aged females may mechanistically increase bone strength via modulation of remodeling signals that enhance bone matrix composition on the cellular and subcellular level.

In contrast to, but consistent with our findings, Nrf2 deficiency (C57BL6/129SV $Nrf2^{-/-}$) significantly decreased femoral long bone and vertebral compression strength as determined by femoral 3-point bending and lumbar vertebral compression testing, respectively [148]. These Nrf2-knockout mice also had significantly decreased vertebral stiffness, a finding inversely consistent with our study given that phytochemical activation of Nrf2 significantly increased 15-month-old female Hartley guinea pig femur stiffness. Further, Ibáñez et al. demonstrated that both sham-operated and ovariectomized Nrf2 deficient (C57BL/6J $Nrf2^{-/-}$) mice had significantly reduced volumetric bone mineral density in femoral cancellous

bone as well as reduced cortical bone area in the lumbar vertebrae [149]. Thus, Nrf2 may be required for homeostasis and Nrf2-activator supplementation may increase anabolic effects on bone.

On a cellular level, Nrf2 deficiency promotes RANKL-induced osteoclastogenesis and the formation of resorption pits by means of increased oxidative stress and diminished antioxidant levels [131]. In our study, there was a significant interaction between sex and treatment on the expression of RUNX2, a gene implemented in osteoblastogenesis, in musculoskeletal tissue from animals treated for 3-months with a Nrf2a; Nrf2a treated males trended towards decreased expression while treated females had increased RUNX2 expression (Supplemental Table 2.1). These findings may further suggest that Nrf2-deficiency induces osteoclastogenic effects, while Nrf2-activity stimulates osteoblastogenic effects on musculoskeletal tissues. Collectively, these findings demonstrate that the Nrf2 pathway plays a dynamic role in bone metabolism and maintenance, may enhance bone formation, and potentially serve as a therapeutic target in osteoporotic patients.

An inherent limitation in this study is that both age and treatment effects are reflected in the comparison between groups. Future work includes more rigorously controlling for age and treatment effects, investigating the utility of Nrf2-activators on bone matrix composition at the cellular and subcellular level, and exploring the utility of more senior-aged Hartley guinea pigs as a natural model of osteoporosis. Further, in addition to assessment of biomechanical stress, we plan to measure biomechanical strain and thus characterize femur toughness, which will provide a more comprehensive assessment of mechanical parameters that contribute to overall fracture resistance. In conclusion, this study demonstrates that Nrf2-activation enhances long bone strength in aging female Hartley guinea pigs, findings of which may serve as promise in the utilization of Nrf2-activators in the clinical management of age-related bone disorders.

# CHAPTER 5: CLINICAL AND HISTOLOGIC MANIFESTATIONS OF A NOVEL RECTUS FEMORIS MYOTENDINOUS JUNCTION INJURY IN RATS

## 5.1: Overview

Animal models of muscle injury have primarily relied on methods which do not mimic chronic scarring that typically occurs adjacent to the myotendinous junction (MTJ). The goal of this study was three-fold: (1) to create a strain-induced *in vivo* model of rectus femoris MTJ injury in rats; (2) to document clinical manifestations of injury using longitudinal tracking of individual animals via voluntary and compulsory (treadmill) mobility analysis and (3) to validate and assess the model for persistent scarring through serial histologic assessment and development of a semi-quantitative grading scheme to characterize injury response over time. Strain-induced MTJ injury was generated in male Sprague Dawley rats via needle tension directed along the transverse axis between the rectus femoris muscle and distal tendon that attaches to the patella. Animals received mobility assessments (gait analysis using a DigiGait Treadmill System and weight bearing using a Tekscan Rodent Walkway System) at days 0, 1, 3, 6, 13, 20, and 27 of the experimental protocol. Rats were euthanized at 1-, 3-, 7-, 14-, and 28-days post-injury (n=6 rats per time-point) and hindlimbs were processed for histology. Significant changes in locomotor parameters included injured and contralateral limb paw area, max dA/dt (limb deceleration/breaking time), stride time, stance time, force time impulse, and fore/hind symmetry, and injured limb maximum force. The most significant and consistent histologic finding was a pathologic fibrotic adhesive lesion at the muscle and tendon interface along the proximal aspect of the patella just distal to the injury site**.** This lesion was composed of reactive fibroblasts, disorganized collagen fibers, vascular profiles, and a myxomatous ground substance stroma. This work is the first to characterize the clinical and pathologic development of a chronic model of rectus femoris MTJ injury, which results in altered mobility likely caused by a strain-induced fibrotic scar along the anterior patella. Notably, both the functional and pathologic changes recapitulate the course of injury progression similar to what is described in humans. This work provides a unique model to study MTJ

injury mechanisms for the identification of enhanced treatment options for patients who suffer from activity-related muscle conditions.

### 5.2: Introduction

The myotendinous junction (MTJ) is as a highly specialized transition zone composed of many interacting tendinous and muscular filaments, which contribute to physiologic adhesion and anchoring [150]. This site is responsible for the transmission of force between the muscle, tendon, and bone, which ultimately dictates skeletal movement and gait patterns. As the connection between two different tissue types, the MTJ represents the weakest link along the greater muscle-tendon unit, making it highly vulnerable to tension-induced impairment [151,152]. Activities that induce eccentric loading, such as high-speed running and kicking, pose an increased risk of MTJ injury [153]. While the mechanical contributions of MTJ strains (stretch) during eccentric loading are fairly well described [153,154], little is known about the clinical (gait and weight bearing parameters) or structural (histopathologic) responses to injury.

The quadriceps, hamstrings, and gastrocnemius muscles are uniquely prone to MTJ injury due to their superficial location and extension across two joints [151,155]. Indeed, lower limb orthopedic injuries affect 25-48% [156–158], 62.4% [159], and 32.3% [160] of military, athletic, and occupational populations, respectively, with strains of the aforementioned muscles accounting for the majority of these conditions. Depending on the severity of MTJ injury, patients present with swelling, tenderness, and pain [161]. Due to the complicated structural organization and cell signaling at the MTJ, endogenous healing for structural and functional recovery is difficult. Current treatment regimens for MTJ injuries remain conservative and include the RICE method (rest, ice (cold), compression, elevation) followed by gradual exposure to physical exercise modalities [151]. If not addressed, persistent scarring within the muscle directly adjacent to the MTJ can lead to reduced flexibility, weakness, and muscle atrophy, making previous injuries a leading risk factor associated with injury recurrence [156,162,163]. Therefore, the controlled study of MTJ injury progression in a clinically relevant pre-clinical model may allow for the development of novel therapeutics and treatment strategies for patients who suffer from such injuries.

Animal models of muscle injury include chemical [164], traumatic [165–167], acute high intensity exercise [168], contusion [166,169,170], and contraction [171] methods. While valuable, the majority of current models do not specifically target the MTJ, a common site of clinical strain-induced activity-related injuries [151,152]. Recently, a model of gastrocnemius MTJ injury was developed in the rat [172]. Through a needle core puncture directed along the transverse axis of the MTJ, grade I-II muscle lesions were generated as early as 1-day post-injury. Of note, muscle lesions in this model resolved by 26-46 days post-injury. Similarly, models that utilize mechanically and tetanically induced strain injuries replicate acute muscle damage near the MTJ without lesion development [173,174]. While these provide suitable models of inherent muscle regeneration and healing, a model that recapitulates the persistent scarring seen clinically would be advantageous for testing new methods of clinical management and reduction of re-injury rates. Therefore, the development of a chronic animal model is needed to better characterize factors leading to high re-injury rates and investigate interventions that may expedite patient recovery.

While gastrocnemius MTJ injury has been studied to date [172], no published reports exist that employ an animal model of quadriceps MTJ injury. The most commonly reported site of quadriceps MTJ injury in humans is the distal MTJ of the rectus femoris muscle belly where it inserts on the proximal aspect of the knee joint [153,175,176]. More specifically, given its short length, MTJ injuries of the rectus femoris usually occur near the osteotendinous junction approximately 2cm from the insertion of the quadriceps tendon on the patella [177]. Indeed, as a bipennate muscle with short muscle fibers, a steep oblique tendon attachment, and a large MTJ transition zone [178], the rectus femoris is highly susceptible to strain during stretching [179]. Owing to this, the goal of this study was to create a strain-induced in vivo model of rectus femoris MTJ injury in rats. Findings were characterized by: (i) documenting clinical manifestations and progression of injury using longitudinal tracking of individual animals via voluntary and compulsory (treadmill) mobility analysis; and (ii) validating and assessing the model for persistent scaring through temporal histologic assessment and development of a semi-quantitative grading scheme to characterize injury response over time. The controlled study and application of this model of MTJ injury may allow for the development of novel therapeutics and treatment strategies for patients who suffer from such injuries.

## 5.3: Materials and Methods

### 5.3.1: Animals

All procedures were approved by the university's Institutional Animal Care and Use Committee (Protocol #16-6927A) and were performed in accordance with the NIH Guide for the Care and Use of Laboratory Animals. Thirty (30) male Sprague Dawley rats were purchased from a commercial vendor (Charles River Laboratory, Wilmington, MA) at 70 days of age and allowed to acclimate to the vivarium for 14 days. A single sex was chosen to standardize the model as 1) injury severity was dictated by the needle size relative to the targeted region, 2) rectus femoris injury in males is better characterized clinically, and 3) due to their size, males offered a larger targeted area for initial model development. Animals were monitored daily by a veterinarian. All rats were housed singly in solid bottom cages with corncob bedding and were maintained at 22–24 °C on a 12-h light/dark cycle. Commercially available irradiated water and food were available ad libitum during the experiments.

### 5.3.2: Rectus Femoris Injury at the Myotendinous Junction

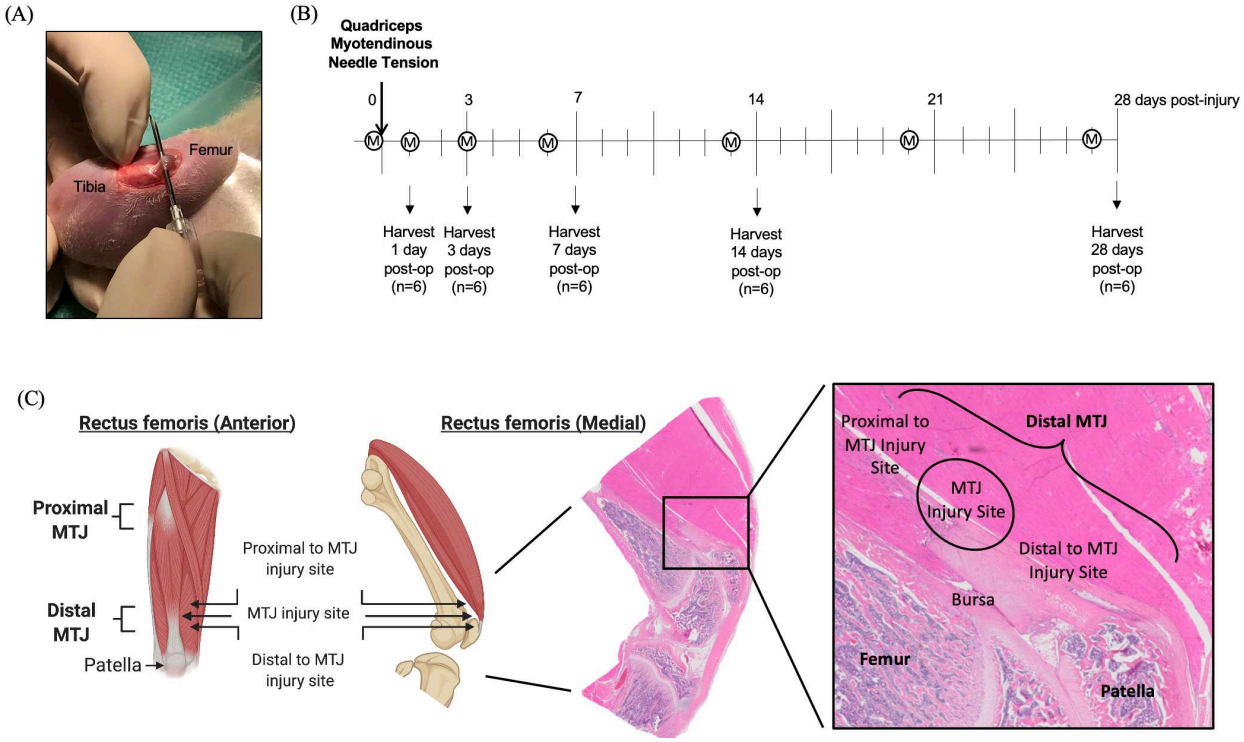


**Figure 5.1. Surgical approach, experimental time course, and histoanatomic injury location.** (**A**) Strain induced MTJ injury generated via 18G needle tension directed along the transverse axis of the MTJ. (**B**) Experimental time-course following injury. Rats were euthanized at 1-, 3-, 7-, 14-, and 28-days post-injury (n=6/time-point) and their limbs taken for histology. The 28-day time-point animals received mobility assessments (marked with M) at days 0, 1, 3, 6, 13, 20, and 27 of the experimental protocol. (**C**) Anatomic location of quadriceps distal MTJ injury with a representative subgross sections demonstrating a naïve/control MTJ. The MTJ anchors the distal quadriceps muscle belly to the proximal patellar tendon. There are well differentiated adipocytes along the proximal and posterior aspect of the tendon and bursa. Cranial to the distal metaphysis of the femur is a large fibrovascular bursa that is continuous with a fat pad proximally and the synovial membrane and joint space distally. The skeletal muscle contains low numbers of mast cells. *H&E, subgross image.*

Animals were anesthetized using a mixture of isoflurane and oxygen (2-4%) and both limbs were shaved and surgically prepped using chlorohexidine and isopropyl alcohol. The surgical region of interest was visualized via a 1cm incision along anterior aspect of the knee. Strain-induced MTJ injury was induced on the right hind limb via needle tension (using an 18G hypodermic needle) that was directed along the transverse axis between the rectus femoris muscle and quadriceps tendon (**Figure 5.1A**). Specifically, this injury focused on tissue plane separation and stretching [155] to induce strain between the tendon/muscle and surrounding structures, as contrasted to a coring needle puncture biopsy utilized in previous reports [172]. For matched comparisons and clinical translatability, the left limb was utilized as a sham surgery

control, receiving an anterior superficial surgical incision without subsequent needle injury. Rats were randomized to end-points and sacrificed at either day 1-, 3-, 7-, 14-, and 28-days post-injury (n=6/time-point; **Figure 5.1B**) in accordance with approved protocols (CO2 inhalation with confirmatory cervical dislocation).

### 5.3.3: Mobility Assessments

The 28-day time-point rats underwent compulsory gait analysis using a DigiGait Treadmill System (Mouse Specifics, Framingham, MA) and voluntary weight bearing using a Tekscan Rodent Walkway System (South Boston, MA) on Days 0, 1, 3, 6, 13, 20, and 27 of the experimental protocol. Prior to start of the experiments, rats were acclimated to both systems over one week. For gait analysis, rats were run for three consecutive replicates per time-point on a flat treadmill at 30 cm/sec, and videos were analyzed for 22 gait parameters including stride length, % swing stride, % stance stride, % brake stride, % propel stride, and stride frequency. For weight bearing, rats were allowed to walk voluntarily over the Tekscan walkway for 3 times/day, and videos were analyzed for 12 weight bearing and gait parameters including maximum force, force time impulse, and maximum force symmetry values (front/hind, left/right, left front/right front, left hind/right hind). For both gait analysis and weight bearing, the three runs taken at each time-point were averaged and utilized for statistical comparisons. For information regarding how specific mobility parameters were calculated see equipment specific manuals.

### 5.3.4: Histology and Histopathology

Following euthanasia, hind limbs were removed at the coxofemoral joint and placed into 10% neutral buffered formalin for 48 hours. Limbs were then transferred to a 10% solution of ethylenediaminetetraacetic acid (EDTA) at pH 7 for decalcification. EDTA was replaced twice weekly for 8-10 weeks. Limbs were trimmed in the sagittal plane, routinely processed and embedded, sectioned at 5um, and stained with hematoxylin and eosin (H&E). Histologic sections were evaluated by one author blinded to the groups.

A semi-quantitative grading scheme was developed to characterize injury-related histologic changes associated with needle puncture. The three sites assessed included: 1) the MTJ at the needle insertion/injury site; 2) the MTJ immediately distal to the injury site; and 3) the MTJ immediately proximal to the injury site (**Figure 5.1C**). At each location, the following parameters were scored: 1) lesion size, 2) degree of fibrosis (a measure of scarring), 3) ground substance (myxomatous degeneration), and 4) vascularity, with each having an allowable score of 0-3. Additionally, secondary changes were documented including bursal cellularity/vascularity, and the presence or absence of reactive synovium and joint space effusion, with each having an allowable score of 0-2. Animals were assessed for the aforementioned histologic changes at days 1, 3, 7, 14, and 28 post-surgery (n=6 males per group). Based on the degree of injury-associated pathology in each individual animal, the minimum possible score was 0 and the maximum possible score was 41.

### 5.3.5: Statistics

The experimental sample size (6 animals per time-point) was calculated using GPower Version 3.1.1 [180]. Specifically, an *a-priori* power analysis was conducted using pilot gait data (stride length) obtained using this injury model in rats. This power analysis resulted in a power of 80%, using a 95% confidence interval and typical standard deviation of 1.00 within groups. All *post-hoc* statistics were conducted in GraphPad Prism 8.3.0 (San Diego, CA). For gait analysis and weight bearing parameters that quantify individual limb changes (stride length, % swing stride, etc.), groups were compared using repeated measures, mixed effects analysis with limb (injured right hind, sham left hind, right fore, and left fore), time (days 0, 1, 3, 6, 13, 20, and 27 post-op) and limb/time interaction factors. Tukey's *post-hoc* tests were used to compare individual groups when the factors (limb, time, and limb/time) showed significance. For gait analysis and weight bearing parameters that demonstrate the relationship between limbs (e.g. stance factor, step angle, overlap distance, paw placement positioning, and weight bearing symmetry parameters), a repeated measures One-Way ANOVA with Tukey's *post-hoc* tests was utilized. For all graded pathology parameters, time-points were compared using a Kruskal-Wallis non-parametric One-Way ANOVA with

Dunn's *post-hoc* tests. For correlation between parameters, a Pearson Correlation Analysis was conducted. Significance was set to $p<0.05$ for all comparisons.

## 5.4: Results

### 5.4.1: Mobility Assessments

#### 5.4.1.1: DigiGait™ Treadmill-Based Gait Analysis

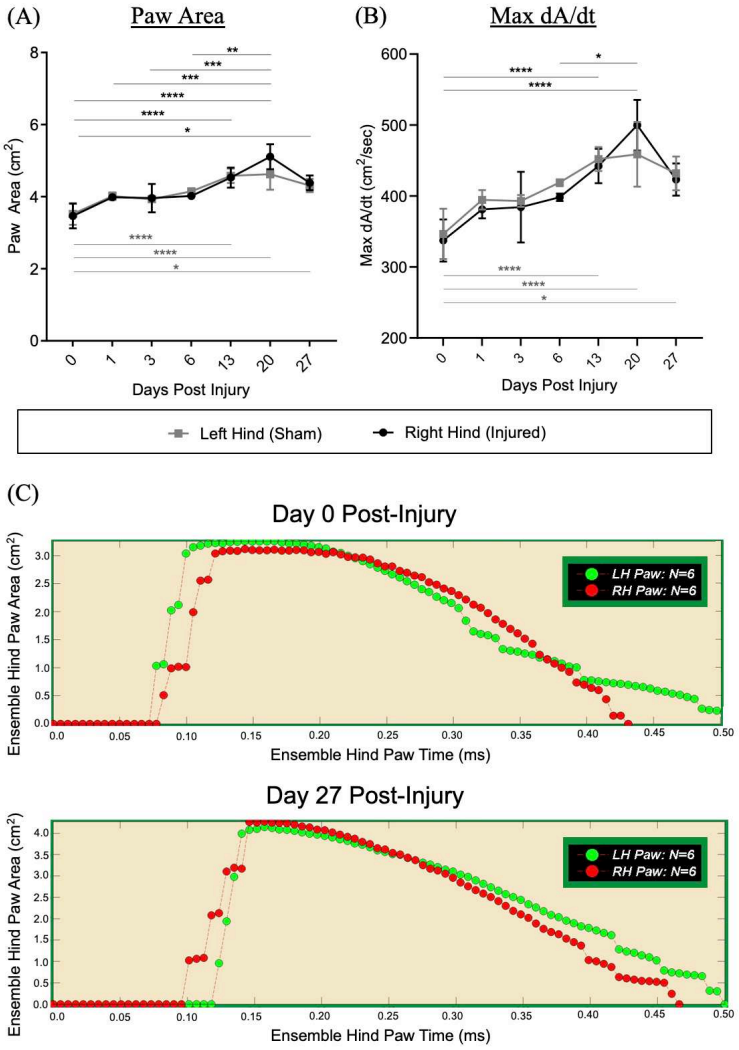


**Figure 5.2. Treadmill based gait analysis parameters (Digigait Treadmill System) following quadriceps MTJ injury in the right hind limbs of rats.** Significant spatiotemporal parameters include (**A**) paw area ($cm^2$) and (**B**) Max dA/dt ($cm^2$/sec). Right hind (injured) differences are in black at the top and left hind (sham) differences in grey at the bottom. No statistically relevant differences between hind limbs were noted. Values are represented as Mean +/- Standard Deviation. (**C**) Representative output paw area curves demonstrating altered stance phase parameters at 27 days post-injury. *$p<0.05$, **$p<0.01$, ***$p<0.001$, ****$p<0.0001$

For treadmill-based gait analysis parameters, paw area significantly increased over time for both the injured right hind and sham left hind limbs (**Figure 5.2A**). This was associated with a greater Max dA/dt (increased deceleration or breaking time during the stance phase) over time for both hind limbs (**Figure 5.2B**). Representative paw area output curves qualitatively demonstrate altered stance phase parameters up to 27 days post-injury (**Figure 5.2C**). No statistically significant differences were found for stride length (cm), %swing stride, %brake stride, %brake stance, %propel stride, %propel stance, %stance stride, stance/swing, stride frequency (steps/sec), absolute paw angle (degrees), min dA/dt ($cm^2$/sec), gait symmetry, ataxia coefficient, midline distance (cm), axis distance (cm), stance width (cm), stance factor, step angle (degrees), overlap distance (cm), or paw placement positioning (cm).

### 5.4.1.2: Tekscan™ Walkway-Based Gait Analysis

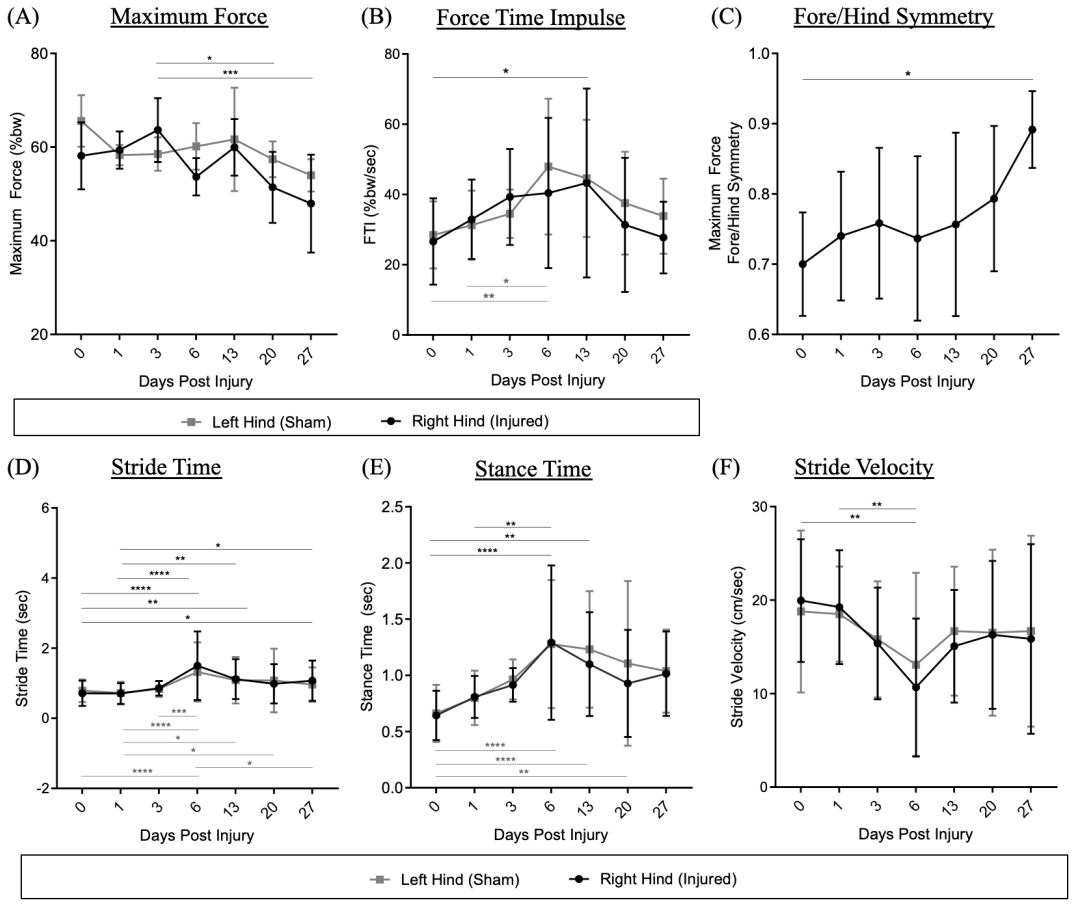


**Figure 5.3. Voluntary weight bearing and gait parameters (Tekscan Rodent Walkway System) following quadriceps MTJ injury in the right hind limbs of rats.** Significant parameters over time include (**A**) maximum force (% body weight (bw)), (**B**) force time impulse (FTI; %bw/sec), (**C**) maximum force fore/hind symmetry, (**D**) stride time (sec), (**E**) stance time (sec), and (**F**) stride velocity. No statistically relevant between limb differences were noted. Values are represented as Mean +/- Standard Deviation with right hind (injured) differences in black at the top and left hind (sham) differences in grey at the bottom. **p<0.05, **p<0.01, ***p<0.001, ****p<0.0001*

For voluntary weight bearing parameters, a decrease in maximum force was seen in the injured right hind limb out to 27 days post-injury, but not the sham left hind limb (**Figure 5.3A**). Importantly, no appreciable correlation ($p=0.36$, $R^2=0.02$) was found between maximum force and maximum velocity, demonstrating that animal speed did not dictate force measurements. Increases in the force time impulse increased for both the injured right hind and sham left hind limbs; however, this normalized by 27 days post-injury (**Figure 5.3B**). Interestingly, altered hind limb loading was associated with an increase in the fore/hind limb

symmetry value, suggesting decreased hind limb loading was associated with increased fore limb loading (**Figure 5.3C**). In contrast to obligatory treadmill walking at a set speed (where no differences in temporal parameters of the stride and stance phases were appreciated), voluntary walking demonstrated a significantly increased stride time (**Figure 5.3D**) and stance time (**Figure 5.3E**) out to 27- and 20-days post-injury, respectively, with peaks at 6 days post-injury. These changes were associated with a decreased stride velocity (**Figure 5.3F**) at 6 days post-injury with normalization by 27 days post-injury. No significant differences were found for maximum peak pressure (MPa), maximum force left/right symmetry, maximum force left hind/right hind symmetry, stride length (cm) swing time (sec), or stride acceleration ($cm^2$/sec).

### 5.4.2: Histology and Histopathology

For rectus femoris MTJ injury, a novel grading scheme (**Table 5.1**) was developed that separately and cumulatively assessed the following regions of the MTJ: 1) needle injury site; 2) MTJ proximal to the injury site; and 3) MTJ distal to the injury site. The joint, synovium, and bursa were also evaluated. Of note, the following site descriptions are for the injured right hind limbs; no pathologic findings were appreciated in the sham left hind limbs at any time-points (score of 0 for all parameters).

**Table 5.1. Histopathologic grading scale for quadriceps MTJ injury-associated pathology.** The MTJ injury site, MTJ proximal to the injury site, and MTJ distal to the injury site were each graded independently on a scale of 0-3pts, with a maximum score of 12 possible for each site. The synovium, bursa, and joint were graded separately on a scale of 0-2pts each. Total MTJ injury score consisted of the sum of all sites and parameters with a maximum score of 41.

| Score | 0 | 1 | 2 | 3 |
|---|---|---|---|---|
| **MTJ Injury Sites (0-3pts)** | | | | |
| Size | Normal/ Inconspicuous | Mild (lesion measure between 0-75um) | Moderate (lesion measures between 75-150um) | Marked (lesion measures greater than 150um) |
| Ground Substance | Absent/ Normal | Mild myxomatous degeneration mildly separating collagen bundles | Moderate myxomatous degeneration disrupting collagen fiber organization | Marked myxomatous degeneration effacing collagen bundles with cartilaginous and/or osseous metaplasia and or enthesophytes at tendon insertion |
| Fibrosis | Normal | Mildly increased numbers of interstitial fibroblasts with maintenance of fiber organization | Fibroblasts disrupt collagen fiber organization and/or fiber polarization | Fibroblasts efface collagen fibers |
| Vascularity | Normal | 1-2 cross-sectional vascular profiles per high powered field | 3-6 cross-sectional vascular profiles per high powered field | Over 7 cross-sectional vascular profiles per high powered field |
| **Joint Space, Bursa, and Synovium (0-2pts)** | | | | |
| Joint Space Effusion | Normal | Proteinaceous fluid | Intracapsular leukocytes +/- proteinaceous fluid | N/A |
| Bursa | Normal | Hypercellularity | Vascularization +/- hypercellularity | N/A |
| Synovium | Normal | Hypertrophied/reactive and/or hyperplastic synoviocytes | N/A | N/A |

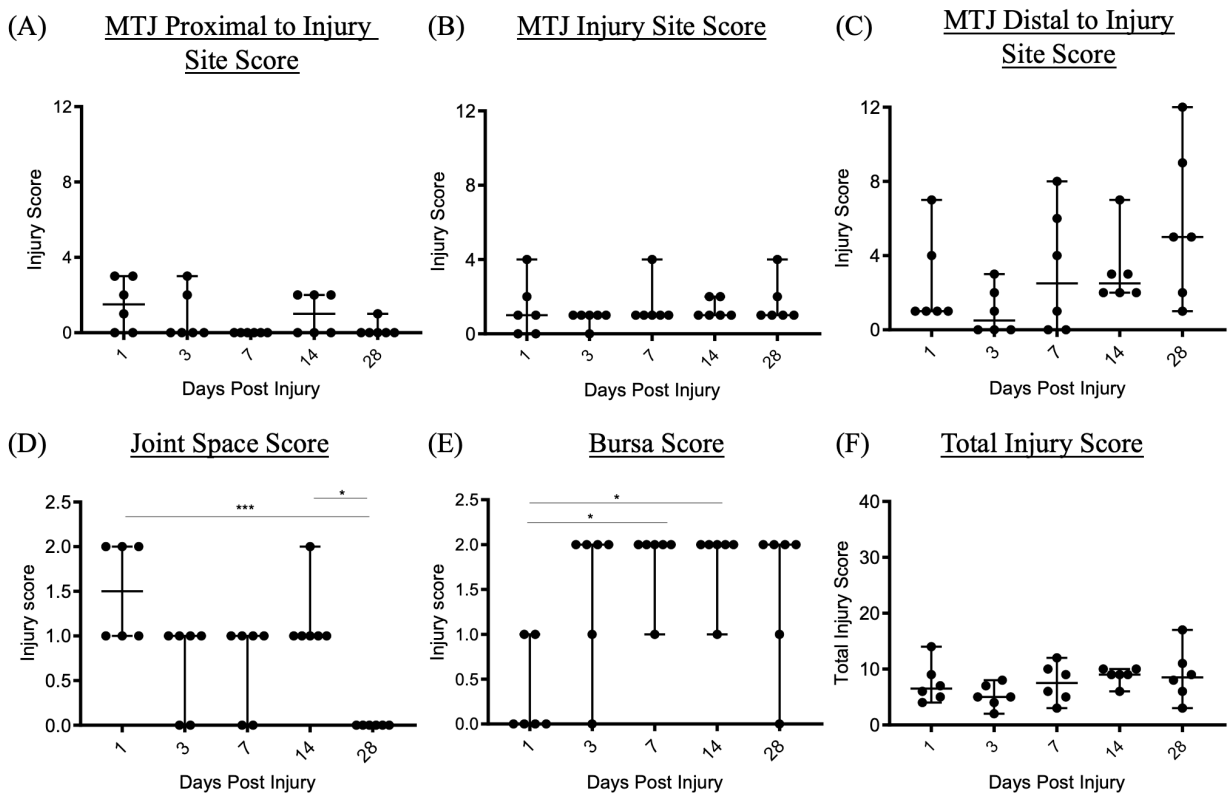


**Figure 5.4. Individual MTJ Site Scores and Total MTJ Injury Score for the injured right hind limbs at 1-, 3-, 7-, 14-, and 28-days post-surgery**. Injury scores for (**A**) MTJ proximal to the injury site, (**B**) MTJ at the injury site, (**C**) MTJ distal to injury site, as well as secondary changes within the (**D**) joint space and (**E**) bursa. (**F**) Total MTJ injury score reflects the sum of all pathology scores, with the maximal/maximum range of the scoring scheme provided on the y axis. Values are represented as median with range and individual animals marked as dots. **p<0.05, **p<0.01, ***p<0.001, ****p<0.0001*

Overall, the most significant and consistent qualitative finding was a pathologic fibrotic adhesive lesion at the muscle and tendon interface along the anterior/cranial aspect of the patella (**Figure 5.5**) at the MTJ distal to the injury site.

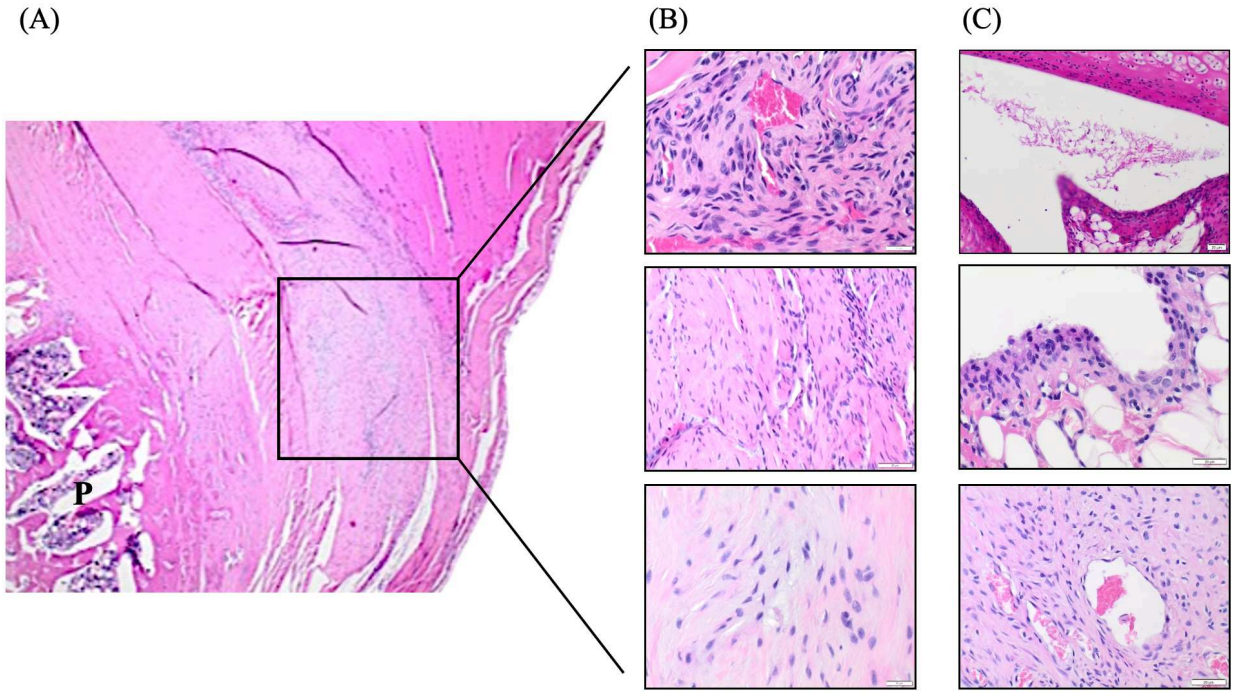


**Figure 5.5. Representative photomicrographs of MTJ injury-associated pathology.** (**A**) Representative low power photomicrograph of MTJ-injury distal to the needle site (2x). The anterior surface of the patella and associated fascial planes are expanded by scar tissue (black box). (**B**) Scar tissue is composed of vascularized and proliferative fibrous connective tissue supported by a variable distinct ground substance stroma (40x). (**C**) Other findings include: (1) joint space effusion, (2) synovial hypertrophy and hyperplasia, and (3) vascularized hypercellular bursa (20x).

The injury typically measured 25-400um and was composed of reactive fibroblasts and disorganized collagen fibers, variably prominent myxomatous ground substance stroma, and vascular profiles. When focusing on individual parameters that contributed to these findings, lesion size (p=0.34), vascularity (p=0.33), and fibrosis (p=0.06) at the MTJ distal to the injury site were not significantly different between time-points. However, the ground substance (p=0.02) score was significant at the MTJ distal to the injury site, suggesting that this parameter may have the greatest contribution to the injury response and the overall pathology score.

In spite of the finding that the MTJ distal to the injury site progressively worsened over time, no significant differences were appreciated for the total injury score (p=0.18, **Figure 5.4F**), the MTJ proximal to the injury site (p=0.10, **Figure 5.4A**), MTJ injury site (p=0.54, **Figure 5.4B**), or MTJ distal to the injury site (p=0.11, **Figure 5.4C**). When considering the individual components which made up these scores, no

significant differences in lesion size, fibrosis, ground substance, and vascularity were appreciated at the MTJ injury site. For the MTJ proximal to injury site, a significant decrease in fibrosis ($p=0.02$; between 1-day post-injury and both 7- and 28-days post-injury) was seen, with no significant changes in lesion size ($p=0.15$), vascularity ($p=0.20$), and ground substance. It was observed that the changes at the MTJ injury site and MTJ proximal to the needle site were subtle and the biological relevance of these findings remains undetermined.

With respect to secondary pathology changes, no significant differences between time-points were appreciated for the synovium ($p=0.84$). However, significant differences were appreciated for joint space effusion (**Figure 5.4D**) and bursa (**Figure 5.4E**), although the pathology at both these sites seemed to decrease over time.

### 5.5: Discussion

This animal model utilized needle tension to produce strain along the tendon-MTJ-muscle interface, a common site of impairment clinically [151,152]. Importantly, this work has resulted in a chronic model (up to 28 days post-injury) that histologically recapitulates muscle lesions adjacent to the MTJ compared to published models which focus on acute muscle injury [172–174]. Therefore, this translational model of MTJ injury can be used for the study of aberrant or delayed healing and chronic scarring that may lead to high re-injury rates. Importantly, this strain-induced model also results in mobility changes associated with injured limb disuse, which can be used to study how therapeutics and rehabilitation strategies not only effect injury pathology but also mitigate decreased activity related to pain in clinical populations.

The major symptom and chief complaint of patients with muscle injuries is altered and/or painful mobility, yet there are few pre-clinical models which study functional alterations in gait and/or weight bearing. Many studies focus on changes to muscle force production [171–174]; however, a direct association to limb alterations has not been established. Indeed, previous studies have shown that locomotive changes following injury precede muscle force changes [169], suggesting that re-establishment of functional mobility may initiate muscle activation and subsequent force production. Therefore, mobility

measures may more accurately demonstrate early symptom modifications post-injury. Mobility in pre-clinical models can be studied using spatial (position-based), temporal (time-based), or kinetic (force-based) methods. To the authors' knowledge, this is the first study quantitatively analyzing all forms of functional mobility alterations using both voluntary and compulsory methods (temporal, spatial, and weight bearing) in an animal model of MTJ injury. In this study, the longitudinal tracking of individual animals throughout the experimental time-course using multiple methods has provided a comprehensive understanding of clinical manifestations of rectus femoris-specific MTJ injury.

With respect to temporal and spatial movement parameters, there were decreases in temporal parameters with voluntary movement (decreased velocity and increased stance time and stride time which peaks at 6 days post-injury) in the current model. Indeed, non-invasive kinetic methods to evaluate weight bearing distribution have been shown to sensitively predict limb dysfunction post-injury [181]. With respect to weight bearing, subjective gait scoring following muscle contusion injury demonstrated decrease limb loading in a mouse model [170]. As a less severe model was utilized in the current study, quantitative dynamic weight bearing was undertaken, and similar results were obtained. Rats placed less weight on their hind limbs over time (decreased maximum force and increased force time impulse) and shifted their weight to their forelimbs (increased maximum force for fore/hind limb symmetry). Clinically, rectus femoris injury of the quadriceps muscle group typically occurs during the swing phase due to eccentric contractions of the muscle that occur during that portion of the gait cycle [153]. Following rectus femoris MTJ injury in this study, animals were avoiding limb rotation (swing phase), which was associated with decreased animal movement. Therefore, it is likely that post-injury animals are attempting to avoid this swing phase to minimize rectus femoris muscle contraction. Of note, the functional mobility changes seen in the injured hind limb are also occurring in the contralateral hind limb that received a sham surgery.

Interestingly, no changes in temporal parameters post-injury with compulsory treadmill-based gait analysis were appreciated. Given the set treadmill speed and the fact that only data where the animal maintained speed with the treadmill were utilized for analysis, it can be difficult to appreciate natural gait differences. However, alterations in spatial parameters were documented with this obligatory method.

Specifically, rats exhibited increased paw area and altered spatiotemporal parameters including increased Max dA/dt (impaired braking capacity). Collectively, our results suggest that following strain induced MTJ injury, rats are favoring the stance phase to minimize limb rotation and movement during the swing phase. These results are corroborated by previous reports. Changes in ankle angle and calcaneus height have been shown in contusion models of anterior tibialis muscle injury [169], suggesting impaired joint rotation/movement. Additionally, voluntary walking impairment has previously been shown in a rat model of traumatic muscle injury [166]. In this study, treadmill-based walking trials were performed in triplicate to assess reproducibility in our clinical assessments. This necessitated 10 minutes of animal activity per time-point, which was divided into short segments of non-strenuous compulsory movement followed by resting periods. We do not anticipate this level of movement modulated tissue remodeling in our model as more intense long term (>60 minutes/day for 3-16 weeks) running protocols are typically utilized to induce muscle and tendon injury in rodents [168,182,183]. Along this vein, more intense running protocols may be employed in future investigations to assess if chronic MTJ scarring, a unique characteristic of this model, may lead to high re-injury rates.

To determine a relationship between the observed mobility alterations and histoanatomic manifestations of injury, we created a semi-quantitative grading scheme to characterize the inflammatory and structural response to MTJ injury throughout the experimental time-course. Our approach was to evaluate not only the MTJ but also nearby structures to gain a comprehensive understanding of how the entire region is responding to needle injury and to identify key contributors to injury progression. The grading scheme included evaluation of the needle puncture site, the region proximal and distal to the needle site, as well as nearby fat pads, bursa, synovial membranes, and knee joint spaces. Currently there is a lack of histopathologic data describing the acute and chronic manifestations of MTJ injuries in humans. Clinicians tend to rely on magnetic resonance imaging for injury evaluation and studies have demonstrated the presence of hemorrhage, edema, fatty infiltration, and muscle atrophy directly adjacent to the MTJ [155]. Similarly, we have documented acute mixed inflammation and edema acutely after injury. In the later stages

of healing, we see more chronic changes including fibrosis, vascularization, and secondary changes to nearby structures including the joint space, bursae, and synovium.

The most striking and consistent qualitative histologic finding was a fairly large (50-300um) adhesive lesion along the MTJ distal to the needle injury site 28 days post injury, which resulted in a significantly increased ground substance score at this time-point. It is anticipated that the development of this lesion was associated with an aberrant healing response resulting in early chronic injury progression [151]. In regards to normal tissue healing, an initial injury (independent of severity) is followed by: (1) an inflammatory cell reaction and formation of a hematoma; (2) phagocytosis of the damaged tissue (3) repair and/or regeneration of myofibers; and lastly (4) reorganization and remodeling with the aim of full functional recovery [151]. Tissue regeneration at the MTJ can be particularly difficult due to the complex organization and anchoring between muscle myofibers and tendon collagen fibers [150]. Indeed, in the current model, an excessive and disorganized fibroblastic response with diminished remodeling was seen as evidenced by the generation of a fibrotic scar 28 days post injury, which mimics the repair phase following muscle injury [151].

When identifying associations between histology and gait pattern outcome measures, it is noteworthy that the bursa score peaks at 7 days post-injury, which corresponds to decreases in voluntary movement at 6 days post-injury. Therefore, this may be a critical timeframe to target the local microenvironment towards a reparative vs. delayed/dysregulated healing process. Cellular and tissue level variations at this time-point may identify pathways that could be manipulated for organized healing. Future work is needed to investigate the functional role of these structures and the influence they may have on resident progenitor cells such as skeletal muscle satellite cells, fibroadipogenic precursors, interstitial tenocytes, fibroblasts, nerves, endothelial cells and inflammatory cells. As many of these cell types were present in both injured and sham limbs natively and at different time points post-injury their specific role in driving the histoanatomic manifestations of injury progression requires further study.

Rats were chosen due to their large size (relative to mice), inherent exercise ability for mobility outcomes, and the fact that the Crl:CD(SD) rats are an outbred strain. Weight and skeletal measurements taken during the experimental time-course also demonstrate that rats were still growing, with skeletal maturity obtained

at 16 weeks of age. Therefore, the results presented here are particularly relevant for adolescents and young adults (13-22 years of age) who experience MTJ associated sports-injuries. Notably, multiple prospective studies have identified that age is not a risk factor for quadriceps MTJ specifically, unlike in other MTJ etiologies [163,184,185]. Future studies will determine whether age plays a significant role in quadriceps MTJ injury and healing with this model.

Caveats of this study include the use of the contralateral limb as a control for both mobility and histopathological assessments. While this was undertaken due to clinical applicability, no significant changes between the injured right hind and contralateral sham limb were appreciated. Therefore, further study on the compensatory effects in quadruped animals is warranted to fully characterize this model. Additionally, all outcomes demonstrate sustained changes out to 28 days post-injury. Future directions include characterizing the injury at later (56 and 120 day) time-points to evaluate histologic changes (we suspect there will be adhesion contracture and remodeling) and mobility alterations later on throughout the repair process. Based on our findings out to 28 days post-injury, we anticipate that, while mobility measurements may normalize at 56- and 120-day time-points, pathologic and scored features may be more distinct during these later stages of chronic tissue remodeling. The authors acknowledge that the exact strain which was induced during injury was not directly measured. However, the use of an 18G needle provided consistency among animals and dictated the degree of tissue plane separation as no excessive force was utilized.

The results from this study demonstrate the development of a chronic model of rectus femoris MTJ injury, altered mobility, and strain-induced fibrotic scarring along the anterior patella. Notably, these pathologic and functional changes recapitulate the course of injury progression similar to what is described in humans [153,175,176]. Collectively, this work provides a unique pre-clinical model to study quadriceps MTJ injury mechanisms for the identification of enhanced treatment options for patients who suffer from such activity-related muscle conditions.

# CHAPTER 6: CONCLUSIONS

## 6.1: Concluding Remarks

As reviewed and introduced in Chapter 1, the Hartley guinea pig serves as an underutilized model of idiopathic musculoskeletal aging. We documented an age-associated decline in transcriptional and functional activity of Nrf2 in knee joint tissue (Chapter 1). During the early-stages of OA, Nrf2-activator treatment modified gait and activity patterns, altered transcriptional activity in articular cartilage and the IFP, and mitigated patellofemoral knee joint OA (Chapter 2). Further, during more advanced stages of OA we demonstrated that Nrf2-activator treatment mitigated whole knee joint OA pathology, modified articular cartilage and IFP gene expression profiles, and modified voluntary mobility patterns characteristic of end-stage disease in this strain (Chapter 3). Of additional interest, Nrf2-activation enhanced long bone strength in aging female Hartley guinea pigs, a finding which may serve as promise in the utilization of Nrf2-activators in the clinical management of age-related bone degeneration (Chapter 4). Lastly, the longitudinal clinical and histologic manifestations of a novel rectus femoris myotendinous junction injury model was also characterized in rats (Chapter 5).

## 6.2: Future Direction

Future work is necessary to further characterize and develop our understanding of the Hartley guinea pig model of idiopathic musculoskeletal aging. Advanced analysis of our mRNA and gait data from both ageing and Nrf2-activator treated animals (pathway analysis and principal component analysis, respectively) is necessary to better correlate meaningful biomarkers between the sexes and OA progression. Further, our group is interested in investigating sex specific differences in the phenotypic manifestation of age-related knee joint pathology as well as the longitudinal assessment of other pathologies we hypothesize may be present in non-weight bearing joints containing articular discs (temporomandibular and lumbar vertebral joints).

Current clinical treatment and strategies for managing OA are limited; nutraceuticals and specifically Nrf2-activators may hold promise when managing OA patients with long-term disease. Structural changes within the joint noted with PB125 treatment are intriguing, however; future studies, such as repeating this study as well as implementing a study in a larger (and monogastric foregut fermenter) model of OA, are necessary to evaluate the efficacy and safety of this nutraceutical in mitigating the age-related decline in structural and functional mobility associated with osteoarthritis and bone degeneration in the elderly.

This work also highlights the first study quantitatively analyzing all forms of functional mobility alterations using both voluntary and compulsory methods (temporal, spatial, and weight bearing) in an animal model of myotendinous junction injury. Studies are underway to validate this injury model in female rats. Further, future studies on the compensatory effects in quadruped animals are warranted to fully characterize this model. Additionally, all outcomes demonstrate sustained changes out to 28 days post-injury. Future directions include characterizing the injury at later (56 and 120 day) time-points to evaluate histologic changes (we suspect there will be adhesion contracture and remodeling) and mobility alterations later on throughout the repair process.

## REFERENCES


[1] Y. Zhang, J.M. Jordan, Epidemiology of osteoarthritis, Clin. Geriatr. Med. (2010). https://doi.org/10.1016/j.cger.2010.03.001.

[2] M.G. Cisternas, L. Murphy, J.J. Sacks, D.H. Solomon, D.J. Pasta, C.G. Helmick, Alternative Methods for Defining Osteoarthritis and the Impact on Estimating Prevalence in a US Population-Based Survey, Arthritis Care Res. (2016). https://doi.org/10.1002/acr.22721.

[3] R.F. Loeser, Age-related changes in the musculoskeletal system and the development of osteoarthritis, Clin. Geriatr. Med. (2010). https://doi.org/10.1016/j.cger.2010.03.002.

[4] J. Axford, C. Heron, F. Ross, C.R. Victor, Management of knee osteoarthritis in primary care: Pain and depression are the major obstacles, J. Psychosom. Res. (2008). https://doi.org/10.1016/j.jpsychores.2007.11.009.

[5] L.B. Murphy, M.G. Cisternas, D.J. Pasta, C.G. Helmick, E.H. Yelin, Medical Expenditures and Earnings Losses Among US Adults With Arthritis in 2013, Arthritis Care Res. (2018). https://doi.org/10.1002/acr.23425.

[6] R. Meliconi, L. Pulsatelli, O. Addimanda, V. Brusi, B. Pavloska, New findings in osteoarthritis pathogenesis: Therapeutic implications, Ther. Adv. Chronic Dis. (2013). https://doi.org/10.1177/2040622312462734.

[7] World Health Organisation, WHO | Ageing and Life Course, WHO. (2019).

[8] A.M. McCoy, Animal Models of Osteoarthritis: Comparisons and Key Considerations., Vet. Pathol. 52 (2015) 803–18. https://doi.org/10.1177/0300985815588611.

[9] U. Styrkarsdottir, S.H. Lund, G. Thorleifsson, F. Zink, O.A. Stefansson, J.K. Sigurdsson, K. Juliusson, K. Bjarnadottir, S. Sigurbjornsdottir, S. Jonsson, K. Norland, L. Stefansdottir, A. Sigurdsson, G. Sveinbjornsson, A. Oddsson, G. Bjornsdottir, R.L. Gudmundsson, G.H. Halldorsson, T. Rafnar, I. Jonsdottir, E. Steingrimsson, G.L. Norddahl, G. Masson, P. Sulem, H. Jonsson, T. Ingvarsson, D.F. Gudbjartsson, U. Thorsteinsdottir, K. Stefansson, Meta-analysis of Icelandic and UK data sets identifies missense variants in SMO, IL11, COL11A1 and 13 more new loci associated with osteoarthritis, Nat. Genet. (2018). https://doi.org/10.1038/s41588-018-0247-0.

[10] M.A. McNulty, R.F. Loeser, C. Davey, M.F. Callahan, C.M. Ferguson, C.S. Carlson, A comprehensive histological assessment of osteoarthritis lesions in mice, Cartilage. (2011). https://doi.org/10.1177/1947603511402665.

[11] M.A. McNulty, R.F. Loeser, C. Davey, M.F. Callahan, C.M. Ferguson, C.S. Carlson, Histopathology of naturally occurring and surgically induced osteoarthritis in mice, Osteoarthr. Cartil. (2012). https://doi.org/10.1016/j.joca.2012.05.001.

[12] R. Stoop, P.M. Van Der Kraan, P. Buma, A.P. Hollander, R.C. Billinghurst, A.R. Poole, W.B. Van Den Berg, Type II collagen degradation in spontaneous osteoarthritis in C57Bl/6 and BALB/c mice, Arthritis Rheum. (1999). https://doi.org/10.1002/1529-0131(199911)42:11<2381::AID-ANR17>3.0.CO;2-E.

[13] S.S. Glasson, M.G. Chambers, W.B. Van Den Berg, C.B. Little, The OARSI histopathology initiative - recommendations for histological assessments of osteoarthritis in the mouse, Osteoarthr. Cartil. (2010). https://doi.org/10.1016/j.joca.2010.05.025.

[14] P.M. van der Kraan, R. Stoop, T.H.M. Meijers, A.R. Poole, W.B. van den Berg, Expression of type X collagen in young and old C57BI/6 and Balb/c mice. Relation with articular cartilage degeneration, Osteoarthr. Cartil. (2001). https://doi.org/10.1053/joca.2000.0364.

[15] L.C. Strong, Genetic nature of the constitutional states of cancer susceptibility and resistance in mice and men, Yale J. Biol. Med. (2000).

[16] J. Chayen, L. Bitensky, M.G. Chambers, Modulation of murine osteoarthritis, Cell Biochem. Funct. (1996). https://doi.org/10.1002/cbf.643.

[17] B.M. S Mahr, J Menard, V Krenn, Sexual dimorphism in the osteoarthritis of STR/ort mice may be

linked to articular cytokines., Ann. Rheum. Dis. 62 (2003) 1234–1237.
[18] B. Poulet, R. De Souza, C.B. Knights, C. Gentry, A.M. Wilson, S. Bevan, Y.M. Chang, A.A. Pitsillides, Modifications of gait as predictors of natural osteoarthritis progression in Str/Ort mice, Arthritis Rheumatol. (2014). https://doi.org/10.1002/art.38616.
[19] L. Sokoloff, L.B. Crittenden, R.S. Yamamoto, G.E. Jay, The genetics of degenerative joint disease in mice, Arthritis Rheum. (1962). https://doi.org/10.1002/art.1780050602.
[20] P.J. Watson, L.D. Hall, A. Malcolm, J.A. Tyler, Degenerative joint disease in the guinea pig: Use of magnetic resonance imaging to monitor progression of bone pathology, Arthritis Rheum. (1996). https://doi.org/10.1002/art.1780390810.
[21] R. V. Musci, M.A. Walsh, A.R. Konopka, C.A. Wolff, F.F. Peelor, R.F. Reiser, K.S. Santangelo, K.L. Hamilton, The Dunkin Hartley Guinea Pig Is a Model of Primary Osteoarthritis That Also Exhibits Early Onset Myofiber Remodeling That Resembles Human Musculoskeletal Aging, Front. Physiol. (2020). https://doi.org/10.3389/fphys.2020.571372.
[22] V.B. Kraus, J.L. Huebner, J. DeGroot, A. Bendele, The OARSI histopathology initiative - recommendations for histological assessments of osteoarthritis in the guinea pig, Osteoarthr. Cartil. (2010). https://doi.org/10.1016/j.joca.2010.04.015.
[23] P.A. Jimenez, S.S. Glasson, O. V Trubetskoy, H.B. Haimes, Spontaneous osteoarthritis in Dunkin Hartley guinea pigs: histologic, radiologic, and biochemical changes., Lab. Anim. Sci. 47 (1997) 598–601. http://www.ncbi.nlm.nih.gov/pubmed/9433695.
[24] L.B. Radakovich, A.J. Marolf, J.P. Shannon, S.C. Pannone, V.D. Sherk, K.S. Santangelo, Development of a microcomputed tomography scoring system to characterize disease progression in the Hartley guinea pig model of spontaneous osteoarthritis, Connect. Tissue Res. (2017). https://doi.org/10.1080/03008207.2017.1409218.
[25] E.L. Kuyinu, G. Narayanan, L.S. Nair, C.T. Laurencin, Animal models of osteoarthritis: classification, update, and measurement of outcomes, J. Orthop. Surg. Res. 11 (2016) 19. https://doi.org/10.1186/s13018-016-0346-5.
[26] K.S. Santangelo, A.C. Kaeding, S.A. Baker, A.L. Bertone, Quantitative Gait Analysis Detects Significant Differences in Movement between Osteoarthritic and Nonosteoarthritic Guinea Pig Strains before and after Treatment with Flunixin Meglumine, Arthritis. (2014). https://doi.org/10.1155/2014/503519.
[27] D.C. Bauer, D.J. Hunter, S.B. Abramson, M. Attur, M. Corr, D. Felson, D. Heinegård, J.M. Jordan, T.B. Kepler, N.E. Lane, T. Saxne, B. Tyree, V.B. Kraus, (V Kraus, Chair) For the Osteoarthritis Biomarkers Network, Classification of osteoarthritis biomarkers: a proposed approach, Osteoarthr. Cartil. (2006). https://doi.org/10.1016/j.joca.2006.04.001.
[28] T.M. Griffin, R.P. Main, C.T. Farley, Biomechanics of quadrupedal walking: How do four-legged animals achieve inverted pendulum-like movements?, J. Exp. Biol. (2004). https://doi.org/10.1242/jeb.01177.
[29] J.S. Thomsen, T.S. Straarup, C.C. Danielsen, H. Oxlund, A. Brüel, Relationship between articular cartilage damage and subchondral bone properties and meniscal ossification in the Dunkin Hartley guinea pig model of osteoarthritis, Scand. J. Rheumatol. (2011). https://doi.org/10.3109/03009742.2011.571218.
[30] A.M. McCoy, Animal Models of Osteoarthritis: Comparisons and Key Considerations, Vet. Pathol. (2015). https://doi.org/10.1177/0300985815588611.
[31] R.F. Loeser, S.R. Goldring, C.R. Scanzello, M.B. Goldring, Osteoarthritis: A disease of the joint as an organ, Arthritis Rheum. (2012). https://doi.org/10.1002/art.34453.
[32] A.P. Hollander, I. Pidoux, A. Reiner, C. Rorabeck, R. Bourne, A.R. Poole, Damage to type II collagen in aging and osteoarthritis starts at the articular surface, originates around chondrocytes, and extends into the cartilage with progressive degeneration, J. Clin. Invest. (1995). https://doi.org/10.1172/JCI118357.
[33] J.L. Huebner, J.M. Williams, M. Deberg, Y. Henrotin, V.B. Kraus, Collagen fibril disruption occurs early in primary guinea pig knee osteoarthritis, Osteoarthr. Cartil. (2010).

https://doi.org/10.1016/j.joca.2009.09.011.
[34] P.J. Roughley, J.S. Mort, The role of aggrecan in normal and osteoarthritic cartilage, J. Exp. Orthop. (2014). https://doi.org/10.1186/s40634-014-0008-7.
[35] R.D. Pasternak, S.J. Hubbs, R.G. Caccese, R.L. Marks, J.M. Conaty, G. DiPasquale, Interleukin-1 stimulates the secretion of proteoglycan- and collagen-degrading proteases by rabbit articular chondrocytes, Clin. Immunol. Immunopathol. (1986). https://doi.org/10.1016/0090-1229(86)90006-1.
[36] K.S. Santangelo, E.M. Pieczarka, G.J. Nuovo, S.E. Weisbrode, A.L. Bertone, Temporal expression and tissue distribution of interleukin-1β in two strains of guinea pigs with varying propensity for spontaneous knee osteoarthritis, Osteoarthr. Cartil. (2011). https://doi.org/10.1016/j.joca.2011.01.004.
[37] K.S. Santangelo, G.J. Nuovo, A.L. Bertone, In vivo reduction or blockade of interleukin-1β in primary osteoarthritis influences expression of mediators implicated in pathogenesis, Osteoarthr. Cartil. (2012). https://doi.org/10.1016/j.joca.2012.08.011.
[38] A. Liacini, J. Sylvester, W.Q. Li, W. Huang, F. Dehnade, M. Ahmad, M. Zafarullah, Induction of matrix metalloproteinase-13 gene expression by TNF-α is mediated by MAP kinases, AP-1, and NF-κB transcription factors in articular chondrocytes, Exp. Cell Res. (2003). https://doi.org/10.1016/S0014-4827(03)00180-0.
[39] M.J. Pearson, D. Herndler-Brandstetter, M.A. Tariq, T.A. Nicholson, A.M. Philp, H.L. Smith, E.T. Davis, S.W. Jones, J.M. Lord, IL-6 secretion in osteoarthritis patients is mediated by chondrocyte-synovial fibroblast cross-talk and is enhanced by obesity, Sci. Rep. (2017). https://doi.org/10.1038/s41598-017-03759-w.
[40] E. V. Medvedeva, E.A. Grebenik, S.N. Gornostaeva, V.I. Telpuhov, A. V. Lychagin, P.S. Timashev, A.S. Chagin, Repair of damaged articular cartilage: Current approaches and future directions, Int. J. Mol. Sci. (2018). https://doi.org/10.3390/ijms19082366.
[41] B.D. Boyan, L. Tosi, R. Coutts, R. Enoka, D.A. Hart, D.P. Nicolella, K. Berkley, K. Sluka, K. Kwoh, M.I. O'Connor, W. Kohrt, Sex differences in osteoarthritis of the knee, J. Am. Acad. Orthop. Surg. (2012). https://doi.org/10.5435/JAAOS-20-10-668.
[42] S. Linn, B. Murtaugh, E. Casey, Role of Sex Hormones in the Development of Osteoarthritis, PM R. (2012). https://doi.org/10.1016/j.pmrj.2012.01.013.
[43] R.C. Kinney, Z. Schwartz, K. Week, M.K. Lotz, B.D. Boyan, Human articular chondrocytes exhibit sexual dimorphism in their responses to 17β-estradiol, Osteoarthr. Cartil. (2005). https://doi.org/10.1016/j.joca.2004.12.003.
[44] R.S. Richmond, C.S. Carlson, T.C. Register, G. Shanker, R.F. Loeser, Functional estrogen receptors in adult articular cartilage: Estrogen replacement therapy increases chondrocyte synthesis of proteoglycans and insulin-like growth factor binding protein 2, Arthritis Rheum. (2000). https://doi.org/10.1002/1529-0131(200009)43:9<2081::AID-ANR20>3.0.CO;2-I.
[45] B.D. Boyan, D.A. Hart, R.M. Enoka, D.P. Nicolella, E. Resnick, K.J. Berkley, K.A. Sluka, C.K. Kwoh, L.L. Tosi, M.I. O'Connor, R.D. Coutts, W.M. Kohrt, Hormonal modulation of connective tissue homeostasis and sex differences in risk for osteoarthritis of the knee, Biol. Sex Differ. (2013). https://doi.org/10.1186/2042-6410-4-3.
[46] J.E. Stevens-Lapsley, W.M. Kohrt, Osteoarthritis in women: Effects of estrogen, obesity and physical activity, Women's Heal. (2010). https://doi.org/10.2217/whe.10.38.
[47] V.B. Kraus, J.L. Huebner, J. DeGroot, A. Bendele, The OARSI histopathology initiative - recommendations for histological assessments of osteoarthritis in the guinea pig, Osteoarthr. Cartil. 18 (2010). https://doi.org/10.1016/j.joca.2010.04.015.
[48] R.F. Loeser, J.A. Collins, B.O. Diekman, Ageing and the pathogenesis of osteoarthritis, Nat. Rev. Rheumatol. (2016). https://doi.org/10.1038/nrrheum.2016.65.
[49] S. Koelling, N. Miosge, Sex differences of chondrogenic progenitor cells in late stages of osteoarthritis, Arthritis Rheum. (2010). https://doi.org/10.1002/art.27311.
[50] M.L. Ricks, J.T. Farrell, D.J. Falk, D.W. Holt, M. Rees, J. Carr, T. Williams, B.A. Nichols, L.C.

Bridgewater, P.R. Reynolds, D.L. Kooyman, R.E. Seegmiller, Osteoarthritis in temporomandibular joint of Col2a1 mutant mice, Arch. Oral Biol. (2013). https://doi.org/10.1016/j.archoralbio.2013.02.008.
[51] L. Zhong, X. Huang, M. Karperien, J.N. Post, Correlation between gene expression and osteoarthritis progression in human, Int. J. Mol. Sci. (2016). https://doi.org/10.3390/ijms17071126.
[52] Y. Luo, D. Sinkeviciute, Y. He, M. Karsdal, Y. Henrotin, A. Mobasheri, P. Önnerfjord, A. Bay-Jensen, The minor collagens in articular cartilage, Protein Cell. (2017). https://doi.org/10.1007/s13238-017-0377-7.
[53] J.M. McCord, B.M. Hybertson, A. Cota-Gomez, K.P. Geraci, B. Gao, Nrf2 activator pb125® as a potential therapeutic agent against covid-19, Antioxidants. (2020). https://doi.org/10.3390/antiox9060518.
[54] S. Kasai, J. Mimura, T. Ozaki, K. Itoh, Emerging regulatory role of Nrf2 in iron, heme, and hemoglobin metabolism in physiology and disease, Front. Vet. Sci. (2018). https://doi.org/10.3389/fvets.2018.00242.
[55] K.S. Santangelo, L.B. Radakovich, J. Fouts, M.T. Foster, Pathophysiology of obesity on knee joint homeostasis: Contributions of the infrapatellar fat pad, Horm. Mol. Biol. Clin. Investig. (2016). https://doi.org/10.1515/hmbci-2015-0067.
[56] J. Gallagher, P. Tierney, P. Murray, M. O'Brien, The infrapatellar fat pad: Anatomy and clinical correlations, Knee Surgery, Sport. Traumatol. Arthrosc. (2005). https://doi.org/10.1007/s00167-004-0592-7.
[57] R. Lago, R. Gomez, M. Otero, F. Lago, R. Gallego, C. Dieguez, J.J. Gomez-Reino, O. Gualillo, A new player in cartilage homeostasis: adiponectin induces nitric oxide synthase type II and pro-inflammatory cytokines in chondrocytes, Osteoarthr. Cartil. (2008). https://doi.org/10.1016/j.joca.2007.12.008.
[58] L.M. Gierman, S. Wopereis, B. Van El, E.R. Verheij, B.J.C. Werff-Van Der Vat, Y.M. Bastiaansen-Jenniskens, G.J.V.M. Van Osch, M. Kloppenburg, V. Stojanovic-Susulic, T.W.J. Huizinga, A.M. Zuurmond, Metabolic profiling reveals differences in concentrations of oxylipins and fatty acids secreted by the infrapatellar fat pad of donors with end-stage osteoarthritis and normal donors, Arthritis Rheum. (2013). https://doi.org/10.1002/art.38081.
[59] L.B. Radakovich, A.J. Marolf, L.A. Culver, K.S. Santangelo, Calorie restriction with regular chow, but not a high-fat diet, delays onset of spontaneous osteoarthritis in the Hartley guinea pig model, Arthritis Res. Ther. (2019). https://doi.org/10.1186/s13075-019-1925-8.
[60] T.H. Chen, L. Chen, M.S. Hsieh, C.P. Chang, D.T. Chou, S.H. Tsai, Evidence for a protective role for adiponectin in osteoarthritis, Biochim. Biophys. Acta - Mol. Basis Dis. (2006). https://doi.org/10.1016/j.bbadis.2006.06.008.
[61] S. Honsawek, M. Chayanupatkul, Correlation of Plasma and Synovial Fluid Adiponectin with Knee Osteoarthritis Severity, Arch. Med. Res. (2010). https://doi.org/10.1016/j.arcmed.2010.11.007.
[62] P.J. Francin, A. Abot, C. Guillaume, D. Moulin, A. Bianchi, P. Gegout-Pottie, J.Y. Jouzeau, D. Mainard, N. Presle, Association between adiponectin and cartilage degradation in human osteoarthritis, Osteoarthr. Cartil. (2014). https://doi.org/10.1016/j.joca.2014.01.002.
[63] E.H. Kang, Y.J. Lee, T.K. Kim, C.B. Chang, J.H. Chung, K. Shin, E.Y. Lee, E.B. Lee, Y.W. Song, Adiponectin is a potential catabolic mediator in osteoarthritis cartilage, Arthritis Res. Ther. (2010). https://doi.org/10.1186/ar3218.
[64] J.H. Ku, C.K. Lee, B.S. Joo, B.M. An, S.H. Choi, T.H. Wang, H.L. Cho, Correlation of synovial fluid leptin concentrations with the severity of osteoarthritis, Clin. Rheumatol. (2009). https://doi.org/10.1007/s10067-009-1242-8.
[65] V.K. Singh, G. Shah, P.K. Singh, D. Saran, Extraskeletal ossifying chondroma in Hoffa's fat pad: An unusual cause of anterior knee pain, Singapore Med. J. (2009).
[66] E. Distel, T. Cadoudal, S. Durant, A. Poignard, X. Chevalier, C. Benelli, The infrapatellar fat pad in knee osteoarthritis: An important source of interleukin-6 and its soluble receptor, Arthritis Rheum. (2009). https://doi.org/10.1002/art.24881.

[67] B. Chuckpaiwong, H.C. Charles, V.B. Kraus, F. Guilak, J.A. Nunley, Age-associated increases in the size of the infrapatellar fat pad in knee osteoarthritis as measured by 3T MRI, J. Orthop. Res. (2010). https://doi.org/10.1002/jor.21125.
[68] L. Prut, C. Belzung, The open field as a paradigm to measure the effects of drugs on anxiety-like behaviors: A review, Eur. J. Pharmacol. (2003). https://doi.org/10.1016/S0014-2999(03)01272-X.
[69] D.J. Leong, M. Choudhury, D.M. Hirsh, J.A. Hardin, N.J. Cobelli, H.B. Sun, Nutraceuticals: Potential for chondroprotection and molecular targeting of osteoarthritis, Int. J. Mol. Sci. (2013). https://doi.org/10.3390/ijms141123063.
[70] S. Harirforoosh, W. Asghar, F. Jamali, Adverse effects of nonsteroidal antiinflammatory drugs: An update of gastrointestinal, cardiovascular and renal complications, J. Pharm. Pharm. Sci. (2013). https://doi.org/10.18433/j3vw2f.
[71] J.A. Bolduc, J.A. Collins, R.F. Loeser, Reactive oxygen species, aging and articular cartilage homeostasis, Free Radic. Biol. Med. (2019). https://doi.org/10.1016/j.freeradbiomed.2018.08.038.
[72] N. Robledinos-Antón, R. Fernández-Ginés, G. Manda, A. Cuadrado, Activators and Inhibitors of NRF2: A Review of Their Potential for Clinical Development, Oxid. Med. Cell. Longev. (2019). https://doi.org/10.1155/2019/9372182.
[73] P. Zhang, A. Singh, S. Yegnasubramanian, D. Esopi, P. Kombairaju, M. Bodas, H. Wu, S.G. Bova, S. Biswal, Loss of kelch-like ECH-associated protein 1 function in prostate cancer cells causes chemoresistance and radioresistance and promotes tumor growth, Mol. Cancer Ther. (2010). https://doi.org/10.1158/1535-7163.MCT-09-0589.
[74] L. Ji, H. Li, P. Gao, G. Shang, D.D. Zhang, N. Zhang, T. Jiang, Nrf2 Pathway Regulates Multidrug-Resistance-Associated Protein 1 in Small Cell Lung Cancer, PLoS One. (2013). https://doi.org/10.1371/journal.pone.0063404.
[75] M.-K. Kwak, K. Itoh, M. Yamamoto, T.W. Kensler, Enhanced Expression of the Transcription Factor Nrf2 by Cancer Chemopreventive Agents: Role of Antioxidant Response Element-Like Sequences in the nrf2 Promoter, Mol. Cell. Biol. (2002). https://doi.org/10.1128/MCB.22.9.2883-2892.2002.
[76] S. Mukherjee, H. Gangopadhyay, D.K. Das, Broccoli: A unique vegetable that protects mammalian hearts through the redox cycling of the thioredoxin superfamily, J. Agric. Food Chem. (2008). https://doi.org/10.1021/jf0728146.
[77] E.L. Donovan, J.M. McCord, D.J. Reuland, B.F. Miller, K.L. Hamilton, Phytochemical activation of Nrf2 protects human coronary artery endothelial cells against an oxidative challenge, Oxid. Med. Cell. Longev. (2012). https://doi.org/10.1155/2012/132931.
[78] D.W. Hwang, J.H. Kang, J.M. Jeong, J.K. Chung, M.C. Lee, S. Kim, D.S. Lee, Noninvasive in vivo monitoring of neuronal differentiation using reporter driven by a neuronal promoter, Eur. J. Nucl. Med. Mol. Imaging. (2008). https://doi.org/10.1007/s00259-007-0561-8.
[79] M.R. Vargas, D.A. Johnson, D.W. Sirkis, A. Messing, J.A. Johnson, Nrf2 activation in astrocytes protects against neurodegeneration in mouse models of familial amyotrophic lateral sclerosis, J. Neurosci. (2008). https://doi.org/10.1523/JNEUROSCI.4099-08.2008.
[80] A.T. Dinkova-Kostova, R. V. Kostov, A.G. Kazantsev, The role of Nrf2 signaling in counteracting neurodegenerative diseases, FEBS J. (2018). https://doi.org/10.1111/febs.14379.
[81] A.S. Marchev, P.A. Dimitrova, A.J. Burns, R. V. Kostov, A.T. Dinkova-Kostova, M.I. Georgiev, Oxidative stress and chronic inflammation in osteoarthritis: Can NRF2 counteract these partners in crime?, Ann. N. Y. Acad. Sci. (2017). https://doi.org/10.1111/nyas.13407.
[82] R.K. Davidson, O. Jupp, R. De Ferrars, C.D. Kay, K.L. Culley, R. Norton, C. Driscoll, T.L. Vincent, S.T. Donell, Y. Bao, I.M. Clark, Sulforaphane represses matrix-degrading proteases and protects cartilage from destruction in vitro and in vivo, Arthritis Rheum. (2013). https://doi.org/10.1002/art.38133.
[83] D. Cai, S. Yin, J. Yang, Q. Jiang, W. Cao, Histone deacetylase inhibition activates Nrf2 and protects against osteoarthritis, Arthritis Res. Ther. 17 (2015) 269. https://doi.org/10.1186/s13075-015-0774-3.

[84] R.K. Davidson, O. Jupp, R. de Ferrars, C.D. Kay, K.L. Culley, R. Norton, C. Driscoll, T.L. Vincent, S.T. Donell, Y. Bao, I.M. Clark, Sulforaphane represses matrix-degrading proteases and protects cartilage from destruction in vitro and in vivo, Osteoarthr. Cartil. (2014). https://doi.org/10.1016/j.joca.2014.02.597.

[85] J.Y. Ko, Y.J. Choi, G.J. Jeong, G. Il Im, Sulforaphane-PLGA microspheres for the intra-articular treatment of osteoarthritis, Biomaterials. (2013). https://doi.org/10.1016/j.biomaterials.2013.03.066.

[86] K. Sun, J. Luo, X. Jing, J. Guo, X. Yao, X. Hao, Y. Ye, S. Liang, J. Lin, G. Wang, F. Guo, Astaxanthin protects against osteoarthritis via Nrf2: A guardian of cartilage homeostasis, Aging (Albany. NY). (2019). https://doi.org/10.18632/aging.102474.

[87] Y. Wang, X. Zhao, M. Lotz, R. Terkeltaub, R. Liu-Bryan, Mitochondrial biogenesis is impaired in osteoarthritis chondrocytes but reversible via peroxisome proliferator-activated receptor γ coactivator 1α, Arthritis Rheumatol. (2015). https://doi.org/10.1002/art.39182.

[88] N.M. Khan, I. Ahmad, T.M. Haqqi, Nrf2/ARE pathway attenuates oxidative and apoptotic response in human osteoarthritis chondrocytes by activating ERK1/2/ELK1-P70S6K-P90RSK signaling axis, Free Radic. Biol. Med. (2018). https://doi.org/10.1016/j.freeradbiomed.2018.01.013.

[89] J.P. Pelletier, D. V. Jovanovic, V. Lascau-Coman, J.C. Fernandes, P.T. Manning, J.R. Connor, M.G. Currie, J. Martel-Pelletier, Selective inhibition of inducible nitric oxide synthase reduces progression of experimental osteoarthritis in vivo: Possible link with the reduction in chondrocyte apoptosis and caspase 3 level, Arthritis Rheum. (2000). https://doi.org/10.1002/1529-0131(200006)43:6<1290::AID-ANR11>3.0.CO;2-R.

[90] M. Deberg, A. Labasse, S. Christgau, P. Cloos, D.B. Henriksen, J.P. Chapelle, B. Zegles, J.Y. Reginster, Y. Henrotin, New serum biochemical markers (Coll 2-1 and Coll 2-1 NO2) for studying oxidative-related type II collagen network degradation in patients with osteoarthritis and rheumatoid arthritis, Osteoarthr. Cartil. (2005). https://doi.org/10.1016/j.joca.2004.12.002.

[91] C. Yang, S.W. Li, H.J. Helminen, J.S. Khillan, B. Yunhua, D.J. Prockop, Apoptosis of chondrocytes in transgenic mice lacking collagen II, Exp. Cell Res. (1997). https://doi.org/10.1006/excr.1997.3692.

[92] O. Bruyère, R.D. Altman, J.Y. Reginster, Efficacy and safety of glucosamine sulfate in the management of osteoarthritis: Evidence from real-life setting trials and surveys, Semin. Arthritis Rheum. (2016). https://doi.org/10.1016/j.semarthrit.2015.11.011.

[93] B. Mazieres, B. Combe, A.P. Van, J. Tondut, M. Grynfeltt, Chondroitin sulfate in osteoarthritis of the knee: A prospective, double blind, placebo controlled multicenter clinical study, J. Rheumatol. (2001).

[94] L. Bucsi, G. Poor, Efficacy and tolerability of oral chondroitin sulfate as a symptomatic slow-acting drug for osteoarthritis (SYSADOA) in the treatment of knee osteoarthritis, in: Osteoarthr. Cartil., 1998. https://doi.org/10.1016/S1063-4584(98)80009-5.

[95] J. Abusarah, H. Benabdoune, Q. Shi, B. Lussier, J. Martel-Pelletier, M. Malo, J.C. Fernandes, F.P. de Souza, H. Fahmi, M. Benderdour, Elucidating the Role of Protandim and 6-Gingerol in Protection Against Osteoarthritis, J. Cell. Biochem. (2017). https://doi.org/10.1002/jcb.25659.

[96] B.M. Hybertson, B. Gao, S. Bose, J.M. McCord, Phytochemical combination PB125 activates the Nrf2 pathway and induces cellular protection against oxidative injury, Antioxidants. (2019). https://doi.org/10.3390/antiox8050119.

[97] H.J. Mankin, L. Lippiello, The glycosaminoglycans of normal and arthritic cartilage., J. Clin. Invest. (1971). https://doi.org/10.1172/JCI106660.

[98] S.L. Carney, M.E.J. Billingham, H. Muir, J.D. Sandy, Demonstration of increased proteoglycan turnover in cartilage explants from dogs with experimental osteoarthritis, J. Orthop. Res. (1984). https://doi.org/10.1002/jor.1100020301.

[99] P.M. Van der Kraan, E.L. Vitters, H.M. Van Beuningen, W.B. Van den Berg, Proteoglycan synthesis and osteophyte formation in “metabolically” and “mechanically” induced murine degenerative joint disease: An in-vivo autoradiographic study, Int. J. Exp. Pathol. (1992).

[100] L. Troeberg, H. Nagase, Proteases involved in cartilage matrix degradation in osteoarthritis, Biochim. Biophys. Acta - Proteins Proteomics. (2012). https://doi.org/10.1016/j.bbapap.2011.06.020.
[101] P.M. Van Der Kraan, The changing role of TGFβ in healthy, ageing and osteoarthritic joints, Nat. Rev. Rheumatol. (2017). https://doi.org/10.1038/nrrheum.2016.219.
[102] M. Zhu, D. Tang, Q. Wu, S. Hao, M. Chen, C. Xie, R.N. Rosier, R.J. O'Keefe, M. Zuscik, D. Chen, Activation of β-catenin signaling in articular chondrocytes leads to osteoarthritis-like phenotype in adult β-catenin conditional activation mice, J. Bone Miner. Res. (2009). https://doi.org/10.1359/jbmr.080901.
[103] Q. Wu, M. Zhu, R.N. Rosier, M.J. Zuscik, R.J. O'Keefe, D. Chen, β-catenin, cartilage, and osteoarthritis, in: Ann. N. Y. Acad. Sci., 2010. https://doi.org/10.1111/j.1749-6632.2009.05212.x.
[104] P.M. Van Der Kraan, H.L. Glansbeek, E.L. Vitters, W.B. Van Den Berg, Early elevation of transforming growth factor-β, decorin, and biglycan mRNA levels during cartilage matrix restoration after mild proteoglycan depletion, J. Rheumatol. (1997).
[105] T. Aigner, K. Fundel, J. Saas, P.M. Gebhard, J. Haag, T. Weiss, A. Zien, F. Obermayr, R. Zimmer, E. Bartnik, Large-scale gene expression profiling reveals major pathogenetic pathways of cartilage degeneration in osteoarthritis, Arthritis Rheum. (2006). https://doi.org/10.1002/art.22174.
[106] G. Tsuji, M. Koshiba, H. Nakamura, H. Kosaka, S. Hatachi, C. Kurimoto, M. Kurosaka, Y. Hayashi, J. Yodoi, S. Kumagai, Thioredoxin protects against joint destruction in a murine arthritis model, Free Radic. Biol. Med. (2006). https://doi.org/10.1016/j.freeradbiomed.2006.01.006.
[107] C.C. Hong, C.B. Ambrosone, J. Ahn, J.Y. Choi, M.L. McCullough, V.L. Stevens, C. Rodriguez, M.J. Thun, E.E. Calle, Genetic variability in iron-related oxidative stress pathways (Nrf2, NQ01, NOS3, and HO-1), iron intake, and risk of postmenopausal breast cancer, Cancer Epidemiol. Biomarkers Prev. (2007). https://doi.org/10.1158/1055-9965.EPI-07-0247.
[108] S. Wyllie, J.G. Liehr, Release of iron from ferritin storage by redox cycling of stilbene and steroid estrogen metabolites: A mechanism of induction of free radical damage by estrogen, Arch. Biochem. Biophys. (1997). https://doi.org/10.1006/abbi.1997.0306.
[109] V.C. Chang, M. Cotterchio, E. Khoo, Iron intake, body iron status, and risk of breast cancer: A systematic review and meta-analysis, BMC Cancer. (2019). https://doi.org/10.1186/s12885-019-5642-0.
[110] P.A. Dieppe, L.S. Lohmander, Pathogenesis and management of pain in osteoarthritis, in: Lancet, 2005. https://doi.org/10.1016/S0140-6736(05)71086-2.
[111] Y. Ellen, P. Flecknell, M. Leach, Evaluation of using behavioural changes to assess post-operative pain in the Guinea pig (cavia porcellus), PLoS One. (2016). https://doi.org/10.1371/journal.pone.0161941.
[112] R. Longhi, R.F. Almeida, L.F. Pettenuzzo, D.G. Souza, L. Machado, A. Quincozes-Santos, D.O. Souza, Effect of a trans fatty acid-enriched diet on mitochondrial, inflammatory, and oxidative stress parameters in the cortex and hippocampus of Wistar rats, Eur. J. Nutr. (2018). https://doi.org/10.1007/s00394-017-1474-3.
[113] I. Mouse Specifics, DigiGait ™ Imaging System - Indices, (n.d.).
[114] N. Volpi, Chondroitin sulfate safety and quality, Molecules. (2019). https://doi.org/10.3390/molecules24081447.
[115] R. Strong, R.A. Miller, A. Antebi, C.M. Astle, M. Bogue, M.S. Denzel, E. Fernandez, K. Flurkey, K.L. Hamilton, D.W. Lamming, M.A. Javors, J.P. de Magalhães, P.A. Martinez, J.M. McCord, B.F. Miller, M. Müller, J.F. Nelson, J. Ndukum, G.E. Rainger, A. Richardson, D.M. Sabatini, A.B. Salmon, J.W. Simpkins, W.T. Steegenga, N.L. Nadon, D.E. Harrison, Longer lifespan in male mice treated with a weakly estrogenic agonist, an antioxidant, an α-glucosidase inhibitor or a Nrf2-inducer, Aging Cell. (2016). https://doi.org/10.1111/acel.12496.
[116] Q. Zheng, G. Zhou, R. Morello, Y. Chen, X. Garcia-Rojas, B. Lee, Type X collagen gene regulation by Runx2 contributes directly to its hypertrophic chondrocyte-specific expression in vivo, J. Cell Biol. (2003). https://doi.org/10.1083/jcb.200211089.

[117] K. Morita, T. Miyamoto, N. Fujita, Y. Kubota, K. Ito, K. Takubo, K. Miyamoto, K. Ninomiya, T. Suzuki, R. Iwasaki, M. Yagi, H. Takaishi, Y. Toyama, T. Suda, Reactive oxygen species induce chondrocyte hypertrophy in endochondral ossification, J. Exp. Med. (2007). https://doi.org/10.1084/jem.20062525.
[118] T. Jikimoto, Y. Nishikubo, M. Koshiba, S. Kanagawa, S. Morinobu, A. Morinobu, R. Saura, K. Mizuno, S. Kondo, S. Toyokuni, H. Nakamura, J. Yodoi, S. Kumagai, Thioredoxin as a biomarker for oxidative stress in patients with rheumatoid arthritis, Mol. Immunol. (2002). https://doi.org/10.1016/S0161-5890(01)00113-4.
[119] L.H. Burton, L.B. Radakovich, A.J. Marolf, K.S. Santangelo, Systemic iron overload exacerbates osteoarthritis in the strain 13 guinea pig, Osteoarthr. Cartil. (2020). https://doi.org/10.1016/j.joca.2020.06.005.
[120] C.P. Anderson, M. Shen, R.S. Eisenstein, E.A. Leibold, Mammalian iron metabolism and its control by iron regulatory proteins, Biochim. Biophys. Acta - Mol. Cell Res. (2012). https://doi.org/10.1016/j.bbamcr.2012.05.010.
[121] L. Kennish, M. Attur, C. Oh, S. Krasnokutsky, J. Samuels, J.D. Greenberg, X. Huang, S.B. Abramson, Age-dependent ferritin elevations and HFE C282Y mutation as risk factors for symptomatic knee osteoarthritis in males: A longitudinal cohort study, BMC Musculoskelet. Disord. (2014). https://doi.org/10.1186/1471-2474-15-8.
[122] A.H. Warriner, N.M. Patkar, J.R. Curtis, E. Delzell, L. Gary, M. Kilgore, K. Saag, Which fractures are most attributable to osteoporosis?, J. Clin. Epidemiol. (2011). https://doi.org/10.1016/j.jclinepi.2010.07.007.
[123] M. Almeida, L. Han, M. Martin-Millan, L.I. Plotkin, S.A. Stewart, P.K. Roberson, S. Kousteni, C.A. O'Brien, T. Bellido, A.M. Parfitt, R.S. Weinstein, R.L. Jilka, S.C. Manolagas, Skeletal involution by age-associated oxidative stress and its acceleration by loss of sex steroids, J. Biol. Chem. (2007). https://doi.org/10.1074/jbc.M702810200.
[124] C.J. Jagger, J.M. Lean, J.T. Davies, T.J. Chambers, Tumor necrosis factor-α mediates osteopenia caused by depletion of antioxidants, Endocrinology. (2005). https://doi.org/10.1210/en.2004-1058.
[125] K. Reziwan, D. Sun, B. Zhang, Z. Zhao, MicroRNA-1225 activates Keap1-Nrf2-HO-1 signalling to inhibit TNFα-induced osteoclastogenesis by mediating ROS generation, Cell Biochem. Funct. (2019). https://doi.org/10.1002/cbf.3394.
[126] A.S. Schreurs, S. Torres, T. Truong, E.L. Moyer, A. Kumar, C.G.T. Tahimic, J.S. Alwood, R.K. Globus, Skeletal tissue regulation by catalase overexpression in mitochondria, Am. J. Physiol. - Cell Physiol. (2020). https://doi.org/10.1152/ajpcell.00068.2020.
[127] M. Sova, L. Saso, Design and development of Nrf2 modulators for cancer chemoprevention and therapy: A review, Drug Des. Devel. Ther. (2018). https://doi.org/10.2147/DDDT.S172612.
[128] M.S.P.H.K. Smith, Robert; Tran, Kevin; Smith, Cynthia; McDonald, The Role of the Nrf2/ARE Antioxidant System in Preventing Cardiovascular Diseases, Diseases. 4 (2016).
[129] J. Kim, Y.N. Cha, Y.J. Surh, A protective role of nuclear factor-erythroid 2-related factor-2 (Nrf2) in inflammatory disorders, Mutat. Res. - Fundam. Mol. Mech. Mutagen. 690 (2010) 12–23. https://doi.org/10.1016/j.mrfmmm.2009.09.007.
[130] Y. Kubo, C.J. Wruck, A. Fragoulis, W. Drescher, H.C. Pape, P. Lichte, H. Fischer, M. Tohidnezhad, F. Hildebrand, T. Pufe, H. Jahr, Role of Nrf2 in Fracture Healing: Clinical Aspects of Oxidative Stress, Calcif. Tissue Int. (2019). https://doi.org/10.1007/s00223-019-00576-3.
[131] S. Hyeon, H. Lee, Y. Yang, W. Jeong, Nrf2 deficiency induces oxidative stress and promotes RANKL-induced osteoclast differentiation, Free Radic. Biol. Med. (2013). https://doi.org/10.1016/j.freeradbiomed.2013.08.005.
[132] X. Li, Y. Chen, Y. Mao, P. Dai, X. Sun, X. Zhang, H. Cheng, Y. Wang, I. Banda, G. Wu, J. Ma, S. Huang, T. Forouzanfar, Curcumin Protects Osteoblasts From Oxidative Stress-Induced Dysfunction via GSK3β-Nrf2 Signaling Pathway, Front. Bioeng. Biotechnol. (2020). https://doi.org/10.3389/fbioe.2020.00625.
[133] H. Li, C. Huang, J. Zhu, K. Gao, J. Fang, H. Li, Lutein suppresses oxidative stress and inflammation

by Nrf2 activation in an osteoporosis rat model, Med. Sci. Monit. (2018). https://doi.org/10.12659/MSM.908699.
[134] C.J. Wruck, A. Fragoulis, A. Gurzynski, L.O. Brandenburg, Y.W. Kan, K. Chan, J. Hassenpflug, S. Freitag-Wolf, D. Varoga, S. Lippross, T. Pufe, Role of oxidative stress in rheumatoid arthritis: Insights from the Nrf2-knockout mice, Ann. Rheum. Dis. (2011). https://doi.org/10.1136/ard.2010.132720.
[135] L.F. Bonewald, D.P. Kiel, T.L. Clemens, K. Esser, E.S. Orwoll, R.J. O'Keefe, R.A. Fielding, Forum on bone and skeletal muscle interactions: Summary of the proceedings of an ASBMR workshop, J. Bone Miner. Res. (2013). https://doi.org/10.1002/jbmr.1980.
[136] D.J. Digirolamo, D.P. Kiel, K.A. Esser, Bone and skeletal muscle: Neighbors with close ties, J. Bone Miner. Res. (2013). https://doi.org/10.1002/jbmr.1969.
[137] L.M. Wancket, Animal Models for Evaluation of Bone Implants and Devices: Comparative Bone Structure and Common Model Uses, Vet. Pathol. (2015). https://doi.org/10.1177/0300985815593124.
[138] I.S. Maggiano, C.M. Maggiano, V.G. Tiesler, J.R. Chi-Keb, S.D. Stout, Drifting Diaphyses: Asymmetry in Diametric Growth and Adaptation Along the Humeral and Femoral Length, Anat. Rec. (2015). https://doi.org/10.1002/ar.23201.
[139] M.I. Carter, P.S. Hinton, Physical activity and bone health., Mo. Med. (2014).
[140] A. Creecy, S. Uppuganti, M.R. Girard, S.G. Schlunk, C. Amah, M. Granke, M. Unal, M.D. Does, J.S. Nyman, The age-related decrease in material properties of BALB/c mouse long bones involves alterations to the extracellular matrix, Bone. (2020). https://doi.org/10.1016/j.bone.2019.115126.
[141] V. Gorbunova, M.J. Bozzella, A. Seluanov, Rodents for comparative aging studies: From mice to beavers, Age (Omaha). (2008). https://doi.org/10.1007/s11357-008-9053-4.
[142] A.L. Boskey, R. Coleman, Aging and Bone, J. Dent. Res. (2010). https://doi.org/10.1177/0022034510377791.
[143] A.G. Robling, The interaction of biological factors with mechanical signals in bone adaptation: Recent developments, Curr. Osteoporos. Rep. (2012). https://doi.org/10.1007/s11914-012-0099-y.
[144] S.S. Mao, D. Li, Y. Luo, Y.S. Syed, M.J. Budoff, Application of quantitative computed tomography for assessment of trabecular bone mineral density, microarchitecture and mechanical property, Clin. Imaging. (2016). https://doi.org/10.1016/j.clinimag.2015.09.016.
[145] P. Ammann, R. Rizzoli, Bone strength and its determinants., Osteoporos. Int. (2003). https://doi.org/10.1007/s00198-002-1345-4.
[146] D.D. Sosa, E.F. Eriksen, Reduced Bone Material Strength is Associated with Increased Risk and Severity of Osteoporotic Fractures. An Impact Microindentation Study, Calcif. Tissue Int. (2017). https://doi.org/10.1007/s00223-017-0256-5.
[147] E.F. Eriksen, Commentary on sclerostin deficiency is linked to altered bone composition, J. Bone Miner. Res. (2014). https://doi.org/10.1002/jbmr.2346.
[148] Y.X. Sun, L. Li, K.A. Corry, P. Zhang, Y. Yang, E. Himes, C.L. Mihuti, C. Nelson, G. Dai, J. Li, Deletion of Nrf2 reduces skeletal mechanical properties and decreases load-driven bone formation, Bone. (2015). https://doi.org/10.1016/j.bone.2014.12.066.
[149] L. Ibáñez, M.L. Ferrándiz, R. Brines, D. Guede, A. Cuadrado, M.J. Alcaraz, Effects of Nrf2 deficiency on bone microarchitecture in an experimental model of osteoporosis, Oxid. Med. Cell. Longev. (2014). https://doi.org/10.1155/2014/726590.
[150] B. Charvet, F. Ruggiero, D. Le Guellec, The development of the myotendinous junction. A review, Muscles. Ligaments Tendons J. (2012).
[151] T.A.H. Järvinen, T.L.N. Järvinen, M. Kääriäinen, H. Kalimo, M. Järvinen, Muscle injuries: Biology and treatment, Am. J. Sports Med. (2005). https://doi.org/10.1177/0363546505274714.
[152] J. Garrett, Muscle strain injuries, Am. J. Sports Med. (1996). https://doi.org/10.1249/00005768-199008000-00003.
[153] J. Mendiguchia, E. Alentorn-Geli, F. Idoate, G.D. Myer, Rectus femoris muscle injuries in football: A clinically relevant review of mechanisms of injury, risk factors and preventive strategies, Br. J.

Sports Med. (2013). https://doi.org/10.1136/bjsports-2012-091250.
[154] U. Proske, T.J. Allen, Damage to skeletal muscle from eccentric exercise, Exerc. Sport Sci. Rev. (2005). https://doi.org/10.1097/00003677-200504000-00007.
[155] J.T. Bencardino, Z.S. Rosenberg, R.R. Brown, A. Hassankhani, E.S. Lustrin, J. Beltran, Traumatic musculotendinous injuries of the knee: Diagnosis with MR imaging, Radiographics. (2000). https://doi.org/10.1148/radiographics.20.suppl_1.g00oc16s103.
[156] B.H. Jones, D.N. Cowan, J.P. Tomlinson, J.R. Robinson, D.W. Polly, P.N. Frykman, Epidemiology of injuries associated with physical training among young men in the army, Med. Sci. Sports Exerc. (1993). https://doi.org/10.1249/00005768-199302000-00006.
[157] P.L. Davidson, D.J. Chalmers, B.D. Wilson, D. McBride, Lower limb injuries in New Zealand Defence Force personnel: Descriptive epidemiology, Aust. N. Z. J. Public Health. (2008). https://doi.org/10.1111/j.1753-6405.2008.00195.x.
[158] S.A. Almeida, K.M. Williams, R.A. Shaffer, S.K. Brodine, Epidemiological patterns of musculoskeletal injuries and physical training, Med. Sci. Sports Exerc. (1999). https://doi.org/10.1097/00005768-199908000-00015.
[159] M.C. Drakos, B. Domb, C. Starkey, L. Callahan, A.A. Allen, Injury in the National Basketball Association: A 17-year overview, Sports Health. (2010). https://doi.org/10.1177/1941738109357303.
[160] J. Shi, S. Gardner, K.K. Wheeler, M.C. Thompson, B. Lu, L. Stallones, H. Xiang, Characteristics of nonfatal occupational injuries among U.S. workers with and without disabilities, Am. J. Ind. Med. (2015). https://doi.org/10.1002/ajim.22395.
[161] T.J. Noonan, W.E. Garrett, Muscle strain injury: diagnosis and treatment., J. Am. Acad. Orthop. Surg. (1999). https://doi.org/10.5435/00124635-199907000-00006.
[162] K.R. Kaufman, S. Brodine, R. Shaffer, Military training-related injuries: Surveillance, research, and prevention, Am. J. Prev. Med. (2000). https://doi.org/10.1016/S0749-3797(00)00114-8.
[163] J.W. Orchard, Intrinsic and extrinsic risk factors for muscle strains in Australian football, Am. J. Sports Med. (2001). https://doi.org/10.1177/03635465010290030801.
[164] Z. Yan, S. Choi, X. Liu, M. Zhang, J.J. Schageman, S.Y. Lee, R. Hart, L. Lin, F.A. Thurmond, R.S. Williams, Highly coordinated gene regulation in mouse skeletal muscle regeneration, J. Biol. Chem. (2003). https://doi.org/10.1074/jbc.M209879200.
[165] C.A. Mitchell, J.K. McGeachie, M.D. Grounds, Cellular differences in the regeneration of murine skeletal muscle: a quantitative histological study in SJL/J and BALB/c mice, Cell Tissue Res. (1992). https://doi.org/10.1007/BF00384736.
[166] L.S. dos Santos, J.C. Saltorato, M.G. Monte, R.L. Marcos, R.Á.B. Lopes-Martins, S.S. Tomazoni, E.C.P. Leal-Junior, R.L. de Paiva Carvalho, PBMT and topical diclofenac as single and combined treatment on skeletal muscle injury in diabetic rats: effects on biochemical and functional aspects, Lasers Med. Sci. (2019). https://doi.org/10.1007/s10103-018-2580-z.
[167] S.E. Anderson, W.M. Han, V. Srinivasa, M. Mohiuddin, M.A. Ruehle, J.Y. Moon, E. Shin, C.L. San Emeterio, M.E. Ogle, E.A. Botchwey, N.J. Willett, Y.C. Jang, Determination of a critical size threshold for volumetric muscle loss in the mouse quadriceps, Tissue Eng. - Part C Methods. (2019). https://doi.org/10.1089/ten.tec.2018.0324.
[168] A. Thirupathi, S. Freitas, H.R. Sorato, G.S. Pedroso, P.S. Effting, A.P. Damiani, V.M. Andrade, R.T. Nesi, R.C. Gupta, A.P. Muller, R.A. Pinho, Modulatory effects of taurine on metabolic and oxidative stress parameters in a mice model of muscle overuse, Nutrition. (2018). https://doi.org/10.1016/j.nut.2018.03.058.
[169] A. Iwata, S. Fuchioka, K. Hiraoka, M. Masuhara, K. Kami, Characteristics of locomotion, muscle strength, and muscle tissue in regenerating rat skeletal muscles, Muscle and Nerve. (2010). https://doi.org/10.1002/mus.21567.
[170] F.T.G. Rahusen, P.S. Weinhold, L.C. Almekinders, Nonsteroidal anti-inflammatory drugs and acetaminophen in the treatment of an acute muscle injury, Am. J. Sports Med. (2004). https://doi.org/10.1177/0363546504266069.

[171] S.J.P. Pratt, M.W. Lawlor, S.B. Shah, R.M. Lovering, An in vivo rodent model of contraction-induced injury in the quadriceps muscle, Injury. (2012). https://doi.org/10.1016/j.injury.2011.09.015.
[172] P. Contreras-Muñoz, A. Fernández-Martín, R. Torrella, X. Serres, M. De La Varga, G. Viscor, T.A.H. Järvinen, V. Martínez-Ibáñez, J.L. Peiró, G. Rodas, M. Marotta, A New Surgical Model of Skeletal Muscle Injuries in Rats Reproduces Human Sports Lesions, Int. J. Sports Med. (2016). https://doi.org/10.1055/s-0035-1555933.
[173] T.M. Best, R.P. Mccabe, D. Corr, R. Vanderby, Evaluation of a new method to create a standardized muscle stretch injury, Med. Sci. Sports Exerc. (1998). https://doi.org/10.1097/00005768-199802000-00005.
[174] S.L. Brickson, R.P. McCabe, A.W. Pala, R. Vanderby, A model for creating a single stretch injury in murine biarticular muscle, BMC Sports Sci. Med. Rehabil. (2014). https://doi.org/10.1186/2052-1847-6-14.
[175] K.P. Speer, J. Lohnes, W.E. Garrett, E. Eriksson, Radiographic imaging of muscle strain injury, Am. J. Sports Med. (1993). https://doi.org/10.1177/036354659302100116.
[176] C. Hughes, C.T. Hasselman, T.M. Best, S. Martinez, W.E. Garrett, Incomplete, Intrasubstance Strain Injuries of the Rectus Femoris Muscle, Am. J. Sports Med. (1995). https://doi.org/10.1177/036354659502300422.
[177] A.H. Sonin, S.W. Fitzgerald, M.E. Bresler, M.D. Kirsch, F.L. Hoff, H. Friedman, MR imaging appearance of the extensor mechanism of the knee: functional anatomy and injury patterns., Radiographics. (1995). https://doi.org/10.1148/radiographics.15.2.7761641.
[178] D. V. Flores, C.M. Gómez, M. Estrada-Castrillón, E. Smitaman, M.N. Pathria, MR imaging of muscle trauma: Anatomy, biomechanics, pathophysiology, and imaging appearance, Radiographics. (2018). https://doi.org/10.1148/rg.2018170072.
[179] A.F. Costa, G.A. Di Primio, M.E. Schweitzer, Magnetic resonance imaging of muscle disease: A pattern-based approach, Muscle and Nerve. (2012). https://doi.org/10.1002/mus.23370.
[180] F. Faul, E. Erdfelder, A.G. Lang, A. Buchner, G*Power 3: A flexible statistical power analysis program for the social, behavioral, and biomedical sciences, in: Behav. Res. Methods, 2007. https://doi.org/10.3758/BF03193146.
[181] A.M. Pardes, B.R. Freedman, L.J. Soslowsky, Ground reaction forces are more sensitive gait measures than temporal parameters in rodents following rotator cuff injury, J. Biomech. (2016). https://doi.org/10.1016/j.jbiomech.2015.12.027.
[182] S.I. Rooney, E. Loro, J.J. Sarver, C.D. Peltz, M.W. Hast, W.J. Tseng, A.F. Kuntz, X. Sherry Liu, T.S. Khurana, L.J. Soslowsky, Exercise protocol induces muscle, tendon, and bone adaptations in the rat shoulder, Muscles. Ligaments Tendons J. (2014). https://doi.org/10.11138/mltj/2014.4.4.413.
[183] L. Jafari, P. Vachon, F. Beaudry, E. Langelier, Histopathological, biomechanical, and behavioral pain findings of achilles tendinopathy using an animal model of overuse injury, Physiol. Rep. (2015). https://doi.org/10.14814/phy2.12265.
[184] J. Ekstrand, M. Hägglund, M. Waldén, Epidemiology of muscle injuries in professional football (soccer), Am. J. Sports Med. (2011). https://doi.org/10.1177/0363546510395879.
[185] P.S. Bradley, M.D. Portas, The relationship between preseason range of motion and muscle strain injury in elite soccer players, J. Strength Cond. Res. (2007). https://doi.org/10.1519/R-20416.1.

# APPENDIX

## Chapter 2 Supplemental Tables

**Supplemental Table 2.1. Normalized absolute mRNA counts from pooled articular cartilage and menisci of 5-month-old control and Nrf2-activator treated Hartley guinea pigs.** Data is depicted as mean and standard deviation. Trending (*p<0.15, italic)* and significant (**p<0.05, bold**) sources of variation (determined via 2-way ANOVA, factors signifying sex and treatment) are depicted in table 1. Trending *(p<0.15, italic)* and significant (**p<0.05, bold**) differences between groups (determined via Bonferroni multiple comparisons) are listed in the last column.

*2-way ANOVA key:*
- $^{\S}$*sex*
- $^{\ddagger}$*treatment*
- $^{\dagger}$*interaction*
- *NS no significant or trending source of variation identified*

*Bonferroni multiple comparisons key:*
- $^{*}$*Difference between control males and PB125 males*
- $^{\infty}$*Difference between control females and PB125 females*
- $^{\Psi}$*Difference between control males and control females*
- $^{\Delta}$*Difference between PB125 males and PB125 females*
- *NS no significant or trending difference*

| Gene | Description | Male Control (n=12) | Male PB125 (n=14) | Female Control (n=13) | Female PB125 (n=13) | 2-way ANOVA p-values | Bonferroni p-values |
|---|---|---|---|---|---|---|---|
| **Aggrecan** | Cartilage structure | 14177.6; 4450.7 | 20365.1; 7514.5 | 16291.7; 6846.1 | 16977.5; 7380.5 | *0.0718*$^{\ddagger}$ *0.1471*$^{\dagger}$ | **0.047**$^{*}$ |
| **Adiponectin** | Glucose & FA metabolism | 18416.1; 12670.1 | 11598.8; 5703.4 | 20295.0; 10224.6 | 19656.3; 14195.5 | *0.1121*$^{\S}$ | *0.1288*$^{\Delta}$ |
| **AKT** | Cellular survival and proliferation | 6155.7; 1279.8 | 6144.0; 3997.6 | 4893.5; 729.5 | 5779.6; 1869.9 | NS | NS |
| **BAD** | Inducer of apoptosis | 1060.2; 172.5 | 874.0; 89.7 | 799.0; 111.8 | 867.2; 177.7 | **0.0025**$^{\dagger}$ **0.0016**$^{\S}$ *0.1460*$^{\ddagger}$ | **0.0041**$^{*}$ **<0.0001**$^{\Psi}$ |
| **BAK** | Intrinsic apoptosis | 2348.2; 399.9 | 1970.0; 417.9 | 1848.1; 297.7 | 2238.2; 730.3 | **0.0075**$^{\dagger}$ | **0.0285**$^{\Psi}$ *0.1205*$^{*}$ *0.0967*$^{\infty}$ |
| **BAX** | Intrinsic apoptosis | 1474.3; 231.3 | 1314.1; 158.8 | 1160.8; 139.5 | 1378.8; 307.9 | **0.0035**$^{\dagger}$ **0.0488**$^{\S}$ | **0.0017**$^{\Psi}$ **0.0294**$^{\infty}$ *0.1492*$^{*}$ |
| **BCL-2** | Inhibitor of apoptosis | 1510.0; 272.3 | 1277.2; 333.9 | 1707.1; 368.6 | 1499.7; 499.9 | **0.0418**$^{\ddagger}$ *0.0520*$^{\S}$ | NS |
| **BECN1** | Regulator of autophagy | 2567.5; 416.6 | 2178.6; 373.9 | 2021.3; 284.8 | 2751.6; 1260.3 | **0.0071**$^{\dagger}$ | **0.0232**$^{\infty}$ *0.1206*$^{\Psi}$ *0.0898*$^{\Delta}$ |
| **BIM** | Pro-apoptotic BH3 protein | 364.4; 56.8 | 322.4; 58.2 | 329.1; 67.4 | 385.9; 145.9 | *0.0577*$^{\ddagger}$ | NS |

| | | | | | | | |
|---|---|---|---|---|---|---|---|
| **BMP-7** | Anabolic effect on cartilage | 83.7; 20.7 | 63.2; 20.2 | 70.9; 18.3 | 90.1; 17.9 | **0.0006**$^{\dagger}$ | **0.0211**$^{*}$ **0.0299**$^{\infty}$ **0.0018**$^{\Delta}$ |
| **C3** | Activator of complement | 2224.3; 1108.6 | 1525.6; 617.9 | 1680.4; 621.9 | 2265.2; 1381.1 | **0.0224**$^{\ddagger}$ | *0.1519*$^{*}$ *0.1113*$^{\Delta}$ |
| **Caspase-1** | Initiator of apoptosis | 144.8; 28.6 | 162.0; 37.2 | 176.9; 40.2 | 169.7; 83.7 | NS | NS |
| **Caspase-3** | Executioner of apoptosis | 412.5; 57.4 | 377.4; 52.1 | 348.2; 62.5 | 350.5; 79.2 | **0.0128**$^{\S}$ | **0.0294**$^{\Psi}$ |
| **Caspase-8** | Executes extrinsic apoptosis | 228.3; 23.5 | 232.9; 78.4 | 224.4; 33.8 | 248.3; 58.9 | NS | NS |
| **Caspase-9** | Executes intrinsic apoptosis | 277.1; 47.4 | 221.1; 46.8 | 218.3; 38.6 | 266.3; 71.4 | **0.0010**$^{\dagger}$ | **0.0215**$^{*}$ **0.0487**$^{\infty}$ **0.0152**$^{\Psi}$ *0.0669*$^{\Delta}$ |
| **Catalase** | Protects from oxidative damage via degradation of $2H_2O_2 \rightarrow O_2 + 2H_2O$ | 12115.3; 2026.9 | 9989.9; 2069.6 | 13639.4; 2128.4 | 11808.5; 2044.6 | **0.0055**$^{\S}$ **0.0012**$^{\ddagger}$ | *0.1438*$^{\Psi}$ *0.0539*$^{\Delta}$ |
| **CBS** | Mediates early transsulfuration | 37.5; 6.9 | 34.3; 10.6 | 35.2; 8.3 | 37.4; 10.4 | NS | NS |
| **CCL-2** | Chemoattractant agent for myeloid and lymphoid cells | 3656.6; 1672.1 | 2892.9; 1574.8 | 3013.4; 1733.0 | 2195.7; 1834.6 | *0.1014*$^{\ddagger}$ | NS |
| **CD163** | Scavenger receptor for hemoglobin-haptoglobin | 3025.1; 934.8 | 2880.2; 513.2 | 2782.8; 612.9 | 2360.1; 567.8 | **0.0454**$^{\S}$ *0.1326*$^{\ddagger}$ | *0.0976*$^{\Delta}$ |
| **COL10A1** | Marker of chondrocytes hypertrophy | 266.3; 125.5 | 256.5; 130.1 | 360.8; 227.1 | 530.8; 414.1 | **0.0116**$^{\S}$ | *0.0141*$^{\Delta}$ |
| **COL2A1** | Structural component of cartilage | 1152287.9; 328219.0 | 1177245.8; 591386.6 | 803744.3; 291273.9 | 998664.2; 268734.5 | **0.0212**$^{\S}$ | *0.0675*$^{\Psi}$ |
| **CUL3** | Ubiquitin ligase | 3416.3; 167.7 | 2962.5; 597.4 | 3392.9; 277.0 | 3027.3; 681.6 | **0.0042**$^{\ddagger}$ | **0.0478**$^{*}$ *0.1221*$^{\infty}$ |
| **FGF-18** | Anabolic effect on cartilage | 3367.9; 962.1 | 3212.8; 1160.9 | 2760.3; 614.4 | 2930.1; 840.3 | *0.0882*$^{\S}$ | NS |
| **FTH-1** | Intracellular iron storage protein | 135133.2; 14696.6 | 122858.1; 15046.7 | 128022.6; 14204.5 | 128593.6; 20333.7 | NS | NS |
| **Glutathione peroxidase** | Nrf2 mediated antioxidant; $2H_2O_2 \rightarrow O_2 + 2H_2O$ $O_2^{=} \rightarrow O_2 + OH$ | 12656.4; 2538.3 | 10727.6; 2286.6 | 10201.5; 2684.3 | 15019.2; 5518.2 | **0.0013**$^{\dagger}$ *0.1508*$^{\ddagger}$ | **0.0022**$^{\infty}$ **0.0065**$^{\Delta}$ |
| **GSK3β** | Inactivates nuclear Nrf2 | 3029.9; 368.2 | 2425.6; 433.3 | 2550.7; 281.6 | 2417.9; 436.7 | **0.0330**$^{\dagger}$ **0.0279**$^{\S}$ **0.0012**$^{\ddagger}$ | **0.0005**$^{*}$ **0.0065**$^{\Psi}$ |

| | | | | | | | |
|---|---|---|---|---|---|---|---|
| **HAMP** | Regulates iron absorption | 22.6; 5.8 | 22.3; 9.6 | 19.9; 5.9 | 25.2; 8.2 | NS | NS |
| **HIF1-a** | Transcriptional response to hypoxia | 19769.0; 7249.6 | 19230.3; 6000.9 | 14781.3; 5331.7 | 12752.1; 5523.1 | **0.0013**$^{\S}$ | **0.0154**$^{\Delta}$ *0.0894*$^{\Psi}$ |
| **HMGB1** | Proinflammatory alarmin | 15989.9; 2165.9 | 14522.2; 2265.3 | 15002.0; 1206.5 | 14094.7; 2719.9 | *0.0538*$^{\ddagger}$ | NS |
| **HMOX-1** | Nrf2 regulated antioxidant that degrades heme | 2773.6; 907.6 | 2523.4; 887.9 | 1973.4; 528.4 | 2619.0; 1186.3 | *0.0849*$^{\dagger}$ | *0.0653*$^{\Psi}$ |
| **IFN-γ** | Implemented in rheumatoid arthritis | 11.8; 3.7 | 14.7; 5.2 | 11.7; 3.8 | 15.9; 6.1 | *0.0107*$^{\ddagger}$ | *0.0556*$^{\infty}$ |
| **IL-10** | Anti-inflammatory cytokine | 29.5; 5.9 | 34.9; 14.7 | 30.0; 8.1 | 34.6; 6.7 | *0.0717*$^{\ddagger}$ | NS |
| **IL-1β** | Proinflammatory cytokine | 113.5; 47.9 | 114.6; 51.8 | 132.5; 47.8 | 158.5; 62.4 | **0.0373**$^{\S}$ | *0.0724*$^{\Delta}$ |
| **IL-4** | T-cell differentiation and Th2 immune response | 69.3; 15.1 | 68.2; 28.0 | 56.2; 15.5 | 59.8; 13.8 | **0.0498**$^{\S}$ | NS |
| **IL-5** | Induced eosinophil differentiation | 27.2; 6.6 | 30.6; 10.8 | 26.0; 6.8 | 26.7; 6.9 | NS | NS |
| **IL-6** | Proinflammatory cytokine | 166.6; 92.9 | 163.7; 81.1 | 161.6; 156.4 | 115.8; 48.5 | NS | NS |
| **KEAP1** | Degrades cytoplasmic Nrf2 | 2127.8; 280.5 | 2006.5; 521.1 | 1900.1; 337.5 | 2455.2; 819.4 | **0.0293**$^{\dagger}$ | **0.0227**$^{\infty}$ *0.0767*$^{\Delta}$ |
| **LEP** | Adipokine and regulator of appetite | 4316.5; 3828.0 | 2415.9; 3816.8 | 3325.3; 3989.9 | 4302.8; 10469.6 | NS | NS |
| **MAPK** | Cell differentiation, proliferation, and survival | 4229.8; 393.5 | 3610.4; 513.6 | 3741.9; 291.6 | 3571.8; 672.6 | **0.0057**$^{\ddagger}$ *0.1062*$^{\dagger}$ *0.0596*$^{\S}$ | **0.0333**$^{\Psi}$ **0.0048**$^{*}$ |
| **MCL1** | Inhibitor of apoptosis | 8323.5; 849.5 | 7284.9; 925.1 | 7497.6; 639.7 | 7118.5; 1253.8 | *0.0647*$^{\S}$ **0.0095**$^{\ddagger}$ | *0.0678*$^{\Psi}$ **0.0149**$^{*}$ |
| **MMP-13** | Cleaves type II collagen | 5182.3; 2267.4 | 4999.4; 1857.7 | 5879.9; 2153.6 | 7074.5; 3052.9 | **0.0402**$^{\S}$ | *0.0547*$^{\Delta}$ |
| **MMP-2** | Cleaves type IV collagen | 61945.9; 12277.3 | 64706.1; 23118.5 | 48541.4; 8796.2 | 48396.6; 13700.5 | **0.0013**$^{\S}$ | **0.0190**$^{\Delta}$ *0.0755*$^{\Psi}$ |
| **MMP-3** | Cleaves type II-IV, IX and X collagens | 760.2; 165.0 | 717.3; 154.5 | 691.3; 198.0 | 624.5; 211.9 | *0.1197*$^{\S}$ | NS |
| **MMP-9** | Cleaves type IV & V collagen, activates neutrophils | 3709.7; 1374.7 | 3430.6; 1585.7 | 3553.5; 1136.3 | 5149.5; 1586.0 | **0.0230**$^{\dagger}$ *0.0562*$^{\S}$ *0.1056*$^{\ddagger}$ | **0.0064**$^{\Delta}$ **0.0135**$^{\infty}$ |
| **MTOR** | Regulator of cell metabolism and growth | 1356.8; 342.1 | 978.2; 180.9 | 1012.9; 236.9 | 1270.3; 599.7 | **0.0042**$^{\dagger}$ | **0.0311**$^{*}$ *0.0543*$^{\Psi}$ *0.1079*$^{\Delta}$ |

| | | | | | | | |
|---|---|---|---|---|---|---|---|
| **NF-κB-1** | Proinflammatory transcription factor | 488.6; 68.3 | 448.2; 45.9 | 459.6; 46.4 | 469.5; 92.6 | NS | NS |
| **NFE-2** | Oxidant induced anti-inflammatory transcription factor | 450.6; 346.5 | 405.5; 196.2 | 605.4; 369.6 | 636.5; 400.6 | NS | NS |
| **NFE2L2** | Oxidant induced anti-inflammatory transcription factor | 5140.5; 540.1 | 4475.7; 566.0 | 4803.4; 357.5 | 4737.1; 703.4 | **0.0216**$^{\ddagger}$ *0.0578*$^{\dagger}$ | **0.0080**$^{*}$ |
| **NOS1** | Neuronal and constitutively expressed; synthesizes NO | 73.8; 21.4 | 70.7; 30.1 | 61.7; 17.2 | 75.1; 22.3 | NS | NS |
| **NOS2** | Cytokine induced NO synthesis | 423.1; 116.0 | 376.9; 138.6 | 329.1; 105.0 | 389.9; 104.3 | *0.1085*$^{\dagger}$ | *0.1002*$^{\Psi}$ |
| **NOS3** | Endothelial induced NO in shear stress | 143.9; 59.4 | 114.0; 31.4 | 103.2; 30.6 | 134.7; 75.9 | **0.0435**$^{\dagger}$ | *0.1210*$^{\Psi}$ |
| **NQO1** | Nrf2 mediated removal of toxic intermediates | 6966.7; 832.9 | 6897.3; 932.6 | 5978.1; 740.7 | 6267.6; 701.9 | **0.0008**$^{\S}$ | **0.0074**$^{\Psi}$ *0.0979*$^{\Delta}$ |
| **NURR1** | Neuroinflammatory transcription factor | 2492.3; 1122.8 | 1841.2; 654.0 | 1778.9; 864.1 | 1907.1; 814.9 | **0.1098**$^{\dagger}$ | *0.0914*$^{\Psi}$ *0.1256*$^{*}$ |
| **Nrf1** | Transcriptional modulation of metabolism, growth, and development | 505.6; 55.4 | 497.1; 51.1 | 544.5; 57.2 | 564.9; 75.6 | **0.0026**$^{\S}$ | **0.0108**$^{\Delta}$ |
| **PCSK9** | LDL-cholesterol metabolism | 17.0; 7.0 | 13.8; 2.8 | 11.5; 3.0 | 16.4; 22.0 | NS | NS |
| **PPARγ** | Adipocyte differentiation; senescence | 480.4; 230.7 | 330.4; 82.5 | 443.6; 135.6 | 491.4; 201.1 | **0.0400**$^{\dagger}$ | **0.0315**$^{\Delta}$ *0.0595*$^{*}$ |
| **PRDX1** | Nrf2 antioxidant; detoxifies peroxides | 10976.2; 1277.7 | 10803.7; 1444.5 | 9970.1; 1208.4 | 8545.8; 2649.9 | **0.0018**$^{\S}$ *0.1112*$^{\ddagger}$ | |
| **PTGS-1** | Proinflammatory enzyme | 703.6; 145.5 | 761.5; 492.9 | 630.2; 122.1 | 1000.4; 953.4 | NS | NS |
| **PTGS-2** | Proinflammatory enzyme | 179.1; 108.7 | 165.3; 73.1 | 168.5; 108.1 | 153.0; 102.0 | NS | NS |
| **RIPK1** | Driver of apoptosis and necroptosis | 1581.3; 113.7 | 1499.5; 145.1 | 1517.7; 117.7 | 1400.0; 247.9 | **0.0359**$^{\ddagger}$ *0.0840*$^{\S}$ | *0.1499*$^{\infty}$ |
| **RUNX2** | Osteoblast differentiation | 1210.9; 261.8 | 1024.9; 260.5 | 1156.2; 263.2 | 1345.9; 389.3 | **0.0278**$^{\dagger}$ *0.1145*$^{\S}$ | **0.0138**$^{\Delta}$ |

| | | | | | | | |
|---|---|---|---|---|---|---|---|
| **SCL11A2** | Metal transport, iron uptake | 1376.7; 158.3 | 1414.5; 376.2 | 1252.4; 193.8 | 1607.2; 768.5 | *0.1253*[‡] | *0.0989*[∞] |
| **SESN2** | Stress-induced metabolic regulator | 146.4; 35.9 | 115.0; 23.8 | 122.2; 37.7 | 139.4; 58.7 | **0.0401**[†] | *0.1246*[*] |
| **SLC39A14** | Divalent metal transporter | 1607.1; 726.4 | 1522.4; 547.6 | 1158.3; 459.8 | 1532.4; 1166.9 | NS | NS |
| **SLC40A1** | Ferroportin; transports iron | 2373.8; 443.4 | 2425.2; 286.2 | 2740.7; 380.1 | 2354.4; 456.2 | *0.1305*[‡] *0.0500*[†] | **0.0494**[Ψ] **0.0289**[∞] |
| **SLC7A11** | Cystine/glutamate antiporter; preserves redox balance | 76.6; 19.9 | 77.4; 17.6 | 57.3; 18.3 | 71.0; 44.0 | *0.0992*[§] | NS |
| **SOD-1** | Cytoplasmic dismutation of $O_2^- \rightarrow O_2 + H_2O_2$ | 9109.6; 401.6 | 8899.6; 876.4 | 8818.8; 768.3 | 9287.7; 1228.2 | NS | NS |
| **SOD-2** | Mitochondrial dismutation of $O_2^- \rightarrow O_2 + H_2O_2$ | 21789.7; 9020.4 | 19333.1; 4950.9 | 19101.2; 9289.0 | 15365.0; 7151.7 | 0.1234[§] | NS |
| **SOD-3** | Extracellular dismutation of $O_2^- \rightarrow O_2 + H_2O_2$ | 3950.4; 1100.8 | 3058.8; 1140.5 | 3239.4; 1017.3 | 4364.9; 2214.7 | **0.0171**[†] | *0.0563*[Δ] *0.1138*[∞] |
| **TFRC** | Transferrin receptor; cellular uptake of iron | 1677.2; 512.3 | 1540.0; 427.4 | 1805.2; 653.0 | 1824.8; 713.2 | NS | NS |
| **TGFβ1** | Secretory peptide; cell growth, differentiation, and apoptosis | 2017.3; 245.2 | 1644.9; 294.4 | 1661.0; 248.8 | 2079.7; 570.5 | **0.0004**[†] | **0.0296**[*] **0.0112**[∞] **0.0388**[Ψ] **0.0083**[Δ] |
| **TIMP-1** | Inhibits ECM degradation | 8450.0; 2482.7 | 7402.1; 1670.5 | 6875.4; 1852.8 | 8027.1; 3270.6 | *0.1087*[†] | NS |
| **TIMP-2** | Inhibits ECM degradation | 42795.2; 6818.1 | 41424.2; 6636.4 | 38960.4; 5591.7 | 36823.3; 8335.2 | **0.0346**[§] | NS |
| **TNF** | Proinflammatory cytokine involved in the acute phase stress response | 30.1; 6.9 | 27.4; 8.9 | 28.3; 6.6 | 31.7; 11.5 | NS | NS |
| **TXN** | Nrf2 induced antioxidant; reduces oxidized cysteine residues and cleaves disulfide bonds | 15090.5; 2635.8 | 13431.1; 3251.7 | 12606.9; 1945.5 | 11696.3; 4446.8 | **0.0223**[§] | *0.1237*[Ψ] |
| **ULK1** | Inducer of autophagy | 1577.2; 174.1 | 1362.6; 304.2 | 1469.7; 250.9 | 1709.8; 571.5 | **0.0292**[†] | **0.0358**[Δ] |

| | | | | | | | |
|---|---|---|---|---|---|---|---|
| **VEGF** | Promotes growth of new blood vessels | 12.2; 5.1 | 12.5; 4.9 | 13.3; 3.7 | 14.0; 6.7 | NS | NS |
| **WNT** | Regulates the proliferation of cells | 15.0; 5.3 | 16.1; 9.5 | 13.4; 6.2 | 24.3; 10.0 | **0.0358**$^{\dagger}$ **0.0102**$^{\ddagger}$ *0.1497*$^{\S}$ | **0.0238**$^{\Delta}$ **0.0025**$^{\infty}$ |
| **β-CAT** | Component of canonical Wnt signaling; cell growth and adhesion | 24800.6; 3794.0 | 21997.0; 1954.2 | 20918.3; 2232.7 | 24234.3; 4831.0 | **0.0024**$^{\dagger}$ | **0.0129**$^{\Psi}$ **0.0332**$^{\infty}$ *0.0902*$^{*}$ |
| **p65 (RELA)** | Nuclear translocation and activation of NF-κB | 5800.5; 957.0 | 4768.1; 727.7 | 4800.6; 660.5 | 5462.4; 1667.0 | **0.0075**$^{\dagger}$ | ***0.0424***$^{*}$ *0.0508*$^{\Psi}$ |
| **ACTB** | Housekeeper gene; constitutively expressed cytoskeletal protein | 167191.7; 19438.2 | 146372.2; 11088.5 | 145915.8; 18080.0 | 148469.0; 24220.3 | **0.0284**$^{\dagger}$ *0.0698*$^{\S}$ *0.0837*$^{\ddagger}$ | **0.0135**$^{\Psi}$ **0.0140**$^{*}$ |
| **EEF1a1**$^{\&}$ | Housekeeper gene; delivery of tRNAs to the ribosome | 171648.9; 0.0 | 171648.9; 0.0 | 171648.9; 0.0 | 171648.9; 0.0 | *0.1125*$^{\dagger}$ | NS |
| **GAPDH** | Housekeeper gene; catalyzes the 6$^{th}$ step of glycolysis | 24722.3; 6993.9 | 27926.1; 16914.3 | 22352.4; 7152.2 | 32476.4 | NS | NS |
| **SDH-a** | Housekeeper gene; involved in complex II of the mitochondrial electron transport chain | 1886.4; 215.3 | 2260.0; 1082.6 | 2004.5; 173.7 | 2616.3; 1933.4 | *0.1258*$^{\dagger}$ | NS |

$^{\&}$*Selected housekeeper gene utilized in data normalization*

**Supplemental Table 2.2. Normalized absolute mRNA counts from infrapatellar fat pad of 5-mont-old control and Nrf2-activator treated guinea pigs.** Data is depicted as mean and standard deviation. Trending *(p<0.15, italic)* and significant **(p<0.05, bold**) sources of variation (determined via 2-way ANOVA, factors signifying sex and treatment) are depicted in table 1. Trending *(p<0.15, italic)* and significant (**p<0.05, bold**) differences between groups (determined via Bonferroni multiple comparisons) are listed in the last column.

*2-way ANOVA key:*
- *$^{\S}$sex*
- *$^{\ddagger}$treatment*
- *$^{\dagger}$interaction*
- *NS no significant or trending source of variation identified*

*Bonferroni multiple comparisons key:*
- *$^{*}$Difference between control males and PB125 males*
- *$^{\infty}$Difference between control females and PB125 females*
- *$^{\Psi}$Difference between control males and control females*
- *$^{\Delta}$Difference between PB125 males and PB125 females*
- *NS no significant or trending difference*

| Gene | Description | Male Control (n=13) | Male PB125 (n=14) | Female Control (n=13) | Female PB125 (n=14) | 2-way ANOVA p-values | Bonferroni p-values |
|---|---|---|---|---|---|---|---|
| **Aggrecan** | Cartilage structure | 184.1; 98.3 | 207.3; 129.9 | 184.6; 144.9 | 154.2; 40.9 | NS | NS |
| **Adiponectin** | Glucose & FA metabolism | 107502.9; 29708.8 | 101251.7; 27382.9 | 143535.8; 36358.4 | 130632.4; 28836.2 | **0.0003$^{\S}$** | **0.0085$^{\Psi}$** **0.0288$^{\Delta}$** |
| **AKT** | Cellular survival and proliferation | 2942.5; 530.4 | 3060.1; 610.4 | 2805.6; 448.3 | 2776.8; 451.7 | *0.1408$^{\S}$* | NS |
| **BAD** | Inducer of apoptosis | 777.6; 102.7 | 807.8; 115.0 | 722.3; 126.3 | 719.7; 80.7 | **0.0176$^{\S}$** | *0.0690$^{\Delta}$* |
| **BAK** | Intrinsic apoptosis | 1545.3; 251.3 | 1616.5; 340.3 | 1371.8; 226.2 | 1430.8; 257.9 | **0.0197$^{\S}$** | NS |
| **BAX** | Intrinsic apoptosis | 833.0, 106.4 | 827.6; 132.7 | 758.4; 136.2 | 739.7; 123.2 | **0.0211$^{\S}$** | *0.1384$^{\Delta}$* |
| **BCL-2** | Inhibitor of apoptosis | 1160.1; 223.1 | 1265.8; 257.8 | 1309.2; 276.4 | 1485.3; 293.9 | **0.0136$^{\S}$** *0.0562$^{\ddagger}$* | *0.0658$^{\Delta}$* |
| **BECN1** | Regulator of autophagy | 1642.5; 239.8 | 1632.1; 308.6 | 1555.5; 198.9 | 1528.7; 141.4 | *0.1361$^{\S}$* | NS |
| **BIM** | Pro-apoptotic | 324.7; 73.7 | 336.8; 79.2 | 351.0; 124.2 | 284.1; 36.4 | 0.0873$^{\dagger}$ | 0.0853$^{\infty}$ |
| **BMP-7** | Anabolic effect on cartilage | 67.7; 43.4 | 68.1; 46.6 | 64.5; 45.4 | 56.7; 22.4 | NS | NS |
| **C3** | Activator of complement | 5784.7; 1930.1 | 4795.1; 1001.8 | 6241.1; 1824.4 | 5470.7; 1287.1 | **0.0415$^{\ddagger}$** | NS |
| **Caspase-1** | Initiator of apoptosis | 487.7; 111.0 | 492.5; 159.7 | 375.8; 102.2 | 405.8; 89.5 | **0.0035$^{\S}$** | **0.0406$^{\Psi}$** *0.1199$^{\Delta}$* |
| **Caspase-3** | Executioner of apoptosis | 510.3; 95.2 | 533.8; 152.3 | 457.6; 169.9 | 455.6; 73.3 | *0.0674$^{\S}$* | NS |

| | | | | | | | |
|---|---|---|---|---|---|---|---|
| **Caspase-8** | Executes extrinsic apoptosis | 313.5; 34.8 | 307.6; 37.8 | 299.6; 54.3 | 292.5; 29.5 | NS | NS |
| **Caspase-9** | Executes intrinsic apoptosis | 188.8; 37.3 | 181.4; 29.2 | 186.6; 46.7 | 178.3; 24.1 | NS | NS |
| **Catalase** | Protects from oxidative damage via degradation of $2H_2O_2 \rightarrow O_2+2H_2O$ | 27085.3; 4991.0 | 23187.3; 4993.1 | 31188.1; 5865.2 | 29816.9; 4430.6 | **0.0003**$^{\S}$ *0.0627*$^{\ddagger}$ | **0.0023**$^{\Delta}$ *0.1038*$^{*}$ |
| **CBS** | Mediates early transsulfuration | 62.4; 15.2 | 69.6; 31.9 | 71.2; 15.7 | 66.6; 11.4 | NS | NS |
| **CCL-2** | Chemoattractant agent for myeloid and lymphoid cells | 4165.7; 2363.9 | 3752.4; 1614.8 | 3312.4; 1178.4 | 3940.8; 1674.2 | NS | NS |
| **CD163** | Scavenger receptor for hemoglobin-haptoglobin | 8374.6; 1542.4 | 9079.9; 2534.8 | 7002.1; 1535.0 | 7797.0; 1881.9 | **0.0148**$^{\S}$ | NS |
| **COL10A1** | Marker of chondrocytes hypertrophy | 94.7; 72.0 | 100.7; 108.9 | 98.3; 95.1 | 72.2; 37.4 | NS | NS |
| **COL2A1** | Structural component of cartilage | 431.7; 463.8 | 687.4; 553.7 | 251.5; 133.9 | 700.0; 611.3 | **0.0104**$^{\ddagger}$ | **0.0385**$^{\infty}$ |
| **CUL3** | Ubiquitin ligase | 34889.0; 336.3 | 3629.4; 440.0 | 3205.7; 239.2 | 3457.0; 281.8 | **0.0157**$^{\S}$ **0.0364**$^{\dagger}$ | *0.0713*$^{\Psi}$ *0.1133*$^{\infty}$ |
| **FGF-18** | Anabolic effect on cartilage | 2013.4; 792.5 | 1947.0; 365.6 | 2334.0; 740.7 | 2268.5; 672.4 | *0.0799*$^{\S}$ | NS |
| **FTH-1** | Intracellular iron storage protein | 105628.4; 18656.3 | 102444.2; 12637.8 | 101435.9; 13217.6 | 100003.3; 10091.8 | NS | NS |
| **Glutathione peroxidase** | Nrf2 mediated antioxidant; $2H_2O_2 \rightarrow O_2 + 2H_2O$ $O_2^{=} \rightarrow O_2 + OH$ | 6321.7; 1261.5 | 6380.0; 1138.7 | 6232.6; 1608.1 | 6224.1; 1120.2 | NS | NS |
| **GSK3β** | Inactivates nuclear Nrf2 | 2076.3; 128.6 | 2187.5; 201.8 | 1957.9; 254.9 | 2084.8; 167.4 | **0.0410**$^{\S}$ **0.0283**$^{\ddagger}$ | NS |
| **HAMP** | Regulates iron absorption | 98.3; 61.4 | 91.1; 73.3 | 97.1; 73.4 | 78.4; 29.4 | NS | NS |
| **HIF1-a** | Transcriptional response to hypoxia | 6719.3; 1882.2 | 8389.3; 2811.2 | 5841.1; 1194.6 | 5736.1; 1209.6 | **0.0013**$^{\S}$ *0.0933*$^{\dagger}$ *0.1377*$^{\ddagger}$ | **0.0543**$^{*}$ **0.0011**$^{\Delta}$ |
| **HMGB1** | Proinflammatory alarmin | 15477.0; 1495.0 | 15444.7; 1349.8 | 13922.9; 990.8 | 14924.2; 916.1 | **0.0028**$^{\S}$ *0.1231*$^{\dagger}$ *0.1478*$^{\ddagger}$ | **0.0038**$^{\Psi}$ *0.0731*$^{\infty}$ |
| **HMOX-1** | Nrf2 regulated antioxidant that degrades heme | 1600.7; 391.9 | 1526.2; 347.0 | 1374.8; 440.9 | 1216.8; 322.7 | **0.0134**$^{\S}$ | *0.0787*$^{\Delta}$ |
| **IFN-γ** | Implemented in rheumatoid arthritis | 33.0; 20.6 | 34.1; 25.1 | 32.9; 26.5 | 31.4; 13.5 | NS | NS |
| **IL-10** | Anti-inflammatory cytokine | 103.9; 46.4 | 108.5; 55.8 | 97.1; 52.9 | 90.9; 20.1 | NS | NS |
| **IL-1β** | Proinflammatory cytokine | 177.1; 61.0 | 163.5; 86.0 | 139.2; 42.7 | 143.0; 30.5 | *0.0761*$^{\S}$ | NS |
| **IL-4** | T-cell differentiation and | 67.9; 43.4 | 69.1; 59.4 | 66.5; 45.5 | 52.6; 15.0 | NS | NS |

| | | | | | | | |
|---|---|---|---|---|---|---|---|
| | Th2 immune response | | | | | | |
| **IL-5** | Induced eosinophil differentiation | 43.0; 16.2 | 44.3; 19.9 | 47.3; 24.0 | 43.2; 13.4 | NS | NS |
| **IL-6** | Proinflammatory cytokine | 267.7; 147.3 | 206.2; 140.1 | 182.5; 146.7 | 131.6; 41.5 | **0.0242**$^{\S}$ *0.1084*$^{\ddagger}$ | NS |
| **KEAP1** | Degrades cytoplasmic Nrf2 | 1234.3; 219.7 | 1294.0; 242.2 | 1192.6; 220.3 | 1217.1; 201.0 | NS | NS |
| **LEP** | Adipokine and regulator of appetite | 71135.1; 38306.7 | 69985.0; 40246.5 | 61065.7; 20423.6 | 47909.3; 16989.8 | *0.0611*$^{\S}$ | *0.1274*$^{\Delta}$ |
| **MAPK** | Cell differentiation, proliferation, and survival | 3199.4; 360.2 | 3404.1; 284.3 | 2996.7; 311.6 | 3311.3; 292.3 | **0.0036**$^{\ddagger}$ *0.0887*$^{\S}$ | **0.0236**$^{\infty}$ |
| **MCL1** | Inhibitor of apoptosis | 9922.9; 1027.0 | 9438.1; 1020.1 | 8792.3; 1185.1 | 8822.4; 1211.9 | **0.0059**$^{\S}$ | **0.0253**$^{\Psi}$ |
| **MMP-13** | Cleaves type II collagen | 106.6; 61.5 | 112.7; 53.8 | 116.2; 88.6 | 106.0; 47.8 | NS | NS |
| **MMP-2** | Cleaves type IV collagen | 23817.8; 5723.6 | 28484.9; 9573.6 | 22754.2; 5190.8 | 20932.2; 4958.9 | **0.0217**$^{\S}$ *0.0804*$^{\dagger}$ | **0.0085**$^{\Delta}$ |
| **MMP-3** | Cleaves type II-IV, IX and X collagens | 456.2; 117.4 | 415.7; 87.1 | 318.8; 79.8 | 273.9; 79.2 | **<0.0001**$^{\S}$ *0.0984*$^{\ddagger}$ | **0.0008**$^{\Psi}$ **0.0004**$^{\Delta}$ |
| **MMP-9** | Cleaves type IV & V collagen, activates neutrophils | 59.0; 26.1 | 62.6; 27.5 | 64.8; 46.1 | 57.9; 36.9 | NS | NS |
| **MTOR** | Cell metabolism and growth | 529.6; 106.7 | 543.2; 152.9 | 496.5; 108.2 | 462.6; 70.6 | *0.0722*$^{\S}$ | *0.1327*$^{\Delta}$ |
| **NF-κB-1** | Proinflammatory transcription factor | 337.3; 46.7 | 338.1; 43.7 | 313.7; 62.5 | 318.4; 45.7 | *0.1179*$^{\S}$ | NS |
| **NFE-2** | Oxidant induced anti-inflammatory transcription factor | 144.2; 29.0 | 133.9; 22.4 | 146.6; 35.0 | 153.8; 34.5 | NS | NS |
| **NFE2L2** | Oxidant induced anti-inflammatory transcription factor | 4880.3; 453.1 | 4969.5; 394.9 | 4624.5; 533.2 | 4855.8; 347.4 | *0.1254*$^{\S}$ | NS |
| **NOS1** | Neuronal and constitutively expressed; synthesizes NO | 27.8; 19.0 | 36.0; 27.1 | 23.8; 14.2 | 27.9; 33.4 | NS | NS |
| **NOS2** | Cytokine induced NO synthesis | 157.7; 99.2 | 166.4; 144.9 | 150.4; 115.7 | 116.8; 54.4 | NS | NS |
| **NOS3** | Endothelial induced NO in shear stress | 135.3; 34.9 | 123.5; 28.6 | 133.5; 36.9 | 112.7; 24.2 | *0.0626*$^{\ddagger}$ | NS |
| **NQO1** | Nrf2 mediated removal of toxic intermediates | 6980.9; 620.0 | 7331.1; 1007.0 | 6283.8; 637.3 | 7063.7; 818.1 | **0.0299**$^{\S}$ **0.0116**$^{\ddagger}$ | **0.0273**$^{\infty}$ *0.0586*$^{\Psi}$ |
| **NURR1** | Neuroinflammatory transcription factor | 1405.8; 782.1 | 915.0; 230.2 | 827.2; 297.4 | 833.6; 405.6 | **0.0136**$^{\S}$ *0.0664*$^{\ddagger}$ *0.0598*$^{\dagger}$ | **0.0061**$^{\Psi}$ **0.0195**$^{*}$ |
| **Nrf1** | Transcriptional modulation of metabolism, | 515.3; 44.3 | 510.4; 64.1 | 488.6; 81.9 | 507.7; 51.2 | NS | NS |

| | | | | | | | |
|---|---|---|---|---|---|---|---|
| | growth, and development | | | | | | |
| **PCSK9** | LDL-cholesterol metabolism | 56.4; 37.6 | 47.6; 40.4 | 45.5; 32.9 | 37.8; 14.9 | NS | NS |
| **PPARγ** | Adipocyte differentiation; senescence | 1834.3; 473.4 | 1616.4; 463.8 | 2107.6; 503.6 | 1986.3; 601.2 | **0.0259$^{Ŝ}$** | *0.1256$^{Δ}$* |
| **PRDX1** | Nrf2 antioxidant; detoxifies peroxides | 14163.4; 2077.5 | 14550.4; 1606.0 | 12950.4; 1490.2 | 14374.8; 1578.5 | *0.0559$^{‡}$* *0.1399$^{Ŝ}$* | *0.1495$^{Ψ}$* *0.0686$^{∞}$* |
| **PTGS-1** | Proinflammatory enzyme | 1044.1; 201.3 | 1018.5; 174.6 | 927.5; 194.1 | 945.7; 160.0 | *0.0628$^{Ŝ}$* | NS |
| **PTGS-2** | Proinflammatory enzyme | 220.9; 86.5 | 189.9; 90.3 | 192.1; 116.6 | 172.0; 47.0 | NS | NS |
| **RIPK1** | Driver of apoptosis and necroptosis | 1674.7; 145.0 | 1723.5; 186.1 | 1530.2; 211.0 | 1610.2; 139.6 | **0.0085$^{Ŝ}$** | *0.0755$^{Ψ}$* |
| **RUNX2** | Osteoblast differentiation | 109.8; 38.9 | 118.6; 43.1 | 102.7; 57.9 | 84.9; 18.8 | *0.0784$^{Ŝ}$* | *0.0752$^{Δ}$* |
| **SCL11A2** | Metal transport, iron uptake | 902.9; 140.9 | 949.6; 195.6 | 866.0; 235.9 | 829.1; 82.4 | *0.1005$^{Ŝ}$* | *0.1417$^{Δ}$* |
| **SESN2** | Stress-induced metabolic regulator | 55.2; 11.7 | 58.4; 13.2 | 50.0; 12.6 | 47.9; 8.6 | **0.0179$^{Ŝ}$** | **0.0434$^{Δ}$** |
| **SLC39A14** | Divalent metal transporter | 397.9; 206.4 | 423.9; 254.8 | 335.8; 165.8 | 353.6; 217.8 | NS | NS |
| **SLC40A1** | Ferroportin; transports iron | 2791.5; 548.5 | 2820.0; 497.7 | 2835.4; 472.8 | 2657.8; 358.0 | NS | NS |
| **SLC7A11** | Cystine/glutamate antiporter; preserves redox balance | 80.7; 40.1 | 94.6; 35.2 | 52.2; 21.9 | 62.3; 29.9 | **0.0012$^{Ŝ}$** | *0.0600$^{Ψ}$* **0.0227$^{Δ}$** |
| **SOD-1** | Cytoplasmic dismutation of $O_2^- \rightarrow O_2 + H_2O_2$ | 10854.7; 1416.3 | 11361.1; 997.4 | 10906.5; 1276.8 | 12065.3; 1495.2 | **0.0235$^{‡}$** | *0.0514$^{∞}$* |
| **SOD-2** | Mitochondrial dismutation of $O_2^- \rightarrow O_2 + H_2O_2$ | 14718.4; 5601.6 | 15816.6; 5787.9 | 12198.1; 3025.7 | 12008.4; 2917.2 | **0.0136$^{Ŝ}$** | *0.0624$^{Δ}$* |
| **SOD-3** | Extracellular dismutation of $O_2^- \rightarrow O_2 + H_2O_2$ | 1123.9; 229.5 | 1041.3; 259.6 | 1351.1; 379.8 | 1193.8; 268.0 | **0.0195$^{Ŝ}$** *0.1337$^{‡}$* | *0.1007$^{Ψ}$* |
| **TFRC** | Transferrin receptor; cellular uptake of iron | 654.4; 104.3 | 678.4; 174.5 | 610.5; 157.4 | 596.1; 91.9 | *0.0964$^{Ŝ}$* | NS |
| **TGFβ1** | Secretory peptide; cell growth, differentiation, and apoptosis | 789.5; 190.9 | 824.7; 241.4 | 751.7; 120.7 | 826.8; 164.5 | NS | NS |
| **TIMP-1** | Inhibits ECM degradation | 5512.5; 1942.0 | 5016.6; 1993.0 | 4615.2; 2435.7 | 4028.5; 1279.7 | *0.0814$^{Ŝ}$* | NS |
| **TIMP-2** | Inhibits ECM degradation | 43302.4; 3924.0 | 44454.8; 6146.0 | 42844; 7046.9 | 41875.2; 5433.6 | NS | NS |
| **TNF** | Proinflammatory cytokine involved in the acute phase stress response | 57.7; 19.7 | 55.3; 29.7 | 52.6; 27.7 | 45.7; 9.8 | NS | NS |

| | | | | | | | |
|---|---|---|---|---|---|---|---|
| **TXN** | Nrf2 induced antioxidant; reduces oxidized cysteine residues and cleaves disulfide bonds | 21391.4; 3790.7 | 21770.3; 3139.9 | 19038.5; 1732.1 | 22511.3; 3242.0 | **0.0258**$^{‡}$ *0.0708*$^{†}$ | **0.0102**$^{∞}$ *0.1136*$^{ψ}$ |
| **ULK1** | Inducer of autophagy | 790.2; 133.7 | 827.8; 198.6 | 774.6; 130.4 | 759.4; 102.4 | NS | NS |
| **VEGF** | Promotes growth of new blood vessels | 50.2; 35.9 | 53.9; 63.8 | 46.1; 31.6 | 45.1; 18.7 | NS | NS |
| **WNT** | Regulates the proliferation of cells | 91.1; 70.3 | 71.7; 53.2 | 88.0; 79.1 | 68.3; 31.0 | NS | NS |
| **β-CAT** | Component of canonical Wnt signaling; cell growth and adhesion | 9730.2; 1062.5 | 10418.6; 1979.5 | 9526.8; 1752.2 | 9328.6; 1383.2 | *0.1413*$^{§}$ | NS |
| **p65 (RELA)** | Nuclear translocation and activation of NF-κB | 2616.0; 555.3 | 2682.3; 540.8 | 2553.0; 542.8 | 2492.0; 477.6 | NS | NS |
| **ACTB** | Housekeeper gene; constitutively expressed cytoskeletal protein | 95417.7; 14725.3 | 95812.3; 21297.0 | 85734.4; 20222.5 | 87110.7; 21259.8 | *0.0918*$^{§}$ | NS |
| **EEF1a1**$^{\&}$ | Housekeeper gene; delivery of tRNAs to the ribosome | 171648.9; 0.0 | 171648.9; 0.0 | 171648.9; 0.0 | 171648.9; 0.0 | NS | NS |
| **GAPDH** | Housekeeper gene; catalyzes the 6$^{th}$ step of glycolysis | 8660.6; 1603.0 | 10946.8; 6462.6 | 8102.7; 1992.5 | 9261.6; 3698.2 | *0.1200*$^{‡}$ | NS |
| **SDH-a** | Housekeeper gene; involved in complex II of the mitochondrial electron transport chain | 2912.2; 258.5 | 2958.9; 430.3 | 2920.0; 330.2 | 2864.0; 314.1 | NS | NS |

$^{\&}$Selected housekeeper gene utilized in data normalization

**Supplemental Table 2.3. Any-maze indices depicted as means and standard deviation from 5-month-old control and Nrf2-activator treated guinea pigs.** Trending *(p<0.15, italic)* and significant (**p<0.05, bold**) sources of variation (determined via 2-way ANOVA, factors signifying sex and treatment) are shown. Trending *(p<0.15, italic)* and significant (**p<0.05, bold**) differences between groups (determined via Bonferroni multiple comparisons) are listed in the last column.

*2-way ANOVA key:*

$^{\S}$*sex*
$^{\ddagger}$*treatment*
$^{\dagger}$*interaction*$^{\dagger}$
*NS no significant or trending source of variation identified*

*Bonferroni multiple comparisons key:*

$^{*}$*Difference between control males and PB125 males*
$^{\infty}$*Difference between control females and PB125 females*
$^{\Psi}$*Difference between control males and control females*
$^{\Delta}$*Difference between PB125 males and PB125 females*
*NS no significant or trending difference*

| **Description** | **Male Control (n=14)** | **Male PB125 (n=14)** | **Female Control (n=14)** | **Female PB125 (n=14)** | **2-way ANOVA p-values** | **Bonferroni p-values** |
|---|---|---|---|---|---|---|
| Distance Traveled (m) | 6.99; 5.11 | 9.54; 6.42 | 10.91; 7.47 | 7.46; 5.31 | *0.0737*$^{\dagger}$ | NS |
| Average Speed (m/s) | 0.012; 0.009 | 0.016; 0.011 | 0.018; 0.013 | 0.013; 0.009 | *0.0769*$^{\dagger}$ | NS |
| Time Mobile (s) | 89.58; 62.36 | 114.0; 78.03 | 115.3; 59.59 | 99.58; 72.88 | NS | NS |
| % Time Mobile | 14.93; 10.39 | 19.00; 13.01 | 19.22; 9.93 | 16.60; 12.15 | NS | NS |
| Time in Hut (s) | 282.2; 189.0 | 152.5; 170.9 | 260.6; 149.9 | 296.7; 186.3 | 0.0817$^{\dagger}$ | *0.0670*$^{\Delta}$ *0.1096*$^{*}$ |
| % Time in Hut | 59.31; 31.94 | 25.41; 28.49 | 43.44; 24.99 | 37.18; 25.99 | **0.0097**$^{\ddagger}$ *0.0703*$^{\dagger}$ | **0.0046**$^{*}$ |

**Supplemental Table 2.4. Digigait indices depicted as means and standard deviation from 5-month-old control and Nrf2-activator treated guinea pigs.** Trending (*p<0.15, italic)* and significant (**p<0.05, bold**) sources of variation (determined by 2-way ANOVA, factors signifying sex and treatment) are listed. Trending *(p<0.15, italic)* and significant (**p<0.05, bold**) differences between groups (determined by Bonferroni multiple comparisons post hoc analysis) are listed in the last column.

*2-way ANOVA key:*

$^{\S}$*sex*
$^{\ddagger}$*treatment*
$^{\dagger}$*interaction*
*NS no significant or trending source of variation identified*

*Bonferroni multiple comparisons key:*

$^{*}$*Difference between control males and PB125 males*
$^{\infty}$*Difference between control females and PB125 females*
$^{\Psi}$*Difference between control males and control females*
$^{\Delta}$*Difference between PB125 males and PB125 females*
*NS no significant or trending difference*

| Indice | Male Control (N=9) | Male PB125 (N=11) | Female Control (N=10) | Female PB125 (N=12) | 2-way ANOVA P-values | Bonferroni P-values |
|---|---|---|---|---|---|---|
| **Swing** | 0.100; 0.009 | 0.098; 0.009 | 0.092; 0.009 | 0.091; 0.010 | **0.0158**$^{\S}$ | *0.1426*$^{\Psi}$ |
| **% Swing Stride** | 32.678; 2.849 | 31.580; 2.654 | 31.100; 2.747 | 31.938; 3.438 | NS | NS |
| **Brake** | 0.041; 0.015 | 0.037; 0.015 | 0.034; 0.018 | 0.045; 0.026 | NS | NS |
| **% Brake Stride** | 13.29; 4.44 | 11.98; 4.52 | 11.37; 6.23 | 15.46; 8.32 | NS | NS |
| **Propel** | 0.165; 0.013 | 0.175; 0.017 | 0.170; 0.019 | 0.150; 0.026 | **0.0203**$^{\dagger}$ *0.1356*$^{\S}$ | **0.0403**$^{\infty}$ **0.0136**$^{\Delta}$ |
| **% Propel Stride** | 54.03; 4.53 | 56.07; 3.97 | 57.55; 5.32 | 52.60; 6.75 | **0.0465**$^{\dagger}$ | *0.0682*$^{\infty}$ |
| **Stance** | 0.206; 0.015 | 0.212; 0.019 | 0.204; 0.017 | 0.195; 0.024 | *0.1279*$^{\S}$ | *0.0988*$^{\Delta}$ |
| **% Stance Stride** | 67.32; 2.85 | 68.42; 2.65 | 68.90; 2.75 | 68.06; 3.44 | NS | NS |
| **Stride** | 0.306; 0.016 | 0.309; 0.021 | 0.296; 0.020 | 0.286; 0.028 | **0.0199**$^{\S}$ | **0.0337**$^{\Delta}$ |
| **% Brake Stance** | 19.71; 6.30 | 17.36; 6.20 | 16.37; 8.64 | 22.37; 10.74 | NS | NS |
| **% Propel Stance** | 80.29; 6.30 | 82.64; 6.20 | 83.63; 8.64 | 77.63; 10.74 | *0.1177*$^{\dagger}$ | NS |
| **Stance/Swing** | 2.083; 0.263 | 2.190; 0.238 | 2.255; 0.285 | 2.175; 0.393 | NS | NS |
| **Stride Length** | 16.806; 0.866 | 17.015; 1.154 | 16.282; 1.106 | 15.692; 1.543 | **0.0194**$^{\S}$ | **0.0308**$^{\Delta}$ |

| | | | | | | |
|---|---|---|---|---|---|---|
| **Stride Frequency** | 3.317; 0.237 | 3.295; 0.243 | 3.445; 0.208 | 3.588; 0.405 | **0.0250$^{\S}$** | **0.0483$^{\Delta}$** |
| **Paw Angle** | -0.394; 1.748 | -0.325; 3.315 | -0.055; 2.518 | -1.613; 3.029 | NS | NS |
| **Absolute Paw Angle** | 13.339; 2.906 | 11.745; 4.062 | 16.227; 5.314 | 14.821; 4.940 | **0.0389$^{\S}$** | NS |
| **Paw Angle Variability** | 5.633; 4.679 | 6.415; 6.740 | 4.091; 1.945 | 7.138; 4.235 | NS | NS |
| **Stance Width** | 2.811; 0.549 | 3.000; 0.558 | 2.809; 0.464 | 2.900; 0.602 | NS | NS |
| **Step Angle** | 72.767; 5.151 | 68.990; 8.418 | 70.864; 4.351 | 72.400; 5.910 | NS | NS |
| **Stride Length Variability** | 2.612; 1.546 | 2.024; 1.506 | 1.418; 0.438 | 2.393; 1.258 | *0.0500$^{\dagger}$* | *0.0787$^{\Psi}$* *0.1362$^{\infty}$* |
| **Stance Width Variability** | 0.470; 0.305 | 0.319; 0.142 | 0.352; 0.164 | 0.448; 0.245 | *0.0793$^{\dagger}$* | NS |
| **Step Angle Variability** | 7.177; 1.861 | 8.710; 7.628 | 6.595; 3.323 | 9.398; 3.111 | *0.1285$^{\ddagger}$* | NS |
| **Number of Steps** | 5.500; 0.820 | 6.100; 0.868 | 5.955; 0.748 | 5.458; 0.509 | **0.0215$^{\dagger}$** | *0.0977$^{\Delta}$* |
| **Stride Length CV** | 15.443; 8.739 | 11.804; 8.496 | 8.744; 2.759 | 15.527; 8.414 | **0.0303$^{\dagger}$** | *0.1059$^{\Psi}$* *0.0714$^{\infty}$* |
| **Stance Width CV** | 16.790; 11.097 | 11.124; 5.838 | 13.233; 8.302 | 16.530; 10.723 | *0.1265$^{\dagger}$* | NS |
| **Step Angle CV** | 9.959; 2.901 | 14.426; 17.257 | 9.386; 5.001 | 13.298; 5.255 | NS | NS |
| **Swing Duration CV** | 16.315; 9.942 | 16.890; 11.445 | 14.688; 8.212 | 13.829; 7.790 | NS | NS |
| **Paw Area at Peak Stance ($cm^2$)** | 3.717; 1.673 | 3.229; 0.700 | 2.717; 0.467 | 3.245; 1.130 | *0.1319$^{\dagger}$* *0.1448$^{\S}$* | *0.0865$^{\Psi}$* |
| **Paw Variability at Peak Stance** | 0.413; 0.572 | 0.303; 0.296 | 0.198; 0.268 | 0.593; 0.670 | *0.1039$^{\dagger}$* | *0.1205$^{\infty}$* |
| **Hind Limb Shared Stance Time** | 0.116; 0.018 | 0.136; 0.023 | 0.121; 0.026 | 0.114; 0.028 | *0.0840$^{\dagger}$* | *0.0846$^{\Delta}$* |
| **% Shared Stance** | 56.39; 5.90 | 64.25; 11.71 | 58.99; 8.80 | 57.78; 7.86 | *0.1069$^{\dagger}$* | *0.1212$^{*}$* |
| **Stance Factor** | 0.993; 0.037 | 0.972; 0.048 | 0.981; 0.039 | 0.966; 0.107 | NS | NS |
| **Gait Symmetry** | 1.050; 0.114 | 0.994; 0.044 | 1.014; 0.054 | 0.992; 0.028 | *0.0586$^{\ddagger}$* | *0.1322$^{*}$* |
| **MAX dA/dT** | 370.845; 155.355 | 325.387; 72.542 | 287.122; 40.530 | 310.653; 82.524 | *0.0978$^{\S}$* | *0.1068$^{\Psi}$* |
| **MIN dA/dT** | -71.012; 72.487 | -51.365; 25.377 | -47.649; 24.624 | -58.261; 40.799 | NS | NS |

| | | | | | | |
|---|---|---|---|---|---|---|
| **Tau Propulsion** | 0.140; 0.050 | 0.118; 0.023 | 0.124; 0.024 | 0.136; 0.036 | *0.1156*[†] | NS |
| **Overlap Distance** | -1.712; 2.204 | -1.045; 1.089 | -1.627; 1.437 | -0.649; 1.569 | *0.1058*[‡] | NS |
| **Ataxia Coefficient** | 0.394; 0.246 | 0.311; 0.249 | 0.223; 0.082 | 0.404; 0.240 | *0.0540*[†] | *0.0999*[∞] |
| **Midline Distance** | 4.116; 1.112 | 3.921; 0.816 | 3.830; 0.821 | 4.038; 0.794 | NS | NS |
| **Axis Distance** | 0.031; 0.221 | 0.137; 0.214 | 0.068; 0.250 | 0.200; 0.213 | *0.0964*[‡] | NS |
| **Paw Drag** | -21.472; 4.876 | -16.496; 4.609 | -15.425; 4.708 | -16.216; 14.003 | NS | NS |

**Chapter 3 Supplemental Figures**

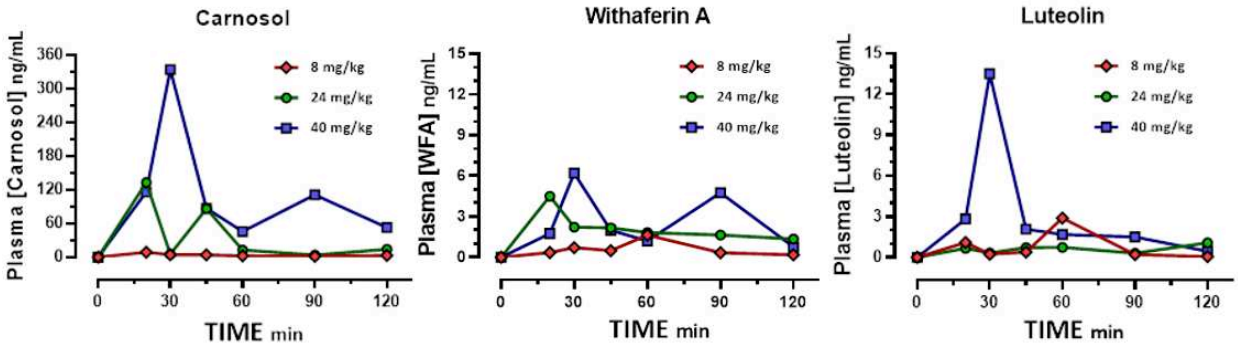


**Supplemental Figure 3.1. Pharmacokinetic analyses of PB125-derived phytochemical concentrations in plasma.** OA-prone Dunkin Hartley guinea pigs were treated with one of 3 doses (8 mg/kg, 24 mg/kg, 40 mg/kg) of PB125, and plasma was collected at 0-, 20-, 30-, 40-, 60-, 90-, and 120-minutes post oral dosing. The 3 active phytochemical compound concentrations in PB125 – carnosol, withaferin A, and luteolin – were detected using HPLC/MS/MS.

**Chapter 3 Supplemental Tables**

**Supplemental Table 3.1. Normalized absolute mRNA counts from pooled articular cartilage and menisci from 15-month-old control and Nrf2-activator treated guinea pigs.** Data is depicted as mean and standard deviation. Trending *(p<0.15, italic)* and significant (**p<0.05, bold**) sources of variation (determined via 2-way ANOVA, factors signifying sex and treatment) are depicted in table 1. Trending *(p<0.15, italic)* and significant (**p<0.05, bold**) differences between groups (determined via Bonferroni multiple comparisons) are listed in the last column.

*2-way ANOVA key:*
- *$^{\S}$sex*
- *$^{\ddagger}$treatment*
- *$^{\dagger}$interaction*
- *NS no significant or trending source of variation identified*

*Bonferroni multiple comparisons key:*
- *$^{*}$Difference between control males and PB125 males*
- *$^{\infty}$Difference between control females and PB125 females*
- *$^{\Psi}$Difference between control males and control females*
- *$^{\Delta}$Difference between PB125 males and PB125 females*
- *NS no significant or trending difference*

| Gene | Description | Male Control (n=14) | Male PB125 (n=11) | Female Control (n=11) | Female PB125 (n=12) | 2-way ANOVA p-values | Bonferroni p-values |
|---|---|---|---|---|---|---|---|
| **Aggrecan** | Cartilage structure | 10196.57 ; 3886.91 | 9736.42; 2034.92 | 10789.02; 3357.60 | 10403.14 ; 4464.15 | NS | NS |
| **Adiponectin** | Glucose & FA metabolism | 4252.82; 4613.74 | 6345.40; 3451.71 | 17063.92; 14989.08 | 9992.19; 5345.52 | **0.0012$^{\S}$** *0.0605$^{\dagger}$* | **0.0007$^{\Psi}$** *0.0894$^{\infty}$* |
| **AKT** | Cellular survival and proliferation | 4716.10; 721.57 | 4899.87; 658.15 | 5252.91; 1122.28 | 5836.54; 2102.04 | *0.0538$^{\S}$* | NS |
| **BAD** | Inducer of apoptosis | 871.51; 123.45 | 951.21; 108.38 | 923.46; 155.82 | 981.16; 166.21 | *0.0978$^{\ddagger}$* | NS |
| **BAK** | Intrinsic apoptosis | 1942.90; 348.29 | 1968.62; 284.90 | 2082.01; 461.42 | 2318.70; 797.21 | *0.1063$^{\S}$* | NS |
| **BAX** | Intrinsic apoptosis | 1270.94; 135.79 | 1290.35; 130.40 | 1245.56; 253.02 | 1329.24; 277.98 | NS | NS |
| **BCL-2** | Inhibitor of apoptosis | 1253.30; 392.08 | 1205.89; 350.26 | 1893.64; 293.46 | 1726.66; 469.34 | **<0.0001$^{\S}$** | **0.0003$^{\Psi}$** **0.0045$^{\Delta}$** |
| **BECN1** | Regulator of autophagy | 1940.17; 312.62 | 1984.32; 229.71 | 2119.92; 362.43 | 2365.91; 916.38 | *0.0746$^{\S}$* | |
| **BIM** | Pro-apoptotic BH3 protein | 344.85; 59.32 | 329.20; 64.10 | 339.22; 46.17 | 361.97; 139.70 | NS | NS |
| **BMP-7** | Anabolic effect on cartilage | 50.28; 21.88 | 44.57; 24.52 | 73.80; 21.36 | 86.59; 84.06 | **0.0189$^{\S}$** | *0.0706$^{\Delta}$* |
| **C3** | Activator of complement | 924.44; 976.69 | 1301.55; 619.02 | 2568.08; 1330.31 | 2720.54; 2002.10 | **0.0003$^{\S}$** | **0.0075$^{\Psi}$** **0.0285$^{\Delta}$** |
| **Caspase-1** | Initiator of apoptosis | 134.96; 46.24 | 123.49; 31.44 | 148.39; 25.05 | 159.57; 55.00 | **0.0478$^{\S}$** | *0.0901$^{\Delta}$* |

| | | | | | | | |
|---|---|---|---|---|---|---|---|
| **Caspase-3** | Executioner of apoptosis | 296.41; 40.69 | 288.04; 54.77 | 303.80; 60.56 | 324.58; 47.97 | *0.1432*$^{\S}$ | NS |
| **Caspase-8** | Executes extrinsic apoptosis | 203.85; 31.93 | 196.58; 23.81 | 223.42; 30.79 | 228.47; 59.53 | **0.0284**$^{\S}$ | *0.1146*$^{\Delta}$ |
| **Caspase-9** | Executes intrinsic apoptosis | 220.22; 31.97 | 221.12; 35.65 | 250.67; 42.33 | 256.89; 46.87 | **0.0058**$^{\S}$ | *0.1225*$^{\Psi}$ *0.0696*$^{\Delta}$ |
| **Catalase** | Protects from oxidative damage via degradation of $2H_2O_2 \rightarrow O_2 + 2H_2O$ | 8021.13; 1925.62 | 7959.08; 1356.03 | 10739.70; 3373.83 | 9978.47; 1675.72 | **0.0006**$^{\S}$ | *0.0071*$^{\Psi}$ *0.0651*$^{\Delta}$ |
| **CBS** | Mediates early transsulfuration | 30.93; 7.33 | 35.27; 6.52 | 33.96; 10.53 | 37.11; 7.45 | *0.1156*$^{\ddagger}$ | NS |
| **CCL-2** | Chemoattractant agent for myeloid and lymphoid cells | 2336.10; 897.68 | 3248.39; 1484.86 | 3014.08; 1773.30 | 3149.81; 1316.45 | NS | NS |
| **CD163** | Scavenger receptor for hemoglobin-haptoglobin | 3149.90; 857.07 | 3069.91; 747.06 | 2855.13; 713.82 | 2898.79; 934.99 | NS | NS |
| **COL10A1** | Marker of chondrocytes hypertrophy | 191.72; 158.87 | 129.46; 59.36 | 398.45; 269.24 | 217.24; 175.68 | **0.0079**$^{\S}$ **0.0262**$^{\ddagger}$ | **0.0135**$^{\Psi}$ **0.0460**$^{\infty}$ |
| **COL2A1** | Structural component of cartilage | 206537.96; 104364.05 | 201805.86; 85158.90 | 141386.42; 78751.15 | 165333.84; 52775.05 | **0.0417**$^{\S}$ | *0.1185*$^{\Psi}$ |
| **CUL3** | Ubiquitin ligase | 2876.94; 291.26 | 2968.99; 364.50 | 2998.10; 249.56 | 3304.55; 518.97 | **0.0389**$^{\S}$ *0.0699*$^{\ddagger}$ | *0.1067*$^{\infty}$ *0.0703*$^{\Delta}$ |
| **FGF-18** | Anabolic effect on cartilage | 3423.05; 1007.51 | 3508.37; 771.96 | 3868.03; 931.38 | 3609.23; 743.87 | NS | NS |
| **FTH-1** | Intracellular iron storage protein | 113601.55; 29412.44 | 102927.44; 17622.90 | 136200.74; 14430.79 | 120306.06; 18791.19 | **0.0025**$^{\S}$ **0.0387**$^{\ddagger}$ | **0.0247**$^{\Psi}$ *0.1183*$^{\Delta}$ |
| **Glutathione peroxidase** | Nrf2 mediated antioxidant; $2H_2O_2 \rightarrow O_2 + 2H_2O$ $O_2^{=} \rightarrow O_2 + OH$ | 8614.78; 2060.12 | 8396.54; 1633.05 | 10077.96; 2329.85 | 12925.10; 8617.74 | **0.0317**$^{\S}$ | **0.0488**$^{\Delta}$ |
| **GSK3β** | Inactivates nuclear Nrf2 | 2532.35; 334.69 | 2558.44; 318.90 | 2613.30; 332.86 | 2719.90; 348.90 | NS | NS |
| **HAMP** | Regulates iron absorption | 16.05; 6.86 | 22.04; 4.40 | 21.81; 4.78 | 23.57; 8.88 | **0.0481**$^{\ddagger}$ *0.0623*$^{\S}$ | *0.0576*$^{*}$ *0.0703*$^{\Psi}$ |
| **HIF1-a** | Transcriptional response to hypoxia | 19325.81; 5447.74 | 20745.04; 5823.86 | 13605.62; 5052.92 | 14422.68; 6214.05 | **0.0006**$^{\S}$ | **0.0315**$^{\Psi}$ **0.0206**$^{\Delta}$ |
| **HMGB1** | Proinflammatory alarmin | 14358.48; 1746.89 | 14018.34; 1062.08 | 13799.47; 1231.10 | 14296.03; 1651.36 | NS | NS |
| **HMOX-1** | Nrf2 regulated antioxidant that degrades heme | 1881.02; 441.57 | 1706.95; 317.57 | 1691.53; 372.41 | 1889.59; 678.43 | NS | NS |

| | | | | | | | |
|---|---|---|---|---|---|---|---|
| **IFN-γ** | Proinflammatory cytokine; implemented in rheumatoid arthritis | 11.18; 6.74 | 9.28; 3.65 | 16.85; 7.35 | 12.15; 4.96 | **0.0181**$^{\S}$ *0.0646*$^{\ddagger}$ | **0.0442**$^{\Psi}$ *0.1398*$^{\infty}$ |
| **IL-10** | Anti-inflammatory cytokine | 27.19; 5.55 | 28.22; 7.62 | 30.73; 6.71 | 28.34; 6.04 | NS | NS |
| **IL-1β** | Proinflammatory cytokine | 67.77; 31.50 | 52.96; 14.59 | 82.42; 16.81 | 79.52; 24.99 | **0.0049**$^{\S}$ | **0.0235**$^{\Delta}$ |
| **IL-4** | Proinflammatory cytokine; induces T-cell differentiation and Th2 response | 30.31; 12.05 | 32.30; 7.86 | 36.06; 10.46 | 38.40; 18.36 | *0.1204*$^{\S}$ | NS |
| **IL-5** | Proinflammatory cytokine; induces eosinophil differentiation | 23.28; 6.83 | 26.75; 3.48 | 26.58; 10.86 | 23.40; 5.48 | *0.1148*$^{\dagger}$ | NS |
| **IL-6** | Proinflammatory cytokine | 95.39; 46.55 | 120.29; 88.86 | 98.11; 43.29 | 75.82; 19.95 | *0.1491*$^{\dagger}$ | *0.1155*$^{\Delta}$ |
| **KEAP1** | Degrades cytoplasmic Nrf2 | 1710.23; 273.93 | 1692.95; 288.65 | 1934.83; 319.60 | 2176.19; 839.59 | **0.0167**$^{\S}$ | **0.0455**$^{\Delta}$ |
| **LEP** | Adipokine and regulator of appetite | 604.66; 963.99 | 781.76; 456.23 | 2981.53; 3651.76 | 1490.31; 998.48 | **0.0079**$^{\S}$ *0.1391*$^{\dagger}$ | **0.0071**$^{\Psi}$ *0.1356*$^{\infty}$ |
| **MAPK** | Cell differentiation, proliferation, and survival | 3575.89; 529.80 | 3547.14; 570.55 | 3801.75; 448.78 | 3919.69; 394.56 | **0.0416**$^{\S}$ | NS |
| **MCL1** | Inhibitor of apoptosis | 7421.54; 677.51 | 7774.36; 657.29 | 7793.30; 992.70 | 8097.62; 790.35 | *0.1334*$^{\S}$ | NS |
| **MMP-13** | Cleaves type II collagen | 3755.37; 2096.13 | 2630.96; 1297.63 | 2701.14; 1433.47 | 3234.27; 1677.57 | *0.0977*$^{\dagger}$ | NS |
| **MMP-2** | Cleaves type IV collagen | 75276.95; 18836.98 | 81354.65; 14836.86 | 53495.02; 17844.95 | 55273.61; 21814.05 | **<0.0001**$^{\S}$ | **0.0114**$^{\Psi}$ **0.0033**$^{\Delta}$ |
| **MMP-3** | Cleaves type II-IV, IX and X collagens | 725.05; 192.07 | 708.66; 211.86 | 500.32; 159.27 | 553.95; 160.71 | **0.0008**$^{\S}$ | **0.0076**$^{\Psi}$ *0.0968*$^{\Delta}$ |
| **MMP-9** | Cleaves type IV & V collagen, activates neutrophils | 2054.25; 1295.40 | 1268.12; 329.87 | 1792.67; 865.07 | 2022.01; 881.41 | *0.0695*$^{\dagger}$ | *0.0879*$^{*}$ *0.1227*$^{\Delta}$ |
| **MTOR** | Regulator of cell metabolism and growth | 836.63; 208.77 | 888.87; 177.86 | 985.92; 207.25 | 1055.74; 312.82 | **0.0240**$^{\S}$ | NS |
| **NF-κB-1** | Proinflammatory transcription factor | 490.23; 80.41 | 479.99; 78.16 | 538.84; 96.25 | 557.95; 132.85 | **0.0329**$^{\S}$ | *0.1321*$^{\Delta}$ |
| **NFE-2** | Oxidant induced anti-inflammatory | 209.40; 148.72 | 128.34; 76.05 | 152.86; 49.93 | 237.38; 78.19 | **0.0076**$^{\dagger}$ | **0.0256**$^{\Delta}$ *0.1037*$^{*}$ *0.1124*$^{\infty}$ |

| | | | | | | | |
|---|---|---|---|---|---|---|---|
| | transcription factor | | | | | | |
| **NFE2L2** | Oxidant induced anti-inflammatory transcription factor | 4429.32; 596.56 | 4411.79; 732.67 | 4921.33; 608.58 | 5011.73; 738.92 | **0.0073**[§] | *0.1497*[Ψ] *0.0746*[Δ] |
| **NOS1** | Neuronal and constitutively expressed; synthesizes NO | 27.08; 17.08 | 33.92; 13.76 | 32.52; 13.37 | 47.41; 30.45 | *0.1106*[§] *0.0681*[‡] | NS |
| **NOS2** | Cytokine induced NO synthesis | 130.28; 61.85 | 131.05; 35.59 | 177.72; 59.04 | 172.80; 46.01 | **0.0053**[§] | *0.0591*[Ψ] *0.1251*[Δ] |
| **NOS3** | Endothelial induced NO in shear stress | 115.34; 27.37 | 121.53; 28.77 | 145.39; 35.55 | 186.65; 141.93 | **0.0357**[§] | *0.0906*[Δ] |
| **NQO1** | Nrf2 mediated removal of toxic intermediates | 5872.38; 1008.72 | 5661.17; 610.55 | 5694.75; 623.73 | 5753.22; 620.41 | NS | NS |
| **NURR1** | Neuroinflammatory transcription factor | 1662.88; 719.38 | 1982.48; 1053.89 | 2147.18; 1237.19 | 2188.71; 1234.34 | NS | NS |
| **Nrf1** | Transcriptional modulation of metabolism, growth, and development | 477.96; 86.07 | 445.64; 56.88 | 528.10; 58.98 | 504.05; 44.85 | **0.0061**[§] *0.1418*[‡] | *0.1237*[Ψ] *0.0734*[Δ] |
| **PCSK9** | LDL-cholesterol metabolism | 12.24; 4.23 | 13.44; 4.04 | 10.81; 3.26 | 14.14; 4.40 | *0.0593*[‡] | *0.1082*[∞] |
| **PPARγ** | Adipocyte differentiation; senescence | 250.83; 143.31 | 297.65; 77.61 | 487.33; 205.27 | 421.53; 187.13 | **0.0004**[§] | **0.0014**[Ψ] *0.1424*[Δ] |
| **PRDX1** | Nrf2 antioxidant; detoxifies peroxides | 10663.02; 1216.09 | 11704.03; 1723.34 | 10253.08; 1118.60 | 10248.92; 2178.14 | *0.0516*[§] | *0.0710*[Δ] |
| **PTGS-1** | Proinflammatory enzyme | 718.25; 151.97 | 658.71; 141.64 | 785.57; 147.62 | 777.42; 179.12 | **0.0459**[§] | NS |
| **PTGS-2** | Proinflammatory enzyme | 146.43; 42.83 | 167.77; 64.43 | 177.48; 78.50 | 125.78; 41.35 | **0.0341**[†] | *0.0739*[∞] |
| **RIPK1** | Driver of apoptosis and necroptosis | 1481.71; 142.44 | 1450.54; 157.35 | 1515.17; 94.66 | 1516.17; 108.00 | NS | NS |
| **RUNX2** | Osteoblast differentiation | 996.17; 292.93 | 922.98; 257.00 | 1049.46; 351.40 | 1036.85; 222.29 | NS | NS |
| **SCL11A2** | Metal transport, iron uptake | 1248.54; 116.97 | 1253.20; 112.92 | 1187.25; 188.47 | 1184.51; 211.48 | NS | NS |
| **SESN2** | Stress-induced metabolic regulator | 116.36; 31.77 | 111.45; 21.39 | 118.02; 31.78 | 139.77; 46.54 | *0.1385*[§] | *0.1078*[Δ] |
| **SLC39A14** | Divalent metal transporter | 1344.21; 427.99 | 1487.09; 210.58 | 1610.41; 453.78 | 1468.61; 515.39 | NS | NS |
| **SLC40A1** | Ferroportin; transports iron | 2466.73; 381.46 | 2576.18; 393.73 | 2030.77; 320.13 | 2110.30; 319.47 | **<0.0001**[§] | **0.0080**[Ψ] **0.0062**[Δ] |

| | | | | | | | |
|---|---|---|---|---|---|---|---|
| **SLC7A11** | Cystine/glutamate antiporter; preserves redox balance | 42.10; 11.19 | 42.23; 6.58 | 38.43; 12.27 | 46.51; 13.02 | NS | NS |
| **SOD-1** | Cytoplasmic dismutation of $O_2^- \rightarrow O_2 + H_2O_2$ | 7645.76; 961.52 | 7774.87; 766.37 | 8247.52; 655.96 | 8273.01; 843.33 | **0.0265**$^{\S}$ | NS |
| **SOD-2** | Mitochondrial dismutation of $O_2^- \rightarrow O_2 + H_2O_2$ | 28113.88; 10092.25 | 28039.45; 6317.31 | 29433.45; 10317.57 | 27616.92; 9483.86 | NS | NS |
| **SOD-3** | Extracellular dismutation of $O_2^- \rightarrow O_2 + H_2O_2$ | 2969.85; 1297.25 | 2753.23l 982.23 | 4353.92; 1180.98 | 4957.62; 3324.50 | **0.0027**$^{\S}$ | **0.0191**$^{\Delta}$ |
| **TFRC** | Transferrin receptor; cellular uptake of iron | 863.94; 249.85 | 813.26; 199.78 | 819.05; 144.99 | 872.88; 171.57 | NS | NS |
| **TGFβ1** | Secretory peptide; cell growth, differentiation, and apoptosis | 1621.61; 290.68 | 1505.54; 242.70 | 1792.21; 413.77 | 1928.23; 481.77 | **0.0080**$^{\S}$ | **0.0171**$^{\Delta}$ |
| **TIMP-1** | Inhibits ECM degradation | 6942.11; 1521.22 | 6893.72; 691.48 | 7401.73; 1776.44 | 8047.94; 2854.76 | *0.1468*$^{\S}$ | NS |
| **TIMP-2** | Inhibits ECM degradation | 48380.75; 5617.56 | 50132.28; 6345.82 | 42835.52; 5435.70 | 40667.01; 5468.65 | **<0.0001**$^{\S}$ | **0.0406**$^{\Psi}$ **0.0005**$^{\Delta}$ |
| **TNF** | Proinflammatory cytokine involved in the acute phase stress response | 23.56; 6.21 | 21.74; 3.91 | 24.46; 9.44 | 26.79; 5.44 | *0.1227*$^{\S}$ | *0.1405*$^{\Delta}$ |
| **TXN** | Nrf2 induced antioxidant; reduces oxidized cysteine residues and cleaves disulfide bonds | 12217.15; 2006.44 | 13611.82; 1633.17 | 11495.56; 1756.17 | 12352.95; 2490.11 | *0.0968*$^{\S}$ *0.0601*$^{\ddagger}$ | NS |
| **ULK1** | Inducer of autophagy | 1128.54; 202.61 | 1143.63; 183.80 | 1262.98; 182.05 | 1366.35; 396.83 | **0.0215**$^{\S}$ | *0.0895*$^{\Delta}$ |
| **VEGF** | Promotes growth of new blood vessels | 14.23; 4.61 | 16.93; 6.08 | 14.23; 4.51 | 17.33; 8.81 | *0.1153*$^{\ddagger}$ | NS |
| **WNT** | Regulates the proliferation of cells | 12.72; 5.77 | 12.54; 5.86 | 18.59; 9.52 | 28.42; 33.23 | **0.0401**$^{\S}$ | *0.0747*$^{\Delta}$ |
| **β-CAT** | Component of canonical Wnt signaling; cell growth and adhesion | 21479.90; 2604.29 | 21345.03; 1579.98 | 20658.21; 2769.05 | 21695.43; 3224.27 | NS | NS |
| **p65 (RELA)** | Nuclear translocation and activation of NF-κB | 4772.86; 865.29 | 4789.05; 743.94 | 5506.77; 878.28 | 5662.20; 1497.04 | **0.0108**$^{\S}$ | *0.1011*$^{\Delta}$ |

| | | | | | | | |
|---|---|---|---|---|---|---|---|
| **ACTB** | Housekeeper gene; constitutively expressed cytoskeletal protein | 151359.39; 19649.35 | 146820.63; 10869.07 | 142927.95; 17078.86 | 145166.96; 19146.06 | NS | NS |
| **EEF1a1**[&] | Housekeeper gene; delivery of tRNAs to the ribosome | 171648.89; 0.00 | 171648.89; 0.00 | 171648.89; 0.00 | 171648.89; 0.00 | NS | NS |
| **GAPDH** | Housekeeper gene; catalyzes the 6th step of glycolysis | 17829.47; 4519.31 | 18988.50; 3692.00 | 18827.07; 4106.95 | 25472.24; 9560.10 | **0.0367**[§] **0.0297**[‡] *0.1212*[†] | **0.0256**[Δ] **0.0217**[∞] |
| **SDH-a** | Housekeeper gene; involved in complex II of the mitochondrial electron transport chain | 1769.00; 209.78 | 1749.61; 198.44 | 1915.61; 237.70 | 2063.01; 395.43 | **0.0055**[§] | **0.0167**[Δ] |

[&]Selected housekeeper gene utilized in data normalization

**Supplemental Table 3.2. Normalized absolute mRNA counts from infrapatellar fat pad from 15-month-old control and Nrf2-activator treated guinea pigs.** Data is depicted as mean and standard deviation. Trending *(P<0.15, italic)* and significant (**P<0.05, bold**) sources of variation (determined via 2-way ANOVA, factors signifying sex and treatment) are depicted in table 1. Trending *(P<0.15, italic)* and significant (**P<0.05, bold**) differences between groups (determined via Bonferroni multiple comparisons) are listed in the last column.

*2-way ANOVA key:*
- $^{\S}$*sex*
- $^{\ddagger}$*treatment*
- $^{\dagger}$*interaction*
- *NS no significant or trending source of variation identified*

*Bonferroni multiple comparisons key:*
- $^{*}$*Difference between control males and PB125 males*
- $^{\infty}$*Difference between control females and PB125 females*
- $^{\Psi}$*Difference between control males and control females*
- $^{\Delta}$*Difference between PB125 males and PB125 females*
- *NS no significant or trending difference*

| Gene | Description | Male Control (n=14) | Male PB125 (n=12) | Female Control (n=8) | Female PB125 (n=11) | 2-way ANOVA p-values | Bonferroni p-values |
|---|---|---|---|---|---|---|---|
| **Aggrecan** | Cartilage structure | 483.15; 227.06 | 405.33; 200.63 | 431.31; 191.67 | 812.95; 720.02 | *0.0747*$^{\dagger}$ | **0.0408**$^{\Delta}$ *0.0998*$^{\infty}$ |
| **Adiponectin** | Glucose & FA metabolism | 40352.45; 26675.63 | 54425.15; 26873.51 | 72666.59; 36645.28 | 54132.49; 14843.95 | **0.0499**$^{\dagger}$ *0.0539*$^{\S}$ | **0.0176**$^{\Psi}$ |
| **AKT** | Cellular survival and proliferation | 2874.67; 1187.16 | 2290.84; 583.55 | 2507.11; 373.50 | 2276.31; 719.39 | *0.1097*$^{\ddagger}$ | NS |
| **BAD** | Inducer of apoptosis | 938.06; 234.86 | 767.53; 118.51 | 865.12; 143.59 | 954.05; 379.10 | *0.0907*$^{\dagger}$ | *0.1465*$^{\Delta}$ |
| **BAK** | Intrinsic apoptosis | 1370.42; 345.55 | 1219.96; 194.80 | 1169.91; 133.33 | 1130.93; 300.39 | *0.0836*$^{\S}$ | NS |
| **BAX** | Intrinsic apoptosis | 844.89; 251.04 | 715.17; 124.22 | 753.11; 146.76 | 881.29; 350.77 | *0.0863*$^{\dagger}$ | NS |
| **BCL-2** | Inhibitor of apoptosis | 1336.30; 296.18 | 1140.23; 338.95 | 1580.36; 251.46 | 1724.57; 627.61 | **0.0018**$^{\S}$ | **0.0025**$^{\Delta}$ |
| **BECN1** | Regulator of autophagy | 1560.65; 483.72 | 1316.67; 239.08 | 1352.10; 144.45 | 1275.09; 285.03 | *0.1192*$^{\ddagger}$ | *0.1421*$^{*}$ |
| **BIM** | Pro-apoptotic BH3 protein | 509.09; 195.40 | 403.60; 123.67 | 464.08; 115.34 | 655.17; 330.37 | **0.0278**$^{\dagger}$ *0.1199*$^{\S}$ | **0.0134**$^{\Delta}$ *0.1185*$^{\infty}$ |
| **BMP-7** | Anabolic effect on cartilage | 171.59; 101.04 | 119.54; 72.55 | 158.12; 45.76 | 247.64; 219.04 | *0.0826*$^{\dagger}$ | **0.0444**$^{\Delta}$ |
| **C3** | Activator of complement | 3836.42; 2121.00 | 3574.49; 1523.13 | 4872.85; 1840.14 | 4272.73; 2342.16 | NS | NS |
| **Caspase-1** | Initiator of apoptosis | 720.64; 254.38 | 539.76; 180.36 | 617.78; 289.09 | 788.49; 403.95 | *0.0521*$^{\dagger}$ | *0.0860*$^{\Delta}$ |
| **Caspase-3** | Executioner of apoptosis | 922.92; 413.92 | 773.19; 297.74 | 758.28; 249.21 | 1120.98; 602.67 | *0.0526*$^{\dagger}$ | *0.1043*$^{\Delta}$ *0.1386*$^{\infty}$ |

| | | | | | | | |
|---|---|---|---|---|---|---|---|
| **Caspase-8** | Executes extrinsic apoptosis | 397.11; 106.62 | 327.95; 89.23 | 364.87; 49.82 | 485.14; 238.86 | **0.0356**$^{\dagger}$ | **0.0221**$^{\Delta}$ |
| **Caspase-9** | Executes intrinsic apoptosis | 222.31; 75.41 | 201.54; 40.86 | 215.84; 36.73 | 322.26; 150.57 | **0.0260**$^{\dagger}$ **0.0443**$^{\S}$ *0.1275*$^{\ddagger}$ | **0.0048**$^{\Delta}$ **0.0290**$^{\infty}$ |
| **Catalase** | Protects from oxidative damage via degradation of $2H_2O_2 \rightarrow O_2 + 2H_2O$ | 17823.42; 11617.98 | 17987.86; 6635.21 | 22141.68; 8164.31 | 22347.70; 6876.70 | *0.1078*$^{\S}$ | NS |
| **CBS** | Mediates early transsulfuration | 97.20; 49.97 | 64.77; 35.81 | 86.74; 33.37 | 76.60; 40.65 | *0.0966*$^{\ddagger}$ | *0.1078*$^{*}$ |
| **CCL-2** | Chemoattractant agent for myeloid and lymphoid cells | 2793.06; 1232.32 | 2601.51; 1148.29 | 2835.34; 759.41 | 3565.85; 2206.12 | NS | NS |
| **CD163** | Scavenger receptor for hemoglobin-haptoglobin | 9415.29; 2477.74 | 8753.88; 2046.82 | 7578.76; 1771.99 | 8311.30; 2769.04 | *0.1152*$^{\S}$ | NS |
| **COL10A1** | Marker of chondrocytes hypertrophy | 372.65; 278.78 | 249.69; 192.36 | 315.39; 194.19 | 430.00; 328.34 | *0.1388*$^{\ddagger}$ | NS |
| **COL2A1** | Structural component of cartilage | 1073.39; 1460.77 | 718.00; 735.41 | 537.58; 359.76 | 636.41; 474.31 | NS | NS |
| **CUL3** | Ubiquitin ligase | 3911.25; 651.88 | 3738.00; 442.26 | 3436.01; 349.49 | 3997.52; 863.21 | *0.0601*$^{\dagger}$ | *0.1159*$^{\infty}$ |
| **FGF-18** | Anabolic effect on cartilage | 2603.55; 1593.22 | 1894.30; 481.45 | 2547.10; 918.38 | 2244.03; 824.15 | *0.1271*$^{\ddagger}$ | NS |
| **FTH-1** | Intracellular iron storage protein | 81041.24; 30554.27 | 68897.78; 16496.07 | 84662.52; 27513.67 | 67932.92; 14230.84 | *0.0453*$^{\ddagger}$ | NS |
| **Glutathione peroxidase** | Nrf2 mediated antioxidant; $2H_2O_2 \rightarrow O_2 + 2H_2O$ $O_2^{-} \rightarrow O_2 + OH$ | 6692.14; 2237.15 | 5425.76; 743.38 | 6634.61; 1141.29 | 6483.80; 2182.09 | NS | NS |
| **GSK3β** | Inactivates nuclear Nrf2 | 2151.09; 325.56 | 2009.92; 258.19 | 2093.32; 267.38 | 2348.53; 449.16 | *0.0592*$^{\dagger}$ | **0.0375**$^{\Delta}$ |
| **HAMP** | Regulates iron absorption | 265.43; 173.82 | 207.72; 138.04 | 228.83; 117.77 | 454.56; 402.13 | *0.0596*$^{\dagger}$ | **0.0337**$^{\Delta}$ *0.0962*$^{\infty}$ |
| **HIF1-a** | Transcriptional response to hypoxia | 7170.09; 1543.40 | 8625.97; 3040.93 | 5983.98; 3710.34 | 7336.97; 4006.80 | *0.1478*$^{\ddagger}$ | NS |
| **HMGB1** | Proinflammatory alarmin | 16823.34; 1606.66 | 16075.66; 1061.53 | 15187.25; 1241.57 | 16526.64; 2375.65 | **0.0477**$^{\dagger}$ | *0.0730*$^{\Psi}$ |
| **HMOX-1** | Nrf2 regulated | 1235.05; 395.43 | 1030.48; 333.64 | 1019.37; 273.04 | 1050.40; 362.29 | NS | NS |

| | | | | | | | |
|---|---|---|---|---|---|---|---|
| | antioxidant that degrades heme | | | | | | |
| **IFN-γ** | Proinflammatory cytokine; implemented in rheumatoid arthritis | 94.67; 67.00 | 87.49; 67.11 | 76.13; 34.72 | 169.07; 130.99 | *0.0579*[†] *0.1024*[‡] | **0.0477**[Δ] **0.0429**[∞] |
| **IL-10** | Anti-inflammatory cytokine | 244.98; 140.39 | 173.69; 101.40 | 197.45; 93.59 | 337.09; 248.82 | **0.0372**[†] | **0.0362**[Δ] *0.1340*[∞] |
| **IL-1β** | Proinflammatory cytokine | 264.94; 102.16 | 188.67; 90.15 | 227.43; 79.01 | 314.29; 178.96 | **0.0314**[†] | **0.0305**[Δ] |
| **IL-4** | Proinflammatory cytokine; induces T-cell differentiation and Th2 response | 198.41; 124.34 | 128.63; 93.10 | 164.55; 89.08 | 239.22; 175.39 | *0.0685*[†] | *0.0812*[Δ] |
| **IL-5** | Proinflammatory cytokine; induces eosinophil differentiation | 82.17; 38.70 | 72.79; 41.25 | 71.25; 29.13 | 140.64; 95.02 | **0.0306**[†] *0.1134*[§] *0.0957*[‡] | **0.0137**[Δ] **0.0255**[∞] |
| **IL-6** | Proinflammatory cytokine | 408.75; 235.68 | 342.98; 173.49 | 356.62; 168.64 | 596.21; 399.65 | *0.0652*[†] | *0.0509*[Δ] *0.1131*[∞] |
| **KEAP1** | Degrades cytoplasmic Nrf2 | 1217.63; 508.26 | 972.28; 189.55 | 1085.77; 146.34 | 1027.60; 393.99 | NS | NS |
| **LEP** | Adipokine and regulator of appetite | 28327.96; 22927.21 | 38940.88; 24892.30 | 39111.87; 25026.75 | 19747.23; 10687.24 | **0.0281**[†] | *0.0791*[Δ] *0.1219*[∞] |
| **MAPK** | Cell differentiation, proliferation, and survival | 3708.57; 559.12 | 3327.90; 591;63 | 3399.41; 381.54 | 3818.65; 834.24 | **0.0407**[†] | *0.1252*[Δ] |
| **MCL1** | Inhibitor of apoptosis | 8393.87; 1599.40 | 8991.26; 1081.65 | 7703.74; 972.97 | 8680.52; 1334.90 | *0.0531*[‡] | NS |
| **MMP-13** | Cleaves type II collagen | 401.30; 342.03 | 215.69; 144.23 | 215.07; 96.30 | 406.51; 318.89 | **0.0252**[†] | NS |
| **MMP-2** | Cleaves type IV collagen | 25139.19; 16800.43 | 20004.95; 5547.09 | 15423.99; 3191.92 | 17646.93; 6364.71 | *0.0603*[§] | *0.0814*[Ψ] |
| **MMP-3** | Cleaves type II-IV, IX and X collagens | 437.61; 167.70 | 481.07; 151.24 | 343.83; 117.30 | 461.41; 199.90 | *0.1142*[‡] | NS |
| **MMP-9** | Cleaves type IV & V collagen, activates neutrophils | 94.15; 102.21 | 50.20; 18.90 | 92.62; 91.06 | 98.63; 56.76 | NS | NS |

| | | | | | | | |
|---|---|---|---|---|---|---|---|
| **MTOR** | Regulator of cell metabolism and growth | 705.84; 430.26 | 512.93; 74.22 | 531.62; 125.32 | 584.03; 238.90 | *0.1480*$^{\dagger}$ | NS |
| **NF-κB-1** | Proinflammatory transcription factor | 363.42; 104.90 | 302.63; 28.90 | 342.79; 41.36 | 387.66; 147.96 | *0.0814*$^{\dagger}$ | *0.0797*$^{\Delta}$ |
| **NFE-2** | Oxidant induced anti-inflammatory transcription factor | 145.71; 42.66 | 152.16; 53.84 | 140.87; 24.99 | 192.75; 84.51 | *0.0993*$^{\ddagger}$ | *0.1087*$^{\infty}$ |
| **NFE2L2** | Oxidant induced anti-inflammatory transcription factor | 4929.47; 711.66 | 4484.20; 384.13 | 4686.45; 579.30 | 4865.93; 891.77 | *0.1337*$^{\dagger}$ | NS |
| **NOS1** | Neuronal and constitutively expressed; synthesizes NO | 82.07; 56.46 | 50.48; 35.87 | 63.99; 38.45 | 81.90; 75.83 | *0.1461*$^{\dagger}$ | NS |
| **NOS2** | Cytokine induced NO synthesis | 451.83; 281.40 | 334.35; 247.59 | 371.59; 213.02 | 636.20; 489.12 | *0.0636*$^{\dagger}$ | *0.0635*$^{\Delta}$ |
| **NOS3** | Endothelial induced NO in shear stress | 171.74; 77.52 | 148.39; 26.75 | 157.20; 30.19 | 196.73; 77.50 | *0.0967*$^{\dagger}$ | *0.1213*$^{\Delta}$ |
| **NQO1** | Nrf2 mediated removal of toxic intermediates | 6556.86; 1363.07 | 5749.52; 756.93 | 5862.57; 855.90 | 5247.37; 710.87 | **0.0217**$^{\ddagger}$ *0.0513*$^{\S}$ | *0.0886*$^{*}$ |
| **NURR1** | Neuroinflammatory transcription factor | 1031.78; 347.21 | 942.36; 378.08 | 1084.90; 619.08 | 1430.74; 1168.98 | NS | NS |
| **Nrf1** | Transcriptional modulation of metabolism, growth, and development | 553.01; 94.69 | 493.40; 76.41 | 538.10; 35.79 | 599.45; 165.45 | *0.0704*$^{\dagger}$ | **0.0415**$^{\Delta}$ |
| **PCSK9** | LDL-cholesterol metabolism | 136.34; 83.40 | 102.18; 68.76 | 117.51; 56.18 | 190.29; 163.55 | *0.0969*$^{\dagger}$ | *0.0903*$^{\Delta}$ |
| **PPARγ** | Adipocyte differentiation; senescence | 972.61; 352.49 | 1226.46; 487.21 | 1658.93; 576.47 | 1583.89; 454.63 | **0.0006**$^{\S}$ | **0.0038**$^{\Psi}$ *0.1288*$^{\Delta}$ |
| **PRDX1** | Nrf2 antioxidant; detoxifies peroxides | 13668.84; 1421.21 | 12009.52; 2295.25 | 12520.57; 1093.81 | 10240.74; 2058.15 | **0.0121**$^{\S}$ **0.0010**$^{\ddagger}$ | **0.0185**$^{\infty}$ **0.0453**$^{\Delta}$ *0.0576*$^{*}$ |
| **PTGS-1** | Proinflammatory enzyme | 1023.58; 165.66 | 958.68; 213.06 | 959.75; 214.06 | 1104.10; 343.39 | NS | NS |
| **PTGS-2** | Proinflammatory enzyme | 408.40; 213.99 | 330.41; 181.65 | 360.25; 121.95 | 650.51; 479.63 | **0.0428**$^{\dagger}$ *0.1303*$^{\S}$ | **0.0209**$^{\Delta}$ *0.0707*$^{\infty}$ |

| | | | | | | | |
|---|---|---|---|---|---|---|---|
| **RIPK1** | Driver of apoptosis and necroptosis | 1693.55; 326.94 | 1595.11; 238.23 | 1595.52; 220.73 | 1758.79; 359.32 | NS | NS |
| **RUNX2** | Osteoblast differentiation | 313.99; 165.49 | 253.75; 135.61 | 208.13; 79.98 | 354.39; 217.25 | **0.0421**$^{\dagger}$ | *0.1132*$^{\infty}$ |
| **SCL11A2** | Metal transport, iron uptake | 1397.18; 460.36 | 1171.89; 327.93 | 1204.38; 326.13 | 1682.34; 882.16 | **0.0438**$^{\dagger}$ | *0.0628*$^{\Delta}$ *0.1384*$^{\infty}$ |
| **SESN2** | Stress-induced metabolic regulator | 68.01; 25.69 | 58.40; 12.03 | 58.53; 8.76 | 74.54; 38.86 | *0.1030*$^{\dagger}$ | NS |
| **SLC39A14** | Divalent metal transporter | 388.16; 199.69 | 360.79; 195.34 | 419.78; 438.94 | 388.78; 320.15 | NS | NS |
| **SLC40A1** | Ferroportin; transports iron | 2685.99; 970.83 | 2488.04; 528.16 | 2461.87; 721.59 | 2824.75; 491.61 | NS | NS |
| **SLC7A11** | Cystine/glutamate antiporter; preserves redox balance | 102.63; 66.94 | 83.36; 55.27 | 65.86; 67.18 | 71.40; 48.81 | NS | NS |
| **SOD-1** | Cytoplasmic dismutation of $O_2^- \rightarrow O_2 + H_2O_2$ | 10336.38; 1424.74 | 8607.13; 1331.80 | 10451.31; 1298.46 | 8640.51; 1914.10 | **0.0004**$^{\ddagger}$ | **0.0125**$^{*}$ **0.0258**$^{\infty}$ |
| **SOD-2** | Mitochondrial dismutation of $O_2^- \rightarrow O_2 + H_2O_2$ | 22097.40; 11105.05 | 14652.76; 4033.65 | 23340.67; 18478.98 | 18801.14; 10104.33 | *0.0838*$^{\ddagger}$ | NS |
| **SOD-3** | Extracellular dismutation of $O_2^- \rightarrow O_2 + H_2O_2$ | 1113.69; 630.56 | 768.47; 262.77 | 1283.51; 256.33 | 1070.01; 487.50 | *0.0517*$^{\ddagger}$ *0.0985*$^{\S}$ | *0.1299*$^{*}$ |
| **TFRC** | Transferrin receptor; cellular uptake of iron | 720.04; 161.14 | 643.99; 164.29 | 679.52; 68.45 | 818.41; 274.62 | *0.0657*$^{\dagger}$ | *0.0577*$^{\Delta}$ |
| **TGFβ1** | Secretory peptide; cell growth, differentiation, and apoptosis | 931.51; 523.01 | 618.84; 181.20 | 724.33; 168.16 | 624.46; 199.71 | **0.0437**$^{\ddagger}$ | **0.0405**$^{*}$ |
| **TIMP-1** | Inhibits ECM degradation | 4626.07; 1798.98 | 4324.85; 1658.78 | 4341.08; 2529.31 | 3927.60; 1613.94 | NS | NS |
| **TIMP-2** | Inhibits ECM degradation | 34609.63; 13169.56 | 38314.48; 7699.04 | 36173.61; 11874.57 | 37576.73; 6251.78 | NS | NS |
| **TNF** | Proinflammatory cytokine involved in the acute | 124.29; 71.33 | 93.45; 53.42 | 105.48; 47.68 | 147.72; 91.01 | *0.0895*$^{\dagger}$ | *0.1274*$^{\Delta}$ |

| | | | | | | | |
|---|---|---|---|---|---|---|---|
| | phase stress response | | | | | | |
| **TXN** | Nrf2 induced antioxidant; reduces oxidized cysteine residues and cleaves disulfide bonds | 22780.48; 3115.58 | 20101.63; 2906.41 | 21076.25; 2856.01 | 19238.02; 2444.49 | **0.0125**[‡] *0.1450*[§] | **0.0472**[*] |
| **ULK1** | Inducer of autophagy | 744.54; 288.02 | 655.57; 113.96 | 660.43; 92.98 | 692.71; 199.60 | NS | NS |
| **VEGF** | Promotes growth of new blood vessels | 231.84; 170.94 | 125.79; 101.60 | 188.27; 136.94 | 209.63; 179.55 | NS | NS |
| **WNT** | Regulates the proliferation of cells | 369.18; 262.94 | 212.64; 153.83 | 305.24; 205.17 | 398.53; 313.79 | *0.0990*[†] | *0.1419*[Δ] |
| **β-CAT** | Component of canonical Wnt signaling; cell growth and adhesion | 8658.16; 2248.69 | 8707.59; 1730.61 | 8346.85; 2020.08 | 9321.88; 2086.15 | NS | NS |
| **p65 (RELA)** | Nuclear translocation and activation of NF-κB | 2582.30; 1256.25 | 1947.81; 431.40 | 2212.50; 359.79 | 1829.99; 271.46 | **0.0355**[‡] | *0.0840*[*] |
| **ACTB** | Housekeeper gene; constitutively expressed cytoskeletal protein | 68273.60; 32602.19 | 70883.51; 14881.38 | 62222.79; 25181.78 | 68962.47; 17213.49 | NS | NS |
| **EEF1a1**[&] | Housekeeper gene; delivery of tRNAs to the ribosome | 171648.89; 0.00 | 171648.89; 0.01 | 171648.89; 0.00 | 171648.89; 0.00 | NS | NS |
| **GAPDH** | Housekeeper gene; catalyzes the 6$^{th}$ step of glycolysis | 10094.98; 4575.99 | 9734.80; 6654.79 | 8177.56; 1773.70 | 6660.94; 1951.86 | *0.0740*[§] | NS |
| **SDH-a** | Housekeeper gene; involved in complex II of the mitochondrial electron transport chain | 2168.62; 468.69 | 2276.05; 479.01 | 2277.90; 266.99 | 1981.20; 281.42 | NS | NS |

[&]Selected housekeeper gene utilized in data normalization

## Chapter 4 Supplemental Tables

### Supplemental Table 4.1. ANY-maze enclosure monitoring descriptive statistics.

| | | Female - Young | | | | | Female – Late Middle Aged | | | | |
|---|---|---|---|---|---|---|---|---|---|---|---|
| | | 5-mo. Control (n=13) | | 5-mo. Nrf2a (n=14) | | p-value | 15-mo. Control (n=12) | | 15-mo. Nrf2a (n=12) | | p-value |
| Property | Unit | mean | SD | mean | SD | | mean | SD | mean | SD | |
| *Enclosure Monitoring* | | | | | | | | | | | |
| Distance traveled | m | 10.90 | 7.47 | 7.46 | 5.31 | 0.1705 | 1.67 | 2.11 | 2.85 | 2.10 | 0.1943 |
| Average speed | m/s | 0.018 | 0.013 | 0.013 | 0.01 | 0.1685 | 0.003 | 0.004 | 0.005 | 0.004 | 0.2294 |
| Time mobile | s | 115.31 | 59.59 | 99.58 | 72.88 | 0.5373 | 20.07 | 22.13 | 36.89 | 25.17 | 0.1049 |
| Time in hut | s | 260.61 | 149.93 | 296.69 | 186.28 | 0.5772 | 365.32 | 227.78 | 318.7 | 151.89 | 0.5613 |
| Moving speed | m/s | 0.085 | 0.029 | 0.071 | 0.026 | 0.1878 | 0.071 | 0.054 | 0.070 | 0.027 | 0.9778 |

| | | Male - Young | | | | | Male – Late Middle Aged | | | | |
|---|---|---|---|---|---|---|---|---|---|---|---|
| | | 5-mo. Control (n=11) | | 5-mo. Nrf2a (n=13) | | p-value | 15-mo. Control (n=12) | | 15-mo. Nrf2a (n=12) | | p-value |
| Property | Unit | mean | SD | mean | SD | | mean | SD | mean | SD | |
| *Enclosure Monitoring* | | | | | | | | | | | |
| Distance traveled | m | 6.99 | 5.11 | 9.54 | 6.19 | 0.2556 | 6.02 | 4.17 | 6.63 | 0.011 | 0.7203 |
| Average speed | m/s | 0.012 | 0.009 | 0.016 | 0.011 | 0.2717 | 0.010 | 0.007 | 0.011 | 0.007 | 0.7379 |
| Time mobile | s | 89.58 | 62.36 | 113.99 | 78.03 | 0.3689 | 58.04 | 38.16 | 66.42 | 37.31 | 0.5783 |
| Time in hut | s | 282.21 | 189.00 | 152.47 | 170.93 | 0.0679 | 129.98 | 173.85 | 186.78 | 218.73 | 0.4678 |
| Moving speed | m/s | 0.071 | 0.025 | 0.082 | 0.046 | 0.4143 | 0.095 | 0.034 | 0.089 | 0.030 | 0.6546 |

*Mo=month; SD=Standard Deviation; m=meters; m/s=meters/second; s=seconds.*

**Supplemental Table 4.2. Descriptive statistics on female body weight, selected properties from uCT, and four-point bending.**

| | | Female - Young | | | | | Female – Late Middle Aged | | | | |
|---|---|---|---|---|---|---|---|---|---|---|---|
| | | 5-mo. Control (n=13) | | 5-mo. Nrf2a (n=14) | | p-value | 15-mo. Control (n=12) | | 15-mo. Nrf2a (n=12) | | p-value |
| Property | Unit | mean | SD | mean | SD | | mean | SD | mean | SD | |
| Body Mass | g | 755.04 | 48.864 | 738.57 | 72.592 | 0.4875 | 1008.3 | 79.163 | 985.85 | 122.17 | 0.5687 |
| *Femoral head* | | | | | | | | | | | |
| BV/TV | % | 0.4404 | 0.0403 | 0.4545 | 0.0537 | 0.4372 | 0.5231 | 0.0539 | 0.5155 | 0.0423 | 0.7032 |
| Tb. Number | (1/mm) | 3.9260 | 0.2292 | 3.9583 | 0.2060 | 0.7034 | *3.7159* | *0.2480* | *3.9225* | *0.2379* | ***0.0491*** |
| Tb. Thickness | mm | 0.1244. | 0.0162 | 0.1253 | 0.0152 | 0.8624 | 0.1444 | 0.0116 | 0.1385 | 0.0092 | 0.1806 |
| Tb. Spacing | mm | 0.2113 | 0.0160 | 0.2081 | 0.0178 | 0.6225 | 0.2266 | 0.0284 | 0.2137 | 0.0188 | 0.2016 |
| *Diaphyseal cortex* | | | | | | | | | | | |
| Thickness | mm | 0.8149 | 0.0484 | 0.8267 | 0.0689 | 0.6019 | 0.9431 | 0.0668 | 0.9624 | 0.0986 | 0.5749 |
| Cortical spacing | mm | 0.0966 | 0.0394 | 0.0855 | 0.0352 | 0.4399 | *0.1557* | *0.0310* | *0.1180* | *0.0405* | ***0.0211*** |
| Porosity | % | 0.0506 | 0.0061 | 0.0501 | 0.0052 | 0.8200 | 0.0436 | 0.0078 | 0.0407 | 0.0086 | 0.4072 |
| *Femoral condyle* | | | | | | | | | | | |
| BV/TV | % | 0.3103 | 0.0396 | 0.3283 | 0.0509 | 0.2850 | 0.3332 | 0.0454 | 0.3384 | 0.0487 | 0.7909 |
| Tb. Number | (1/mm) | 3.3288 | 0.2508 | 3.3493 | 0.2243 | 0.9050 | 3.2502 | 0.2806 | 3.1886 | 0.1950 | 0.5386 |
| Tb. Thickness | mm | 0.1060 | 0.0068 | 0.1119 | 0.0152 | 0.2176 | 0.1188 | 0.0094 | 0.1198 | 0.0129 | 0.8302 |
| Tb. Spacing | mm | 0.2815 | 0.0325 | 0.2734 | 0.0251 | 0.4649 | 0.3019 | 0.0401 | 0.2930 | 0.0227 | 0.5109 |
| *Four-Point Bending* | | | | | | | | | | | |
| Bending Load | N*mm | 912.58 | 126.25 | 897.70 | 143.83 | 0.7734 | *1163.33* | *214.50* | *1379.80* | *544.64* | ***0.0082*** |
| Displacement | mm | -2.46 | 0.53 | -2.32 | 0.75 | 0.5747 | -1.92 | 0.51 | -2.29 | 0.65 | 0.1491 |
| Stiffness | N/mm | 204.57 | 36.93 | 196.18 | 50.47 | 0.6202 | *267.65* | *50.18* | *312.21* | *43.22* | ***0.0326*** |
| Length | mm | 33.67 | 0.76 | 33.36 | 0.84 | 0.3238 | 34.52 | 1.08 | 34.56 | 0.99 | 0.9393 |
| Moment arm | mm | 11.22 | 0.25 | 11.12 | 0.28 | 0.3238 | 11.51 | 0.36 | 11.63 | 0.32 | 0.4038 |
| Major radius | mm | 2.93 | 0.10 | 2.87 | 0.16 | 0.2151 | 3.23 | 0.16 | 3.18 | 0.19 | 0.4769 |
| Minor radius | mm | *2.02* | *0.10* | *1.91* | *0.08* | ***0.0047*** | 2.07 | 0.14 | 2.10 | 0.11 | 0.5229 |
| $I_{xx}$ | $mm^4$ | 16.72 | 3.40 | 14.11 | 5.48 | 0.1409 | 18.98 | 4.87 | 17.57 | 3.57 | 0.4357 |
| $I_{yy}$ | $mm^4$ | 22.47 | 2.79 | 21.08 | 4.28 | 0.3173 | 31.51 | 6.60 | 32.86 | 6.40 | 0.6235 |
| $I_{xy}$ | $mm^4$ | *-4.72* | *2.87* | *-2.15* | *3.32* | ***0.0377*** | -0.46 | 7.15 | -1.39 | 4.58 | 0.7095 |
| $I_{max}$ | $mm^4$ | 26.14 | 2.58 | 23.92 | 4.26 | 0.1075 | 35.16 | 5.44 | 34.34 | 6.03 | 0.7374 |
| $I_{min}$ | $mm^4$ | *13.06* | *1.78* | *11.27* | *1.53* | ***0.0083*** | 15.33 | 3.39 | 16.09 | 3.13 | 0.5817 |
| Bending Stress | Mpa | 141.79 | 18.82 | 152.31 | 7.17 | 0.1103 | *159.03* | *21.28* | *182.91* | *18.31* | ***0.0087*** |

*SD=Standard Deviation; g=grams; mm=millimeter; N=Newton; MPa=Megapascal; Tb.=Trabecular; BV/TV=bone volume/total volume; I=Inertia*

**Supplemental Table 4.2. Descriptive statistics on male body weight, selected properties from uCT, and four-point bending.**

| | | Male - Young | | | | | Male – Late Middle Aged | | | | |
|---|---|---|---|---|---|---|---|---|---|---|---|
| | | 5-mo. Control (n=11) | | 5-mo. Nrf2a (n=13) | | p-value | 15-mo. Control (n=12) | | 15-mo. Nrf2a (n=12) | | p-value |
| Property | Unit | mean | SD | mean | SD | | mean | SD | mean | SD | |
| Body Mass | g | 893.98 | 88.747 | 899.87 | 72.547 | 0.8513 | 1191.3 | 117.03 | 1223.5 | 83.781 | 0.4351 |
| *Femoral head* | | | | | | | | | | | |
| BV/TV | % | 0.4063 | 0.0360 | 0.4095 | 0.0371 | 0.8332 | 0.4813 | 0.0314 | 0.4969 | 0.0644 | 0.4313 |
| Tb. Number | (1/mm) | 3.7914 | 0.1330 | 3.7627 | 0.2558 | 0.7395 | 3.8352 | 0.1599 | 3.7657 | 0.2113 | 0.3497 |
| Tb. Thickness | mm | 0.1195 | 0.0087 | 0.1199 | 0.0079 | 0.9167 | 0.1314 | 0.0078 | 0.1380 | 0.0167 | 0.1965 |
| Tb. Spacing | mm | 0.2262 | 0.0109 | 0.2314 | 0.0195 | 0.4389 | 0.2221 | 0.0142 | 0.2227 | 0.0244 | 0.9463 |
| *Diaphyseal cortex* | | | | | | | | | | | |
| Thickness | mm | 0.9401 | 0.0975 | 0.9021 | 0.1420 | 0.5213 | 1.0923 | 0.0820 | 1.1027 | 0.0935 | 0.7690 |
| Cortical spacing | mm | 0.1089 | 0.0567 | 0.1040 | 0.0685 | 0.8741 | 0.1571 | 0.0550 | 0.1574 | 0.0497 | 0.9872 |
| Porosity | % | 0.0451 | 0.0078 | 0.0493 | 0.0073 | 0.2767 | 0.0411 | 0.0080 | 0.0416 | 0.0062 | 0.8859 |
| *Femoral condyle* | | | | | | | | | | | |
| BV/TV | % | 0.3394 | 0.0282 | 0.3464 | 0.0440 | 0.6328 | 0.3558 | 0.0451 | 0.3599 | 0.0567 | 0.8424 |
| Tb. Number | (1/mm) | 3.2553 | 0.2199 | 3.3382 | 0.3094 | 0.4385 | 3.2358 | 0.2040 | 3.2133 | 0.2765 | 0.8120 |
| Tb. Thickness | mm | 0.1183 | 0.0074 | 0.1215 | 0.0122 | 0.4306 | 0.1259 | 0.0134 | 0.1232 | 0.0141 | 0.6249 |
| Tb. Spacing | mm | 0.2830 | 0.0248 | 0.2858 | 0.0396 | 0.8308 | 0.2953 | 0.0318 | 0.2943 | 0.0353 | 0.9419 |
| *Four-Point Bending* | | | | | | | | | | | |
| Bending load | N*mm | 1043.60 | 177.36 | 1001.93 | 169.90 | 0.6348 | *1353.13* | *326.87* | *1640.96* | *188.64* | ***0.0138*** |
| Displacement | mm | -2.74 | 0.87 | -2.78 | 0.72 | 0.9052 | -3.23 | 1.13 | -2.86 | 1.28 | 0.4461 |
| Stiffness | N/mm | *198.41* | *30.52* | *172.08* | *32.73* | ***0.0408*** | 296.60 | 41.01 | 319.39 | 56.08 | 0.2554 |
| Femur length | mm | 33.70 | 0.71 | 33.90 | 0.82 | 0.5044 | 35.33 | 1.25 | 35.91 | 1.08 | 0.2225 |
| Moment arm | mm | 11.23 | 0.24 | 11.30 | 0.27 | 0.5044 | 11.78 | 0.42 | 11.97 | 0.36 | 0.2225 |
| Major radius | mm | 3.09 | 0.07 | 3.04 | 0.19 | 0.5024 | 3.46 | 0.20 | 3.45 | 0.18 | 0.8923 |
| Minor radius | mm | 2.02 | 0.09 | 2.04 | 0.10 | 0.6347 | 2.18 | 0.10 | 2.26 | 0.12 | 0.0869 |
| $I_{xx}$ | $mm^4$ | 17.49 | 3.40 | 16.01 | 3.33 | 0.3879 | 23.88 | 6.08 | 25.32 | 4.93 | 0.5236 |
| $I_{yy}$ | $mm^4$ | 30.42 | 5.15 | 30.23 | 6.12 | 0.9462 | 42.02 | 9.10 | 45.62 | 7.40 | 0.2913 |
| $I_{xy}$ | $mm^4$ | -4.36 | 4.56 | -1.20 | 4.48 | 0.1767 | -7.31 | 4.67 | -6.43 | 6.28 | 0.6939 |
| $I_{max}$ | $mm^4$ | 33.17 | 4.49 | 31.64 | 6.04 | 0.5572 | 46.83 | 5.89 | 49.31 | 6.80 | 0.3396 |
| $I_{min}$ | $mm^4$ | 14.75 | 2.52 | 14.61 | 2.15 | 0.9080 | *19.07* | *2.44* | *21.63* | *3.11* | ***0.0305*** |
| Bending stress | Mpa | 144.34 | 18.90 | 140.89 | 20.57 | 0.7254 | 155.13 | 33.8 | 172.65 | 14.45 | 0.1088 |

*SD=Standard Deviation; g=grams; mm=millimeter; N=Newton; MPa=Megapascal; Tb.=Trabecular; BV/TV=bone volume/total volume; I=Inertia*

**Supplemental Table 4.4. Correlations between ultimate bending stress and various dependent variables.**

| Dependent Variable | Pearson (r) | 95% CI | P-value |
|---|---|---|---|
| **Weight** | 0.2473 | 0.0447 to 0.4303 | **0.0175** |
| *5-months* | | | |
| Male control | -0.0451 | -0.6886 to 0.6382 | 0.9084 |
| Male Nrf2a | 0.0077 | -0.7497 to 0.7564 | 0.9869 |
| Female control | -0.2448 | -0.6862 to 0.3285 | 0.3990 |
| Female Nrf2a | 0.1355 | -0.4256 to 0.6214 | 0.6441 |
| *15-months* | | | |
| Male control | 0.1161 | -0.4646 to 0.6270 | 0.7057 |
| Male Nrf2a | 0.0613 | -0.5313 to 0.6136 | 0.8500 |
| Female control | -0.4908 | -0.8653 to -0.0073 | *0.1253* |
| Female Nrf2a | -0.5788 | -0.8653 to -0.0073 | **0.0486** |
| **Femur length** | 0.2041 | 0.0004 to 0.3915 | **0.0497** |
| *5-months* | | | |
| Male control | -0.1569 | -0.7158 to 0.5245 | 0.6651 |
| Male Nrf2a | -0.7780 | -0.9654 to -0.0602 | **0.0394** |
| Female control | -0.2587 | -0.6940 to 0.3152 | 0.3719 |
| Female Nrf2a | 0.2826 | -0.2917 to 0.7071 | 0.3276 |
| *15-months* | | | |
| Male control | 0.5066 | -0.0616 to 0.8268 | *0.0773* |
| Male Nrf2a | -0.1934 | -0.6906 to 0.4280 | 0.5470 |
| Female control | -0.3190 | -0.7713 to 0.3474 | 0.3390 |
| Female Nrf2a | -0.6089 | -0.8765 to -0.0538 | **0.0356** |
| **Distance traveled** | -0.2887 | -0.4650 to -0.0903 | **0.0050** |
| *5-months* | | | |
| Male control | 0.0891 | -0.5727 to 0.6805 | 0.8067 |
| Male Nrf2a | -0.2934 | -0.8571 to 0.5900 | 0.5230 |
| Female control | -0.0916 | -0.5933 to 0.4614 | 0.7555 |
| Female Nrf2a | -0.1090 | -0.6046 to 0.4475 | 0.7107 |
| *15-months* | | | |
| Male control | -0.2922 | -0.7263 to 0.3085 | 0.3327 |
| Male Nrf2a | -0.2896 | -0.7404 to 0.3410 | 0.3613 |
| Female control | 0.4296 | -0.2294 to 0.8185 | 0.1873 |
| Female Nrf2a | 0.0918 | -0.5089 to 0.6324 | 0.7766 |
| **Time mobile** | -0.2965 | -0.4718 to -0.0988 | **0.0039** |
| *5-months* | | | |
| Male control | 0.2532 | -0.4478 to 0.7614 | 0.4803 |
| Male Nrf2a | -0.4072 | -0.8880 to 0.4988 | 0.3646 |
| Female control | -0.0908 | -0.5928 to 0.4621 | 0.7577 |
| Female Nrf2a | -0.2072 | -0.6647 to 0.3633 | 0.4773 |
| *15-months* | | | |
| Male control | -0.2871 | -0.7236 to 0.3135 | 0.3416 |
| Male Nrf2a | -0.3562 | -0.7722 to 0.2737 | 0.2558 |
| Female control | -0.1688 | -0.6980 to 0.4797 | 0.6199 |
| Female Nrf2a | 0.0420 | -0.5450 to 0.6014 | 0.8969 |
| **Average speed** | -0.2905 | -0.4666 to -0.0922 | **0.0047** |
| *5-months* | | | |
| Male control | 0.0843 | -0.5759 to 0.6780 | 0.8168 |
| Male Nrf2a | -0.2934 | -0.8571 to 0.5900 | 0.5230 |
| Female control | -0.0897 | -0.5921 to 0.4629 | 0.7603 |
| Female Nrf2a | -0.1120 | -0.6065 to 0.4450 | 0.7031 |
| *15-months* | | | |
| Male control | -0.2887 | -0.7245 to 0.3119 | 0.3387 |
| Male Nrf2a | -0.2942 | -0.7427 to 0.3365 | 0.3533 |
| Female control | 0.3900 | -0.2739 to 0.8022 | 0.2357 |
| Female Nrf2a | 0.1326 | -0.4777 to 0.6565 | 0.6813 |